TRADE-OFFS IN AUTOMOTIVE ACTIVE SUSPENSION DESIGN

Semiha TÜRKAY

Ph.D. Dissertation

Graduate School of Sciences

Electrical and Electronics Engineering

June 2010

ABSTRACT

Ph.D. Dissertation

TRADE-OFFS IN AUTOMOTIVE ACTIVE SUSPENSION DESIGN

Semiha TÜRKAY

Anadolu University
Graduate School of Sciences
Electrical and Electronics Engineering Program

Supervisor: Prof. Dr. Hüseyin AKÇAY

2010, 219 pages

In this thesis, a strongly consistent subspace algorithm for the identification of discrete-time, linear time invariant systems from nonuniformly spaced power spectrum measurements is proposed. A byproduct subspace algorithm to construct analytic functions from evaluations of their real or imaginary parts on finite subsets of the unit circle is developed. A connection between the subspace identification and the Lagrange-Sylvester interpolation problems is established.

Pointwise constraints and trade-offs on closed-loop frequency responses are derived for a quarter-car active suspension model. The influence of tire damping on the design of an active suspension system is analyzed. The rms and the rms gain constraints for the quarter, half, and full-car suspension models are studied in the $\mathcal{H}_2$-optimal and multi-objective control frameworks. For the quarter and half-car models, the dependance of closed-loop rms responses on the tire damping is investigated. The multi-objective suspension control problem is formulated as a convex mixed $\mathcal{H}_2/\mathcal{H}_\infty$ synthesis problem for the quarter, half, and full-car models and solved by using linear matrix inequalities. Next, the problem is re-formulated as a non-convex and non-smooth optimization problem for the quarter and full-car models and is solved by using HIFOO toolbox. Then, for the quarter and half-car models the assumption that tire

damping coefficient is exactly known is relaxed and robust controllers to cope with polytopic tire damping uncertainties are designed. Finally, a prototype three-degrees-of freedom cabin model for a commercial truck is derived and an active suspension system is designed by using the linear-quadratic-Gaussian design methodology.

Keywords: System identification; Active suspension; Tire damping; Multi–objective control; Linear matrix inequality; Non-convex optimization.

ÖZET

Doktora Tezi

OTOMOTİV SÜSPANSİYON TASARIMINDA UZLAŞIM EĞRİLERİ

Semiha TÜRKAY

Anadolu Üniversitesi
Fen Bilimleri Enstitüsü
Elektrik-Elektronik Mühendisliği Anabilim Dalı

Danışman: Prof. Dr. Hüseyin AKÇAY

2010, 219 sayfa

Bu tezde, kesikli zaman, doğrusal, zamandan bağımsız sistemlerin tanıyımı için düzgün aralıklı olmayan spectrum ölçümleri kullanılarak yüksek tutarlı altuzay algoritması önerilmiştir. Bunun yanında, analitik fonksiyonları, birim çemberin sonlu alt setleri üzerindeki reel ve imajiner ölçümlerinden elde eden altuzay algoritması geliştirilmiştir. Altuzay tanıyımı ve Lagrange-Sylvester interpolasyon problemi arasındaki ilişki kurulmuştur.

Çeyrek araç aktif süspansiyon modeli için kapalı döngü frekans yanıtları üzerindeki noktasal kısıtlamalar ve uzlaşım eğrileri türetilmiştir. Lastik sönümleme katsayısının aktif süspansiyon sistem tasarımı üzerindeki etkisi analiz edilmiştir. $\mathcal{H}_2$-optimal ve çok amaçlı kontrol kapsamında çeyrek, yarım ve tam araç modelleri için rms ve rms kazanç kısıtlamaları çalışılmıştır. Çok amaçlı süspansiyon kontrol problemi konveks, karışık $\mathcal{H}_2/\mathcal{H}_\infty$ sentez problemi olarak formüle edilmiştir ve doğrusal matris eşitsizlikleri kullanılarak çözülmüştür. Çeyrek ve yarım araç modellerinde kapalı döngü rms yanıtlarının lastik sönümleme katsayısına olan bağlılığı araştırılmıştır. Daha sonra problem çeyrek ve tam araç modelleri için konveks ve düzgün olmayan optimizasyon problemi olarak yeniden formüle edilmiştir ve HIFOO araç kutusu kullanılarak çözülmüştür. Çeyrek ve yarım araç modellerinde lastik sönümleme katsayısının tam olarak bilinmediği varsayılarak politopik lastik sönümleme katsayısı be-

lirsizlikleri için gürbüz kontrolcüler tasarlanmıştır. Son olarak, ticari kamyon için üç serbestlik derecesine sahip kabin modeli türetilmiştir ve doğrusal-kare-Gaussian (LQG) tasarım yöntemi kullanılarak aktif süspansiyon sistemi tasarlanmıştır.

Anahtar Kelimeler: Sistem tanıyımı; Aktif süspansiyon; Lastik sönümleme katsayısı; Çok amaçlı kontrol; Doğrusal matris eşitsizlikleri; Konveks olmayan optimizasyon.

ACKNOWLEDGMENTS

First and foremost I want to express my sincerest gratitude to my supervisor, Prof. Akçay , who has supported me throughout my thesis with his patience and unsurpassed knowledge. I thank him for his guidance and encouragement where the good advice, support and friendship has been invaluable on both an academic and a personal level.

I also want to express my gratitude to Prof. Lohmann and the people in his group for their hospitality and support during my visit to the Institute of Automatic Control, Technical University of Munich in Germany supported by Deutsche Akademische Austauschdienst (DAAD). I am also grateful to Dipl.-Ing. Andreas Unger for his valuable research discussions on the practical aspects of automotive control.

I would like to thank Dr. Suat Gümüşsoy for his valuable comments on applying the $\mathcal{H}_\infty$ fixed-order optimization toolbox.

I gretefully acknowledge finacial support I received from Ford Motor Company-OTOSAN Inc. for the research project "Semi-active cabin suspension design for cargo truck" and funding from Turkish Scientific and Technical Research Council (TÜBİTAK) under the Grant 106E180.

Finally, I would like to express my eternal gratitude to my parents for their everlasting love, support and confidence in me.

TABLE OF CONTENTS

LIST OF FIGURES

LIST OF TABLES

GLOSSARY

$\mathbf{R}$	Set of the real numbers
$\mathbf{C}$	Set of the complex numbers
$\mathbf{T}$	Unit circle in the complex plane
$\mathbf{D}$	Open unit disk in the complex plane
$\bar{z}$	Complex conjugate of z
$\mathrm{Re}(z)$	Real part of z
$\mathrm{Im}(z)$	Imaginary part of z
j	$\sqrt{-1}$
A^T	Transpose of A
A^*	Complex conjugate of A
A^H	Complex conjugate transpose of A
δ_{kl}	Kronecker delta, i.e. $\delta_{kl} = 1$ if $k = l$ and 0 otherwise
$X \otimes Y$	Kronecker product of $X \in \mathbf{C}^{m \times n}$ and Y defined as $\begin{bmatrix} X_{11}Y & \cdots & X_{1n}Y \\ X_{m1}Y & \cdots & X_{mn}Y \end{bmatrix}$.

$\text{vec}(A)$	Vector formed by stacking the columns of $A = [a_1 \cdots a_n]$ into one long vector $\begin{bmatrix} a_1 \\ \vdots \\ a_n \end{bmatrix}$.
$\mathcal{C}(X)$	Number of elements in a given set X
I_n	n by n identity matrix
0_{mxn}	m by n null matrix
$\text{diag}(\cdot)$	Block diagonal matrix
$\|\eta_k\|_F = [\text{Tr}(\eta_k^H \eta_k)]^{\frac{1}{2}}$	Frobenius norm of η_k
$M^\dagger = (M^T M)^{-1} M^T$	Moore-Penrose inverse of a full column matrix M
$\text{Tr}(X)$	Trace of a given square matrix X
$\delta(\tau)$	Unit impulse function
$a(s) = O(s^\gamma)$	$\exists \ \alpha, \ \beta > 0$ such that $\alpha\|s\|^\gamma \leq \|a(s)\| \leq \beta\|s\|^\gamma$
$\text{E}(x)$	Expected value of random variable x
$\mathcal{L}_2$	Hilbert space of complex functions on the imaginary axis (unit circle)
$\mathcal{H}_2$	Hilbert space of complex functions analytic on the open right half plane (open unit disk)
$\mathcal{L}_\infty$	Lebesque space of complex functions bounded on the imaginary axis (unit circle)
$\mathcal{H}_\infty$	Banach space of complex functions analytic and bounded on the open right half plane (open unit disk)

$\mathcal{RH}_\infty^{\mathrm{pq}}$	Set of stable p by q real-rational proper transfer matrices analytic and bounded on the open right half plane (open unit disk)
$\mathcal{H}_2^\perp$	Orthogonal complement of $\mathcal{H}_2$ in $\mathcal{L}_2$
Π	Orthogonal projections from $\mathcal{L}_2$ onto $\mathcal{H}_2$
$\Pi^\perp$	Orthogonal projections from $\mathcal{L}_2$ onto $\mathcal{H}_2^\perp$
$\sigma_{\max}$	Largest singular value
$\|G\|_\infty$	$\sup_{w\in IR}\sigma_{\max}(G(jw))$ when the domain of $G \in \mathcal{L}_\infty$ is the imaginary axis and $\sup_{0\le\theta<2\pi}\sigma_{\max}(G(e^{j\theta}))$ when the domain of $G \in \mathcal{L}_\infty$ is the unit circle
$\|G\|_2$	$(\frac{1}{2\pi}\int_{-\infty}^{\infty}\|G(jw)\|^2dw)^{1/2}$ when the domain of $G \in \mathcal{L}_2$ is the imaginary axis and $(\frac{1}{2\pi}\int_0^{2\pi}\|G(e^{j\theta}))\|^2dw)^{1/2}$ when the domain of $G \in \mathcal{L}_2$ is the unit circle
$H^\sim(s)$	$H^T(-s)$
(A, B, C, D)	Quadruplet representing the state-space realization of $G(s) = D + C(sI - A)^{-1}B$

1 INTRODUCTION

1.1 Motivation and Background

The suspension system is the main tool to achieve ride comfort and drive safety for a vehicle. Passive suspension systems have been designed to obtain a good compromise between these objectives, but intrinsic limitations prevent them from obtaining the best performances for both goals. Lower the vertical acceleration, the better is the ride comfort. However, structural features of a vehicle place a hard limit on the amount of suspension deflection available to reduce the car body acceleration; and good road holding is important for vehicle handling, and in general for enhanced safety. Additional constraints are also imposed by overall system robustness, reliability and cost requirements. Compared with passive suspension systems, active and semi-active suspension systems can achieve a better compromise during various driving conditions.

The use of active and semi-active control on vehicle suspensions has been considered for many years. A large number of different arrangements from semi-active to fully active schemes have been investigated. See, for example, [1–12] and the references therein. The three main performance requirements for advanced vehicle suspensions are to isolate passengers from vibrations arising from road roughness, to suppress the vibrations of the wheels in order to maintain firm and uninterrupted contact of wheels for good road handling, and to keep suspension strokes within specified limits.

In order to provide a compromise among these conflicting goals various approaches, *i.e*, Linear-quadratic Gaussian (LQG), adaptive control, robust control, and nonlinear control have been proposed and a significant progress has been made, [1, 3, 5, 11, 13–16].

A common point of these approaches is that all control requirements are weighted and formulated in a single objective function, which is minimized

to find an optimal controller. Specifying all different requirements in a single objective function and minimizing it may yield a conservative suspension design. Moreover, in single objective approach the trade-offs among conflicting requirements are managed by choosing appropriate, possibly frequency dependent weightings, which is, however, nontrivial [17].

Constraints and trade-offs on achievable suspension performance have been studied in [18–22]. As put forward in [20], in a study of constraints and trade-offs from a control systems point of view, one has to properly address:

(i) What can and can not be achieved with general dynamic compensation,

(ii) How much freedom is gained by the selection of measurements for feedback purpose?

In [18, 22], constraints on achievable frequency responses were derived from an *invariant point* perspective. A framework using mechanical multi-port networks to study the performance capabilities and constraints was developed in [21]. In [20], for a quarter-car model of an automotive suspension a *complete* set of constraints on several transfer functions of interest from the road and the load disturbances were determined by making use of the *factorization* approach to feedback stability and the Youla *parameterization* of stabilizing controllers. Roughly speaking, completeness means that from a given set of constraints, one can identify a quarter-car model within the model class matching the given constraints. Such an approach reveals the degrees-of-freedom in shaping the response of the vehicle to disturbances and determines a minimum set of measurements to exploit this freedom.

In [20], constraints on the frequency responses of the sprung mass position, the suspension travel, and the tire deflection were derived for various choices of measurements ranging from the suspension travel to a full set of state variables. These constraints typically arise in the form of finite and nonzero invariant frequency points and the growth restrictions on the frequency responses and their derivatives at zero and infinite frequencies. The quarter-

car model studied in that work does not include passive suspension elements spring and damper; and also tire damping is neglected.

Actually in most works, tire damping is set to zero when modeling automotive active suspension systems. This is due to the facts that tire damping is typically small and it is difficult to estimate. It is generally accepted that damping ratio in a vehicle tire ranges between 0.03 and 0.10 depending on tire size, applied pressure, whether the tire is free or rotating, if it is new or worn, and also on tire type *i.e.,* whether it is all season or snow [23–25]. In fact, tire damping by itself has little influence on the wheel-hop vibration since this mode is mainly damped by the shock absorber.

The ignorance of damping in tire models compelled misleading conclusions that at the wheel-hop frequency, no matter what forces are exerted between sprung and unsprung masses, their motion are uncoupled, and the vertical acceleration of the sprung mass will be unaffected [18, 20, 22]. It is pointed out in [26] that by taking tire damping to be small but nonzero, the motions of the sprung and unsprung masses are coupled at all frequencies, and control forces can be used to reduce the sprung mass vertical acceleration at the wheel-hop frequency. The results in this thesis show that tire damping can have a significant influence on the closed-loop performance of an active suspension system.

The study of the constraints on the achievable performance has remained largely restricted to pointwise constraints in the frequency domain while ride comfort and safety criteria are mostly expressed in terms of the root-mean square (rms) values of the sprung mass vertical acceleration, the suspension travel, and the tire deflection. The performance requirements on rms values or rms gains of response variables can easily be described by using linear matrix inequalities (LMIs). It is straightforward to express closed-loop pole placement constraints and robustness requirements arising from various uncertainties such as unmodelled tire unbalance and nonlinearities, and parametric uncertainties as LMIs. The resulting multi-objective control problems

can efficiently be solved by using convex optimization techniques [27].

Multi-objective control of vehicle suspensions by using LMIs has emerged as a powerful design technique for a variety of linear control problems such as mixed $\mathcal{H}_2/\mathcal{H}_\infty$ synthesis. In [2], a constrained $\mathcal{H}_\infty$ control scheme with output and control constraints were studied. In [28], problems with $\mathcal{H}_2$ or $\mathcal{H}_\infty$ cost under positive realness constraint on controller structures based on matrix inequalities were considered. The control objective similar to that in [28] was studied in [29]. In [30] where two separate Lyapunov functions were considered for the $\mathcal{H}_2$ performance and the positive real constraint, an iterative LMI procedure was proposed. Robust multi-objective controllers were also synthesized to cope with parameter uncertainties in system matrices characterized by a given polytope [31, 32]. Application of non-convex and non-smooth optimization algorithms [33] to suspension control problems was reported in the recent work [34]. In [35], static output feedback $\mathcal{H}_\infty$ controller and non-fragile static output feedback $\mathcal{H}_\infty$ controller design procedures via LMIs and genetic algorithm were presented. The $\mathcal{H}_\infty$ control problem for active vehicle suspension systems with actuator time delay was studied in [36] and a delay-dependent memoryless state feedback $\mathcal{H}_\infty$ controller was designed using LMIs.

A problem in vehicle active suspension control is to insulate the vehicle body from both road and load disturbances. It is well known that these are conflicting requirements when passive suspensions are used, but the conflict can be removed when active control is employed with appropriate hardware structure, *e.g*, choice of sensor location, number, and type [20,37,38]. When the active control is employed with appropriate hardware structure the design for each disturbance path can be carried out successively, which provides sufficient freedom to adjust the responses independently. In [37, 38], the disturbance response decoupling problems were studied for half and full-car models as well. In [21, 39], some simplifying assumptions were used to perform energy-preserving transformations of the external disturbance variables to achieve decoupling. It was noted in [37] that under certain conditions the half-car model by possibly violating the energy-preserving property can be decoupled

into *bounce* and *rotation* quarter-car models in order to exploit the simplified structure of the latter. The details can be found in [37]. Further decoupling examples were given in [14, 38, 40]. For example in [38], a full-car motion was decomposed into the *heave*, the *pitch*, and the *roll* components for the vehicle body and additionally a *warp* component for the wheels which are in contact with the road.

In [41], an active suspension system for seven-degrees-of-freedom vehicle model was designed as a full-state, optimal, LQG regulator. In [42], feedback control of a full-vehicle suspension system featuring magnetorheological dampers was investigated. Sliding mode control of active suspensions for a full-car model was studied in [43] and neural network based robust control was designed in [44] to control the vibration of vehicle's suspensions. In contrast to motion decoupling strategies in [37], the seven-degrees-of-freedom ride model considered in [41–44] allows simultaneous investigation of the heave, the pitch, and the roll motions of a full vehicle model, which are in fact strongly coupled. It is necessary that a high performing suspension system takes all possible couplings into account. In this thesis it is demonstrated by a case study that multi-objective control methods in [11, 45, 46] can be applied to large-scale active suspension design problems without resorting to such motion decoupling procedures.

In this thesis, we also consider active suspension design problem for a mid-size commercial truck cabin. Heavy road vehicles are typically used for transportation and they have dynamic behavior which is significantly different than that of cars, and thus require distinct suspension design approaches. The issue of ride comfort for vehicle operations has generated considerable interest recently, especially in heavy vehicle systems since long-distance drivers are more likely to experience high levels of vibration. Vibration-related health problems and ride comfort assessment criteria and methods are discussed in the survey paper [47].

Cabin and seat suspension (secondary suspension) provides the driver

with a comfortable ride without requiring soft primary suspension and consequent problems with vehicle handling, stability, and static deflection. Recent activity [48–51] in the area of cabin and suspension design has focused on the use of controllable suspension elements which provide ride benefits of active/semi-active primary suspension. Although there are many control algorithms available, in this thesis the LQG method is chosen to design an active cabin suspension because it is intuitive and easy to implement.

It is generally agreed that typical road surfaces may be considered as realizations of homogeneous and isotropic two-dimensional Gaussian random processes and these assumptions make it possible to completely describe a road profile by a single power spectral density evaluated from any longitidunal track [52, 53]. Then, the spectral description of the road together with a knowledge of traversal velocity and of the dynamic properties of the vehicle provide an analysis which will describe the response of the vehicle expressed in terms of displacement, acceleration, or stress.

Identification of multi-input/multi-output systems from a measured power spectrum is a problem arising in certain applications; for example, the design of linear shaping filters for noise processes. A practical application is the modeling of stochastic road disturbances experienced by a vehicle moving forward. The goal here is to model road spectrum by a rational transfer function of reasonably low order and to use this approximation for a design of a *linear shaping filter* with a white noise input. Once such an approximation is made, the vehicle control problem can be formulated in standard form. Applications to the modeling of acoustic power spectra and the modeling of passenger sensitivity for car accelerations were presented in [54].

A quarter-car active suspension system can be made to have all the three response variables satisfactory as shown in Section 4.4 when tire damping coefficient is large enough. Conversely, by specifying closed-loop responses one might ask if there exists a feedback controller which produces the specified closed-loop responses when connected with the given passive suspension

system but small tire damping coefficient. This is an interpolation problem with interpolation conditions specified at a set of finite and/or infinite frequencies involving functional and derivative values. In the literature, it is the *so-called* problem of finding Q-parameter of a stabilizing controller arising, for example, in robust controller synthesis [55, 56]. The problem of finding a Q-parameter of a stabilizing controller also arises in active suspension designs as discussed extensively in Chapter 4, which motivated us to undertake a study of the well-known *tangential Lagrange–Sylvester* rational interpolation problem in Chapter 3.

1.2 The Scope of the Work

The contents of this thesis and our contributions are as follows:

In Chapter 2, a subspace-based algorithm to identify multi–input/multi–output systems from corrupted power spectrum samples measured at non uniformly spaced frequencies is presented. The objective is to remove the restriction on the frequencies and show that this algorithm is not only *strongly consistent* but also recovers finite-dimensional rational spectra, given a finite number of noise-free data. The proposed algorithm is illustrated by means of two examples. In the first example, a system that has a power spectrum with sharp peaks is simulated. In the second example, a stochastic road modeling problem is studied to illustrate the practical relevance of the problem. A byproduct subspace algorithm to construct analytic functions from evaluations of their real or imaginary parts on finite subsets of the unit circle is developed. This algorithm exactly retrieves finite-dimensional systems from noise-free data. Its consistency properties are also studied. The results of this chapter have been published in [57–61].

In Chapter 3, the Lagrange-Sylvester interpolation of rational matrix functions which are analytic at infinity is studied and an interpolation algorithm related to the subspace based identification algorithm in [62] is proposed.

The solvability conditions of this interpolation problem are particularly simple and depend only on the total multiplicity of the interpolation nodes. The purpose of this contribution is to pinpoint the kinship between the frequency domain subspace based identification of stable linear systems and the minimal rational interpolation of stable systems. The results of this chapter have been published in [63–65].

In Chapter 4, a quarter-car model is used to study the constraints on the achievable frequency responses for a wide range of suspension parameters. The constraints derived complement existing results in the literature on vehicle dynamics and control. Next, the effect of tire damping on the achievable vehicle performance is investigated. By using the factorization approach to feedback stability it is shown that tire damping couples the motions of the sprung and unsprung masses, and control forces can be used to reduce the sprung mass vertical acceleration at the wheel-hop frequency without sacrificing road holding. The influence of tire damping on the design of an active suspension system for a quarter-car model is also illustrated by a mixture of the LQG methodology and the interpolation approach. Despite its simplicity the quarter-car model is the most widely used suspension model. A significant insight into the suspension design problem can be gained using this simple model. Besides, with the current trend of using four independent suspension systems on a single vehicle, the linear quarter-car model offers quite a reasonable representation of the actual suspension system. In the automotive industry, starting with simple quarter-car models, optimal control theory was used to establish the potential benefits of active suspension systems. The results of this chapter have been published in [66–69].

In Chapter 5, the work initiated in Chapter 4 is continued and the $\mathcal{H}_2$-optimal and the mixed $\mathcal{H}_2/\mathcal{H}_\infty$ syntheses of the quarter-car suspension systems excited by random road disturbances are studied. First, assuming that tire damping is known, a multi-objective suspension control problem is formulated and solved by using LMIs. The influence of tire damping on the solution of this optimization is studied. Later, the assumption that tire damping

coefficient is known is dropped and a multi-objective control problem with tire damping coefficient confined to a prescribed interval is formulated. By using LMIs a controller with guaranteed performance over all suspension models in the uncertainty set is obtained. The closed-loop performance of this robust controller is studied. Next, the multi-objective control is re-formulated as a non-convex and non-smooth optimization problem with controller order less than or equal to the quarter-car model order. For a range of controller orders, controllers are synthesized by using the HIFOO toolbox. A parametric study is performed to assess the dependence of the closed-loop response on tire damping. Parts of this chapter have been published in [70, 71] and some parts have been submitted for publication [72].

In Chapter 6, all achievable rms responses of a four–degrees–of–freedom half-car model subjected to random road excitations are studied. An optimization problem that aims to minimize weighted sums of the rms values of the response variables with respect to the class of all stabilizing controllers is formulated. The solution of this optimization problem is obtained for a range of tire damping ratios and the vehicle forward velocities. Next, assuming that tire damping is precisely known, a multi-objective suspension control problem is formulated and solved by using LMIs. The control objective is to obtain a compromise between ride comfort and road holding. The influence of tire damping on road holding is noteworthy while the other responses are insensitive to changes in tire damping coefficient for the range considered. Later, the assumption that tire damping coefficients are known is dropped and a robust controller is synthesized for a suspension system with polytopic tire uncertainties. It is found that this robust controller does not offer any advantage over an active suspension system designed by neglecting tire damping. The contents of this chapter have been published in [73–75].

In Chapter 7, multi-objective control problems are formulated for a seven-degrees-of-freedom full-car suspension model and solutions to these optimization problems are obtained by using LMIs and the HIFOO toolbox. The contents of this chapter have been submitted for publication [76].

In Chapter 8, a prototype three–degrees–of freedom cabin model for a mid-sized commercial truck is considered. The purpose of this study is to analyze ride motions of the cabin under random road excitations and to improve its ride performance by designing a suitable compensator. An active suspension system is designed using the LQG design methodology. The simulation results show that the cabin vibrations can effectively be suppressed. The content of this chapter have been published in [77].

2 SUBSPACE IDENTIFICATION OF DISCRETE-TIME POWER SPECTRA

In this chapter, we study the problem of fitting a linear discrete-time power spectrum to given measured power spectrum samples. A *parametric* or *model-based* approach to this problem uses a non-linear least-squares criterion, which is optimized by an iterative non-linear search in the parameter space. Discussion of parametric as well as *nonparametric* methods, which mostly use time-domain data, can be found in [78–80]. Drawbacks of this approach are convergence problems and difficulty of parameterizing multi-input/multi-output systems. There has been an extensive amount of research to determine the *so-called* canonical models [81–84].

The subspace approach, on the other hand, does not suffer from any of these inconveniences. In subspace identification algorithms, there is no explicit need for parameterization since full state-space models are used and the only parameter is the order of the system. The major advantage of subspace identification algorithms over the classical prediction error methods [85] is the absence of non-linear parametric optimization problems. Subspace identification algorithms are non-iterative and therefore do not suffer from convergence problems. They always produce results, which are often good for practical data.

Given time domain measurements, there are many state-space subspace identification algorithms available [86–89]. Frequency domain subspace identification algorithms have already appeared in the literature [62, 90–92]. They can be described as direct frequency domain formulations of time-domain subspace algorithms. If the excitation of the system is well-designed, then each measurement in the frequency domain compiled from a large number of time domain measurement is of high quality. Moreover, data originating from different experiments can easily be combined in the frequency domain [93]. However,

these algorithms are not directly applicable for the identification of frequency domain power spectra since rational spectrum models are constrained to have *positive real* transfer functions.

In [54], a subspace algorithm which uses spectrum samples obtained at uniformly spaced frequencies was presented. The algorithm in [54] is based on [62]; and it uses biased impulse response coefficients expressed as functions of the system matrices. However, this algorithm generates *strongly consistent* power spectrum estimates. A related work is [94]. In this work, a subspace algorithm for the time domain identification of mixed causal and anti-causal systems was proposed. The frequency domain extension of this algorithm was given in [95].

The objective of this chapter is to remove the restriction on the frequencies. This problem is precisely formulated in Section 2.1. In Section 2.2, we present our subspace-based algorithm to identify multi–input/multi–output systems from power spectrum samples measured at nonuniformly spaced frequencies and show that this algorithm is not only strongly consistent but also recovers finite-dimensional rational spectra given a finite number of noise-free data (depending on the model order). The proposed algorithm is based on the results in [54, 94, 95]. The proofs are given in Appendix A. In Section 2.3, the properties of the new algorithm are studied by means of two examples. In the first example, we simulate a system that has a power spectrum with sharp peaks. In the second example, we illustrate the practical relevance of the problem treated in this chapter by solving a stochastic road modeling problem.

2.1 Problem Formulation

Consider a multi-input/multi-output square linear time invariant discrete time system represented by the state-space equations:

$$\begin{aligned} x(t+1) &= Ax(t) + Bu(t) \\ y(t) &= Cx(t) + Du(t) \end{aligned} \tag{2.1}$$

where $x(t) \in \mathbf{R}^n$ is the state, $u(t) \in \mathbf{R}^m$ and $y(t) \in \mathbf{R}^m$ are, respectively, the input and the output of the system. The transfer function of the system described by (2.1), denoted by $G(z)$ is computed as

$$G(z) = D + C(zI_n - A)^{-1}B. \tag{2.2}$$

We summarize the requirements on $G(z)$ in the following:

Assumption 2.1.1. *The system in Eq. (2.1) is stable and strictly minimum phase: all eigenvalues of A and $A - BD^{-1}C$ lie strictly inside the unit circle. The pairs $\{A, B\}$ and $\{A, C\}$ are controllable and observable, respectively. All eigenvalues of A are nonzero and distinct.*

Thus, the system in Eq. (2.1) is a minimal stochastic system. Note that since the *Jordan canonical form* is not numerically stable, a slight perturbation of A will lead to distinct eigenvalues if A has repeated eigenvalues.

Assuming that $u(t)$ is zero mean unity variance white noise process, the power spectrum associated with Eq. (2.1) denoted by $S(z)$ is defined as

$$S(z)=G(z)G^T(z^{-1}). \tag{2.3}$$

The system in Eq. (2.1) is called the *innovation form*, unity variance, minimum phase spectral factor associated with the power spectrum $S(z)$. From Eq. (2.3) and Assumption 2.1.1, note that

$$S(e^{j\theta}) > 0, \qquad \text{for all } \theta. \tag{2.4}$$

This is the positive realness condition, and it imposes a constraint on the given spectrum samples S_k, *i.e.*, $S_k > 0$ for each k, as well as on the identified power spectrum denoted by $\widehat{S}_N(z)$.

The problem studied in this paper can be stated as follows:

Given: N noisy samples $S_k \in \mathbf{C}^{m\times m}$ of the power spectrum $S(z)$ evaluated at N points on the unit circle:

$$S_k = S(e^{j\theta_k}) + \eta_k, \qquad k = 1, 2, \cdots, N, \tag{2.5}$$

Find: a quadruplet $(\widehat{A}, \widehat{B}, \widehat{C}, \widehat{D})$ such that the estimated power spectrum

$$\widehat{S}_N(z) = \widehat{G}(z)\widehat{G}^T(z^{-1}) \tag{2.6}$$

is strongly consistent, *i.e.,*

$$\lim_{N\to\infty} \|\widehat{S}_N - S\|_\infty = 0, \qquad \text{w.p.1.} \tag{2.7}$$

where

$$\widehat{G}(z) \triangleq \widehat{C}(zI_n - \widehat{A})^{-1}\widehat{B} + \widehat{D}. \tag{2.8}$$

We also require the algorithm to produce the true model if the noise is zero given a finite amount of data N, *i.e.,* there exists an $N_0 < \infty$ such that

$$\|\widehat{S}_N - S\|_\infty = 0, \qquad \text{for all } N \geq N_0. \tag{2.9}$$

We will assume that the noise η corrupting the spectrum samples is a zero mean complex white noise process with a covariance function satisfying

$$\mathrm{E}\begin{bmatrix} \operatorname{Re}\eta_k \\ \operatorname{Im}\eta_k \end{bmatrix} [\operatorname{Re}\eta_s^T \;\; \operatorname{Im}\eta_s^T] = \begin{bmatrix} \frac{1}{2}\mathcal{R}_k & 0 \\ 0 & \frac{1}{2}\mathcal{R}_k \end{bmatrix} \delta_{ks}. \tag{2.10}$$

Furthermore, we assume that the fourth order moments are bounded above by some $M_\eta < \infty$ as

$$\mathrm{E}\,\|\eta_k\|_F^4 \leq M_\eta, \qquad \text{for all } k. \tag{2.11}$$

We will assume that the frequencies satisfy

$$\lim_{N\to\infty} \inf \frac{1}{N}\,\mathcal{C}(\{\theta_k\}_{k=1}^N \cap [a,b]) \geq \delta(b-a) \tag{2.12}$$

for every $[a,b] \subseteq [0, 2\pi]$ and some fixed $\delta > 0$. This means that every point on the unit circle has a nonzero asymptotic density of frequencies relative to N.

An identification algorithm which satisfies Eq. (2.9) is called *correct algorithm.* In this chapter, we present an algorithm which have these properties. Strong consistency is a most natural requirement for any useful algorithm. As the amount of data increases, asymptotically the correct model should be obtained. In practice, any algorithm has to use a finite amount of data. Then,

correctness of an algorithm becomes important. This is particularly important for spectra with sharp peaks.

The above identification problem can be thought as the design of a linear shaping filter (A, B, C, D) from (corrupted) power spectrum measurements. In this procedure, the zeros of $G(z)$ can be restricted, without loss of generality, to be minimum phase.

2.2 Identification Algorithm

Let us first consider the noise-free case to motivate the derivation of the identification algorithm. We begin by splitting $S(z)$ into the *so-called* spectral summands as follows.

Theorem 2.2.1. *Consider the power spectrum $S(z)$ in Eq. (2.3). Suppose that Assumption 2.1.1 holds. Let P be the solution of the discrete-time Lyapunov equation:*

$$P = APA^T + BB^T. \tag{2.13}$$

Let

$$E{=}CPC^T + DD^T, \tag{2.14}$$

$$F{=}APC^T + BD^T, \tag{2.15}$$

Then $S(z)$ can be split into the sum of two system transfer matrices as follows

$$S(z) = H(z) + H^T(z^{-1}) \tag{2.16}$$

with

$$H(z){=}\frac{1}{2}E + C(zI_n - A)^{-1}F. \tag{2.17}$$

Proof. See, for example, Caines [96].

This splitting of $S(z)$ into the sum of a causal transfer function $H(z)$ and an anti-causal transfer function $H^T(z^{-1})$ is the first step of our subspace-based identification algorithm. It is also the starting point of the subspace algorithm in [54]. As in [54], from the samples S_k we identify a quadruplet

$(A, F, C, \frac{1}{2}E)$ which describes the spectral summand $H(z)$. The algorithm proposed in [54] uses biased Markov parameters of $S(z)$ as in [62]; and requires the discrete frequencies θ_k, $k = 1, 2, \cdots, N$ be uniformly spaced in the interval $[0, \pi]$. The contribution of this chapter is to remove this restriction on the frequencies.

Next, from Eq (2.16) and Eq (2.17) we write a state-representation of $S(z)$ as follows:

$$\begin{aligned} x^{\mathrm{c}}(t+1) &= Ax^{\mathrm{c}}(t) + Fu(t) && (2.18)\\ x^{\mathrm{ac}}(t-1) &= A^T x^{\mathrm{ac}}(t) + C^T u(t) && (2.19)\\ y^{\mathrm{s}}(t) &= Cx^{\mathrm{c}}(t) + F^T x^{\mathrm{ac}}(t) + Eu(t). && (2.20) \end{aligned}$$

These equations are the special cases of the equations considered in [94] for the time-domain subspace identification of mixed causal and anti-causal linear-time invariant systems.

Following [95], we take the discrete Fourier transforms of Eqs (2.18)–(2.20) where we shift Eq (2.19) by $p-1$ samples forward in time:

$$\begin{aligned} e^{j\theta} X^{\mathrm{c}}(\theta) &= AX^{\mathrm{c}}(\theta) + FU(\theta)\\ e^{-j\theta} X^{\mathrm{ac,p}}(\theta) &= A^T X^{\mathrm{ac,p}}(\theta) + C^T e^{j(p-1)\theta} U(\theta)\\ Y^{\mathrm{s}}(\theta) &= CX^{\mathrm{c}}(\theta) + F^T e^{-j(p-1)\theta} X^{\mathrm{ac,p}}(\theta)\\ &\quad + EU(\theta) \end{aligned}$$

where $X^{\mathrm{c}}(\theta)$, $X^{\mathrm{ac,p}}(\theta)$, $U(\theta)$, and $Y^{\mathrm{s}}(\theta)$ denote the discrete Fourier transforms of $x^{\mathrm{c}}(t)$, $x^{\mathrm{ac}}(t+p-1)$, $u(t)$, and $y(t)$, respectively, and $p > 2n$. Let $X_i^{\mathrm{c}}(\theta)$ be the resulting state transform when $U(\theta) = e_i$, the unit vector with 1 on the i^{th} position; and $X_i^{\mathrm{ac,p}}(\theta)$ is defined similarly. By defining the compound state matrices:

$$\begin{aligned} X_{\mathrm{C}}^{\mathrm{c}}(\theta) &= \left[X_1^{\mathrm{c}}(\theta) \;\; X_2^{\mathrm{c}}(\theta) \;\; \cdots \;\; X_m^{\mathrm{c}}(\theta)\right],\\ X_{\mathrm{C}}^{\mathrm{ac,p}}(\theta) &= \left[X_1^{\mathrm{ac,p}}(\theta) \;\; X_2^{\mathrm{ac,p}}(\theta) \;\; \cdots \;\; X_m^{\mathrm{ac,p}}(\theta)\right], \end{aligned} \qquad (2.21)$$

$S(e^{j\theta})$ can be implicitly described as

$$S(e^{j\theta}) = CX_{\mathrm{C}}^{\mathrm{c}}(\theta) + F^T e^{-j(p-1)\theta} X_{\mathrm{C}}^{\mathrm{ac,p}}(\theta) + E$$

with

$$\begin{aligned} e^{j\theta} X_{\mathrm{C}}^{\mathrm{c}}(\theta) &= A X_{\mathrm{C}}^{\mathrm{c}}(\theta) + F, \\ e^{-j\theta} X_{\mathrm{C}}^{\mathrm{ac,p}}(\theta) &= A^T X_{\mathrm{C}}^{\mathrm{ac,p}}(\theta) + C^T e^{j(p-1)\theta}. \end{aligned} \tag{2.22}$$

By iteratively substituting the state-equations, we obtain the relation

$$\begin{aligned} \begin{bmatrix} S(e^{j\theta}) \\ e^{j\theta} S(e^{j\theta}) \\ \vdots \\ e^{j(p-2)\theta} S(e^{j\theta}) \\ e^{j(p-1)\theta} S(e^{j\theta}) \end{bmatrix} &= \Gamma_p \begin{bmatrix} I_m \\ e^{j\theta} I_m \\ \vdots \\ e^{j(p-2)\theta} I_m \\ e^{j(p-1)\theta} I_m \end{bmatrix} \\ &\quad + \mathcal{O}_p \begin{bmatrix} X_{\mathrm{C}}^{\mathrm{c}}(\theta) \\ X_{\mathrm{C}}^{\mathrm{ac,p}}(\theta) \end{bmatrix} \end{aligned} \tag{2.23}$$

where

$$\mathcal{O}_p = \begin{bmatrix} C & F^T (A^T)^{p-1} \\ CA & F^T (A^T)^{p-2} \\ \vdots & \vdots \\ CA^{p-2} & F^T A^T \\ CA^{p-1} & F^T \end{bmatrix} \tag{2.24}$$

and

$$\Gamma_p = \begin{bmatrix} E & F^T C^T & \cdots & F^T (A^T)^{p-2} C^T \\ CF & E & \cdots & \vdots \\ \vdots & \vdots & \ddots & F^T C^T \\ CA^{p-2} F & \cdots & CF & E \end{bmatrix} \tag{2.25}$$

By repeating Eq (2.23) for θ_k, $k = 1, 2, \cdots, N$, we get

$$\mathcal{S}_{\mathrm{C}} = \mathcal{O}_p \mathcal{X}_{\mathrm{C}} + \Gamma_p \mathcal{W}_{\mathrm{C}} \tag{2.26}$$

where $z_k = e^{j\theta_k}$, $k = 1, 2, \cdots, N$ and

$$\mathcal{S}_{\rm C} = \frac{1}{\sqrt{N}} \begin{bmatrix} S(z_1) & \cdots & S(z_N) \\ z_1 S(z_1) & \cdots & z_N S(z_N) \\ \vdots & \ddots & \vdots \\ z_1^{p-1} S(z_1) & \cdots & z_N^{p-1} S(z_N) \end{bmatrix}, \tag{2.27}$$

$$\mathcal{W}_{\rm C} = \frac{1}{\sqrt{N}} \begin{bmatrix} 1 & \cdots & 1 \\ z_1 & \cdots & z_N \\ \vdots & \ddots & \vdots \\ z_1^{p-1} & \cdots & z_N^{p-1} \end{bmatrix} \otimes I_m, \tag{2.28}$$

$$\mathcal{X}_{\rm C} = \frac{1}{\sqrt{N}} \begin{bmatrix} X_{\rm C}^{\rm c}(\theta_1) & \cdots & X_{\rm C}^{\rm c}(\theta_N) \\ X_{\rm C}^{\rm ac,p}(\theta_1) & \cdots & X_{\rm C}^{\rm ac,p}(\theta_N) \end{bmatrix}. \tag{2.29}$$

Now, we consider the noisy data case. From Eqs (2.5), (2.26), and (2.27), we get

$$\widehat{\mathcal{S}}_{\rm C} = \mathcal{O}_p \mathcal{X}_{\rm C} + \Gamma_p \mathcal{W}_{\rm C} + \mathcal{N}_{\rm C} \tag{2.30}$$

where

$$\widehat{\mathcal{S}}_{\rm C} = \frac{1}{\sqrt{N}} \begin{bmatrix} S_1 & \cdots & S_N \\ z_1 S_1 & \cdots & z_N S_N \\ \vdots & \vdots & \ddots & \vdots \\ z_1^{p-1} S_1 & \cdots & z_N^{p-1} S_N \end{bmatrix}, \tag{2.31}$$

$$\mathcal{N}_{\rm C} = \frac{1}{\sqrt{N}} \begin{bmatrix} \eta_1 & \cdots & \eta_N \\ z_1 \eta_1 & \cdots & z_N \eta_N \\ \vdots & \ddots & \vdots \\ z_1^{p-1} \eta_1 & \cdots & z_N^{p-1} \eta_N \end{bmatrix}. \tag{2.32}$$

Since $\mathcal{O}_p$ is a real matrix and we are interested in the real range space, we convert (2.26) into a relation involving only real valued matrices:

$$\begin{aligned} \widehat{\mathcal{S}} &= \mathcal{O}_p \mathcal{X} + \Gamma_p \mathcal{W} + \mathcal{N} \\ &= \mathcal{S} + \mathcal{N} \end{aligned} \tag{2.33}$$

where

$$\widehat{\mathcal{S}} = \left[\mathrm{Re}\,\widehat{\mathcal{S}}_C \;\; \mathrm{Im}\,\widehat{\mathcal{S}}_C\right], \tag{2.34}$$

$$\mathcal{S} = \left[\mathrm{Re}\,\mathcal{S}_C \;\; \mathrm{Im}\,\mathcal{S}_C\right], \tag{2.35}$$

$$\mathcal{X} = \left[\mathrm{Re}\,\mathcal{X}_C \;\; \mathrm{Im}\,\mathcal{X}_C\right], \tag{2.36}$$

$$\mathcal{W} = \left[\mathrm{Re}\,\mathcal{W}_C \;\; \mathrm{Im}\,\mathcal{W}_C\right] \tag{2.37}$$

$$\mathcal{N} = \left[\mathrm{Re}\,\mathcal{N}_C \;\; \mathrm{Im}\,\mathcal{N}_C\right]. \tag{2.38}$$

Let $\mathcal{W}^{\perp}$ be the projection matrix onto the null space of $\mathcal{W}$ given by

$$\mathcal{W}^{\perp}=I_{2mN} - \mathcal{W}^H(\mathcal{W}\mathcal{W}^H)^{-1}\mathcal{W}. \tag{2.39}$$

The term $\Gamma_p\mathcal{W}$ in Eq (2.33) is cancelled when multiplied from right by $\mathcal{W}^{\perp}$. Thus,

$$\begin{aligned}\widehat{\mathcal{S}}\mathcal{W}^{\perp} &= \mathcal{O}_p\mathcal{X}\mathcal{W}^{\perp} + \mathcal{N}\mathcal{W}^{\perp} \\ &= \mathcal{S}\mathcal{W}^{\perp} + \mathcal{N}\mathcal{W}^{\perp}.\end{aligned} \tag{2.40}$$

The range space of $\mathcal{S}\mathcal{W}^{\perp}$ equals the range space of $\mathcal{O}_p$ unless rank cancellations occur. A sufficient condition for the range spaces to be equal is that the intersection between the row spaces of $\mathcal{W}$ and $\mathcal{X}$ is empty. In the following, we present sufficient conditions in terms of the data and the system.

Lemma 2.2.1. *Let $N \geq (p/2) + n + 1$, $\mathcal{W}_{\mathrm{C}}$, and $\mathcal{X}_{\mathrm{C}}$ be given by (2.28) and (2.29) with distinct frequencies θ_k such that z_k is not an eigenvalue of A. Then*

$$\mathrm{rank}\begin{bmatrix}\mathcal{W}\\ \mathcal{X}\end{bmatrix} = pm + 2n \Longleftrightarrow (A, B, C, D) \text{ minimal.} \tag{2.41}$$

Proof. See Appendix A.1. □

If the frequencies are distinct, the number of data satisfies $N \geq (p/2)+ n + 1$, and (A, B, C, D) is minimal, then the two row spaces of $\mathcal{W}$ and $\mathcal{X}$ do not intersect and the range space of $\mathcal{S}\mathcal{W}^{\perp}$ coincides with the range space of $\mathcal{O}_p$. Now, a study of the relation between the column range spaces of $\mathcal{S}\mathcal{W}^{\perp}$ and $\widehat{\mathcal{S}}\mathcal{W}^{\perp}$ for large N is in order.

In [97], it was shown that by using the singular value decomposition of $\widehat{\mathcal{S}}\mathcal{W}^{\perp}$, the $2n$ left singular vectors corresponding to the $2n$ largest singular values form a strongly consistent estimate of the range space of $\mathcal{S}\mathcal{W}^{\perp}$ if the following conditions hold w.p.1

$$\text{(i)} \qquad \lim_{N\to\infty} \mathcal{S}\mathcal{W}^{\perp}(\mathcal{N}\mathcal{W}^{\perp})^T = 0; \tag{2.42}$$

$$\text{(ii)} \qquad \lim_{N\to\infty} \mathcal{N}\mathcal{W}^{\perp}(\mathcal{N}\mathcal{W}^{\perp})^T = \alpha I_{pm} \tag{2.43}$$

for some scalar $\alpha \geq 0$. In [62], it was shown under the assumption in Eq (2.11) that Eq (2.42) holds and

$$\lim_{N\to\infty} \mathcal{N}\mathcal{W}^{\perp}(\mathcal{N}\mathcal{W}^{\perp})^T = \mathcal{K}\mathcal{K}^T, \qquad \text{w.p.1.} \tag{2.44}$$

where $\mathcal{K} \in \mathbf{R}^{pm\times pm}$ is a matrix defined by

$$\begin{aligned} \mathcal{K}\mathcal{K}^T &= \mathrm{Re}\left(\mathcal{W}_{\mathrm{C}}\mathcal{R}\mathcal{W}_{\mathrm{C}}^H\right); \\ \mathcal{R} &= \begin{bmatrix} \mathcal{R}_1 & 0 & \cdots & 0 \\ 0 & \mathcal{R}_2 & \cdots & 0 \\ \vdots & \vdots & \ddots & \vdots \\ 0 & 0 & \cdots & \mathcal{R}_N \end{bmatrix}. \end{aligned} \tag{2.45}$$

The matrix $\mathcal{K}$ can be found by a Cholesky decomposition. Thus, from Eq (2.40) we have the weighted version

$$\mathcal{K}^{-1}\widehat{\mathcal{S}}\mathcal{W}^{\perp} = \mathcal{K}^{-1}\mathcal{S}\mathcal{W}^{\perp} + \mathcal{K}^{-1}\mathcal{N}\mathcal{W}^{\perp} \tag{2.46}$$

satisfying Eq (2.42) and (2.43) with $\alpha = 1$. Hence, the $2n$ left singular vectors corresponding to the $2n$ largest singular values of $\mathcal{K}^{-1}\widehat{\mathcal{S}}\mathcal{W}^{\perp}$ will form a strongly consistent estimate of the range space of $\mathcal{K}^{-1}\mathcal{S}\mathcal{W}^{\perp}$ which equals to the range space of $\mathcal{K}^{-1}\mathcal{O}_p$.

A numerically efficient way of forming $\widehat{\mathcal{S}}\mathcal{W}^{\perp}$ is to use the QR-factorization:

$$\begin{bmatrix} \mathcal{W} \\ \widehat{\mathcal{S}} \end{bmatrix} = \begin{bmatrix} R_{11} & 0 \\ R_{21} & R_{22} \end{bmatrix} \begin{bmatrix} Q_1^T \\ Q_2^T \end{bmatrix}. \tag{2.47}$$

A simple derivation yields

$$\widehat{\mathcal{S}}\mathcal{W}^{\perp} = R_{22}Q_2^T \tag{2.48}$$

and it suffices to use R_{22} since Q_2^T is a matrix of full rank. Thus, the $2n$ left singular vectors corresponding to the $2n$ largest singular values of $\mathcal{K}^{-1}\widehat{\mathcal{S}}\mathcal{W}^{\perp}$ are obtained from the singular value decomposition:

$$\mathcal{K}^{-1}R_{22} = \begin{bmatrix} \widehat{U}_{2n} & \widetilde{U} \end{bmatrix} \begin{bmatrix} \widehat{\Sigma}_{2n} & 0 \\ 0 & \widetilde{\Sigma} \end{bmatrix} \begin{bmatrix} \widehat{V}_{2n} \\ \widetilde{V} \end{bmatrix} \tag{2.49}$$

where this decomposition is partitioned such that $\widehat{\Sigma}_{2n}$ contains the $2n$ largest singular values.

Our consistency analysis has shown that

$$\lim_{N\to\infty} \mathcal{K}\widehat{U}_{2n} = \mathcal{O}_p T, \qquad \text{w.p.1} \tag{2.50}$$

for some nonsingular matrix T. In the calculation of $\widehat{U}_{2n}$, $2n$ elements with fixed indices can be chosen freely subject to the constraint that magnitudes are not greater than unity. Thus, by fixing values of those elements for all N, we see from Eq (2.50) that $\widehat{U}_{2n}$ converges to a matrix denoted by U_{2n} w.p.1 as $N \to \infty$. Hence,

$$\mathcal{K}U_{2n} = \mathcal{O}_p T. \tag{2.51}$$

This asymptotic formula (in the number of data) will be the key in the development of our algorithm. Before undertaking this study, let us record the following result which will be used later.

Lemma 2.2.2. *Let S_k, $k = 1, \cdots, N$ be noise-free samples of the power spectrum of a discrete-time system of order n satisfying Assumption 2.1.1 at N distinct frequencies θ_k. Furthermore, let $N \geq (p/2) + n + 1$ and $\mathcal{K} \in \mathbf{R}^{pm\times pm}$ be any nonsingular matrix. Then, for some nonsingular T*

$$\mathcal{K}\widehat{U}_{2n} = \mathcal{O}_p T. \tag{2.52}$$

Thus, the equations derived from the asymptotic formula are also valid for a finite number of data under the conditions stated in Lemma 2.2.2.

Let J_{u} and J_{d} be the upward and downward shift matrices defined by

$$J_{\mathrm{u}} = \begin{bmatrix} 0_{(p-1)\times m} & I_{(p-1)m} \end{bmatrix}, \tag{2.53}$$

$$J_{\mathrm{d}} = \begin{bmatrix} I_{(p-1)m} & 0_{(p-1)\times m} \end{bmatrix}. \tag{2.54}$$

Then,

$$J_{\rm u}\mathcal{O}_p = J_{\rm d}\mathcal{O}_p A' \tag{2.55}$$

where

$$A'=\begin{bmatrix} A & 0 \\ 0 & (A^T)^{-1} \end{bmatrix}. \tag{2.56}$$

Hence,

$$A' = (J_{\rm d}\mathcal{O}_p)^\dagger J_{\rm u}\mathcal{O}_p = TA''T^{-1} \tag{2.57}$$

and

$$A''=(J_{\rm d}\mathcal{K}U_{2n})^\dagger J_{\rm u}\mathcal{K}U_{2n}. \tag{2.58}$$

From Eq (2.57), we see that A' and A'' are similar matrices. This means that they have the same Jordan blocks in their Jordan canonical representations. Likewise, we have from Eqs (2.24) and (2.51),

$$C'=[C \;\; F^T(A^T)^{p-1}] = J_{\rm f}\mathcal{O}_p = C''T^{-1} \tag{2.59}$$

where

$$J_{\rm f} = [I_m \;\; 0_{m\times(p-1)}], \tag{2.60}$$

$$C'' = J_{\rm f}\mathcal{K}U_{2n}. \tag{2.61}$$

Let us put A'' into the following Jordan canonical form:

$$A'' = [\Pi_{\rm c} \;\; \Pi_{\rm ac}] \begin{bmatrix} \Sigma_{\rm c} & 0 \\ 0 & \Sigma_{\rm ac} \end{bmatrix} [\Pi_{\rm c} \;\; \Pi_{\rm ac}]^{-1} \tag{2.62}$$

where the eigenvalues of $\Sigma_{\rm c}$ lie inside the unit circle. Since $H(z)$ is invariant to similarity transformations, we may let

$$A=\Sigma_{\rm c} \tag{2.63}$$

in Eq (2.1). The canonical form (2.62) is invariant to ordering of eigenvalues as long as the eigenvalues and the corresponding eigenvectors of $\Sigma_{\rm c}$ are permuted accordingly, in complex pairs. Moreover, from the similarity of A'' to A', in Eq (2.1) we may let

$$\Sigma_{\rm ac} = (\Sigma_{\rm c}^T)^{-1}. \tag{2.64}$$

This, of course, imposes a certain structure on T. Let

$$\Pi = [\Pi_{\rm c} \;\; \Pi_{\rm ac}]\,. \tag{2.65}$$

Then, Eq (2.62) can be written as

$$A' = \Pi^{-1} A'' \Pi \tag{2.66}$$

Hence from Eqs (2.57) and (2.66),

$$A' = T A'' T^{-1} = \Pi^{-1} A'' \Pi. \tag{2.67}$$

The relations among Σ, Π, and T are captured in the following lemma. Recall that A has distinct eigenvalues.

Lemma 2.2.3. *Let A'' be as in (2.58). Consider the Jordan canonical form of A'' given by Eq (2.62) where A and $\Sigma_{\rm ac}$ satisfy Eqs (2.63) and (2.64). Then, $\Sigma_{\rm c}$ is a block diagonal matrix*

$$\Sigma_{\rm c} = \begin{bmatrix} \Sigma_1 & 0 & \cdots & 0 \\ 0 & \Sigma_2 & \cdots & 0 \\ \vdots & \vdots & \ddots & \vdots \\ 0 & 0 & \cdots & \Sigma_k \end{bmatrix}, \qquad \Sigma_i \in \mathbf{R}^{n_i \times n_i} \tag{2.68}$$

where $n_i \in \{1, 2\}$, $\nu_i \neq 0$, and

$$\Sigma_i = \begin{cases} \mu_i, & \text{if } \; n_i = 1 \\ \begin{bmatrix} \mu_i & \nu_i \\ -\nu_i & \mu_i \end{bmatrix}, & \text{if } \; n_i = 2. \end{cases} \tag{2.69}$$

Also, $\Sigma_{\rm ac}$ is a block diagonal matrix with block types and sizes compatible with $\Sigma_{\rm c}$. For some $\Lambda_{\rm c}$ and $\Lambda_{\rm ac}$ compatible with $\Sigma_{\rm c}$, the following holds

$$\Pi = T^{-1} \Lambda \tag{2.70}$$

where

$$\Lambda = \begin{bmatrix} \Lambda_{\rm c} & 0 \\ 0 & \Lambda_{\rm ac} \end{bmatrix}. \tag{2.71}$$

Let X and Y be two block diagonal matrices with block sizes and types compatible with $\Sigma_{\rm c}$, then X^T, XY and X^{-1} are also compatible with $\Sigma_{\rm c}$ and $XY = YX$.

Proof. See Appendix A.2. □

Now, multiplying Eq (2.51) from right by Π, we get

$$\mathcal{K}U_{2n}\Pi = \mathcal{O}_p\Lambda. \tag{2.72}$$

Hence, from Eqs (2.24), (2.65), and (2.71)

$$\begin{aligned}
\mathcal{K}U_{2n}\Pi_{\mathrm{c}} &= \begin{bmatrix} C\Lambda_{\mathrm{c}} \\ C\Sigma_{\mathrm{c}}\Lambda_{\mathrm{c}} \\ \vdots \\ C\Sigma_{\mathrm{c}}^{p-2}\Lambda_{\mathrm{c}} \\ C\Sigma_{\mathrm{c}}^{p-1}\Lambda_{\mathrm{c}} \end{bmatrix}, \\
\mathcal{K}U_{2n}\Pi_{\mathrm{ac}} &= \begin{bmatrix} F^T(\Sigma_{\mathrm{c}}^T)^{p-1}\Lambda_{\mathrm{ac}} \\ F^T(\Sigma_{\mathrm{c}}^T)^{p-2}\Lambda_{\mathrm{ac}} \\ \vdots \\ F^T\Sigma_{\mathrm{c}}^T\Lambda_{\mathrm{ac}} \\ F^T\Lambda_{\mathrm{ac}} \end{bmatrix}.
\end{aligned}$$

Thus,

$$C\Lambda_{\mathrm{c}} = J_{\mathrm{f}}\mathcal{K}U_{2n}\Pi_{\mathrm{c}}, \qquad F^T\Lambda_{\mathrm{ac}} = J_{\mathrm{l}}\mathcal{K}U_{2n}\Pi_{\mathrm{ac}} \tag{2.73}$$

where

$$J_{\mathrm{l}}=[0_{m\times(p-1)} \;\; I_m]. \tag{2.74}$$

The problem of finding the state-space matrices C, F, and E is now reduced to estimating E, Λ_{c}, and Λ_{ac} from the spectral data in Eq. (2.5).

From Lemma 2.2.3, $S(z)$ in Eq. (2.16) can be written as

$$\begin{aligned}
S(z) &= E + C\Lambda_{\mathrm{c}}(z\Lambda_{\mathrm{ac}}^T\Lambda_{\mathrm{c}} - \Lambda_{\mathrm{ac}}^T\Sigma_{\mathrm{c}}\Lambda_{\mathrm{c}})^{-1}\Lambda_{\mathrm{ac}}^T F \\
&\quad + F^T\Lambda_{\mathrm{ac}}(z^{-1}\Lambda_{\mathrm{c}}^T\Lambda_{\mathrm{ac}} - \Lambda_{\mathrm{c}}^T\Sigma_{\mathrm{c}}^T\Lambda_{\mathrm{ac}})^{-1}\Lambda_{\mathrm{c}}^T C^T \\
&= E + C\Lambda_{\mathrm{c}}(zI_n - \Sigma_{\mathrm{c}})^{-1}\Lambda_{\mathrm{c}}^{-1}F \\
&\quad + F^T(\Lambda_{\mathrm{c}}^T)^{-1}(z^{-1}I_n - \Sigma_{\mathrm{c}}^T)^{-1}\Lambda_{\mathrm{c}}^T C^T \\
&= E + \chi(z)\, Z + Z^T\, \chi^T(z^{-1})
\end{aligned} \tag{2.75}$$

where

$$\chi(z) = J_{\mathrm{f}}\mathcal{K}U_{2n}\Pi_{\mathrm{c}}\,(zI_n - \Sigma_{\mathrm{c}})^{-1}, \tag{2.76}$$

$$Z = \Lambda_{\mathrm{c}}^{-1}F. \tag{2.77}$$

Thus, E and Z can be estimated from the data in Eq (2.5) by solving the following linear least-squares problem:

$$E^\sharp, Z^\sharp = \arg\min_{\check{E},\check{Z}} \sum_{k=1}^{N} \|\mathcal{R}_k^{-\frac{1}{2}}(\chi(z_k)\,\check{Z} + \check{Z}^T\,\chi^T(z_k^{-1}) + \check{E} - S(z_k))\|_{\mathrm{F}}^2 \tag{2.78}$$

The formula (2.78) is non-asymptotic in N though asymptotic quantities are used in it. However, it suggests a scheme to consistently estimate the state-space parameters A, C, E, and F.

Recall that when the spectrum samples are noise-free, we can replace U_{2n} with $\widehat{U}_{2n}$ in the above formulae. Thus, we have the following result.

Lemma 2.2.4. *Let $S(z)$ be the power spectrum of a discrete-time system of order n satistying Assumption 2.1.1. Let $\chi(z)$ and Z be as in Eqs. (2.76) and (2.77), respectively. Consider the linear least-squares problem (2.78). If $N \geq (p/2) + n + 1$, then*

$$E^\sharp = E, \qquad Z^\sharp = Z. \tag{2.79}$$

Proof. The proof of this lemma is contained in the proof of Theorem 2.2.3. □

Once we find Z, we calculate C and F from the first equation in (2.73) and (2.77) as

$$C = J_{\mathrm{f}}\mathcal{K}U_{2n}\Pi_{\mathrm{c}}, \qquad F = Z \tag{2.80}$$

which is due to the fact that $H(z)$ defined by Eq (2.17) is invariant to post-multiplication of C by Λ_{c} and pre-multiplication of F by $\Lambda_{\mathrm{c}}^{-1}$ since from Lemma 2.2.3, we have $\Lambda_{\mathrm{c}}^{-1}(zI_n - \Sigma_{\mathrm{c}})^{-1}\Lambda_{\mathrm{c}} = (zI_n - \Sigma_{\mathrm{c}})^{-1}$.

We are left with the determination of the system matrices B and D. To this end, we first solve the following *Riccati* equation for P:

$$P = APA^T + (F - APC^T)(E - CPC^T)^{-1}(F - APC^T)^T. \tag{2.81}$$

Then, we compute B and D as follows

$$B = (F - APC^T)(E - CPC^T)^{-\frac{1}{2}}; \tag{2.82}$$

$$D = (E - CPC^T)^{\frac{1}{2}}. \tag{2.83}$$

Now, we return to the normal case to outline the proposed algorithm. Let

$$\widetilde{A}=(J_{\rm d}\mathcal{K}\widehat{U}_{2n})^{\dagger}J_{\rm u}\mathcal{K}\widehat{U}_{2n} \tag{2.84}$$

and put $\widetilde{A}$ into the Jordan canonical form:

$$\widetilde{A}=\left[\widehat{\Pi}_{\rm c}\ \ \widehat{\Pi}_{\rm ac}\right]\left[\begin{array}{cc}\widehat{\Sigma}_{\rm c} & 0\\ 0 & \widehat{\Sigma}_{\rm ac}\end{array}\right]\left[\widehat{\Pi}_{\rm c}\ \ \widehat{\Pi}_{\rm ac}\right]^{-1} \tag{2.85}$$

where the eigenvalues of $\widehat{\Sigma}_{\rm c}$ lie inside the unit circle. Let

$$\widehat{A} = \widehat{\Sigma}_{\rm c}, \tag{2.86}$$

$$\widehat{C} = J_{\rm f}\mathcal{K}\widehat{U}_{2n}\widehat{\Pi}_{\rm c}. \tag{2.87}$$

From Eqs.(2.50) and (2.58), we have

$$\lim_{N\to\infty}\widetilde{A} = A'', \qquad \text{w.p.1.} \tag{2.88}$$

As in the calculation of $\widehat{U}_{2n}$, we can freely choose $2n$ elements of $\widehat{\Pi}_{\rm c}$ and $\widehat{\Pi}_{\rm ac}$ with fixed indices subject to the constraint that magnitudes are not greater than unity. Then, by fixing values of those elements equal to the values of the corresponding elements in $\Pi_{\rm c}$ and $\Pi_{\rm ac}$ for all N, we see from Eqs. (2.88) and (2.85) that

$$\begin{aligned}&\lim_{N\to\infty}\widehat{\Sigma}_{\rm c} = \Sigma_{\rm c} \quad \text{and} \quad \lim_{N\to\infty}\widehat{\Sigma}_{\rm ac} = \Sigma_{\rm ac}, \qquad \text{w.p.1;}\\ &\lim_{N\to\infty}\widehat{\Pi}_{\rm c} = \Pi_{\rm c} \quad \text{and} \quad \lim_{N\to\infty}\widehat{\Pi}_{\rm ac} = \Pi_{\rm ac}, \qquad \text{w.p.1.}\end{aligned} \tag{2.89}$$

Let

$$\widehat{\chi}(z)=\widehat{C}(zI_n - \widehat{\Sigma}_{\rm c})^{-1}. \tag{2.90}$$

Then, from Eq. (2.89) and the fact that $\widehat{U}_{2n} \to U_{2n}$ w.p.1 as $N \to \infty$ we have

$$\lim_{N\to\infty}\|\widehat{\chi} - \chi\|_{\infty}, \qquad \text{w.p.1.} \tag{2.91}$$

The uniform convergence is due to the fact that the spectral radius of the limit matrix Σ_{c} is less than one.

The estimates of E and F are obtained by solving the following linear least-squares problem:

$$\begin{aligned} \widehat{E}, \widehat{F} \;\; = \;\; & \arg\min_{\check{E},\check{F}} \sum_{k=1}^{N} \| \mathcal{R}_k^{-1/2} (\widehat{\chi}(z_k)\, \check{F} + \check{F}^T\, \widehat{\chi}^T(z_k^{-1}) \\ & + \check{E} - S_k) \|_F^2 \end{aligned} \tag{2.92}$$

Before concluding the consistency analysis, let us summarize the final algorithm in the following.

Algorithm 2.2.1. *Subspace algorithm with nonuniformly spaced spectrum samples:*

1. *Given the data S_k, θ_k, and the covariance data $\mathcal{R}_k$, form the matrices $\mathcal{S}$, $\mathcal{W}_{\mathrm{C}}$, $\mathcal{W}$, and $\mathcal{K}$ defined by Eqs. (2.34), (2.28), (2.37), and (2.45).*
2. *Calculate the QR-factorization in Eq. (2.47).*
3. *Calculate the SVD in Eq. (2.49).*
4. *Determine the system order n by inspecting the singular values and partition the SVD such that $\widehat{\Sigma}_{2n}$ contains the $2n$ largest singular values.*
5. *With J_{u}, J_{d}, and $\widehat{U}_{2n}$ defined by Eqs. (2.53), (2.54), and (2.49), calculate $\widetilde{A}$ from (2.84).*
6. *Block-diagonalize $\widetilde{A}$ as in Eq. (2.85) and let $\widehat{\Pi}_{\mathrm{c}}$ and $\widehat{A}$ be as in Eqs. (2.85) and (2.86).*
7. *With J_{f} defined by Eq. (2.60), let $\widehat{C}$ be as in Eq. (2.87).*
8. *Solve the least-squares problem in Eq. (2.92) for $\widehat{E}$ and $\widehat{F}$ where $\widehat{\chi}$ is defined by Eq. (2.90).*

9. *Solve the Riccati equation for* $\widehat{P}$*:*

$$\widehat{P} = \widehat{A}\widehat{P}\widehat{A}^T + (\widehat{F} - \widehat{A}\widehat{P}\widehat{C}^T)(\widehat{E} - \widehat{C}\widehat{P}\widehat{C}^T)^{-1} \cdot (\widehat{F} - \widehat{A}\widehat{P}\widehat{C}^T)^T \quad (2.93)$$

and calculate $\widehat{B}$ *and* $\widehat{D}$ *from*

$$\widehat{B} = (\widehat{F} - \widehat{A}\widehat{P}\widehat{C}^T)(\widehat{E} - \widehat{C}\widehat{P}\widehat{C}^T)^{-\frac{1}{2}}; \quad (2.94)$$

$$\widehat{D} = (\widehat{E} - \widehat{C}\widehat{P}\widehat{C}^T)^{\frac{1}{2}}. \quad (2.95)$$

10. *Calculate* $\widehat{G}(z)$ *and* $\widehat{S}_N(z)$ *from Eqs. (2.8) and (2.6).*

Combination of Lemma 2.2.2 and Lemma 2.2.4 yields our first result captured in the following.

Theorem 2.2.2. *Consider Algorithm 2.2.1 with N noise-free samples of the power spectrum of a discrete-time system of order n satisfying Assumption 2.1.1 at N distinct frequencies* θ_k*. Let* $\mathcal{K} \in \mathbf{R}^{pm \times pm}$ *be any nonsingular matrix. If* $N \geq (p/2) + n + 1$*, then Algorithm 2.2.1 is correct.*

Now, we finish the consistency analysis of Algorithm 2.2.1.

Theorem 2.2.3. *Consider Algorithm 2.2.1 with corrupted measurements of the power spectrum of a discrete-time system of order n satisfying Assumption 2.1.1 where the corruptions and the frequencies satisfy the assumptions in Eqs. (2.10), (2.11), and (2.12). Then, Algorithm 2.2.1 is strongly consistent.*

Proof. See Appendix A.3. □

The algorithm described in [54] is a special case of Algorithm 2.2.1. The only difference between the algorithms is the choice of the annihilator $\mathcal{W}^{\perp}$. In Algorithm 2.2.1, a maximal rank annihilator is used whereas in [54] an annihilator of much smaller rank is used. In the nonuniform case, we can not *a priori* derive a smaller matrix to cancel $\Gamma_p \mathcal{W}$ in Eq. (2.33) since there is a risk of cancelling some of the row space of $\mathcal{X}$. The details can be found in [62].

Another issue to be addressed is the positivity of the power spectrum. Any physically meaningful power spectrum must be positive real. The power spectrum estimated by the above algorithm may not satisfy this requirement due to noise and undermodeling. This requirement manifests itself as the existence of a positive definite solution of Eq. (2.81). If a positive definite solution fails to exist, then the spectral factor can not be computed. Thus, the positivity of the spectrum should be enforced after the identification. There are many possibilities. Two methods enforcing the positivity condition in Eq. (2.4) are outlined in [54], These methods can be integrated into Algorithm 2.2.1 without modification.

2.3 Examples

In this section, we use two identification examples to illustrate the properties of the developed algorithm. The first example is based on simulated data. This example will show us the role played by the noise covariance information. The second example deals with the design of a linear shaping filter from measured road data.

2.3.1 Simulation Example

Let the true system $G(z) = C(zI_4 - A)^{-1}B + D$ be a fourth-order system described by the state-space model:

$$A = \begin{bmatrix} 0.8876 & 0.4494 & 0 & 0 \\ -0.4494 & 0.7978 & 0 & 0 \\ 0 & 0 & -0.6129 & 0.0645 \\ 0 & 0 & -6.4516 & -0.7419 \end{bmatrix}$$

$$B = \begin{bmatrix} 0.2247 \\ 0.8989 \\ 0.0323 \\ 0.1290 \end{bmatrix}$$

$$C = [0.4719 \;\; 0.1124 \;\; 9.6774 \;\; 1.6129]$$

$$D = 0.9626.$$

We assume N noisy samples S_k of the power spectrum $S(z)$ evaluated at N points on the unit circle are given as

$$S_k = S(e^{j\theta_k}) + \widetilde{S}(e^{j\theta_k})\nu_k, \qquad k = 1, \cdots, N$$

where the noise term $\widetilde{S}(e^{j\theta_k})\nu_k$ is composed of a noise transfer function $\widetilde{S}(z)$, given by a second-order state-space model:

$$\widetilde{S}(z) = \widetilde{C}(zI_2 - \widetilde{A})^{-1}\widetilde{B} + \widetilde{D}$$

with

$$\widetilde{A} = \begin{bmatrix} 0.6296 & 0.0741 \\ -7.4074 & 0.4815 \end{bmatrix}, \quad \widetilde{B} = \begin{bmatrix} 0.04 \\ 0.9 \end{bmatrix}$$

$$\widetilde{C} = [1.6300 \;\; 0.0740], \quad \widetilde{D} = 0.2$$

and ν_k being independent complex identically distributed normal random variables with zero mean and unit variance. The variance of the noise process at

each frequency equals $\mathcal{R}_k = |\widetilde{S}(z_k)|^2$. We picked the frequencies randomly and independently from the intervals

$$\left[\frac{\pi}{N}(k-\frac{1}{2}), \frac{\pi}{N}(k+\frac{1}{2})\right], \qquad k = 1, \cdots, N.$$

Thus, each θ_k has a uniform distribution.

To examine the consistency properties of Algorithm 2.2.1, we performed Monte Carlo simulations estimating the power spectrum, given the samples S_k, using different noise realizations of ν_k. For $N = 400$ and fixed frequencies, 100 different noise realizations were generated, and Algorithm 2.2.1 with $p = 50$ estimated 100 models. To assess the quality of the resulting model both the (measured) supremum norm

$$\|\widehat{S}_n - S\|_{m,\infty} = \max_{1 \le k \le N} |\widehat{S}_N(z_k) - S(z_k)|$$

and the (measured) $\mathcal{H}_2$ norm

$$\|\widehat{S}_n - S\|_{m,2} = \left(\frac{1}{N}\sum_{k=1}^{N} |\widehat{S}_N(z_k) - S(z_k)|^2\right)^{\frac{1}{2}}$$

of the estimation error were determined for each estimated model and averaged over the 100 estimated models. In Figure 2.1, the results for the 100 estimated models using the covariance information are shown. We computed $\|\widehat{S}_n - S\|_{m,2} = 0.3307$ and $\|\widehat{S}_n - S\|_{m,\infty} = 2.4208$.

In Figure 2.2, the results for the 100 estimated models without using the covariance information, *i.e.,* $\mathcal{R}_k = 1$ for all k, are shown. We computed $\|\widehat{S}_n - S\|_{m,2} = 0.4500$ and $\|\widehat{S}_n - S\|_{m,\infty} = 2.6240$.

Comparing $\mathcal{H}_2$ errors, as predicted by the analysis, using the noise covariance information in Algorithm 2.2.1 reduces the estimation error by about 30%.

2.3.2 Stochastic Road Modeling Example

In this subsection, we consider one practical application of Algorithm 2.2.1. Provided that occasional large irregularities such as potholes are removed from

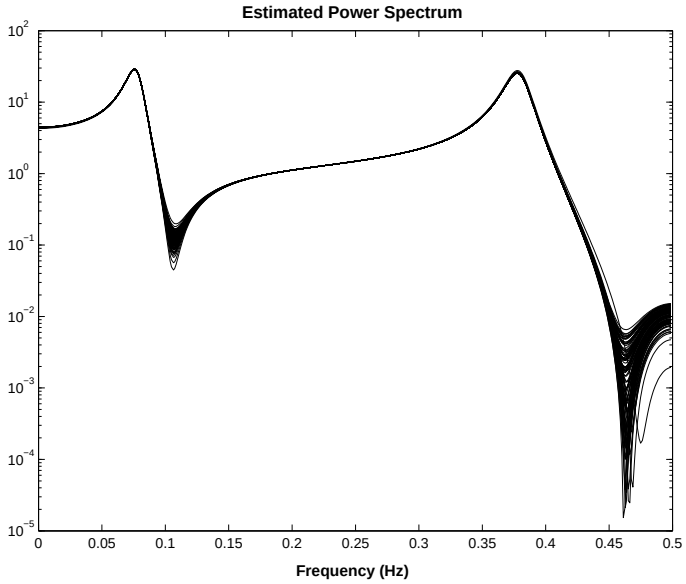

Figure 2.1: The results from Monte Carlo simulations for the 100 estimated models using the covariance information.

the analysis,the road surface may be described as a realization of a stationary random process. This assumption enables one to determine the response of a vehicle traversing a road by accepted techniques of the theory of random vibration. If the road surface is further assumed to be homogeneous and isotropic, then a road profile can be completely described by a single power spectral density evaluated from any single track.

In Figure 2.3 [52], the spectral density of a typical road and its split power law approximation:

$$\widehat{S}(j2\pi\widetilde{n}) = \begin{cases} C|\widetilde{n}/\widetilde{n}_0|^{-2\delta_1}, & 0 < |\widetilde{n}| < \widetilde{n}_0; \\ C|\widetilde{n}/\widetilde{n}_0|^{-2\delta_2}, & \widetilde{n}_0 \leq |\widetilde{n}| < \infty \end{cases}$$

obtained by trial and error for $\widetilde{n}_0 = 0.15708$ cycles/m, $\delta_1 = 1.6$, $\delta_2 = 1.1$, and $C = 0.76 \times 10^{-5}$ are plotted. In the figure, we also show the integrated white noise approximation to the data: $C|\widetilde{n}/\widetilde{n}_0|^{-2}$ which is commonly used in stochastic road modeling. It is clear that the fit by the integrated white-noise modeling is rather poor; in particular at the frequencies below $\widetilde{n}_0$. The problem with the split power approximation is that it can not be generated by

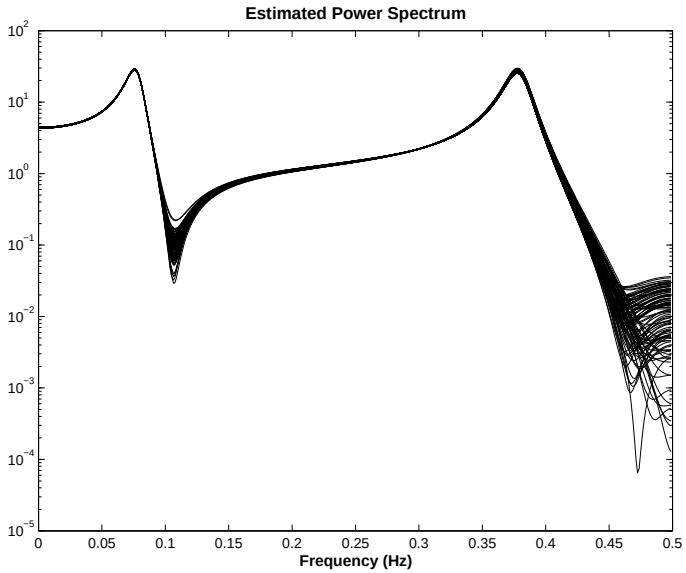

Figure 2.2: The results from Monte Carlo simulations for the 100 estimated models without using the covariance information.

shape filters. Hence, it is not suitable for simulating the response of vehicle. Besides, it is unbounded at $\widetilde{n} = 0$.

In this application, we seek a low order shape filter whose output spectrum matches the spectral data in Figure 2.3 as closely as possible. The continuous-time estimation problem is converted to a discrete one by using the bilinear map:

$$s = \psi(z) = \lambda \frac{z-1}{z+1} \qquad (\lambda > 0).$$

The number of data is $N = 63$. We picked $\lambda = 0.2$ and $p = 32$ in Algorithm 2.2.1. In the first trial, we chose $n = 1$ and $\mathcal{R}_N = I_N$. The continuous-time spectral factor was obtained by substituting $z = \psi^{-1}(s)$ in the discrete-time spectral factor. Thus,

$$\widehat{G}_N(s) = 0.0122 \, \frac{s + 1.1154}{s + 0.0404}. \tag{2.96}$$

In Figure 2.4, the output spectrum and the estimation error of this transfer function are compared with the road data. This figure tells us that the first order rational filter produced by Algorithm 2.2.1 is accurate up to 0.02 cycles/m.

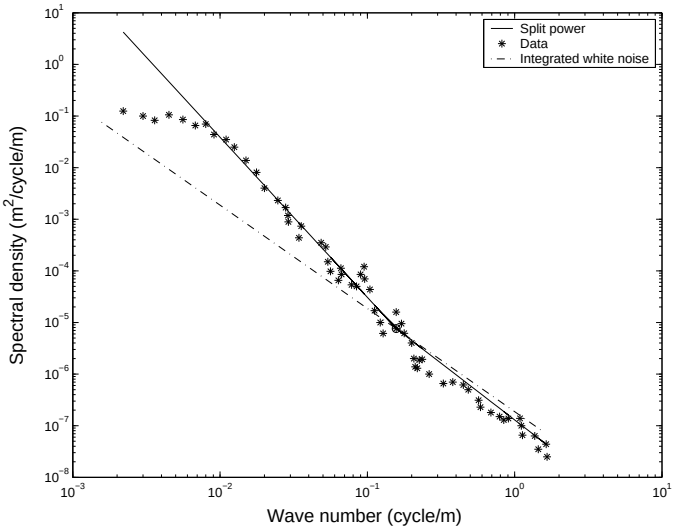

Figure 2.3: The road power spectrum and its approximate modeling by the split power law and the integrated white noise.

To interpret this result, assume that the bandwidth of the vehicle suspension is 10 Hz and the forward velocity of the vehicle is 30 m/sec. Note that the vehicle frequency response rolls off at least 20 decibels per decade. This bandwidth is translated to a (spectral) bandwidth of 1/3 cycles/m in Figure 2.3. Since the road power spectrum rapidly rolls off, we conclude that the first order model provides a good first-degree approximation to the measured data although this model is accurate only in very low frequencies. It should be noted that the power spectrum of this model is not integrable. A convergence factor rolling the frequency response off at high frequencies can be introduced.

Next, we tried higher model orders with $\mathcal{R}$ as a design variable. In Figure 2.5 and Figure 2.6, the output spectra and the estimation errors are compared with the road data for $n = 7$, $p = 32$, and the two cases $\mathcal{R} = I_N$ and $\mathcal{R}_k = S_k$. Clearly, Figure 2.6 indicates improvement in the high frequency rolling caused by weighting.

The purpose of modeling a power spectrum by a rational function of reasonably low order is to use this approximation for the design of a linear shaping filter with a white noise input. Then, the identified road spectrum is

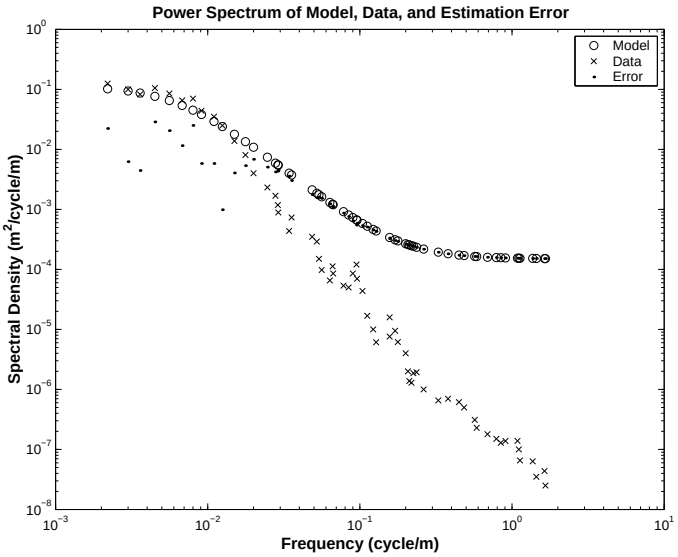

Figure 2.4: The spectral data and its modeling by a rational model of order one produced by Algorithm 2.2.1 with $\mathcal{R} = I_N$.

used, for example in a quarter-car model, to study the response of the vehicle to random road inputs [98].

2.4 Rational interpolation from real or imaginary parts: A subspace-based approach

2.4.1 Motivation for the Problem

Let $f(z)$ denote the transfer function of a given nth order, stable, single-input/single-output, discrete-time system. Then, $f(z)$ is analytic on $\{z \in \mathbf{C} : |z| > \rho\}$ for some $\rho < 1$. In this section, we study construction of $f(z)$ from its real or imaginary parts evaluated on a discrete set of points $e^{j\theta_k} \in \mathbf{T}$, $k = 1, \cdots, N$, not necessarily on a uniform grid of frequencies as in the most existing works [99]. In the classical textbook [100], applications of this construction to representation and efficient sampling of bandpass signals are discussed.

The problem of determining a complex function that is analytic on

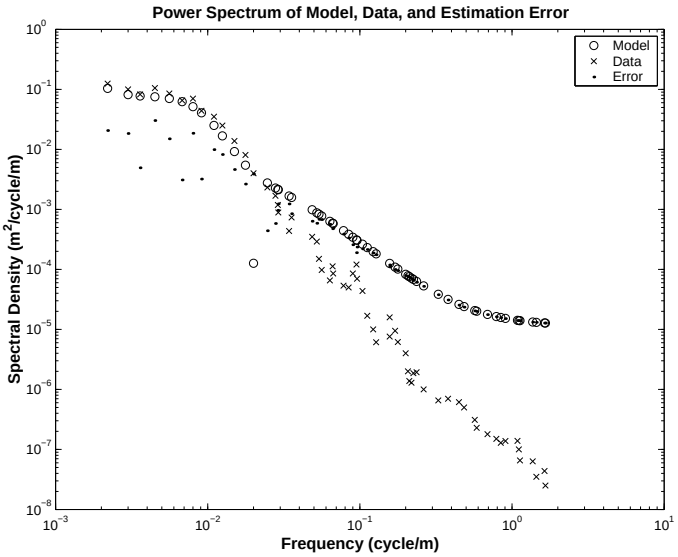

Figure 2.5: The spectral data and its modeling by a rational model of order 7 produced by Algorithm 2.2.1 with $\mathcal{R} = I_N$.

the open unit disk (or its complement, depending on how the z-transform is defined) from evaluations of its real part on the unit circle has a long history in both mathematics [101] and digital signal processing [100]. This construction is given by the following formula, see Lemma 1.2 in Chap. III of [101],

$$v(\theta) = \lim_{\varepsilon \to 0} \frac{1}{2\pi} \int_{|\theta - \phi| > \varepsilon} \cot\left(\frac{\theta - \varphi}{2}\right) u(\varphi) d\varphi \tag{2.97}$$

where $u(\theta)$ and $v(\theta)$ are the real and the imaginary parts of the function we are after evaluated on the unit circle, *that is* $f(e^{j\theta}) = u(\theta) + jv(\theta)$. The harmonic conjugate is normalized so that $v(0) = 0$. The linear mapping sending u to v defined in (2.97) is called the *conjugation operator*. This mapping is commonly known as the *Hilbert transform* in digital signal processing although a different operator, but with similar boundedness behavior, is called with the same name in mathematics [101]. The principal value in (2.97) exists almost everywhere if $|u(\theta)|$ is integrable [101].

In this section, we present a subspace-based algorithm to construct transfer functions of stable, discrete-time systems from their real or imaginary parts evaluated on finite subsets of $\mathbf{T}$. Consistency property of the algorithm

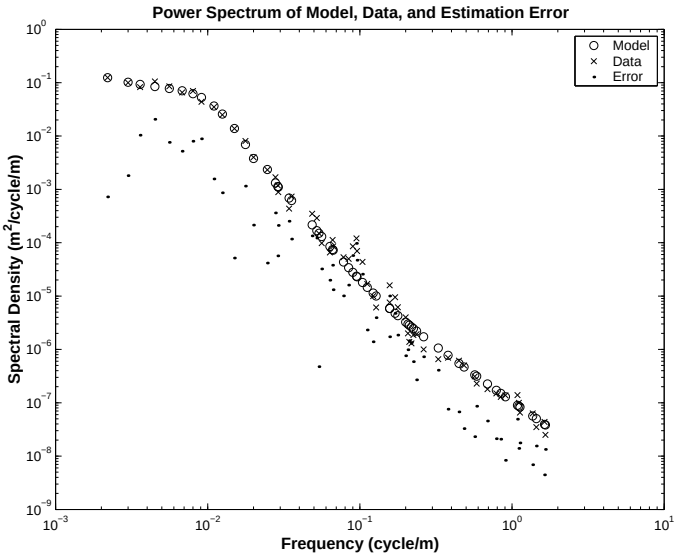

Figure 2.6: The spectral data and its modeling by a rational model of order 7 produced by Algorithm 2.2.1 with $\mathcal{R}_k = S_k$.

with respect to noisy data is also discussed. Our objective is to show that Algorithm 2.2.1 can be used to solve the problem considered in this section.

The problem considered in this section was studied in [99] assuming that the frequencies are uniformly spaced, and finite-impulse response models that interpolate the given data were constructed. Complexity of these models equals $(N-1)/2$ when the number of data, N, is odd and $N/2$ when N is even. The statistical analysis in [99] showed that the transfer function estimate has a variance that equals to noise variance assuming that the corruptions are independent, identically distributed Gaussian random variables. It is easy to understand the reason why the variance does not decrease with N: the number of the parameters to be determined is the half of the number of data.

In contrast, the algorithm of this section does not require model complexity grow unboundedly as N increases. Thus, the proposed algorithm consistently estimates finite-dimensional systems from real or imaginary parts of their transfer functions corrupted by noise.

2.4.2 Main result

Consider a single-input/single-output, linear-time invariant, stable, discrete-time system represented by the state-space equations:

$$\begin{aligned} x(t+1) &= Ax(t) + b\nu(t) \\ y(t) &= 2c^T x(t) + d\nu(t) \end{aligned} \tag{2.98}$$

where $x(t) \in \mathbf{R}^n$ is the state, $\nu(t) \in \mathbf{R}$ and $y(t) \in \mathbf{R}$ are, respectively, the input and the output of the system. The transfer function of the system in Eq. (2.98) denoted by $f(z)$ is computed as

$$f(z) = d + 2c^T(zI_n - A)^{-1}b. \tag{2.99}$$

The pairs (A, b) and (c^T, A) are assumed to be controllable and observable, respectively. The stability of Eq. (2.98) means that all the eigenvalues of A are inside the unit circle and both the controllability and the observability of Eq. (2.98) imply that $f(z)$ is an nth order rational function of z.

From Eq. (2.99), the real part of $f(z)$ can be written as

$$\begin{aligned} u(\theta) &= \frac{1}{2}[f(z) + \overline{f(z)}] \\ &= h(z) + h(z^{-1}) \end{aligned} \tag{2.100}$$

where

$$h(z) = \frac{d}{2} + c^T(zI_n - A)^{-1}b, \tag{2.101}$$

$z = e^{j\theta}$. The second equality in Eq. (2.100) is due to the fact that $f(z)$ is a scalar-valued function of z. In this chapter, we study the problem of determining $v(\theta)$ from corrupted evaluations of $u(\theta)$ on finite subsets of $[0, \pi]$. But, from Eqs. (2.99)–(2.101) this problem is equivalent to determining a realization similar to $(A, b, c, \frac{d}{2})$ from the corrupted evaluations $\hat{u}_k = u(\theta_k) + \eta_k$, $k = 1, \cdots, N$.

Assuming that $\nu(t)$ is zero-mean unity variance white-noise process, the power spectrum associated with Eq. (2.98) is defined as

$$S(z) = f(z)f(z^{-1}). \tag{2.102}$$

If $f(z)$ is minimum-phase, *i.e.,* it has all zeros inside the unit circle, then $S(e^{j\theta}) > 0$ for all θ. This is the positive realness condition, and it imposes a constraint on the given spectrum samples $S_k = S(e^{j\theta_k}) + \eta_k$, *i.e,* $S_k > 0$ for all k. Now, assuming for a moment that $f(z)$ is minimum-phase, let us consider the problem of determining $f(z)$ from corrupted spectrum samples S_k, $k = 1, \cdots, N$. The transfer function $f(z)$ is called the *spectral factor* of $S(z)$.

Suppose $S(z) > 0$ on the unit circle and let P be the solution of the discrete-time Lyapunov equation:

$$P = APA^T + bb^T.$$

Let

$$\begin{aligned} \gamma &= 4c^T Pc + d^2, \\ \beta &= 2APc + db. \end{aligned}$$

Then, $S(z)$ can be split into the sum of two system transfer functions [96] as follows

$$S(z) = \psi(z) + \psi(z^{-1})$$

with

$$\psi(z) = \frac{\gamma}{2} + 2c^T(zI_n - A)^{-1}\beta.$$

This splitting of $S(z)$ into the sum of a causal transfer function $\psi(z)$ and an anti-causal transfer function $\psi(z^{-1})$ is the first step of the subspace-based identification algorithms in [54, 57]. The transfer functions $\psi(z)$ and $\psi(z^{-1})$ are called the *spectral summands* of $S(z)$. In [54, 57], realizations similar to $(A, \beta, 2c, \frac{\gamma}{2})$ are consistently estimated from corrupted power spectrum samples S_k. The subspace-based algorithms proposed in [54, 57] do not require the power spectrum be scalar-valued.

The spectral factor $(A, b, 2c, d)$ is extracted from the quadruplet $(A, \beta, 2c, \frac{\gamma}{2})$ by first solving the Riccati equation for Q:

$$Q = AQA^T + (\beta - 2AQc)(\gamma - 4c^T Qc)^{-1}(\beta - 2AQc)^T \qquad (2.103)$$

and then computing b and d as follows:

$$\begin{aligned} b &= (\beta - 2AQc)(\gamma - 4c^TQc)^{-1/2}, \\ d &= \gamma - 4c^TQc)^{1/2}. \end{aligned}$$

The Riccati equation (2.103) may fail to have a positive definite solution. This may happen due to the finiteness of the data record, undermodelling, and the noise. The positivity of the spectrum can be assured by modifying γ and β. There are many possibilities to ensure this positivity. Two methods enforcing the positivity condition (2.102) are outlined in [54]. (See, also [102] for alternative implementations).

Since the positivity of the spectrum is enforced after the estimation of the spectral summands, the consistency properties carry on to the next stages of the algorithms in [54, 57]. Moreover, the interpolation properties of these algorithms are determined in the estimation step of $\psi(z)$ from the spectrum samples. Thus, the estimation problem of determining $f(z)$ from the corrupted samples of $u(\theta)$ can be viewed as a first step in the spectral estimation problem of determining $f(z)$ from the corrupted samples of $|f(e^{j\theta})|^2$.

The former estimation problem is simpler since the positivity condition is not needed. (The case that $f(z)$ is a positive-real transfer function can be handled similarly to the spectral estimation problem). In [57], the interpolation condition, which links the number of data with the system order, is derived in Lemma 2 there. This condition is obtained under the assumption that the realization $(A, \beta, 2c, \gamma/2)$ is minimal, which is equivalent to the minimality of $(A, b, 2c, d)$. In the current problem however, the latter equivalence is not even needed.

Identification Algorithm

The following algorithm has been derived from Algorithm 2.2.1 by discarding the spectral factor computation component.

Algorithm 2.4.1. *Subspace algorithm.*

1. *Given the data* $\hat{u}_k = u(\theta_k) + \eta_k$, $\mathcal{R}_k$; $k = 1, \cdots, N$ *form the matrices* $\widehat{\mathcal{U}}$, $\mathcal{W}$, *and* $\mathcal{K}$:

$$\begin{aligned} \widehat{\mathcal{U}} &= [\mathrm{Re}\,\widehat{\mathcal{U}}_C \;\; \mathrm{Im}\,\widehat{\mathcal{U}}_C], \\ \mathcal{W} &= [\mathrm{Re}\,\mathcal{W}_C \;\; \mathrm{Im}\,\mathcal{W}_C], \\ \mathcal{K}\mathcal{K}^T &= \mathrm{Re}\left(\mathcal{W}_{\mathrm{C}}\mathcal{R}\mathcal{W}_{\mathrm{C}}^H\right) \end{aligned}$$

where $p > 2n$ *is a free parameter,*

$$\widehat{\mathcal{U}}_{\mathrm{C}} = \frac{1}{\sqrt{N}} \begin{bmatrix} \hat{u}_1 & \cdots & \hat{u}_N \\ z_1\hat{u}_1 & \cdots & z_N\hat{u}_N \\ \vdots & \ddots & \vdots \\ z_1^{p-1}\hat{u}_1 & \cdots & z_N^{p-1}\hat{u}_N \end{bmatrix},$$

and $\mathcal{W}_{\mathrm{C}}$ *is the matrix in Eq. (2.28) evaluated at* $m = 1$.

2. *Calculate the QR-factorization:*

$$\begin{bmatrix} \mathcal{W} \\ \widehat{\mathcal{U}} \end{bmatrix} = \begin{bmatrix} R_{11} & 0 \\ R_{21} & R_{22} \end{bmatrix} \begin{bmatrix} Q_1^T \\ Q_2^T \end{bmatrix}.$$

3. *Calculate the singular value decomposition:*

$$\mathcal{K}^{-1}R_{22} = \begin{bmatrix} \widehat{U}_{2n} & \widetilde{U} \end{bmatrix} \begin{bmatrix} \widehat{\Sigma}_{2n} & 0 \\ 0 & \widetilde{\Sigma} \end{bmatrix} \begin{bmatrix} \widehat{V}_{2n} \\ \widetilde{V} \end{bmatrix}.$$

4. *Determine the system order* n *by inspecting the singular values and partition the SVD such that* $\widehat{\Sigma}_{2n}$ *contains the* $2n$ *largest singular values.*

5. *Calculate*

$$\widetilde{A} = (J_{\mathrm{d}}\mathcal{K}\widehat{U}_{2n})^{\dagger} J_{\mathrm{u}}\mathcal{K}\widehat{U}_{2n}$$

where J_{u} *and* J_{d} *are the upward and downward shift matrices in Eqs. (2.53) and (2.54) evaluated at* $m = 1$.

6. *Block-diagonalize* $\widetilde{A}$*:*

$$\widetilde{A} = \begin{bmatrix} \widehat{\Pi}_{\rm c} & \widehat{\Pi}_{\rm ac} \end{bmatrix} \begin{bmatrix} \widehat{\Sigma}_{\rm c} & 0 \\ 0 & \widehat{\Sigma}_{\rm ac} \end{bmatrix} \begin{bmatrix} \widehat{\Pi}_{\rm c} & \widehat{\Pi}_{\rm ac} \end{bmatrix}^{-1}$$

where the eigenvalues of $\widehat{\Sigma}_{\rm c}$ *lie inside the unit circle and let*

$$\widehat{A} = \widehat{\Sigma}_{\rm c}.$$

7. *Let*

$$\hat{c}^T = J_{\rm f} \mathcal{K} \widehat{U}_{2n} \widehat{\Pi}_{\rm c}$$

where $J_{\rm f}$ *is the matrix in Eq. (2.60) evaluated at* $m = 1$*.*

8. *Solve the linear least-squares problem:*

$$\hat{d}, \hat{b} = \arg\min_{\check{d},\check{b}} \sum_{k=1}^{N} R_k^{-1} [2{\rm Re}(\chi_k \check{b}) + \check{d} - \hat{u}_k]^2$$

for the estimates of d *and* b *where*

$$\chi_k = \hat{c}^T (e^{i\theta_k} I_n - \widehat{\Sigma}_{\rm c})^{-1}.$$

9. *Calculate an estimator of* $f(z)$ *as*

$$\hat{f}(z) = \hat{d} + 2\hat{c}^T (zI_n - \widehat{A})^{-1} \hat{b}.$$

The main result of this section is contained in the following.

Theorem 2.4.1. *Consider Algorithm 2.4.1 with* N *noise-free samples of the real part of the transfer function* $f(z)$ *of a discrete-time stable system of order* n *at* N *distinct frequencies* θ_k*. Assume that the poles of* $f(z)$ *are nonzero and distinct. Choose* $p > 2n$ *and let* $\mathcal{K} \in \mathbf{R}^{p \times p}$ *be any nonsingular matrix. If* $N \geq (p/2) + n + 1$*, then* $\hat{f} = f$*. If the samples are corrupted by noise satisfying Eqs. (2.10) and (2.11), and the frequencies satisfy Eq. (2.12), then Algorithm 2.4.1 is strongly consistent,* i.e.,

$$\lim_{N \to \infty} \sup_{z \in \mathbf{D}} |\hat{f}(z) - f(z)| = 0, \qquad \text{w.p.1.}$$

By picking $p = 2n+1$, it is possible to exactly recover nth order stable systems from real parts of their transfer functions using only $2n+2$ noise-free evaluations on the unit circle whereas polynomial model structures in [99] can only recover finite-impulse responses without error. If the true system is lightly damped, a large number of impulse-response coefficients need to be estimated from data for accurate system representations. But, such representations have large model variability due to the random component of uncertainty as opposed to the strong consistency of Algorithm 2.4.1.

When the samples of $v(\theta)$ are given, its harmonic conjugate $u(\theta)$ is obtained by simply interchanging the roles of u and v by noting $if = -v + iu$. Now, suppose that the samples of $\arg f(z)$ are given and we wish to construct $|f(z)|$ under the minimum-phase constraint. This case is simple if one notes that $\log f(z)$ is analytic whenever $f(z)$ is minimum phase. However, Theorem 2.4.1 does not hold in this case; but, approximations to the true rational system can be obtained with greater precision for large model orders. The converse problem has already been solved by Algorithm 2.2.1.

2.4.3 Example

In this subsection, we use a simulation example to illustrate the properties of the proposed algorithm. Let the true system $f(z) = 2c^T(zI_4 - A)^{-1}b + d$

be a fourth-order system described by the state-space model:

$$A = \begin{bmatrix} 0.8876 & 0.4494 & 0 & 0 \\ -0.4494 & 0.7978 & 0 & 0 \\ 0 & 0 & -0.6129 & 0.0645 \\ 0 & 0 & -6.4516 & -0.7419 \end{bmatrix},$$

$$b = (0.2247 \;\; 0.8989 \;\; 0.0323 \;\; 0.1290)^T,$$

$$2c^T = (0.4719 \;\; 0.1124 \;\; 9.6774 \;\; 1.6129),$$

$$d = 0.9626.$$

We assume N noisy samples $\hat{u}_k$ of $u(\theta)$ evaluated at N points on the unit circle are given as

$$\hat{u}_k = u(\theta_k) + 0.25\eta_k, \qquad k = 1, \cdots, N$$

where η_k are independent identically distributed normal random variables with zero mean and unit variance. We picked the frequencies randomly and independently from the intervals

$$\left[\frac{\pi k}{N}, \frac{\pi(k+1)}{N}\right], \qquad k = 0, \cdots, N-1.$$

Thus, each θ_k has a uniform distribution.

To demonstrate the consistency property of Algorithm 2.4.1, we performed Monte Carlo simulations estimating $f(z)$, given the samples $\hat{u}_k$, using different noise realizations of η_k. For $N = 1000$ and fixed frequencies, 20 different noise realizations were generated, and Algorithm 2.4.1 with $p = 100$ and $\mathcal{R} = I_N$ estimated 20 models. To assess the quality of the resulting model the (measured) $\mathcal{H}_2$ norm:

$$\|\hat{f} - f\|_{m,2} = \left(\frac{1}{N}\sum_{k=1}^{N} |\hat{f}(e^{j\theta_k}) - f(e^{j\theta_k})|^2\right)^{\frac{1}{2}}$$

of the estimation error was determined for each estimated model and averaged over the 20 estimated models. In Figure 2.7, the results for the 20 estimated models are shown. We computed 0.0315 for the average value of $\|\hat{f} - f\|_{m,2}$.

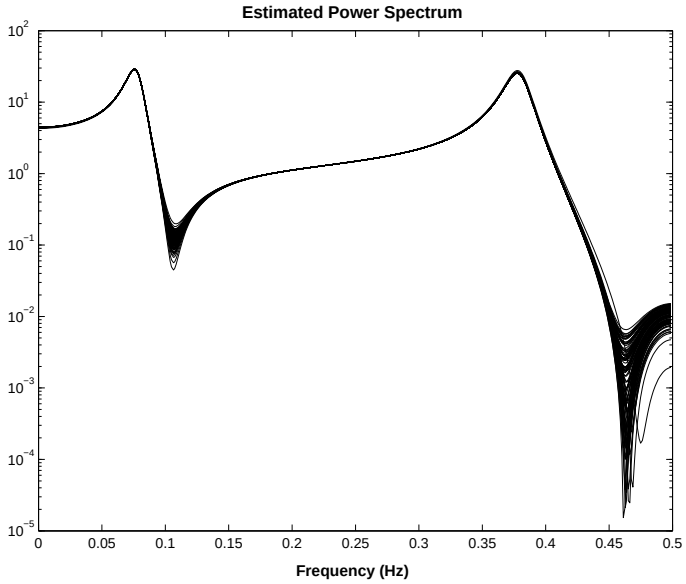

Figure 2.7: The results from Monte Carlo simulations for the 20 estimated models.

Next, we used Algorithm 2.4.1 with $N = p = 9$, randomly chosen frequencies, and $\eta_k = 0$ for all k to verify its interpolation properties. In fact, for this case we computed $\|\hat{f} - f\|_{m,2} = 4.33 \times 10^{-13}$. Since $p > 2n$, the choice for p is appropriate. From Theorem 2.4.1, one would confer $N \geq 10$. However, θ_1 and θ_N are not equal to 0 or π. In this case, the interpolation condition (from the proof of Lemma 2 in [57]) is $2N > p + 2n - 1$, yielding $N = 9$ as the smallest number satisfying this inequality.

2.5 Summary

In this chapter, we presented a strongly consistent subspace algorithm for the identification of square multi-input/multi-output, discrete time, linear time invariant systems from non uniformly spaced power spectrum measurements. The algorithm was illustrated with one practical example that solves a stochastic road modeling problem.

Construction of analytic functions from evaluations of real or imaginary parts on finite subsets of the unit circle was also studied in this chapter.

A subspace-based algorithm, which exactly retrieves finite-dimensional systems from noise-free data, was presented. This algorithm is expected to find applications in the approximation of band-limited filters by rational ones.

3 SUBSPACE-BASED SOLUTION OF LAGRANGE–SYLVESTER INTERPOLATION PROBLEM

Many problems in control, circuit theory, and signal processing can be reduced to the solution of matrix rational interpolation problems which have been widely studied (see, for example, [55,56,103–115] and the references therein). Applications arise, for example, in robust controller synthesis [55,56], in the Q-parameterization of stabilizing controllers for unstable plants [116], in the problem of model validation [117], in circuit theory [118], in spectral estimation [119], and in adaptive filtering and control [114,120].

In the simplest form, given complex numbers z_k and w_k for $k = 1, \ldots, N$, an interpolation problem asks for scalar rational functions $G(z)$ which meet the interpolation conditions

$$G(z_k) = w_k, \qquad k = 1, \ldots, N.$$

The interpolants can further be required to have minimal complexity in terms of their McMillan degree. An extension of this problem to the matrix case is as follows.

Given: a subset $\vartheta \subset \mathbf{C}$, points $z_1, \ldots, z_L$ in ϑ, rational $1 \times p$ row vector functions $v_1(z), \ldots, v_L(z)$ with $v_k(z_k) \neq 0$ for all k, and rational $1 \times m$ row vectors $w_1(z), \ldots, w_L(z)$.

Find: (at least one or all) $p \times m$ rational matrix functions $G(z)$ with no poles in ϑ which satisfy the *tangential* interpolation conditions

$$\frac{d^j}{dz^j}\{v_k(z)G(z)\}\bigg|_{z=z_k} = \frac{d^j}{dz^j}w_k(z)\bigg|_{z=z_k} \tag{3.1}$$

for $0 \leq j \leq N_k$, $1 \leq k \leq L$.

This problem is known as the tangential *Lagrange–Sylvester* rational interpolation problem. One approach to finding a solution is to reduce the

problem to a system of independent scalar problems, which is not interesting from the viewpoint of matrix interpolation theory. In addition, a minimal realization can be obtained only after the elimination of unobservable or/and uncontrollable modes. The contour integral version of this problem is treated in the comprehensive work [107]. The *bitangential* or *bidirectional* version is studied, for example, in [106, 108, 112, 113]. Related problems are the nonhomogenous interpolation problem with metric constraints, as in the various types of Nevanlinna–Pick interpolation and its generalizations [110, 121], and the partial realization problem, that is, finding a rational matrix function analytic at infinity of the smallest possible McMillan degree with prescribed values of itself and a few of its derivatives at infinity [103, 107, 122, 123]. Further applications of interpolation theory to control and systems theory and estimation are presented in [107, 124, 125].

Prior work on the unconstrained tangential interpolation problem has been largely carried out by Ball, Gohberg, and Rodman [107, 108]. The solvability issues of the interpolation problem, i.e., the existence and the uniqueness of the solutions, have been analyzed in [126] by using a *residual interpolation* framework. A more direct algebraic approach in [111] shows that solving a tangential interpolation problem is equivalent to solving a matrix Padé approximation problem with Taylor coefficients obeying a set of linear constraints. In [103–106], the tangential interpolation problem above was studied using a tool called the Löwner matrix. In [106], the problem of finding admissible degrees of complexity of the solutions to the above interpolation problem, that is, finding all positive integers n for which there exits an interpolant with McMillan degree n, and the problem of parameterizing all solutions for a given admissible degree of complexity were investigated. Clearly, the solutions of minimal complexity are of special interest.

The main result in [108] states that the family of rational matrix functions satisfying (3.1) can be parameterized in terms of a certain *linear fractional map*. First, the interpolation data is translated into a so-called *left null pair* that describes the zero structure of a $(p + m) \times (p + m)$ *resolvent*

matrix. The computation of the resolvent matrix requires that the solution of a particular Sylvester equation be invertible. The details can be found in [107]. In [111], a recursive method for computing the resolvent matrix as a product of elementary first-order rational matrix functions is presented. This scheme allows recursive updating of the resolvent matrix whenever a new interpolation point is added to the input data. In the special case when the resolvent matrix is in *column-reduced* form, it is possible to extract the admissible degrees of complexity as well as the minimal degree of complexity from the linear fractional parameterization formula. The resolvent matrix obtained by an unconstrained algorithm can be transformed into column-reduced form via a sequence of elementary unimodular transformations [127]. A detailed algorithm for the construction of a column-reduced rational matrix function from a given *null-pole triple* is given in [128]. This algorithm is not recursive, whereas in [111] a column-reduced transfer function is recursively obtained.

In this chapter, we present a numerically efficient algorithm for solving the unconstrained tangential interpolation problem formulated above. This algorithm is inspired by the recent work on the frequency domain subspace-based identification [62,90–92]. The solvability conditions for the proposed algorithm are simple, and depend only on the total multiplicities of the interpolation points. The resulting interpolating function is in the minimal state-space form. To this date, interpolation properties of the subspace-based methods have not been investigated in the generality of this chapter. Only in [62] was an interpolation result obtained for uniformly spaced data on the unit circle of the complex plane. The problem of curve fitting is also closely related to the interpolation problem. The use of the frequency domain subspace-based methods for curve fitting is briefly described in [129].

Let us reformulate the tangential interpolation problem described above in terms of system properties. More precisely, let us consider a multi-input/multi-output, linear-time invariant, discrete-time system represented by the state-

space equations

$$\begin{aligned} x(k+1) &= Ax(k) + Bu(k), \\ y(k) &= Cx(k) + Du(k), \end{aligned} \tag{3.2}$$

where $x(k) \in \mathbf{R}^n$ is the state and $u(k) \in \mathbf{R}^m$ and $y(k) \in \mathbf{R}^p$ are, respectively, the input and the output of the system. The transfer function of the system (3.2) denoted by $G(z)$ is computed as

$$G(z) = D + C(zI_n - A)^{-1}B. \tag{3.3}$$

We assume that the system (3.2) is stable and the pairs (A, B) and (C, A) are *controllable* and *observable*, respectively. The stability of (3.2) means that $G(z)$ is a *proper rational* matrix that is analytic and bounded in the region $\vartheta = \{z \in \mathbf{C} : |z| \geq 1\}$, and both the controllability and the observability of the pairs (A, B) and (C, A) mean that the quadruplet (A, B, C, D) is a *minimal realization* of $G(z)$.

The interpolation problem studied in this paper can be stated as follows.

Given: noise-free samples of $G(z)$ and its derivatives at L distinct points $z_k \in \vartheta$,

$$\frac{d^j}{dz^j} G(z)\bigg|_{z=z_k} = w_{kj}, \qquad j = 0, 1, \ldots, N_k, \;\; k = 1, 2, \ldots, L. \tag{3.4}$$

Find: a quadruplet $(\widehat{A}, \widehat{B}, \widehat{C}, \widehat{D})$ that is a minimal realization of $G(z)$.

Clearly, Eq. (3.4) is a special case of Eq. (3.1) with suitably selected left vectors $v_k(z)$ and nodes z_k. A subspace-based algorithm handling the tangential-type constraints in Eq. (3.1) as well can be derived along the same lines of the proposed algorithm. The minimality and the uniqueness of the interpolant are the parts of the problem formulation. What is left unanswered is a condition on the number of the interpolation nodes, counting multiplicities. It is also clear that, if it exists, the subspace-based solution is a minimal interpolating function in the set of all possible solutions.

The proposed interpolation scheme is particularly useful when the samples of $G(z)$ and its derivatives are corrupted by noise and the amount of data is large with respect to n. In the noisy case, most interpolation schemes deliver state-space realizations with McMillan degrees tending to infinity as the amount of data grows unboundedly; thus such schemes are sensitive to inaccuracies in the interpolation data. Since our algorithm is subspace-based, it inherits robustness properties of the subspace-based identification algorithms. In particular, there is no need for explicit model parameterization, and this algorithm is computationally efficient since it uses numerically robust QR factorization and the singular value decomposition. In the chapter, we also consider subspace-based system identification with interpolation constraints.

Note that a given interpolation problem on the right half complex plane can be converted to an interpolation problem on the unit disk by using the Möbius transformation:

$$s = \psi(z) = \lambda \frac{z-1}{z+1} \qquad (\lambda > 0). \tag{3.5}$$

We omit the details.

3.1 Subspace-Based Interpolation Algorithm

We begin by taking the z-transform of Eq. (3.2),

$$\begin{aligned} zX(z) &= AX(z) + BU(z), \\ Y(z) &= CX(z) + DU(z), \end{aligned} \tag{3.6}$$

assuming $x(0) = 0$, where $X(z)$, $Y(z)$, and $U(z)$ denote respectively the z-transforms of $x(k)$, $y(k)$, and $u(k)$ defined by

$$U(z) = \sum_{k=0}^{\infty} u(k)\, z^{-k}. \tag{3.7}$$

Let $X_j(x)$ be the resulting state z-transform when

$$u(k) = \begin{cases} e_j, & k = 0, \\ 0, & \text{otherwise}, \end{cases}$$

where e_j denotes the unit vector in $\mathbf{R}^m$ with 1 on the jth position and 0 elsewhere. By defining the compound state z-transform matrix,

$$X_{\mathrm{C}}(z) = [X_1(z) \;\; X_2(z) \;\; \cdots \;\; X_m(z)], \tag{3.8}$$

$G(z)$ can implicitly be described as

$$G(z) = CX_{\mathrm{C}}(z) + D \tag{3.9}$$

with

$$zX_{\mathrm{C}}(z) = AX_{\mathrm{C}}(z) + B. \tag{3.10}$$

By recursive use of Eq. (3.10), we obtain the relation

$$z^k X_{\mathrm{C}}(z) = A^k X_{\mathrm{C}}(z) + \sum_{j=0}^{k-1} A^{k-1-j} B z^j, \qquad k \geq 1. \tag{3.11}$$

Multiplying both sides of Eq. (3.11) with C and using Eq. (3.9), we get

$$z^k G(z) = CA^k X_{\mathrm{C}}(z) + Dz^k + \sum_{j=0}^{k-1} CA^{k-1-j} B z^j, \qquad k \geq 1. \tag{3.12}$$

Now, recall that the impulse response coefficients of $G(z)$ are given by

$$g_k = \begin{cases} D, & k = 0, \\ CA^{k-1}B, & k \geq 1. \end{cases} \tag{3.13}$$

Thus, from Eqs. (3.9), (3.12), and (3.13),

$$z^k G(z) = CA^k X_{\mathrm{C}}(z) + \sum_{j=0}^{k} g_{k-j}\, z^j, \qquad k \geq 0. \tag{3.14}$$

Hence from Eq. (3.14),

$$\begin{bmatrix} G(z) \\ zG(z) \\ \vdots \\ z^{q-1}G(z) \end{bmatrix} = \mathcal{O}_q X_{\mathrm{C}}(z) + \Gamma_q \begin{bmatrix} I_m \\ zI_m \\ \vdots \\ z^{q-1}I_m \end{bmatrix}, \tag{3.15}$$

where

$$\mathcal{O}_q = \begin{bmatrix} C \\ CA \\ \vdots \\ CA^{q-1} \end{bmatrix}, \tag{3.16}$$

$$\Gamma_q = \begin{bmatrix} g_0 & 0 & \cdots & 0 \\ g_1 & g_0 & \cdots & 0 \\ \vdots & \vdots & \ddots & \vdots \\ g_{q-1} & g_{q-2} & \cdots & g_0 \end{bmatrix}. \tag{3.17}$$

For later use, let us write Eq. (3.15) in a compact form. The matrix $\mathcal{O}_q$ is known as the *extended observability matrix* and has full rank n if (A, C) is an observable pair and $q \geq n$.

Let

$$\mathcal{Z}_q(z) = \begin{bmatrix} 1 \\ z \\ \vdots \\ z^{q-1} \end{bmatrix}, \tag{3.18}$$

$$\mathcal{J}_{q,2} = \begin{bmatrix} 0 & & \cdots & & 0 \\ 1 & 0 & & & \\ 0 & 1 & 0 & & \\ \vdots & & & \ddots & \vdots \\ 0 & & \cdots & 1 & 0 \end{bmatrix} \in \mathrm{R}^{q \times q}. \tag{3.19}$$

By a slight abuse of notation, let $\mathcal{J}_{q,1}$ denote the $q \times q$ identity matrix I_q. Observe that $\mathcal{J}_{q,2}$ is obtained by shifting the elements of $\mathcal{J}_{q,1}$ one row down and filling its first row with zeros. Let $\mathcal{J}_{q,j}$ denote the matrix obtained by $j-1$ repeated applications of this process to $\mathcal{J}_{q,1}$ and $J_{q,2}^0 = I_q$. Note the following relations:

$$\mathcal{J}_{q,j} = \begin{cases} \mathcal{J}_{q,2}^{j-1}, & j \leq q \\ 0, & j > q. \end{cases} \tag{3.20}$$

Thus, the lower triangular block Toeplitz matrix in Eq. (3.17) can be written as

$$\Gamma_q = \sum_{j=0}^{q-1} \mathcal{J}_{q,1+j} \otimes g_j. \tag{3.21}$$

Hence, from Eqs. (3.16)–(3.21) we arrive at the following compact expression for Eq. (3.15):

$$\mathcal{Z}_q(z) \otimes G(z) = \mathcal{O}_q X_{\mathrm{C}}(z) + \sum_{j=0}^{q-1} [\mathcal{J}_{q,2}^j \otimes g_j] \, [\mathcal{Z}_q(z) \otimes I_m] \,. \tag{3.22}$$

This equation forms the basis of the frequency domain subspace-based identification algorithms [62, 90]. In subspace-based identification algorithms, $\mathcal{Z}_q(z) \otimes G(z)$ and the right-hand side of Eq. (3.22) are evaluated at a set of distinct points on the unit circle and then stacked into columns of long matrices. This procedure yields a matrix equation *affine* in $\mathcal{O}_q$. From this equation, the range space of $\mathcal{O}_q$ is recovered by a projection. Once the observability range space is recovered, a realization of $G(z)$ is derived in a routine manner. We will adapt the same strategy.

First, we differentiate both sides of Eq. (3.22) l times with respect to z:

$$\begin{aligned} \frac{d^l}{dz^l} H_q(z) &= \sum_{j=0}^{l} \begin{pmatrix} l \\ j \end{pmatrix} \frac{d^j}{dz^j} \mathcal{Z}_q(z) \otimes \frac{d^{l-j}}{dz^{l-j}} G(z) \\ &= \mathcal{O}_q \frac{d^l}{dz^l} X_{\mathrm{C}}(z) + \sum_{j=0}^{q-1} [\mathcal{J}_{q,2}^j \otimes g_j] \left[\frac{d^l}{dz^l} \mathcal{Z}_q(z) \otimes I_m \right], \qquad l \geq 0, \end{aligned} \tag{3.23}$$

where

$$H_q(z) = \mathcal{Z}_q(z) \otimes G(z). \tag{3.24}$$

Then, we augment $H_q(z_k)$ and the first N_k derivatives of $H_q(z)$ at z_k in a data matrix:

$$\mathcal{H}_k = \left[H_q(z) \;\; \frac{d}{dz} H_q(z) \;\; \cdots \;\; \frac{d^{N_k}}{dz^{N_k}} H_q(z) \right]_{z=z_k}, \qquad k = 1, \ldots, L. \tag{3.25}$$

Using the right-hand side of the first equality in (3.23), let us derive a compact

expression for $\mathcal{H}_k$ in terms of the elementary matrices

$$\mathcal{D}_k = \begin{bmatrix} 0 & 1 & 0 & \cdots & 0 \\ & 0 & 2 & & \\ & & 0 & \cdots & \\ \vdots & & & \ddots & N_k \\ 0 & & & \cdots & 0 \end{bmatrix} \in \mathbf{R}^{(N_k+1)\times(N_k+1)} \tag{3.26}$$

and

$$\mathcal{W}_k = \left[\mathcal{Z}_q(z) \;\; \frac{d}{dz}\mathcal{Z}_q(z) \;\; \cdots \;\; \frac{d^{N_k}}{dz^{N_k}}\mathcal{Z}_q(z) \right]_{z=z_k}, \qquad k = 1, \ldots, L, \tag{3.27}$$

as follows:

$$\begin{aligned} \mathcal{H}_k \;=\; & \left[\mathcal{Z}_q(z) \;\; \frac{\mathrm{d}}{dz}\mathcal{Z}_q(z) \;\; \frac{d^2}{dz^2}\mathcal{Z}_q(z) \;\; \cdots \;\; \frac{d^{N_k}}{dz^{N_k}}\mathcal{Z}_q(z) \right]_{z=z_k} \otimes G(z_k) \\ & + \left[0 \;\; \mathcal{Z}_q(z) \;\; 2\frac{d}{\mathrm{d}z}\mathcal{Z}_q(z) \;\; \cdots \;\; \begin{pmatrix} N_k \\ 1 \end{pmatrix} \frac{d^{N_k-1}}{dz^{N_k-1}}\mathcal{Z}_q(z) \right]_{z=z_k} \otimes \frac{d}{dz}G(z_k) \\ & + \left[0 \;\; 0 \;\; \mathcal{Z}_q(z) \;\; \cdots \;\; \begin{pmatrix} N_k \\ 2 \end{pmatrix} \frac{d^{N_k-2}}{dz^{N_k-2}}\mathcal{Z}_q(z) \right]_{z=z_k} \otimes \frac{d^2}{dz^2}G(z_k) + \cdots \\ & + \left[0 \;\; 0 \;\; 0 \;\; \cdots \;\; \mathcal{Z}_q(z) \right]_{z=z_k} \otimes \frac{d^{N_k}}{dz^{N_k}}G(z_k) \\ = \;\; & \mathcal{W}_k \otimes G(z_k) + [\mathcal{W}_k\mathcal{D}_k] \otimes \frac{d}{dz}G(z_k) + \frac{1}{2!}[\mathcal{W}_k\mathcal{D}_k^2] \otimes \frac{d^2}{dz^2}G(z_k) \\ & + \frac{1}{N_k!}[\mathcal{W}_k\mathcal{D}_k^{N_k}] \otimes \frac{d^{N_k}}{dz^{N_k}}G(z_k). \end{aligned}$$

Note that $\mathcal{D}_k^j = 0$ for all $j > N_k$. Hence,

$$\mathcal{H}_k = \sum_{j=0}^{N_k} \frac{1}{j!}[\mathcal{W}_k\,\mathcal{D}_k^j] \otimes w_{kj}, \qquad k = 1, \ldots, L. \tag{3.28}$$

It remains to compute the derivatives of $\mathcal{Z}_q(z)$. To this end, let

$$\mathcal{T}_q = \begin{bmatrix} 0! & 0 & \cdots & 0 \\ 0 & 1! & \cdots & 0 \\ \vdots & \vdots & \ddots & \vdots \\ 0 & 0 & \cdots & (q-1)! \end{bmatrix} \in \mathbf{R}^{q\times q}. \tag{3.29}$$

Then, it is easy to verify that

$$\frac{d^l}{dz^l}\mathcal{Z}_q(z) = \mathcal{T}_q \mathcal{J}_{q,2}^l \mathcal{T}_q^{-1} \mathcal{Z}_q(z), \qquad l \geq 0. \tag{3.30}$$

Hence from Eqs. (3.27) and (3.30),

$$\mathcal{W}_k = \mathcal{T}_q \left[I_q \;\; \mathcal{J}_{q,2} \;\; \cdots \;\; \mathcal{J}_{q,2}^{N_k} \right] \left[I_{N_k+1} \otimes \mathcal{T}_q^{-1} \mathcal{Z}_q(z_k) \right], \qquad k = 1, \ldots, L. \tag{3.31}$$

An alternative compact expression for $\mathcal{H}_k$ is obtained by evaluating the right-hand side of the second equality in Eq. (3.23) for $l = 0, \ldots, N_k$, $k = 1, \ldots, L$, and augmenting the similar terms in compound matrices as follows:

$$\mathcal{H}_k = \mathcal{O}_q \, \mathcal{X}_k + \sum_{j=0}^{q-1} [\mathcal{J}_{q,2}^j \otimes g_j] \, [\mathcal{W}_k \otimes I_m], \qquad k = 1, \ldots, L, \tag{3.32}$$

where

$$\mathcal{X}_k = \left[X_{\mathrm{C}}(z) \;\; \frac{d}{dz} X_{\mathrm{C}}(z) \;\; \cdots \;\; \frac{d^{N_k}}{dz^{N_k}} X_{\mathrm{C}}(z) \right]_{z=z_k}, \qquad k = 1, \ldots, L. \tag{3.33}$$

Now, we collect $\mathcal{H}_k$, $\mathcal{X}_k$, and $\mathcal{W}_k$, $k = 1, \ldots, L$, in the compound matrices

$$\mathcal{H} = [\mathcal{H}_1 \, \mathcal{H}_2 \, \cdots \, \mathcal{H}_L], \tag{3.34}$$

$$\mathcal{X} = [\mathcal{X}_1 \, \mathcal{X}_2 \, \cdots \, \mathcal{X}_L], \tag{3.35}$$

$$\mathcal{W} = [\mathcal{W}_1 \, \mathcal{W}_2 \, \cdots \, \mathcal{W}_L]. \tag{3.36}$$

Hence,

$$\mathcal{H} = \mathcal{O}_q \, \mathcal{X} + \sum_{j=0}^{q-1} [\mathcal{J}_{q,2}^j \otimes g_j] \, [\mathcal{W} \otimes I_m], \tag{3.37}$$

where $\mathcal{H}$ and $\mathcal{W}$ are computed from the problem data $\{z_k, \{w_{kj}\}_{j=0}^{N_k}\}_{k=1}^{L}$ by the formulae (3.18), (3.26),(3.19), (3.28), (3.31), (3.29), (3.34), (3.36). This completes the first stage of our subspace-based interpolation algorithm. Observe that $\mathcal{H}$ is affine in $\mathcal{O}_q$ as advertised.

Since $\mathcal{O}_q$ is a real matrix and we are interested in the real range space, we can convert Eq. (3.37) into a relation involving only real valued matrices:

$$\widehat{\mathcal{H}} = \mathcal{O}_q \, \widehat{\mathcal{X}} + \sum_{j=0}^{q-1} [\mathcal{J}_{q,2}^j \otimes g_j] \, \mathcal{F}, \tag{3.38}$$

where

$$\widehat{\mathcal{H}} = [\mathrm{Re}\mathcal{H}\ \ \mathrm{Im}\mathcal{H}], \tag{3.39}$$

$$\mathcal{F} = [\mathrm{Re}\mathcal{W}\ \ \mathrm{Im}\mathcal{W}] \otimes I_m, \tag{3.40}$$

$$\widehat{\mathcal{X}} = [\mathrm{Re}\mathcal{X}\ \ \mathrm{Im}\mathcal{X}]. \tag{3.41}$$

Let z^* denote the complex conjugate of z. When $z_k \in \mathbf{R}$, from Eq. (3.18) we have $\mathcal{Z}_q(z_k) \in \mathbf{R}^q$. This, by Eq. (3.31), implies that $\mathcal{W}_k \in \mathbf{R}^{q\times(N_k+1)}$. From Eq. (3.10),

$$X_{\mathrm{C}}(z) = (zI_n - A)^{-1}B. \tag{3.42}$$

Then, from Eqs. (3.9), (3.42), and (3.33), it follows that $\mathcal{X}_k \in \mathbf{R}^{n\times m(N_k+1)}$ and, for all $j = 0, \ldots, N_k$, $w_{kj} \in \mathbf{R}^{p\times m}$ whenever $z_k \in \mathbf{R}$. Thus, whenever $z_k \in \mathbf{R}$ from Eq. (3.28) we have $\mathcal{H}_k \in \mathbf{R}^{pq\times m(N_k+1)}$. Hence, the imaginary parts of $\mathcal{H}_k$, $\mathcal{F}$, and $\mathcal{X}_k$ are all zero, and they need not be included in Eqs. (3.39)–(3.41) if $z_k \in \mathbf{R}$; without loss of generality, we will assume this in what follows. Let

$$N = \sum_{k:z_k\in\mathbf{R}} (N_k + 1) + \sum_{k:z_k\in\mathbf{C}-\mathbf{R}} 2(N_k + 1). \tag{3.43}$$

Then, $\widehat{\mathcal{H}} \in \mathbf{R}^{pq\times mN}$, $\mathcal{F} \in \mathbf{R}^{mq\times mN}$, and $\widehat{\mathcal{X}} \in \mathbf{R}^{n\times mN}$.

3.1.1 Projection onto the Observability Range Space

Let $\mathcal{F}^\perp$ be the projection matrix onto the null space of $\mathcal{F}$ given by

$$\mathcal{F}^\perp = I_{mN} - \mathcal{F}^T(\mathcal{F}\mathcal{F}^T)^{-1}\mathcal{F}, \tag{3.44}$$

where $\mathcal{F}^T$ denotes the transpose of $\mathcal{F}$. The summand in Eq. (3.38) is cancelled for all j when multiplied from right by $\mathcal{F}^\perp$. Thus,

$$\widehat{\mathcal{H}}\mathcal{F}^\perp = \mathcal{O}_q\,\widehat{\mathcal{X}}\mathcal{F}^\perp. \tag{3.45}$$

A numerically efficient way of forming $\widehat{\mathcal{H}}\mathcal{F}^\perp$ is to use the QR-factorization

$$\begin{bmatrix} \mathcal{F} \\ \widehat{\mathcal{H}} \end{bmatrix} = \begin{bmatrix} R_{11} & 0 \\ R_{21} & R_{22} \end{bmatrix} \begin{bmatrix} Q_1^T \\ Q_2^T \end{bmatrix}. \tag{3.46}$$

A simple derivation yields

$$\widehat{\mathcal{H}}\mathcal{F}^{\perp} = R_{22}Q_2^T, \tag{3.47}$$

and it suffices to use $R_{22} \in \mathbf{R}^{pq \times m(N-q)}$ in the extraction of the observability range space since Q_2^T is a matrix of full rank.

The range space of $\widehat{\mathcal{H}}\mathcal{F}^{\perp}$ equals the range space of $\mathcal{O}_q$ unless rank cancellations occur. A sufficient condition for the range spaces to be equal is that the intersection of the row spaces of $\mathcal{F}$ and $\widehat{\mathcal{X}}$ be empty. In the following, we present sufficient conditions in terms of the data and the system.

Lemma 3.1.1. *Let $\widehat{\mathcal{X}}$, $\mathcal{F}$, and N be as in Eqs.* (3.41)*,* (3.40)*, and* (3.43)*, respectively. Suppose that $N \geq q+n$ and the eigenvalues of A do not coincide with the distinct complex numbers z_k. Then,*

$$\text{rank} \begin{bmatrix} \mathcal{F} \\ \widehat{\mathcal{X}} \end{bmatrix} = qm + n \qquad \Longleftrightarrow \qquad (A, B) \text{ controllable pair.} \tag{3.48}$$

Proof. See Appendix B.1. □

Since all the eigenvalues of A are inside the unit circle, none of them coincide with any of z_k. Thus, by applying Lemma 3.1.1, we conclude that the two row spaces of $\widehat{\mathcal{X}}$ and $\mathcal{F}$ do not intersect and the range space of $\widehat{\mathcal{H}}\mathcal{F}^{\perp}$ coincides with the range space of $\mathcal{O}_q$. Then, using the singular value factorization of $\widehat{\mathcal{H}}\mathcal{F}^{\perp}$,

$$\begin{aligned} \widehat{\mathcal{H}}\mathcal{F}^{\perp} &= \widehat{U}\widehat{\Sigma}\widehat{V}^T \\ &= \begin{bmatrix} \widehat{U}_s & \widehat{U}_o \end{bmatrix} \begin{bmatrix} \widehat{\Sigma}_s & 0 \\ 0 & \widehat{\Sigma}_o \end{bmatrix} \begin{bmatrix} \widehat{V}_s^T \\ \widehat{V}_o^T \end{bmatrix}, \end{aligned} \tag{3.49}$$

where $\widehat{\Sigma}_s \in \mathbf{R}^{n \times n}$, we determine the system matrices $\widehat{A}$ and $\widehat{C}$ as

$$\begin{aligned} \widehat{A} &= (J_1\widehat{U}_s)^{\dagger} J_2 \widehat{U}_s, \\ \widehat{C} &= J_3 \widehat{U}_s, \end{aligned} \tag{3.50}$$

where

$$J_1 = \begin{bmatrix} I_{(q-1)p} & 0_{(q-1)p\times p} \end{bmatrix}, \tag{3.51}$$

$$J_2 = \begin{bmatrix} 0_{(q-1)p\times p} & I_{(q-1)p} \end{bmatrix}, \tag{3.52}$$

$$J_3 = \begin{bmatrix} I_p & 0_{p\times(q-1)p} \end{bmatrix}, \tag{3.53}$$

Provided that (C, A) is an observable pair, the pseudoinverse in Eq. (3.50) exists if and only if $q > n$. Therefore, in order to apply the lemma it suffices to let $q = n + 1$. In this case, we have the sole requirement $N > 2n$ with N defined by Eq. (3.43). From Lemma 3.1.1, it follows that $\widehat{A}$ and $\widehat{C}$ defined in Eq. (3.50) are related to A and C in Eq. (3.2) by

$$\begin{aligned} \widehat{A} &= T^{-1}AT, \\ \widehat{C} &= CT \end{aligned} \tag{3.54}$$

for some $T \in \mathbf{R}^{n\times n}$.

As noted before, in Eq. (3.49) $\widehat{\mathcal{H}}\mathcal{F}^{\perp}$ can be replaced with R_{22}.

3.1.2 Extracting B and D from the Data

We will now determine B and D matrices in the realization using the given frequency domain data. Repeated application of the differentiation formula

$$\frac{d}{dz}X^{-1} = -X^{-1}\frac{dX}{dz}X^{-1}$$

to $X_{\mathrm{C}}(z) = (zI_n - A)^{-1}B$ yields the derivatives of $G(z)$ as follows:

$$\frac{d^j}{dz^j}G(z) = \delta_{0j}\, D + (-1)^j j!\, C(zI_n - A)^{-j-1}B, \qquad j \geq 0, \tag{3.55}$$

where δ_{ks} is the Kronecker delta. Now, let

$$\mathcal{G}_k = \begin{bmatrix} w_{k0} \\ w_{k1} \\ \vdots \\ w_{kN_k} \end{bmatrix}, \qquad k = 1, \ldots, L, \tag{3.56}$$

and

$$\mathcal{G}=\begin{bmatrix} \mathcal{G}_1 \\ \mathcal{G}_2 \\ \vdots \\ \mathcal{G}_L \end{bmatrix}. \tag{3.57}$$

Observe from Eq. (3.55) that, for fixed A and C, the matrices B and D appear linearly in $\mathcal{G}$. Hence, we can uniquely determine B and D by solving the following linear least-squares problem

$$\widehat{B},\widehat{D} = \arg\min_{B,D} \left\| \widehat{\mathcal{G}} - \widehat{\mathcal{Y}} \begin{bmatrix} B \\ D \end{bmatrix} \right\|_F^2, \tag{3.58}$$

where

$$\widehat{\mathcal{G}} = \begin{bmatrix} \mathrm{Re}\mathcal{G} \\ \mathrm{Im}\mathcal{G} \end{bmatrix} \in \mathbf{R}^{pN\times m}, \tag{3.59}$$

$$\widehat{\mathcal{Y}} = \begin{bmatrix} \mathrm{Re}\mathcal{Y} \\ \mathrm{Im}\mathcal{Y} \end{bmatrix} \in \mathbf{R}^{pN\times (n+p)}, \tag{3.60}$$

and

$$\mathcal{Y}_k=\begin{bmatrix} C(z_kI_n - A)^{-1} & I_p \\ -C(z_kI_n - A)^{-2} & 0 \\ \vdots & \\ (-1)^{N_k}N_k!\,C(z_kI_n - A)^{-N_k-1} & 0 \end{bmatrix}, \tag{3.61}$$

$$\mathcal{Y}=\begin{bmatrix} \mathcal{Y}_1 \\ \mathcal{Y}_2 \\ \vdots \\ \mathcal{Y}_L \end{bmatrix}, \tag{3.62}$$

provided that $\widehat{\mathcal{Y}}$ is not rank deficient. For the last requirement, a sufficient condition is presented next.

Lemma 3.1.2. *Let N and $\widehat{\mathcal{Y}}$ be as in Eqs.* (3.43) *and* (3.60)*, respectively. Suppose that $N > n$ and the eigenvalues of A do not coincide with the distinct complex numbers z_k. Then,*

$$\mathrm{rank}\widehat{\mathcal{Y}} = p + n \qquad \Longleftrightarrow \qquad (C, A) \text{ observable pair.} \tag{3.63}$$

Proof. See Appendix B.2 □

Thus, from Eq. (3.54) and Lemma 3.1.2, if $N \geq q + n$ and $q > n$, we have

$$\begin{aligned} \widehat{B} &= T^{-1}B, \\ \widehat{D} &= D. \end{aligned} \tag{3.64}$$

Moreover,

$$\widehat{G}(z)=\widehat{C}(zI_n - \widehat{A})^{-1}\widehat{B} + \widehat{D} = G(z). \tag{3.65}$$

3.1.3 Solvability Conditions

By picking $q = n+1$ in the subspace-based algorithm developed above, we obtain a sufficient condition for the interpolation of $G(z)$ from its noise-free samples and derivatives evaluated at L distinct points in ϑ as $N \geq 2n + 1$, where N is defined by Eq. (3.43). This condition turns out to be a necessary condition for the interpolation of $G(z)$, as demonstrated next by a simple example.

Consider an nth-order stable single-input/single-output system represented by the transfer function

$$G(z) = \frac{b_0 z^n + b_1 z + \cdots + b_n}{z^n + a_1 z + \cdots + a_n}. \tag{3.66}$$

We are to determine $2n+1$ unknown real coefficients $a_1, \ldots, a_n, b_0, \ldots, b_n$ from the evaluations of $G(z)$ and its derivatives at a given set of distinct frequencies $z_k \in \vartheta$. Let N be as in Eq. (3.43).

Let us first assume in Eq. (3.4) that $N_k = 0$ and $z_k \in \mathbf{C} - \mathbf{R}$ for all k; i.e., the interpolation nodes are simple and purely complex numbers. Then, $N = 2L$. With $q = n + 1$, the subspace-based algorithm delivers a minimal realization of $G(z)$, provided that $2L \geq 2n + 1$. This condition is satisfied by choosing $L = n + 1$. Clearly, this is the least amount of data one could use to interpolate an arbitrary nth-order system, as can directly

be verified by writing $2L$-linear equations down from Eqs. (3.4) and (3.66) to determine the unknowns $a_1, \ldots, a_n, b_0, \ldots, b_n$. Notice that if some interpolation nodes have multiplicities, then the resulting equations become nonlinear in $a_1, \ldots, a_n, b_0, \ldots, b_n$.

Now, as a special case, let us consider the situation that all z_k are on the unit circle excluding the points ± 1. Thus, Algorithm 3.1.1 recovers nth-order stable systems from $n+1$ noise-free frequency response measurements, excluding the frequencies 0 and π. If the frequencies contain 0, from Eq. (3.43) we then have $N = 2L - 1$. Hence, with $q = n + 1$ selected, we must have $2L - 1 \geq 2n + 1$, which is fulfilled by letting $L = n + 1$. If, in addition, the frequencies contain π as well, we end up with the interpolation condition $L = n+2$. The last conclusion extends an interpolation result in [62] derived for the uniformly spaced frequencies case to the nonuniformly spaced frequencies case.

It is easy to see, for example, by the partial fraction expansion or similar techniques, that these results hold for multi-input/multi-output systems with multiple interpolation nodes as well. Therefore, Algorithm 3.1.1 is capable of using a minimum amount of the frequency domain data for the Lagrange–Sylvester interpolation of stable systems.

3.1.4 Summary of the Subspace-Based Interpolation Algorithm

Let us summarize the interpolation algorithm in the following.

Algorithm 3.1.1. *Subspace-based interpolation algorithm.*

1. *Given the data as in Eq.* (3.4)*, compute the matrices* $\widehat{\mathcal{H}}$ *and* $\mathcal{F}$ *defined by Eqs.* (3.39) *and* (3.40) *through Eqs.* (3.34)*,* (3.36)*,* (3.28)*,* (3.31)*,* (3.26)*,* (3.29)*,* (3.19)*, and* (3.18)*.*

2. *Perform the QR-factorization in Eq.* (3.46)*.*

3. *Calculate the singular value decomposition in Eq.* (3.49) *with* $\widehat{\mathcal{H}}\mathcal{F}^{\perp}$ *replaced by* R_{22} *defined in Eq.* (3.46)*.*

4. *Determine the system order by inspecting the singular values, and partition the singular value decomposition such that* $\widehat{\Sigma}_s$ *contains the* n *largest singular values.*

5. *With* J_1, J_2, *and* J_3 *defined by Eqs.* (3.51)–(3.53), *calculate* $\widehat{A}$ *and* $\widehat{C}$ *from Eq.* (3.50).

6. *Solve the least-squares problem* (3.58) *for* $\widehat{B}$ *and* $\widehat{D}$, *where* $\widehat{\mathcal{G}}$ *and* $\widehat{\mathcal{Y}}$ *are defined by Eqs.* (3.59) *and* (3.60) *through Eqs.* (3.61)–(3.62) *and* (3.56)–(3.57).

Clearly, $\widehat{\Sigma}_o = 0$ in Eq. (3.49) when the data are not corrupted by noise, the system that has generated the data is of McMillan degree n, $N \geq q + n$, and $q > n$. As we stated earlier, Algorithm 3.1.1 produces a minimal stable realization of the interpolant, given that the latter exits. In most interpolation problems, the existence and the uniqueness questions are easily settled, and the construction of a solution (or all solutions) with certain properties such as the McMillan degree constraints, in particular minimality, remains a difficult one. The algorithm outlined above is straightforward to implement. In the implementation of the algorithm, it suffices to let $q = n + 1$ and $N = 2n + 1$, where N is defined by Eq. (3.43). The system order, if unknown a priori, can be determined in Step 4 of Algorithm 3.1.1 from the inspection of the singular values. This process also reveals redundancies in the data. Numerically, the most expensive step in the algorithm is the singular value decomposition of R_{22}. Notice with $q = n + 1$ and $N = 2n + 1$ selected, that $R_{22} \in \mathbf{R}^{p(n+1)\times mn}$.

The main result of this chapter is captured in the following.

Theorem 3.1.1. *Consider Algorithm* 3.1.1 *with the data in Eq.* (3.4) *originating from a discrete-time stable system of order* n. *Let* N *be as in Eq.* (3.43). *If* $N \geq q+n$ *and* $q > n$, *then the quadruplet* $(\widehat{A}, \widehat{B}, \widehat{C}, \widehat{D})$ *is a minimal realization of* $G(z)$.

3.1.5 Discussion

In the rest of this section, we will briefly comment on the similarities and the differences between Algorithm 3.1.1 and the Löwner matrix–based approach [103].

The most striking difference between the methods appears to be the formation of data matrices. In [103], elements of a Löwner matrix are computed by taking partial derivatives of the divided differences $[G(z) - G(s)]/(z - s)$ evaluated at $z = z_k$ and $s = z_l$, where the number of the derivatives is determined by the particular choice of the (block) row and column sets and the multiplicities of the nodes. If z_k equals z_l, a limiting process has to be used to define that particular element. It is required that the numbers of the chosen block rows and columns add up to N. The elements of $\mathcal{H}$ in the proposed algorithm, on the other hand, consist of linear combinations of the derivatives of the products $z^l G(z)$ evaluated at $z = z_k$, where for each k, l satisfies $0 \leq l \leq N_k$. A simple transformation that relates $\mathcal{H}$ to a Löwner matrix does not seem possible unless all the z_k are the same, in which case the problem solved reduces to a conventional partial realization problem. In the latter case, notice that this link is provided by the bilinear map as in Eq. (3.5).

Both algorithms rely on the factorization of the data matrices discussed above as a product of two matrices which are directly related to the observability and controllability concepts. In [103], the Löwner matrix is expressed as a product of the so-called generalized observability and the controllability matrices, whereas in the proposed algorithm this relation is recovered after some projections. In fact, the proofs of Lemmas 3.1.1, 3.1.2, and 3.1R in [103] use the same ideas.

The most striking similarity between the algorithms is the condition $N > 2n$. It should be noted that the stability assumption is not essential in the formulation of the interpolation problem, since the data are already assumed to originate from a finite-dimensional dynamical system with a complexity bounded above and the number of the nodes is finite. This assumption

is necessary in an identification setup. Without the knowledge that the data have originated from a dynamical system with a complexity bounded above, the condition $N > 2n$ is precisely one of the requirements for the existence of a unique minimal-order interpolating rational matrix [103]. In addition to this requirement, there is also a more stringent rank condition captured in Assumption 4.1 in [103]. Thus, both algorithms operate under the same conditions which assure the existence of a unique minimal interpolating rational matrix. We have not addressed the properness issue in this chapter due to our standing assumption on the origins of the data. Again, without the knowledge of the origins of the data, one has to secure that the solution of the interpolation problem is a proper transfer function. The properness is guaranteed by Assumption 4.2 in [103]. It is also noted there that this assumption can be eliminated by means of a suitably chosen bilinear transformation.

The Löwner matrix–based and proposed algorithms cannot be directly applied when there does not exist a unique minimal interpolating function and the data are not scalar. This may happen either in the presence of noise which corrupts transfer function evaluations or when the true dynamics is of higher dimension. The problem is then to find the admissible degrees of complexity, i.e., those positive integers n for which there exist solutions $G(z)$ to the interpolation problem (3.4) with $deg\, G = n$, and to construct all corresponding solutions for a given admissible degree n. This problem is known as the partial realization problem. If the original data do not satisfy the criterion for the existence of a unique minimal interpolating function, one needs to add interpolation data until the criterion becomes satisfied. The fact that the data can be found so that the increase in degree is finite is nontrivial. The added data will necessarily drive up the degree of the interpolating transfer function. In the scalar case, dealt with in [104], the way this can be done is set out and is rather complicated. The multivariable case is studied in [106] using the generating system approach. While [106] gives the theory behind the determination of the minimal McMillan degree and all admissible degrees, the current chapter and [103] provide the theory behind the construction in state-space

terms of the solution of admissible degrees.

A departure of Algorithm 3.1.1 from the Löwner matrix–based approach is the determination of the minimal order. Under the stated conditions, in Algorithm 3.1.1 the minimal order and the observability range space are extracted by a singular value decomposition, while in the Löwner matrix–based approach the minimal order is determined by checking ranks of several (generalized) Löwner matrices. The singular value decomposition is not sensitive to random inaccuracies in data; that is, the true singular values and the observability range space are consistently estimated as N increases unboundedly, provided that n is finite or increases more slowly than N [62, 91]. To our best knowledge, an asymptotic error analysis for randomly corrupted transfer function evaluations has not been performed for any of the interpolation algorithms in the literature.

Deficiencies of the proposed interpolation algorithm and the Löwner matrix–based approach are the same. As pointed out in [103], a parameterization of solutions when the original data have to be added and derivation of recursive formulae for allowing update of a realization when one or more interpolation data become available are absent. It would be interesting to develop connections between the constrained interpolation problems such as the Nevanlinna–Pick and the positive-real interpolation and Algorithm 3.1.1. It is worth mentioning that the Nevanlinna–Pick interpolation can be transformed into an interpolation problem without norm constraint by adding the mirror image interpolation points to the original data [105].

3.2 Subspace-Based Identification with Interpolation Constraints

In this section, we will consider identification of an nth-order stable system with transfer function $G(z)$ from noisy samples of the frequency re-

sponse,

$$w_l = G(e^{i\theta_l}) + \eta_l, \qquad l = 1, \ldots, M, \tag{3.67}$$

with the interpolation constraints

$$\frac{d^j}{dz^j} G(z)\bigg|_{z=z_k} = E_{kj}, \qquad j = 0, 1, \ldots, N_k, \;\; k = 1, \ldots, L, \tag{3.68}$$

where $0 \leq \theta_l \leq \pi$, $l = 1, \ldots, M$, denote the discrete-time frequencies and η_l is a sequence of independent zero-mean complex random variables with a known covariance function that is uniformly bounded. The number of the constraints defined in Eq. (3.43) satisfies $N < n$. The interpolation constraints in Eq. (3.68) reflect the prior knowledge on $G(z)$. For example, by taking $E_{kj} = 0$ for all $j \leq N_k$, we enforce a zero with multiplicity $N_k + 1$ at z_k. These constraints may also be used as design variables to focus on a frequency band of interest.

We would like to find an identification algorithm which maps the data $\{w_l, \theta_l\}_{l=1}^M$ to an nth-order model $\widehat{G}_M(z)$ that satisfies the interpolation constraints in (3.68) such that, with probability one,

$$\lim_{M \to \infty} \|\widehat{G}_M - G\|_\infty = 0,$$

Algorithms with this property are called *strongly consistent*. This identification setup except for the constraints in Eq. (3.68) can be found, for example, in [62].

A motivating example for the constraints in Eq. (3.68) is as follows. Suppose that the system to be identified is nth order stable single-input/single-output continuous-time system represented by the transfer function

$$G^c(s) = \frac{b_0 s^m + b_1 s + \cdots + b_m}{s^n + a_1 s + \cdots + a_n}, \tag{3.69}$$

where the denominator degree n is greater than the numerator degree m, and we are given M noise corrupted frequency response measurements

$$w_l = G(i\omega_l) + \eta_l, \qquad l = 1, \ldots, M. \tag{3.70}$$

Assuming $b_0 \neq 0$, the *relative degree* of $G^c(s)$ is defined as $\tau{=}n - m$.

A direct use of the Möbius transform technique in Eq. (3.5) targets

identifying the discrete-time equivalent of $G^c(s)$ defined by

$$G^d(z)=G^c\left(\psi(z)\right), \tag{3.71}$$

using w_l, $l = 1, \ldots, M$, at the transformed discrete-time frequencies

$$\theta_k = 2\arctan\left(\frac{\omega_k}{\lambda}\right), \qquad k = 1, \ldots, M. \tag{3.72}$$

Then, the continuous-time identified transfer function denoted by $\widehat{G}^c_M(s)$ is obtained from the discrete-time identified transfer function denoted by $\widehat{G}^d_M(z)$ by using the inverse Möbius map $z = \psi^{-1}(s)$; i.e., $\widehat{G}^c_M(s) = \widehat{G}^d_M(\psi^{-1}(s))$. Due to noise and unmodeled dynamics, the former is only a proper transfer function.

If maintaining the relative degree as a concern, we then high-pass filter $\widehat{G}^c_M(s)$ as follows:

$$\widehat{G}_M(s) = \frac{\widehat{G}^c_M(s)}{(s+\mu)^\tau},$$

where $\mu > 0$ is chosen sufficiently outside the bandwidth of $\widehat{G}^c_M(s)$. This filtering increases the order of the identified model by τ. This problem can be circumvented by including the constraints

$$\left.\frac{d^j}{dz^j}G^d(z)\right|_{z=-1} = 0, \qquad j = 1, \ldots, \tau,$$

in the problem formulation. Observe that when applied to Eq. (3.69), the Möbius map (3.5) introduces a zero of $G^d(z)$ at $z = -1$ with multiplicity τ.

Now, the solution of the constrained identification problem in Eq. (3.67)–(3.68) is particularly simple if one notes from Eq. (3.55) the following set of equations:

$$\delta_{0j}\, D + (-1)^j j!\, C(z_k I_n - A)^{-j-1} B = E_{kj}, \;\; j = 0, \ldots, N_k, \;\; k = 1, \ldots, L, \tag{3.73}$$

which describe N hyperplanes in the parameter space of B and D for fixed C and A. Hence, it suffices to solve the linear least-squares problem in Eq. (3.58) with the linear constraints in Eq. (3.73). With this modification, the frequency domain subspace-based identification algorithm presented in [62] is strongly

consistent. The inclusion of the noise covariance information in the algorithm is straightforward and can be found in [62]. This extension can be viewed as the tangential version of the Lagrange–Sylvester interpolation problem in Eq. (3.1).

3.3 Example

The purpose of this section is to illustrate Algorithm 3.1.1 with a step-by-step numerical example. Suppose that the system to be found by interpolation has the following state-space representation:

$$A = \begin{bmatrix} -0.5 & 0.5 & 0 & 0 \\ -0.5 & -0.5 & 0 & 0 \\ 0 & 0 & 0.5 & 0 \\ 0 & 0 & 0 & -0.25 \end{bmatrix}, \qquad B = \begin{bmatrix} 1 & 0 & 0 \\ 1 & 1 & 0 \\ 0 & -1 & 0 \\ 1 & 1 & 1 \end{bmatrix},$$

$$C = \begin{bmatrix} 1 & 1 & 1 & 0 \\ 0 & 1 & 0 & 1 \end{bmatrix}, \qquad D = \begin{bmatrix} 1 & -1 & 0 \\ 0 & 1 & 1 \end{bmatrix}.$$

Thus, $n = 4$, $p = 2$, and $m = 3$. This system has the transfer function

$$G(z) = \begin{bmatrix} \dfrac{z^2 + 3z + 1.5}{z^2 + z + 0.5} & -\dfrac{z^3 + 0.5z^2 + 0.5z + 0.75}{z^3 + 0.5z^2 - 0.25} & 0 \\ \dfrac{2z^2 + 1.25z + 0.5}{z^3 + 1.25z^2 + 0.75z + 0.125} & \dfrac{z^3 + 3.25z^2 + 2.5z + 0.75}{z^3 + 1.25z^2 + 0.75z + 0.125} & \dfrac{z + 1.25}{z + 0.25} \end{bmatrix}.$$

Let us assume that the interpolation data are as follows:

$$z_1 = 1 + i,\ N_1 = 0,\ z_2 = 1 - i,\ N_2 = 0,\ z_3 = 2,\ N_3 = 4$$

and

$$w_{10} = \begin{bmatrix} 1.9333 - 0.5333i & -0.8667 + 0.4000i & 0 \\ 0.8878 - 0.5236i & 1.9545 - 0.6569i & 1.4878 - 0.3902i \end{bmatrix},$$

$$w_{20} = \begin{bmatrix} 1.9333 + 0.5333i & -0.8667 - 0.4000i & 0 \\ 0.8878 + 0.5236i & 1.9545 + 0.6569i & 1.4878 + 0.3902i \end{bmatrix},$$

$$
\begin{aligned}
w_{30} &= \begin{bmatrix} 1.7692 & -1.2051 & 0 \\ 0.7521 & 1.8291 & 1.4444 \end{bmatrix}, \\
w_{31} &= \begin{bmatrix} -0.2840 & 0.2433 & 0 \\ -0.2804 & -0.3395 & -0.1975 \end{bmatrix}, \\
w_{32} &= \begin{bmatrix} 0.2003 & -0.4251 & 0 \\ 0.2084 & 0.2757 & 0.1756 \end{bmatrix}, \\
w_{33} &= \begin{bmatrix} -0.2000 & 0.9844 & 0 \\ -0.2333 & -0.3341 & -0.2341 \end{bmatrix}, \\
w_{34} &= \begin{bmatrix} 0.2456 & -2.8518 & 0 \\ 0.3531 & 0.5390 & 0.4162 \end{bmatrix}.
\end{aligned}
$$

Then we set $q = 5$ and compute $N = 9$. Therefore, the inequalities $N \geq q + n$ and $q > n$ are both satisfied. In Step 1, we compute the matrices $\widehat{\mathcal{H}} \in \mathbf{R}^{10\times 27}$ and $\mathcal{F} \in \mathbf{R}^{15\times 27}$. The QR-factorization in Step 2 results in $R_{22} \in \mathbf{R}^{10\times 12}$ given by

$$
R_{22} = \begin{bmatrix}
-0.4622 & 0 & 0 & 0 & 0 & \cdots & 0 \\
0.0381 & -0.0518 & 0 & 0 & \vdots & \ddots & \vdots \\
-0.2544 & 0.0203 & -0.0240 & 0 & & & \\
-0.0176 & 0.0194 & -0.0075 & -0.0009 & & & \\
-0.1144 & -0.0070 & 0.0091 & -0.0089 & & & \\
0.0094 & -0.0110 & 0.0094 & -0.0025 & & & \\
-0.0583 & 0.0035 & -0.0045 & 0.0045 & & & \\
-0.0033 & 0.0057 & -0.0061 & 0.0037 & & & \\
-0.0344 & 0.0033 & -0.0037 & -0.0022 & \vdots & \ddots & \vdots \\
-0.0007 & -0.0013 & 0.0015 & -0.0027 & 0 & \cdots & 0
\end{bmatrix},
$$

which is not unexpected since $n = 4$. In Step 3, we compute the nonzero singular values 0.5460, 0.0609, 0.0249, and 0.0098. The matrices $\widehat{A}$ and $\widehat{C}$

computed in Step 5 are

$$\widehat{A} = \begin{bmatrix} 0.5204 & -0.1361 & 0.3199 & 0.5352 \\ 0.0882 & -0.4983 & 0.4848 & -0.1035 \\ 0.0052 & 0.0820 & -0.4810 & 0.7195 \\ -0.0295 & 0.1919 & -0.3546 & -0.2911 \end{bmatrix},$$

$$\widehat{C} = \begin{bmatrix} 0.8460 & 0.2123 & -0.2149 & -0.3233 \\ -0.0721 & 0.8069 & 0.5289 & 0.1046 \end{bmatrix}.$$

In Step 6, we compute $\widehat{\mathcal{G}} \in \mathbf{R}^{18\times 3}$ and $\widehat{\mathcal{Y}} \in \mathbf{R}^{18\times 6}$ matrices, and the solution of the least-squares problem is

$$\widehat{B} = \begin{bmatrix} 1.0502 & -0.5390 & -0.0816 \\ 2.8626 & 1.8321 & 0.9041 \\ -0.1545 & 1.0984 & 0.4896 \\ -1.4555 & -0.9375 & 0.0547 \end{bmatrix},$$

$$\widehat{D} = \begin{bmatrix} 1.0000 & -1.0000 & -0.0000 \\ -0.0000 & 1.0000 & 1.0000 \end{bmatrix}.$$

The realization $(\widehat{A}, \widehat{B}, \widehat{C}, \widehat{D})$ is similar to (A, B, C, D). In fact, the estimates of the interpolation data computed from the former has a maximum error 5.9746×10^{-14}.

3.4 Summary

In this chapter, we presented a new algorithm for the Lagrange–Sylvester interpolation of rational matrix functions that are analytic at infinity. This algorithm is related to the recent frequency domain subspace-based identification methods and is not sensitive to inaccuracies in data. A necessary and sufficient condition for the existence and the uniqueness of a minimal interpolant was formulated in terms of the total multiplicity of the interpolation nodes. The purpose of this contribution was to pinpoint the kinship between the frequency domain subspace-based identification of stable linear systems and the minimal rational interpolation of stable systems.

4 ACHIEVABLE PERFORMANCE FOR QUARTER-CAR ACTIVE SUSPENSIONS

Active and semi-active control of vehicle suspensions have been the subject of considerable investigation since the late 1960s; see, for example [2, 3,6,8,9,12] and the references therein. Constraints and trade-offs on achievable performances have been studied in [19–22]. As put forward in [20], in a study of constraints and trade-offs from a control systems point of view, one has to properly address:

(i) what can and can not be achieved with general dynamic compensation,

(ii) how much freedom is gained by the selection of measurements for feedback purpose?

In [18, 22], constraints on achievable frequency responses were derived from an *invariant point* perspective. A framework using mechanical multi-port networks to study the performance capabilities and constraints was developed in [21]. In [20], for a quarter-car model of an automative suspension a *complete* set of constraints on several transfer functions of interest from the road and the load disturbances were determined by making use of the *factorization* approach to feedback stability and the Youla *parameterization* of stabilizing controllers. Roughly speaking, completeness means that from a given set of constraints, one can identify a quarter-car model within the model class matching the given constraints. Such an approach reveals the degrees of freedom in shaping the response of the vehicle to disturbances and determines a minimum set of measurements to exploit this freedom.

In [20], constraints on the frequency responses of the sprung mass position, the suspension travel, and the tire deflection were derived for various choices of measurements ranging from the suspension travel to a full set of state variables. These constraints typically arise in the form of finite and

nonzero invariant frequency points and the growth restrictions on the frequency responses and their derivatives at zero and infinite frequencies. The quarter-car model studied in [20] does not include passive suspension elements spring and damper; and also tire damping is neglected.

In most works, tire damping is set to zero when modeling automotive active suspension systems. This is partly due to the fact that tire damping is difficult to estimate. It is generally accepted that damping ratio in a vehicle tire ranges between 0.03 and 0.10 depending on the size, applied pressure, free or rotating, new or worn, and the tire type *i.e.,* all season or snow [23–25]. The tire damping by itself has little influence on the wheel-hop vibration since this mode is mainly damped by the shock absorber.

The ignorance of damping in tire models compelled misleading conclusions that at the wheel-hop frequency, no matter what forces are exerted between sprung and unsprung masses, their motion are uncoupled, and the vertical acceleration of the sprung mass will be unaffected [18, 20, 22]. It is pointed out in [26] that by taking tire damping to be small but nonzero, the motions of the sprung and unsprung masses are coupled at all frequencies, and control forces can be used to reduce the sprung mass vertical acceleration at the wheel-hop frequency. The effect of introducing tire damping can be quite large.

The chapter is structured as follows. First, the results in [20] are complemented assuming that

(i) the sprung mass acceleration measurement instead of the sprung mass position measurement is used for the parametrization of the stabilizing controllers,

(ii) the closed-loop sprung mass acceleration is targeted instead of the closed-loop sprung mass position for the evaluation of ride comfort,

(iii) the passive suspension elements are included in the vehicle model. The differences and the similarities between the derived results and [20] are

emphasized. For example, it is demonstrated that employment of the sprung mass acceleration as a measurement and performance objective in a vehicle model that includes passive suspension elements affects the parameterizability of the stabilizing controllers.

It is reminded that a semi-active suspension consists of in series a spring and damper whose coefficient is changed in a nonlinear fashion. In a semi-active suspension, ride comfort is taken care of by a nonlinear damper while safety requirements are met by a fixed spring.

Next, the effect of tire damping on the achievable performance is investigated. The results predicate the conclusions in [26, 130, 131] that tire damping couples the motions of the sprung and unsprung masses, and control forces can be used to reduce the sprung mass vertical acceleration at the wheel-hop frequency without sacrificing road holding.

4.1 The Quarter-Car Model

A two-degree-of-freedom quarter-car model is shown in Figure 4.1. In this model, the sprung and unsprung masses are denoted, respectively, by m_s and m_u. The suspension system is represented by a linear spring of stiffness k_s and a linear damper with a damping rate c_s. The tire is modeled by a linear spring of stiffness k_t and a linear damper with a damping rate c_t. The parameter values, except c_t, chosen for this study are shown in Table 4.1 [41]. They are typical for a lightly damped passenger car. The parameters m_s, m_u, and k_t are fixed throughout the chapter while the parameters $k_s, c_s,\ c_t$ are freely changed.

Assuming that the tire behaves as a point-contact follower that is in contact with the road at all times, the equations of motion take the form

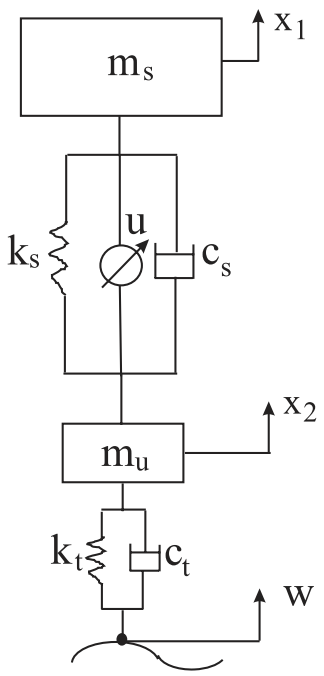

Figure 4.1: The quarter-car model of the vehicle.

$$\begin{aligned} m_s\ddot{x}_1 &= -k_s(x_1 - x_2) - c_s(\dot{x}_1 - \dot{x}_2) - u, \\ m_u\ddot{x}_2 &= k_s(x_1 - x_2) + c_s(\dot{x}_1 - \dot{x}_2) + u - k_t(x_2 - w) - c_t(\dot{x}_2 - \dot{w}) \end{aligned} \tag{4.1}$$

where x_1 and x_2 are respectively the displacements of the sprung and unsprung masses, and w is the road unevenness. The variables x_1, x_2, and w are measured with respect to an inertial frame, and the control input u is a force.

The objective of this chapter is to study the performance limits of an actively controlled vehicle imposed by the road surface unevenness. The vehicle response variables that need to be examined are the vertical acceleration of the sprung mass as an indicator of the vibration isolation, the suspension travel as a measure of the rattling space, and the tire deflection as an indicator

Table 4.1: The vehicle system parameters for the quarter-car model.

Sprung mass	m_s	240 kg
Unsprung mass	m_u	36 kg
Damping coefficient	c_s	980 Ns m^{-1}
Secondary suspension stiffness	k_s	16,000 N m^{-1}
Primary suspension stiffness	k_t	160,000 N m^{-1}

of the road-holding characteristic of the vehicle. These variables, denoted respectively by z_1, z_2, and z_3, can be written in terms of the state variables x_1, x_2, their derivatives, and the exogenous input w as follows:

$$z_1 = \ddot{x}_1, \tag{4.2}$$

$$z_2 = x_1 - x_2, \tag{4.3}$$

$$z_3 = x_2 - w. \tag{4.4}$$

Passenger comfort requires z_1 to be as small as possible while compactness of rattle space, good handling characteristics, and improved road-holding quality require z_2 and z_3 be kept as small as possible.

It is a well-known fact [19] that these objectives can not be met simultaneously with a passive suspension system. In a passive suspension system, the only parameter that can be altered in an optimization study is c_s since k_s is *a priori* fixed to obtain stiffness against rolling. The conflicting three goals can be attained up to a certain level by replacing passive suspension system with an active or semi-active suspension system [5–8, 10, 20, 41].

4.2 Factorization Approach to Feedback Stability

In this section, the factorization approach developed in [20] for the feedback stability of the quarter-car model is briefly reviewed. The reader is referred to Vidyasagar and Zhou *etal.* [17, 132] for a comprehensive treatment.

Let $Z(s)$, $U(s)$, and $W(s)$ denote respectively the Laplace transforms of the signals $z(t) = [z_1(t)\ z_2(t)\ z_3(t)]^T$, $u(t)$, and $w(t)$. From Eqs. (4.1)–(4.4),

$$Z(s) = G_{11}(s)W(s) + G_{12}(s)U(s) \tag{4.5}$$

where

$$\begin{aligned} G_{11}(s) &= \frac{1}{\Delta(s)} \begin{bmatrix} s^2(c_s s + k_s)(c_t s + k_t) \\ -m_s s^2(c_t s + k_t) \\ -s^2\left[m_s m_u s^2 + (m_s + m_u)c_s s + (m_s + m_u)k_s\right] \end{bmatrix}, \\ G_{12}(s) &= \frac{1}{\Delta(s)} \begin{bmatrix} -s^2(m_u s^2 + c_t s + k_t) \\ -[(m_s + m_u)s^2 + c_t s + k_t] \\ m_s s^2 \end{bmatrix}, \end{aligned} \tag{4.6}$$

and

$$\begin{aligned} \Delta(s) &= m_s m_u s^4 + [(m_s + m_u)c_s + m_s c_t]s^3 + (c_s k_t + c_t k_s)s + k_s k_t \\ &\quad + [(m_s + m_u)k_s + m_s k_t + c_s c_t]s^2. \end{aligned} \tag{4.7}$$

A polynomial $\Delta(s)$ is said to be *Hurwitz* if all its zeros lie in the open left-half plane. Note that $\Delta(s)$ is Hurwitz if $k_s, k_t > 0$, and $c_s > 0$ or $c_t > 0$.

For the design of a feedback law, consider the measurements:

$$\begin{aligned} y_1 &= \ddot{x}_1, \\ y_2 &= x_1 - x_2. \end{aligned} \tag{4.8}$$

In the study of the constraints, the cases $y = y_2$ and $y = [y_1\ y_2]^T$ will be considered. When $y = [y_1\ y_2]^T$, from Eqs. (4.1)–(4.4),

$$Y(s) = G_{21}(s)W(s) + G_{22}(s)U(s) \tag{4.9}$$

where

$$G_{21}(s) = \frac{1}{\Delta(s)} \begin{bmatrix} s^2(c_s s + k_s)(c_t s + k_t) \\ -m_s s^2(c_t s + k_t) \end{bmatrix}, \tag{4.10}$$

$$G_{22}(s) = -\frac{1}{\Delta(s)} \begin{bmatrix} s^2(m_u s^2 + c_t s + k_t) \\ (m_s + m_u)s^2 + c_t s + k_t \end{bmatrix}. \tag{4.11}$$

The other case is obtained by simply selecting the second rows of G_{21} and G_{22}. Hence, the generalized plant defined by

$$G(s) = \left[\begin{array}{c|c} G_{11}(s) & G_{12}(s) \\ \hline G_{21}(s) & G_{22}(s) \end{array}\right] \tag{4.12}$$

maps the pair of inputs $[w\ u]^T$ to the pair of outputs $[z^T\ y^T]^T$.

Now, let $K(s)$ denote the transfer function of the controller with input y and the output u. The feedback configuration is shown in Figure 4.2.

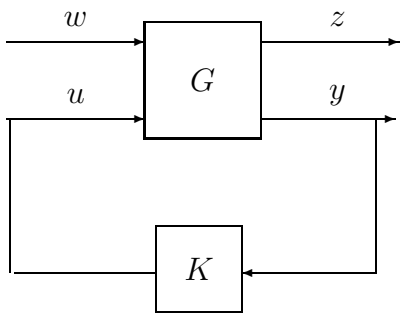

Figure 4.2: Standard block diagram.

The stabilization problem is to find a proper feedback transfer function K such that the closed-loop system in Figure 4.2 is *internally stable*. Assuming that G and G_{22} share the same unstable poles, it is a well-known fact (see, for example, Lemma 12.2 in [17]) that K internally stabilizes G if and only if K internally stabilizes G_{22}. Recall that the unstable poles of G are the roots of $\Delta(s)$ in the closed right-half plane. Assuming that G_{22} is internally stabilizable, the set of all compensators which stabilize G can be parametrized in terms of a *coprime factorization* of G_{22}. This parametrization is called the Youla parametrization.

The Youla parametrization is obtained as follows. Recall that $\mathcal{RH}_\infty^{\mathrm{pq}}$ is the set of stable p by q real-rational transfer matrices. (In what follows, superscripts p and q will be dropped and they will be inferred from the underlying context). Given G_{22}, find matrices N,M,$\widetilde{N}$,$\widetilde{M}$,X,Y, $\widetilde{X}$, and $\widetilde{Y}$ in $\mathcal{RH}_\infty$

such that

$$G_{22} = NM^{-1} = \widetilde{M}^{-1}\widetilde{N}, \tag{4.13}$$

$$\begin{bmatrix} \widetilde{X} & -\widetilde{Y} \\ -\widetilde{N} & \widetilde{M} \end{bmatrix} \begin{bmatrix} M & Y \\ N & X \end{bmatrix} = I. \tag{4.14}$$

The factorization Eq. (4.13) of G_{22} satisfying Eq. (4.14) is called *double* coprime factorization over $\mathcal{RH}_\infty$. Then, the Youla parametrization of all stabilizing controllers takes the form:

$$K = (Y - MQ)(X - NQ)^{-1}, \;\; Q \in \mathcal{RH}_\infty; \; \det(I - X^{-1}NQ)(\infty) \neq 0. \tag{4.15}$$

With this parametrization, the transfer matrix from w to z denoted by $T_{zw}(s)$ takes a particularly convenient form which is affine in Q:

$$T_{zw} = G_{11} + G_{12}(Y - MQ)\widetilde{M}G_{21}. \tag{4.16}$$

As Q varies over $\mathcal{RH}_\infty$, Eq. (4.16) parametrizes all achievable transfer matrices.

4.3 Achievable Performance for Quarter-Car Model

In the design of an active suspension system, it is desirable to keep the road response amplitudes $|T_{z_k w}(j\omega)|$, $k = 1, 2, 3$ as small as possible, at least in the frequency range of interest. The aim of this section is to investigate the limitations on this goal for the two measurement set-ups and several assumptions on k_s, c_s, and c_t. By using the factorization approach, a complete set of constraints on the transfer functions $T_{z_k w}(s)$, $k = 1, 2, 3$ will be derived.

The first case to be treated in the sequel is the case $y = y_2$ with the assumption that k_s, c_s, and c_t are all positive. Then, as noted previously, $\Delta(s)$ is a Hurwitz polynomial and a pair of coprime factors for

$$G_{22} = -\Delta^{-1}[(m_s + m_u)s^2 + c_t s + k_t] \tag{4.17}$$

is easily found as

$$N = \widetilde{N} = G_{22}, \qquad M = \widetilde{M} = 1. \tag{4.18}$$

Furthermore, the choice given by

$$X = \widetilde{X} = G_{22} + 1, \qquad Y = \widetilde{Y} = 1 \tag{4.19}$$

enforces Eq. (4.14) as can directly be verified. Now, put $\widehat{Q} = 1 - Q$ where $Q \in \mathcal{RH}_\infty$. Then, T_{zw} and K in Eqs. (4.16) and (4.15) take the following forms:

$$T_{z_1w} = s^2\Delta^{-1}(c_ts + k_t)\left\{c_ss + k_s + \widehat{Q}m_ss^2\Delta^{-1}(m_us^2 + c_ts + k_t)\right\} \tag{4.20}$$

$$T_{z_2w} = -m_ss^2\Delta^{-1}(c_ts + k_t)\left\{1 - \widehat{Q}\Delta^{-1}[(m_s + m_u)s^2 + c_ts + k_t]\right\} \tag{4.21}$$

$$T_{z_3w} = -s^2\Delta^{-1}[m_sm_us^2 + (m_s + m_u)c_ss + (m_s + m_u)k_s] - \widehat{Q}m_s^2s^4\Delta^{-2}(c_ts + k_t) \tag{4.22}$$

$$K = \widehat{Q}(1 + G_{22}\widehat{Q})^{-1}. \tag{4.23}$$

The first constraint is obtained by observing that the coefficient of $\widehat{Q}$ in the expression for T_{z_1w} is $O(s^4)$ for all sufficiently small complex numbers s and every transfer matrix in $\mathcal{RH}_\infty$ has elements uniformly bounded on the closed right-half plane.

Therefore, a Taylor series expansion of the term $s^2\Delta^{-1}(c_ss + k_s)(c_ts + k_t)$ in a neighborhood of zero which is accurate up to the term $O(s^4)$ will be sufficient to determine the behavior of T_{z_1w} there. By long division,

$$s^2\Delta^{-1}(c_ss + k_s)(c_ts + k_t) = s^2 + O(s^4). \tag{4.24}$$

Hence, for all small s,

$$T_{z_1w} = s^2 + O(s^4), \tag{4.25}$$

which implies,

$$T_{z_1w}(0) = T^{(1)}_{z_1w}(0) = T^{(3)}_{z_1w}(0) = 0, \qquad T^{(2)}_{z_1w}(0) = 2. \tag{4.26}$$

For all large s, observe that the coefficient of $\widehat{Q}$ in the expression for T_{z_1w} is $O(s^{-1})$. Thus, a Taylor series expansion of the term $s^2\Delta^{-1}(c_ss +$

$k_s)(c_t s + k_t)$ around infinity which is accurate up to a term $O(s^{-1})$ is obtained, again by long division, as

$$s^2\Delta^{-1}(c_s s + k_s)(c_t s + k_t) = \frac{c_s c_t}{m_s m_u} + O(s^{-1}). \tag{4.27}$$

Hence,

$$T_{z_1 w} = \frac{c_s c_t}{m_s m_u} + O(s^{-1}). \tag{4.28}$$

It remains to show that Eqs. (4.25) and (4.28) form a complete set of constraints, *i.e.,* no further constraints on $T_{z_1 w}$, which are valid for all $Q \in \mathcal{RH}_\infty$, can be derived. This amounts to showing that given an arbitrary $H_1 \in \mathcal{RH}_\infty$ subject to the constraints Eqs. (4.25) and (4.28), there exists a stabilizing controller such that for some $\widehat{Q} \in \mathcal{RH}_\infty$, Eq. (4.20) holds for H_1. In this case, H_1 is said *admissible*. To this end, from Eq. (4.20)

$$\widehat{Q} = \frac{[T_{z_1 w} - s^2\Delta^{-1}(c_s s + k_s)(c_t s + k_t)]}{m_s s^4 \Delta^{-2}(m_u s^2 + c_t s + k_t)(c_t s + k_t)}.$$

From Eqs. (4.27) and (4.28), the numerator and the denumerator of $\widehat{Q}$ are $O(s^{-1})$. Hence, $\widehat{Q}$ is a proper rational function with a singularity at the origin of multiplicity four. However, the singularity at the origin is removable from Eqs. (4.24) and (4.25). Thus, $\widehat{Q} \in \mathcal{RH}_\infty$ as desired.

It should be noted that as soon as an admissible H_1 is specified, two other admissible functions, be H_2 and H_3, corresponding to $T_{z_2 w}$ and $T_{z_3 w}$ are generated via Eqs. (4.21) and (4.22). Indeed, elimination of $\widehat{Q}$ in Eqs. (4.20)–(4.22) results in the following trade-off relations:

$$H_2 = -\frac{c_t s + k_t}{m_u s^2 + c_t s + k_t} + \frac{(m_s + m_u)s^2 + c_t s + k_t}{s^2(m_u s^2 + c_t s + k_t)} H_1 \tag{4.29}$$

$$H_3 = -\frac{m_u s^2}{m_u s^2 + c_t s + k_t} - \frac{m_s}{m_u s^2 + c_t s + k_t} H_1 \tag{4.30}$$

$$H_3 = -\frac{(m_s + m_u)s^2}{(m_s + m_u)s^2 + c_t s + k_t} - \frac{m_s s^2}{(m_s + m_u)s^2 + c_t s + k_t} H_2. \tag{4.31}$$

The constraints on H_1 and its derivatives at $s = 0$ are partially recovered by Eqs. (4.29) and (4.30). In fact, given an admissible H_2, analyticity of

H_2 at $s = 0$ forces the following function

$$H_1(s) - s^2\Delta^{-1}(c_s s + k_s)(c_t s + k_t)$$

to have at least two zeros there, which implies $H_1(0) = H_1'(0) = 0$. No results on further derivatives of H_1 at $s = 0$ can be deduced from Eqs. (4.29) and (4.30).

The above results are captured in the following.

Proposition 4.3.1. *Consider the quarter car model in Eq. (4.1) with $k_s, c_s, c_t > 0$. Assume that $y = y_2$ and let H_1 be any function in $\mathcal{RH}_\infty$. Then, $H_1 = T_{z_1 w}$ for some stabilizing control law if and only if:*

1. $H_1(s) = \dfrac{c_s c_t}{m_s m_u} + O(s^{-1})$,
2. $H_1(0) = H_1^{(1)}(0) = H_1^{(3)}(0) = 0, \qquad H_1^{(2)}(0) = 2.$

A similar derivation to the above can be carried out for H_2 and H_3 or Proposition 4.3.1 combined with Eqs. (4.29) and (4.30) yields the following results.

Proposition 4.3.2. *Consider the quarter car model in Eq. (4.1) with $k_s, c_s, c_t > 0$. Assume that $y = y_2$ and let H_2 be any function in $\mathcal{RH}_\infty$. Then, $H_2 = T_{z_2 w}$ for some stabilizing control law if and only if:*

1. $H_2(s) = -\dfrac{c_t}{m_u} s^{-1} + \left[\dfrac{m_s + m_u}{m_u}\dfrac{c_s c_t}{m_s m_u} + \dfrac{c_t^2}{m_u^2} - \dfrac{k_t}{m_u}\right] s^{-2} + O(s^{-3})$,
2. $H_2(0) = H_2^{(1)}(0) = 0$.

Proposition 4.3.3. *Consider the quarter car model in Eq. (4.1) with $k_s, c_s, c_t > 0$. Assume that $y = y_2$ and let H_3 be any function in $\mathcal{RH}_\infty$. Then, $H_3 = T_{z_3 w}$ for some stabilizing control law if and only if:*

1. $H_3(s) = -1 + \dfrac{c_t}{m_u} s^{-1} + \left[\dfrac{k_t}{m_u} - \dfrac{(c_s + c_t)c_t}{m_u^2}\right] s^{-2} + O(s^{-3})$,
2. $H_3(0) = H_3^{(1)}(0) = 0,\ H_3^{(2)}(0) = -\dfrac{2(m_s + m_u)}{k_t},\ H_3^{(3)}(0) = \dfrac{6(m_s + m_u)c_t}{k_t^2}$.

Now, assume that $c_t = 0$ and $k_s, c_s > 0$. Then, $\Delta(s)$ is still a Hurwitz polynomial, and it suffices to let $c_t = 0$ in Eqs. (4.20)–(4.22) and Eqs. (4.29)–(4.31). Two new constraints arise at the frequencies:

$$\omega_1 = \sqrt{\frac{k_t}{m_s + m_u}}, \qquad \omega_2 = \sqrt{\frac{k_t}{m_u}} \tag{4.32}$$

which have already been observed in [18, 20]. The results for this case are summarized in the following.

Proposition 4.3.4. *Consider the quarter car model in Eq. (4.1) with $k_s, c_s > 0$, and $c_t = 0$. Assume that $y = y_2$ and let H_1 be any function in $\mathcal{RH}_\infty$. Then, $H_1 = T_{z_1 w}$ for some stabilizing control law if and only if:*

1. $H_1(s) = \dfrac{k_t c_s}{m_s m_u} s^{-1} + O(s^{-2})$,
2. $H_1(0) = H_1^{(1)}(0) = H_1^{(3)}(0) = 0, \qquad H_1^{(2)}(0) = 2$,
3. $H_1(j\omega_2) = -(j\omega_2)^2 \dfrac{m_u}{m_s}$.

Proposition 4.3.5. *Consider the quarter car model in Eq. (4.1) with $k_s, c_s > 0$, and $c_t = 0$. Assume that $y = y_2$ and let H_2 be any function in $\mathcal{RH}_\infty$. Then, $H_2 = T_{z_2 w}$ for some stabilizing control law if and only if:*

1. $H_2(s) = -\dfrac{k_t}{m_u} s^{-2} + \dfrac{(m_s + m_u) c_s k_t}{m_s m_u^2} s^{-3} + O(s^{-4})$,
2. $H_2(0) = H_2^{(1)}(0) = 0$,
3. $H_2(j\omega_1) = -\dfrac{m_s + m_u}{m_s}$.

Proposition 4.3.6. *Consider the quarter car model in Eq. (4.1) with $k_s, c_s > 0$, and $c_t = 0$. Assume that $y = y_2$ and let H_3 be any function in $\mathcal{RH}_\infty$. Then, $H_3 = T_{z_3 w}$ for some stabilizing control law if and only if:*

1. $H_3(s) = -1 + \dfrac{k_t}{m_u} s^{-2} - \dfrac{k_t c_s}{m_u^2} s^{-3} + O(s^{-4})$,
2. $H_3(0) = H_3^{(1)}(0) = H_3^{(3)}(0) = 0, \;\; H_3^{(2)}(0) = -\dfrac{2(m_s + m_u)}{k_t}$.

Propositions 4.3.4–4.3.6 yield Theorems 1–3 in [20] when $c_s = 0$. In [20], T_{x_1w} is constrained instead of T_{z_1w}. The latter is related to the former by the equation $T_{z_1w}(s) = s^2 T_{x_1w}(s)$. Then, the third formula in Proposition 4.3.4 recovers the constraint $T_{x_1w}(j\omega_2) = -m_u/m_s$ derived in [20].

The appearance of c_s in the constraints of Propositions 4.3.4–4.3.6 demonstrates that the damper in Figure 4.1 can not be incorporated to u. Otherwise, for a given proper controller $K^\sharp$ that stabilizes the quarter-car model in Figure 4.1 with $c_s = k_s = 0$, a controller K satisfying Eq. (4.23) and $K^\sharp = K + sc_s + k_s$ would be improper since both controllers have the same input y_2. The same argument also explains absence of k_s in the constraints of Propositions 4.3.1–4.3.6. The reader is cautioned that the first conclusion drawn above is valid for the quarter-car model with a suspension consisting of an actuator in parallel with a spring and a damper as shown in Figure 4.1. There are many possibilities to connect passive elements with an actuator, in which the issue of properness never arises. In hardware implementation of active or semi-active suspensions, parallel connection (without damper) is a preferred configuration.

Although k_s does not appear in the constraint formulae above, a given set of measurements may not be sufficient to parametrize all stabilizing proper controllers if the spring in Figure 4.1 is missing. Recall the internal stabilizability condition: G and G_{22} share the same unstable poles. If $c_s > 0$ or $c_t > 0$ and $k_s > 0$, then this requirement is satisfied by all elements of G_{22} in Eq. (4.11) and one can also use y_1 for the parametrization of the stabilizing controllers. However, in general, different measurements lead to different constraint sets. If $c_s = c_t = k_s = 0$, then Δ and G_{22} in Eqs. (4.7) and (4.11) equal $m_s s^2(m_u s^2 + k_t)$ and

$$\begin{bmatrix} -\dfrac{1}{m_s} \\ -\dfrac{(m_s + m_u)s^2 + k_t}{m_s s^2(m_u s^2 + k_t)} \end{bmatrix}.$$

Clearly, y_1 can not give rise to a parametrization of stabilizing controllers. On the other hand, if $k_s > 0$, then $\Delta(s) = m_s m_u s^4 + [(m_s + m_u)k_s + m_s k_t]s^2 + k_s k_t$,

and since $\Delta(j\omega_1) \neq 0$ and $\Delta(j\omega_2) \neq 0$, no pole-zero cancellation can happen between Δ and any component of G_{22}. Hence, as a measurement, $\ddot{x}_1$ or $x_1 - x_2$ is sufficient for the parametrization of the stabilizing controllers.

The next case to be studied is $y = [y_1\ y_2]^T$.

Let $\widehat{Q} = [\widehat{Q}_1\ \widehat{Q}_2] = (Y - MQ)\widetilde{M}$. Since $Q \in \mathcal{RH}_\infty$ is a 2-dimensional row vector, T_{zw} in Eq. (4.16) can be written as

$$T_{zw} = G_{11} + G_{12}G_{21}^T\widehat{Q}^T. \tag{4.33}$$

Recall that a non-singular matrix is *unimodular* if its determinant is constant. Now, define a product of unimodular matrices by

$$\Pi = \begin{bmatrix} 1 & 0 \\ m_s^{-1}c_s s & 1 \end{bmatrix} \begin{bmatrix} 1 & 0 \\ m_s^{-1}k_s & 1 \end{bmatrix} \tag{4.34}$$

which is a unimodular matrix with the inverse:

$$\Pi^{-1} = \begin{bmatrix} 1 & 0 \\ -m_s^{-1}(c_s s + k_s) & 1 \end{bmatrix}.$$

The chosen matrix Π has the property:

$$G_{21}^T\Pi = -m_s s^2\Delta^{-1}(c_t s + k_t)\,[0\ \ 1]. \tag{4.35}$$

It should be clear how to proceed in order to parametrize the stabilizing controllers if more than two measurements are available for feedback. For example, if y equals $[y_1\ y_2\ \ddot{x}_2\ x_2]^T$, a unimodular matrix Π is constructed such that when premultiplied with G_{21}^T, the result is a row vector with the first three elements being zero, similar to Eq. (4.35). Therefore, the two factors of Π in Eq. (4.34) are exactly elementary column operators. The utility of Eq. (4.35) is to allow a parametrization of T_{zw} in terms of a scalar transfer function.

Since Δ is Hurwitz, coprime factors of G_{22} can be chosen as follows

$$N = \widetilde{N} = G_{22}, \qquad M = 1, \qquad \widetilde{M} = I.$$

Hence,

$$T_{zw} = G_{11} + \widetilde{q}\,G_{12}s^2\Delta^{-1}(c_t s + k_t)(c_s s + k_s)$$

where

$$\widetilde{q} = \widehat{Q}_1 - \widehat{Q}_2 m_s (c_s s + k_s)^{-1}. \tag{4.36}$$

It follows that

$$\begin{aligned}
T_{z_1 w} &= s^2 \Delta^{-1} (c_t s + k_t)(c_s s + k_s) \left\{ 1 - \widetilde{q} s^2 \Delta^{-1} (m_u s^2 + c_t s + k_t) \right\} && (4.37) \\
T_{z_2 w} &= -s^2 \Delta^{-1} (c_t s + k_t) && \\
&\quad \cdot \left\{ m_s + \widetilde{q} \Delta^{-1} [(m_s + m_u) s^2 + c_t s + k_t](c_s s + k_s) \right\} && (4.38) \\
T_{z_3 w} &= -s^2 \Delta^{-1} [m_s m_u s^2 + (m_s + m_u) c_s s + (m_s + m_u) k_s] && \\
&\quad + \widetilde{q}\, m_s s^4 \Delta^{-2} (c_s s + k_s)(c_t s + k_t) && (4.39) \\
K &= \widehat{Q} (I + G_{22} \widehat{Q})^{-1}. && (4.40)
\end{aligned}$$

The range space of $\widetilde{q}$ equals $\mathcal{RH}_\infty$. This means that $\widetilde{q}$ and $\widehat{Q}_2$ can be used to parametrize the set of the stabilizing controllers. Then, $\widehat{Q}_1$ is solved from Eq. (4.36) and plugged in Eq. (4.40).

The trade-off relations among H_1, H_2, and H_3 are the same as Eqs. (4.29)–(4.31). The constraints on the transfer functions H_1, H_2, and H_3 are expressed in the following results.

Proposition 4.3.7. *Consider the quarter car model in Eq. (4.1) with $k_s, c_s, c_t > 0$. Assume that $y = [y_1 \ y_2]^T$ and let H_1 be any function in $\mathcal{RH}_\infty$. Then, $H_1 = T_{z_1 w}$ for some stabilizing control law if and only if:*

$$H_1(0) = H_1^{(1)}(0) = H_1^{(3)}(0) = 0, \qquad H_1^{(2)}(0) = 2.$$

Proposition 4.3.8. *Consider the quarter car model in Eq. (4.1) with $k_s, c_s, c_t > 0$. Assume that $y = y_2$ and let H_2 be any function in $\mathcal{RH}_\infty$. Then, $H_2 = T_{z_2 w}$ for some stabilizing control law if and only if:*

1. $H_2(s) = -\dfrac{c_t}{m_u} s^{-1} + O(s^{-2})$,
2. $H_2(0) = H_2^{(1)}(0) = 0$.

Proposition 4.3.9. *Consider the quarter car model in Eq. (4.1) with $k_s, c_s, c_t > 0$. Assume that $y = [y_1 \ y_2]^T$ and let H_3 be any function in $\mathcal{RH}_\infty$. Then, $H_3 = T_{z_3 w}$ for some stabilizing control law if and only if:*

1. $H_3(s) = -1 + \dfrac{c_t}{m_u} s^{-1} + O(s^{-2})$,

2. $H_3(0) = H_3^{(1)}(0) = 0,\ H_3^{(2)}(0) = -\dfrac{2(m_s + m_u)}{k_t},\ H_3^{(3)}(0) = \dfrac{6(m_s + m_u)c_t}{k_t^2}$.

Based on Propositions 4.3.1–4.3.3 and Propositions 4.3.7–4.3.9, the following conclusions can be drawn. First, extra measurement, *i.e.,* y_1 affects only the Taylor series coefficients of H_1, H_2, and H_3 at infinity. Second, c_s does not show up in the formulae of Propositions 4.3.7–4.3.9 in contrast to those of Propositions 4.3.1–4.3.3. Finally, the trade-off relations are the same for both cases. This implies that a point in the H_2 versus H_1 trade-off curve determined uniquely by the controller in Eq. (4.23) corresponds to an infinite number of controllers in Eq. (4.40). This information can be useful in constraining the controller dynamics. For example, constraining the ℓ_1 norm of K, which is defined as the absolute integral of the impulse response of K, constrains the magnitude of the input to persistent measurements.

The last case to be studied in this chapter is the case $k_s, c_s > 0$, $c_t = 0$, and $y = [y_1\ y_2]^T$. As noted before, Δ is Hurwitz, and it suffices to let $c_t = 0$ in Eqs. (4.37)–(4.39). The trade-off relations are the same as Eqs. (4.29)–(4.31) with $c_t = 0$ substituted. The constraints on H_1, H_2, and H_3 are captured in the following results.

Proposition 4.3.10. *Consider the quarter car model in Eq. (4.1) with $k_s, c_s > 0$, $c_t = 0$. Assume that $y = [y_1\ y_2]^T$ and let H_1 be any function in $\mathcal{RH}_\infty$. Then, $H_1 = T_{z_1 w}$ for some stabilizing control law if and only if:*

1. $H_1(s) = O(s^{-1})$,

2. $H_1(0) = H_1^{(1)}(0) = H_1^{(3)}(0) = 0, \qquad H_1^{(2)}(0) = 2$,

3. $H_1(j\omega_2) = -(j\omega_2)^2 \dfrac{m_u}{m_s}$.

Proposition 4.3.11. *Consider the quarter car model in Eq. (4.1) with $k_s, c_s > 0$, and $c_t = 0$. Assume that $y = [y_1\ y_2]^T$ and let H_2 be any function in $\mathcal{RH}_\infty$. Then, $H_2 = T_{z_2 w}$ for some stabilizing control law if and only if:*

1. $H_2(s) = -\dfrac{k_t}{m_u}s^{-2} + O(s^{-3})$,

2. $H_2(0) = H_2^{(1)}(0) = 0$,

3. $H_2(j\omega_1) = -\dfrac{m_s + m_u}{m_s}$.

Proposition 4.3.12. *Consider the quarter car model in Eq. (4.1) with $k_s, c_s > 0$, $c_t = 0$. Assume that $y = [y_1\ y_2]^T$ and let H_3 be any function in $\mathcal{RH}_\infty$. Then, $H_3 = T_{z_3 w}$ for some stabilizing control law if and only if:*

1. $H_3(s) = -1 + \dfrac{k_t}{m_u}s^{-2} + O(s^{-3})$,

2. $H_3(0) = H_3^{(1)}(0) = H_3^{(3)}(0) = 0,\ \ H_3^{(2)}(0) = -\dfrac{2(m_s + m_u)}{k_t}$.

As in Propositions 4.3.7–4.3.9, c_s does not show up in the above formulae. Thus, whenever $y = [y_1\ y_2]^T$, the damper can be modelled as part of the actuator without affecting the interpolation conditions. The last result is in contrast with the single measurement case of Propositions 4.3.1–4.3.6. When $c_s = c_t = 0$, Δ needs not be Hurwitz; but a slightly more complicated coprime factorization can be performed easily. The reader is referred to [20] for more details on this.

The question of controller approximation is in order. More specifically, let K and $\bar{K}$ be two stabilizing controllers obtained for the quarter-car model with the measurements y_2 and $[y_1\ y_2]^T$ and H_k and $\bar{H}_k$ for $k = 1, 2, 3$ denote the corresponding closed-loop transfer functions, respectively. In [20], when k_s, c_s, and c_t are all zero, it is shown that the closed-loop transfer functions obtained with a stabilizing controller that uses the measurements $y_2, \dot{x}_1, z_3$, and $\dot{x}_2$ can be approximated within a specified tolerance by the closed-loop transfer functions of a stabilizing controller that uses only the suspension travel measurement.

From Eqs. (4.20) and (4.37),

$$H_1 - \bar{H}_1 = (c_t s + k_t)s^4\Delta^{-2}(m_u s^2 + c_t s + k_t)\,[m_s\widehat{Q} + \widetilde{q}(c_s s + k_s)]. \qquad (4.41)$$

Hence,

$$H_1(\infty) - \bar{H}_1(\infty) = \frac{c_s c_t}{m_s^2 m_u}\, \widetilde{q}(\infty).$$

If $\widetilde{q}(\infty) \neq 0$ and $c_t > 0$, there is no way of arbitrarily well approximating $\bar{K}$ by a stabilizing compensator K for the entire range of frequencies. However, if $\widetilde{q}(\infty) = 0$, *i.e.,* when $\widetilde{q}(s)$ is a strictly proper transfer function, by setting $\widehat{Q} = -\widetilde{q}(sc_s + k_s)m_s^{-1}$, we get $H_1(s) \equiv \bar{H}_1(s)$ whether c_t equals zero or not. Note from Eq. (4.36) that $\widetilde{q}(\infty) = 0$ if and only if $\widehat{Q}_1(\infty) = 0$. The latter equality does not require $\bar{K}$ to be strictly proper.

Now, consider the case $c_t = 0$. Let

$$\widehat{Q} = -\frac{\widetilde{q}(sc_s + k_s)}{m_s(1 + \varepsilon s)} \qquad (\varepsilon > 0).$$

As $\varepsilon \to 0$, $m_s\widehat{Q} + \widetilde{q}(sc_s + k_s) \to 0$ uniformly on every internal $[0, j\lambda)$, $\lambda > 0$ though outside this interval it diverges as $O(s)$. However, outside the interval the growth is controlled by the factor $k_t s^4(m_u s^2 + k_t)\Delta^{-2} = O(s^{-2})$. Picking λ sufficiently large and ε sufficiently small, the left hand side of Eq. (4.41) can be made as small as desired. The convergences $H_2 \to \bar{H}_2$ and $H_3 \to \bar{H}_3$ as $\varepsilon \to 0$ follow from the fact that H_2 and H_3 are continuous functions of H_1 on the closed right-half plane. The controller approximation result is captured in the following.

Proposition 4.3.13. *Let $\bar{H}_k$, $k = 1, 2, 3$ be the closed-loop transfer functions obtained for the quarter-car model in Eq. (4.1) with $k_s, c_s > 0$, the measurements y_1, y_2, and some stabilizing controller $\bar{K}$. If $c_t = 0$ or $\widetilde{q}(\infty) = 0$, then for each $\varepsilon > 0$ a stabilizing controller K that uses only y_2 can be found with the corresponding transfer functions H_k satisfying $|\bar{H}_k(j\omega) - H_k(j\omega)| < \varepsilon$ for all ω and $k = 1, 2, 3$.*

When $c_t = 0$, from Propositions 4.3.6 and 4.3.12 we have $T_{z_3 w}(s) = -1 + O(s^{-2})$ for all large s, and in this case Theorem 4 in [20] reads out

$$\int_0^\infty \ln |T_{z_3 w}(j\omega)|\, d\omega = \pi \sum_{k=1}^{n} \sigma_k$$

where σ_k, $k = 1, \cdots, n$ denote the real parts of the zeros of $T_{z_3 w}$ in the open right half plane. This is not a quantitative but a qualitative statement expressing the difficulty of controlling the tire deflection on a broad band of frequencies due to the presence of nonminimum phase zeros.

From Propositions 4.3.1–4.3.13, the following conclusions can be drawn:

- When tire damping is present, utilizing the sprung mass acceleration measurement in addition to the suspension travel measurement in the feedback law affects only the curvatures of $T_{z_2 w}$ and $T_{z_3 w}$ at infinity, and $T_{z_1 w}(\infty)$. If tire damping is neglected, one degree higher order terms of the Taylor series expansions of $T_{z_k w}$, $k = 1, 2, 3$ at infinity are affected by the additional measurement.

- Closed-loop performance of any stabilizing feedback law which uses the sprung mass acceleration and the suspension travel measurements can be obtained within an arbitrary precision by a stabilizing feedback law relying only on the suspension travel measurement provided that either tire damping is neglected or the actuator transfer function satisfies a mild condition in the steady state.

- No matter how small, tire damping couples the wheel-hop and the heave modes. This coupling eliminates the constraints of the conventional quarter-car model, which neglects tire damping at the *so-called* invariant frequencies ω_1 and ω_2. As will be seen in the next section, tire damping improves ride comfort without sacrificing road holding.

- When the suspension travel is the only available measurement, c_s influences $T_{z_1 w}(\infty)$, and the second order terms of the Taylor series expansions of $T_{z_2 w}$ and $T_{z_3 w}$ at infinity if $c_t > 0$. If tire damping is neglected, one degree higher order terms of the Taylor series expansions of $T_{z_k w}$, $k = 1, 2, 3$ at infinity are affected by c_s.

- If the measurements y_1 and y_2 are both used in the parametrization of

the stabilizing controllers, then there is no need to consider c_s separately since it can be included in the feedback law.

The analysis of this chapter and the results in [20] show that the constraints on the closed-loop transfer functions depend on the system parameters as well as the measurements. In the present work, $\ddot{x}_1$ is taken as a measured signal instead of x_1 and $\dot{x}_1$ since in practice, the acceleration is measured, and the velocity and the position are constructed from the former by integration. The sprung mass acceleration measurement rather than velocity or position was also considered in [39][Section 4.5.2]. However, the parameterizability for the stabilizing controllers and the constraints on the closed-loop transfer function, in general, depend on which signal is being used. If x_1 or x_2 is used for the controller parameterization, then one also has to take into the filtering constraints and trade-offs [133], which are beyond the scope of the current work.

The constraints derived in this chapter can be used for the purpose of comparing closed-loop performance of a proposed controller with benchmark values at specific frequencies. They don't give much information about the design of an actual controller, which is an involved process, and besides the road disturbance responses many other factors such as the load disturbance responses and the robustness issues have also to be taken into account. In [20], the constraints on the load response functions are derived. Further applications of the controller parameterization to vehicle active suspension design are reported in [37, 38].

In passing, the constraints in Propositions 4.3.1 and 4.3.7 can be viewed as the interpolation constraints. Then, the problem of finding all stabilizing controllers can be cast into a partial realization problem. Many variants of this formulation, *i.e.,* interpolation with metric and minimal complexity constraints have been considered in the literature on rational interpolation [107].

4.4 Active Control of the Quarter-Car Model

The purpose of this section is to illustrate the effect of tire damping on the controller design for the quarter-car model in Figure 4.1. The vehicle is assumed to traverse a random road profile with a constant forward velocity v. Then, the derivative of $w(t)$ is a random process denoted by $V_i(t)$.

It will be more convenient to define a new set of state variables in terms of the old state variables in Eq. (4.1) as follows:

$$\tilde{x}_1 = x_1 - x_2, \qquad \tilde{x}_2 = x_2 - w, \qquad \tilde{x}_3 = x_3, \qquad \widetilde{x}_4 = x_4. \tag{4.42}$$

Thus, $\dot{\tilde{x}}_1 = x_3 - x_4$, $\dot{\tilde{x}}_2 = x_4 - V_i$, and from Eqs. (4.1), (4.2)–(4.4), (4.8), (4.42),

$$\dot{\widetilde{x}} = A\widetilde{x} + B_1 V_i + B_2 u \tag{4.43}$$

$$z = C_1\widetilde{x} + D_{12}u \tag{4.44}$$

$$y = C_2\widetilde{x} + D_{22}u + \theta \tag{4.45}$$

where

$$A = \begin{bmatrix} 0 & 0 & 1 & -1 \\ 0 & 0 & 0 & 1 \\ -\dfrac{k_s}{m_s} & 0 & -\dfrac{c_s}{m_s} & \dfrac{c_s}{m_s} \\ \dfrac{k_s}{m_u} & -\dfrac{k_t}{m_u} & \dfrac{c_s}{m_u} & -\dfrac{c_s + c_t}{m_u} \end{bmatrix}, \tag{4.46}$$

$$B_1 = \begin{bmatrix} 0 \\ -1 \\ 0 \\ \dfrac{c_t}{m_u} \end{bmatrix}, \; B_2 = \begin{bmatrix} 0 \\ 0 \\ -\dfrac{1}{m_s} \\ \dfrac{1}{m_u} \end{bmatrix}, \tag{4.47}$$

$$C_1 = \begin{bmatrix} -\dfrac{k_s}{m_s} & 0 & -\dfrac{c_s}{m_s} & \dfrac{c_s}{m_s} \\ 1 & 0 & 0 & 0 \\ 0 & 1 & 0 & 0 \end{bmatrix}, \; D_{12} = \begin{bmatrix} -\dfrac{1}{m_s} \\ 0 \\ 0 \end{bmatrix}, \tag{4.48}$$

$$C_2 = \begin{bmatrix} -\dfrac{k_s}{m_s} & 0 & -\dfrac{c_s}{m_s} & \dfrac{c_s}{m_s} \\ 1 & 0 & 0 & 0 \end{bmatrix}, \; D_{22} = \begin{bmatrix} -\dfrac{1}{m_s} \\ 0 \end{bmatrix}. \tag{4.49}$$

and θ is an artificially introduced zero-mean white sensor noise uncorrelated with V_i. Its covariance function denoted by R_θ satisfies

$$R_\theta(\tau) = \mu I \delta(\tau).$$

Here, $\mu > 0$ is a design variable.

For simplicity, the random process V_i is modeled as

$$V_i = 2\pi n_0 \sqrt{\kappa v}\eta(t) \tag{4.50}$$

where $\eta(t)$ is a zero-mean white noise process satisfying $R_\eta(\tau) = \delta(\tau)$; and κ, n_0 are the road roughness parameters [98]. In that work, more general road profile models than the integrated white-noise model defined in Eq. (4.50) are discussed; and the consequences of the road profile modeling on the random vibration characterics of the quarter-car model are studied in detail. The roughness parameters in the current study are set from [98] as $n_0 = 0.15708$ cycles per meter and $\kappa = 0.76 \times 10^{-5}$. Notice the relation $T_{zV_i} = s^{-1} T_{zw}$. Thus, the Q-parametrization of T_{zV_i} can be deduced from the Q-parametrization of T_{zw}. In particular, they share the same invariant frequencies ω_1 and ω_2.

The controller will be designed using the LQG design methodology. Accordingly, $u(t)$ is computed by minimizing

$$J_{LQG} = \lim_{t_f \to \infty} \mathrm{E}\left\{ \int_0^{t_f} \left(\sum_{k=1}^{3} \rho_k^{-2} z_k^2 + \rho_u u^2 \right) dt \right\} \tag{4.51}$$

where ρ_k, ρ_u are nonnegative weights to be chosen by the designer. In the simulation, ρ_u and ρ_k were set, respectively, equal to zero and the rms values of the open-loop z_k denoted by rms_{z_k}. Notice that even if ρ_u were set zero, the control effort is still penalized in Eq. (4.51) through the term $\rho_1^{-2} z_1^2$.

In Figures 4.3–4.5, the frequency response magnitudes of the passive and the active suspensions using either y_2 only or y_1 and y_2 both as measurements are plotted for the parameter values in Table 4.1, $\mu = 10^{-8}$, and $c_t = 0$. The rms values of z_1, z_2, z_3 were computed, respectively, as follows: 0.5424, 0.0046, 0.0017 (the passive suspension); 0.5240, 0.0034, 0.0016 (the active suspension with y_2 measured); 0.5234, 0.0034, 0.0016 (the active suspension with

y_1 and y_2 measured). The frequency responses of the active suspensions for the two measurement cases are almost identical; and thus, confirming the results in Proposition 4.3.13 and [20, 22].

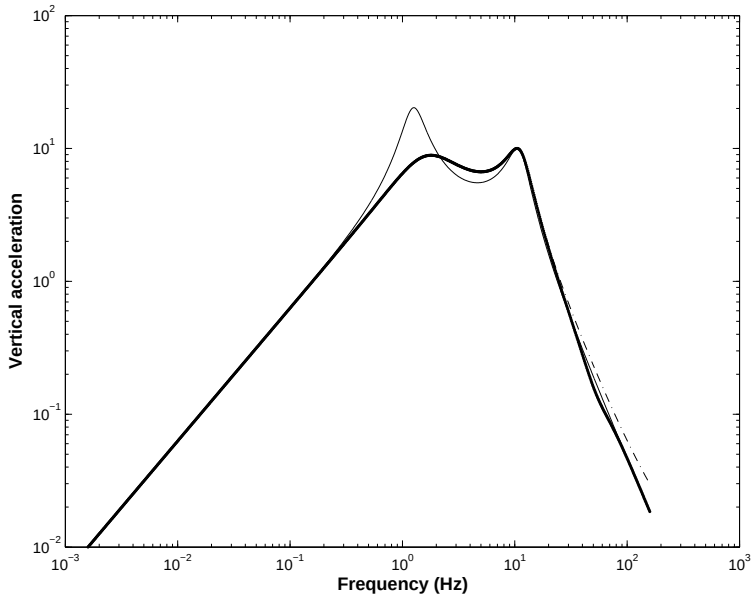

Figure 4.3: The acceleration frequency response magnitude: − Passive suspension; - active suspension using the suspension travel measurement without tire damping; −. active suspension using the acceleration and the suspension travel measurements without tire damping.

The natural frequency and the damping ratio of the heave mode are computed as $w_n^h = 1.2507$ Hz and $\zeta_1^h = 0.2178$ for the passive suspension. For the wheel-hop mode, they are computed as $w_n^{wh} = 11.0247$ Hz and $\zeta_1^{wh} = 0.2013$. The invariant frequencies are calculated from Eq. (4.32) as $\omega_1 = 3.832$ Hz and $\omega_2 = 10.610$ Hz. Since $\omega_2 \approx w_n^{wh}$, it is difficult to control the wheel-hop mode as clearly seen from Figures 4.3–4.5. The 3.5 % drop in the rms vertical acceleration comes from the suppression of the heave mode vibration. This is possible since the natural frequency of the heave mode given approximately by $\sqrt{k_s/(m_s + m_u)}$ is well separated from ω_1.

Now, let $c_t = 2c_s$. This value is unrealistic for tire damping because it yields $w_n^h = 1.2463$ Hz, $\zeta_1^h = 0.2211$; $w_n^{wh} = 11.0628$ Hz, and $\zeta_1^{wh} = 0.5919$.

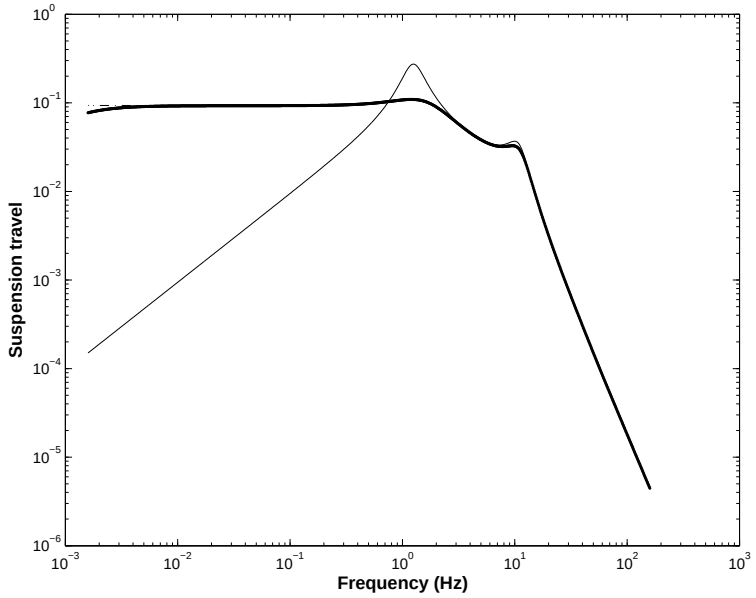

Figure 4.4: The suspension travel frequency response magnitude: − Passive suspension; - active suspension using the suspension travel measurement without tire damping; −. active suspension using the acceleration and the suspension travel measurements without tire damping.

If c_t is set to $0.1c_s$, then $w_n^h = 1.2504$ Hz, $\zeta_1^h = 0.2180$; $w_n^{wh} = 11.0267$ Hz, and $\zeta_1^{wh} = 0.2209$. Hence, the latter seems to be a realistic assumption. In Figs. 4.6–4.8, the counter parts of Figures 4.3–4.5 for the same values of the vehicle and the control design parameters but $c_t = 2c_s$ are plotted.

Clearly, all the three responses have been improved due to the removal of the invariant frequency at ω_2. For the rms values of z_1, z_2, z_3, the following were respectively computed: 0.4513, 0.0043, 0.0011 (the passive suspension); 0.2834, 0.0036, 0.0010 (the active suspension with y_2 measured); 0.2724, 0.0037, 0.0010 (the active suspension with y_1 and y_2 measured). Comparison of Figures 4.6–4.8 with Figures 4.3–4.5, and the modal natural frequencies and the damping ratios shows that the improved responses are achieved by suppressing the wheel-hop vibration.

In Figure 4.9, the vertical acceleration frequency response magnitude is plotted for the case $c_t = 0.1c_s$. The suspension travel and the tire de-

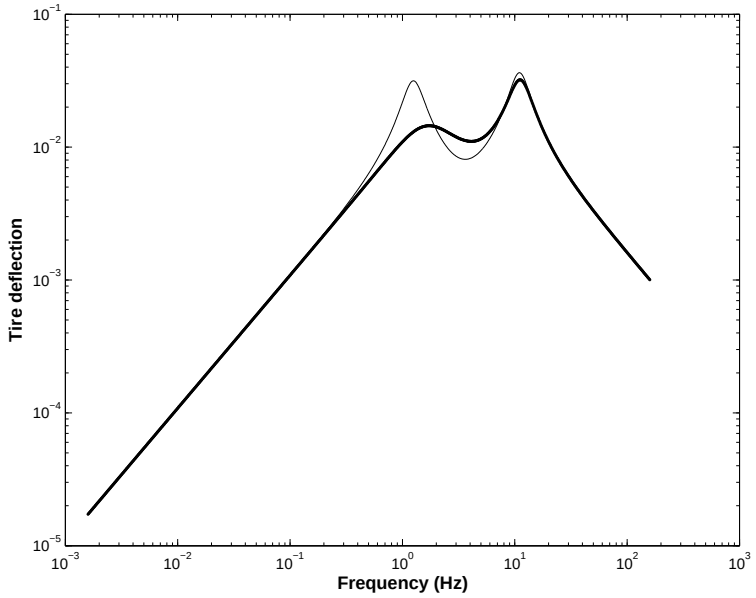

Figure 4.5: The tire deflection frequency response magnitude: − Passive suspension; - active suspension using the suspension travel measurement without tire damping; −. active suspension using the acceleration and the suspension travel measurements without tire damping.

flection responses are similar to those in Figure 4.4 and Figure 4.5. The rms values for this case are, respectively, 0.5259, 0.0045, 0.0017 (the passive suspension); 0.4895, 0.0034, 0.0016 (the active suspension with y_2 measured); 0.4900, 0.0034, 0.0016 (the active suspension with y_1 and y_2 measured). The rms vertical acceleration is reduced by 6.83 % which is about twice of the reduction computed for the case $c_t = 0$. Though as not impressive as the overdamped tire case, the last result shows that the influence of tire damping certainly needs to be taken into account in the design of active suspensions to improve ride quality. The rest of this section will be devoted to further enhancement of the closed-loop performance by means of the interpolation approach of this chapter.

In light of the controller approximation result, it is enough to consider the case $y = y_2$. Recall that $T_{zV_i} = s^{-1}T_{zw}$ which implies from Eq. (4.20) that

$$T_{z_1V_i} = s\Delta^{-1}(c_ts + k_t)\left\{c_ss + k_s + \widehat{Q}m_ss^2\Delta^{-1}(m_us^2 + c_ts + k_t)\right\}. \qquad (4.52)$$

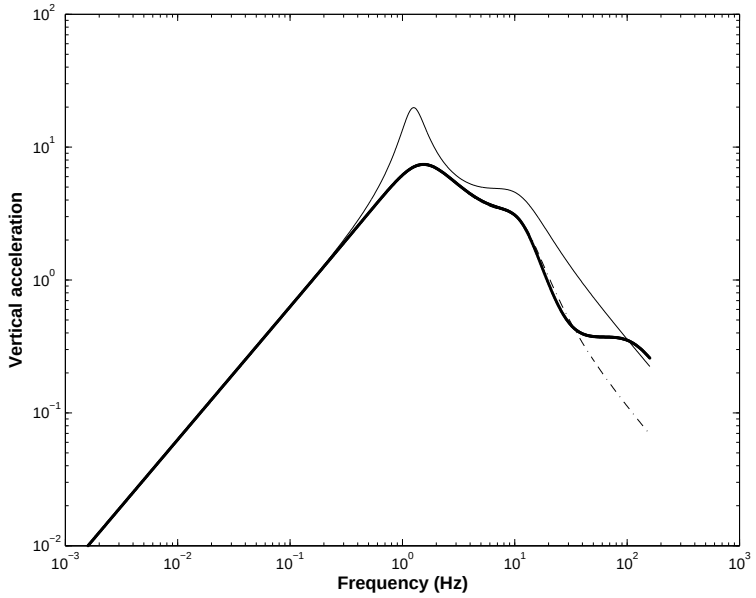

Figure 4.6: The acceleration frequency response magnitude: − Passive suspension; - active suspension using the suspension travel measurement with tire damping $c_t = 2c_s$; −. active suspension using the acceleration and the suspension travel measurements with tire damping $c_t = 2c_s$.

Put $c_t = \alpha c_s$ ($\alpha > 0$) and $H_k(s; \alpha, \widehat{Q}) = T_{z_k V_i}$, $k = 1, 2, 3$, where we have made the dependence on the parameters c_t and $\widehat{Q}$ explicit. Let $\alpha_1 = 0.1$, $\alpha_2 = 2$, and $Q^\dagger$ and $Q^\sharp$ denote the $\widehat{Q}$ parameters of the compensators designed by the above LQG method with $c_t = \alpha_1 c_s$ and $c_t = \alpha_2 c_s$, respectively. As far as the closed-loop responses are concerned, $H_k(s; \alpha_2, Q^\sharp)$, $k = 1, 2, 3$ are satisfactory while $H_k(s; \alpha_1, Q^\dagger)$ are not. Thus, the interpolation problem to be studied is formulated as follows:

Does there exist a $\widehat{Q} \in \mathcal{RH}_\infty$ *such that* $H_1(s; \alpha_1, \widehat{Q}) = H_1(s; \alpha_2, Q^\sharp)$ *?*

If there exists a solution to this problem denoted by $\widehat{Q}$, then the quarter-car model in Figure 4.1 with $c_t = 0.1c_s$ will have the closed-loop responses $H_k(s; \alpha_2, Q^\sharp)$, $k = 1, 2, 3$ using the unique controller K corresponding to this $\widehat{Q}$. Unfortunately, the formulated problem has no solution. To see this, first obtain the complete interpolation conditions for $T_{z_1 V_i}$ from Eq. (4.52) as follows

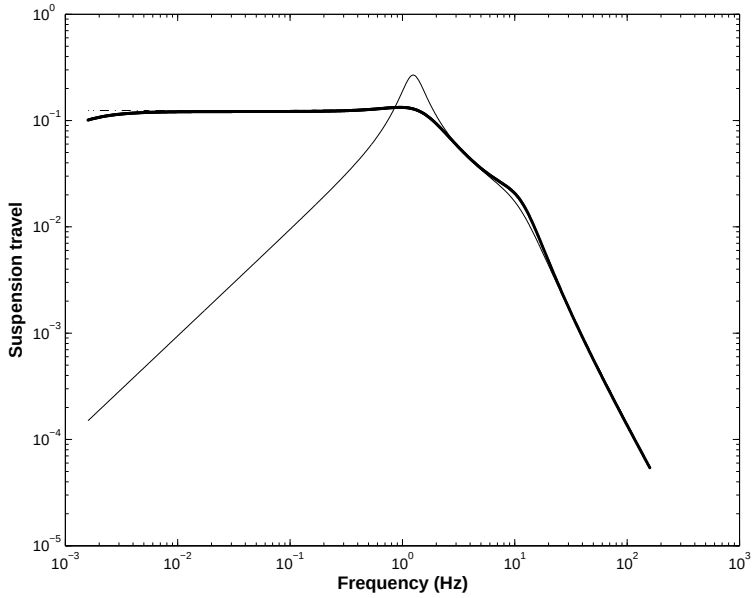

Figure 4.7: The suspension travel frequency response magnitude: − Passive suspension; - active suspension using the suspension travel measurement with tire damping $c_t = 2c_s$; −. active suspension using the acceleration and the suspension travel measurements with tire damping $c_t = 2c_s$.

(i) $H_1(s) = \dfrac{c_s c_t}{m_s m_u} s^{-1} + O(s^{-2})$,

(ii) $H_1(0) = H_1''(0) = 0, \qquad H_1'(0) = 1.$

Then, from the requirement formulated above and (i):

$$s\, H_1(s; \alpha_1, \widehat{Q})|_{s=\infty} = s\, H_1(s; \alpha_2 Q^\sharp)|_\infty,$$

which forces α_1 equal to α_2. Hence, there does not exist any solution.

Having seen the infeasibility of this interpolation problem, consider now the following variant:

Does there exist any $\widehat{Q} \in \mathcal{RH}_\infty$ *such that* $H_1(s; \alpha_1, \widehat{Q}) = H_1(s; \alpha_2, Q^\sharp)\Psi(s)$ *for some* $\Psi \in \mathcal{RH}_\infty$*?*

Fortunately, there exists a solution to the latter problem. In fact, from the interpolation conditions for $T_{z_1 V_i}$, it suffices to pick any $\Psi \in \mathcal{RH}_\infty$ satisfying

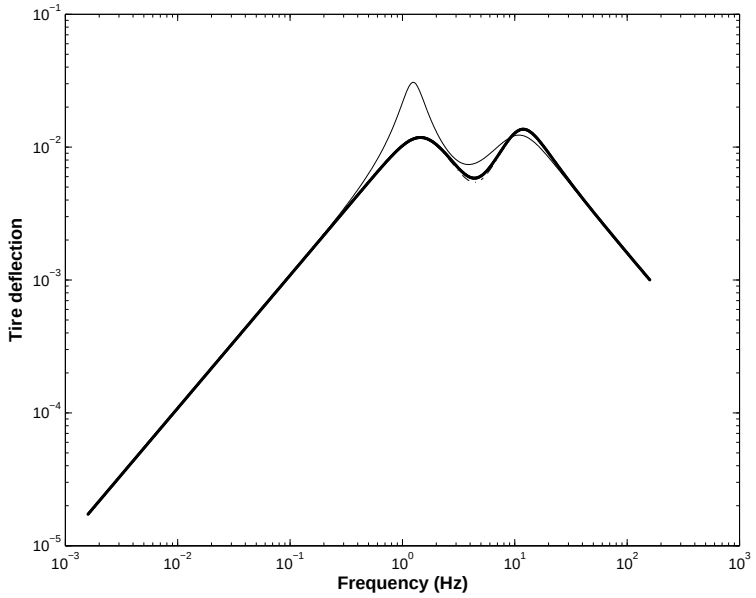

Figure 4.8: The tire deflection frequency response magnitude: − Passive suspension; - active suspension using the suspension travel measurement with tire damping $c_t = 2c_s$; −. active suspension using the acceleration and the suspension travel measurements with tire damping $c_t = 2c_s$.

(iv) $\Psi(0) = 1$,

(v) $\Psi'(0) = 0$,

(vi) $\Psi(\infty) = \alpha_1/\alpha_2$.

It is easy to see that the following transfer function

$$\Psi(s) = \frac{\sigma s^2 + as + b}{s^2 + as + b}, \qquad a, b > 0$$

where $\sigma = \alpha_1/\alpha_2$ has the aforementioned properties. Furthermore, for a given Ω which is sufficiently larger than the wheel-hop frequency ω_n^{wh}, if a and b are chosen so that $\Psi(j\omega)$ is a good approximation to the low-pass filter:

$$L_\Omega(\omega) = \begin{cases} 1, & 0 \le \omega \le \Omega, \\ \sigma, & \omega > \Omega \end{cases}$$

on the frequency band $[0, \Omega]$, then a good match to the vertical acceleration response plotted in Figure 4.6 by the solid line is obtained. From the continuity

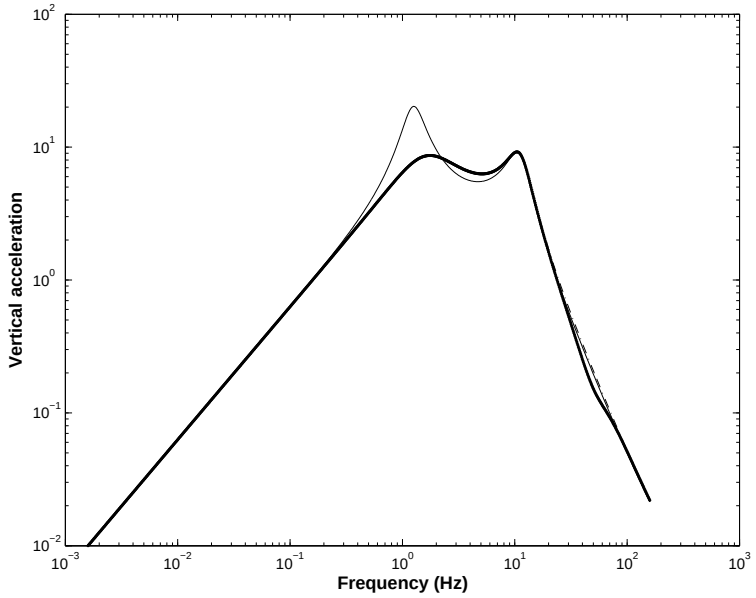

Figure 4.9: The acceleration frequency response magnitude: − Passive suspension; - active suspension using the suspension travel measurement with tire damping $c_t = 0.1c_s$; −. active suspension using the acceleration and the suspension travel measurements with tire damping $c_t = 0.1c_s$.

of the trade-off curves, it follows that the other two responses are satisfactory as well.

It remains to calculate $\widehat{Q}$. To this end, from Eq. (4.52),

$$\widehat{Q} = \frac{H_1(s;\alpha_2,Q^\sharp)\Psi(s)\Delta(s;\alpha_1) - s(\alpha_1 c_s s + k_t)(c_s s + k_s)}{m_s s^3(\alpha_1 c_s s + k_t)(m_u s^2 + \alpha_1 c_s s + k_t)}\,\Delta(s;\alpha_1) \qquad (4.53)$$

where $\Delta(s;\alpha_1)$ is calculated from Eq. (4.7) with $c_t = \alpha_1 c_s$. Since the degree of $H_1(s;\alpha_2,Q^\sharp)$ is 8, the degree of $\widehat{Q}(s)$ is bounded above by 13. The numerator polynomial of $\widehat{Q}$ before cancellations has order 18. Recall how $\Psi(\infty)$ was selected. This drops the order of the numerator polynomial by two. Three more degrees are canceled by the denumerator factor s^3. The end result is a proper transfer function $\widehat{Q}$. Finally, K is calculated from Eq. (4.23) with $\widehat{Q}$ in Eq. (4.53).

It may seem difficult to keep track of pole-zero cancellations. An easy way to circumvent this numerically ill-conditioned procedure is to evaluate

$\widehat{Q}(s)$ and/or its derivatives by computing the right-hand side of Eq. (4.53) and/or its-derivatives at a set of sufficiently many and arbitrarily selected frequencies s_k; and from these evaluations, obtain directly a minimal state-space realization of $\widehat{Q}(s)$. For this purpose, numerically efficient robust algorithms developed in [62,65], which deal with multi-variable data as well, can be used.

In Figure 4.10, the acceleration frequency response magnitude of the active suspension designed by using the suspension travel measurement with the (fictitious) tire damping $c_t = 2c_s$ plotted in Figure 4.6 is reproduced along with the acceleration frequency response magnitude of the active suspension designed by the hybrid algorithm outlined above. The purpose of plotting them together was to show that the approximation $H_1(s;\alpha_1,\widehat{Q}) \approx H_1(s;\alpha_2,Q^\sharp)$ is very accurate in the bandwidth of interest. This, in turn, implies that the approximations $H_2(s;\alpha_1,\widehat{Q}) \approx H_2(s;\alpha_2,Q^\sharp)$ and $H_3(s;\alpha_1,\widehat{Q}) \approx H_3(s;\alpha_2,Q^\sharp)$ are also very accurate in the same band of the frequencies. A comparison of Figure 4.9 with Figure 4.10 reveals impressive closed-loop performance enhancement by the interpolation approach. In the simulation, $\psi(s)$ was chosen as

$$\psi(s) = \frac{0.05s^2 + 500s + 10}{s^2 + 500s + 10}.$$

In Figure 4.11, the actuator frequency response magnitudes of the active suspensions designed by the LOG methodology with tire dampings $c_t = 0.1c_s$ and $c_t = 2c_s$, and the hybrid algorithm with tire damping $c_t = 0.1c_s$ using the suspension travel measurement are plotted. Figure 4.11 shows that the closed-loop performance enhancement by the interpolation approach is achieved at a reasonable price. Actually, the increase in the actuator gain is less than 30 decibels for all frequencies. Simulations for the values of tire damping at the equally spaced 101 points between and including $0.001c_s$ and $0.1c_s$ were also carried out. The numerical results plotted in Figure 4.12 indicate that the actuator frequency response magnitudes of the active suspensions designed by either the LOG methodology or the hybrid algorithm using the suspension

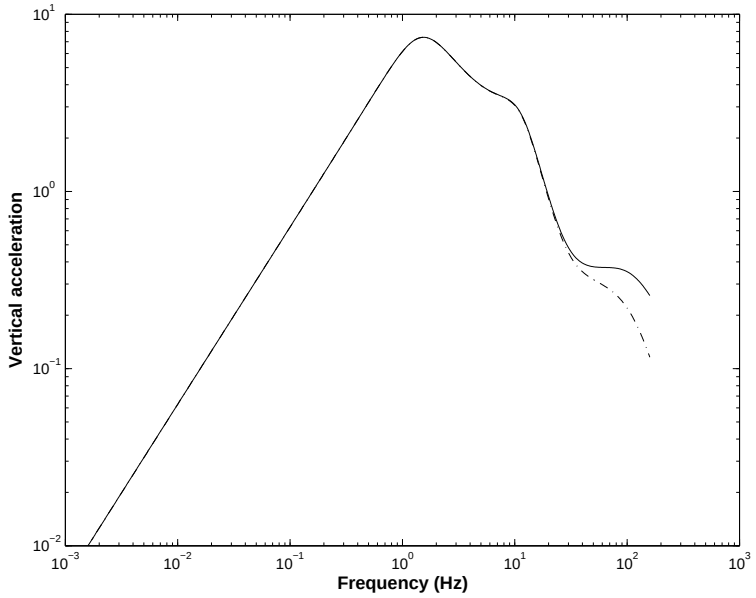

Figure 4.10: The acceleration frequency response magnitude: − Active suspension using the suspension travel measurement with the (fictitious) tire damping $c_t = 2c_s$; −. active suspension designed by a mixture of the LQG methodology and the interpolation approach using the suspension travel measurement with the (actual) tire damping $c_t = 0.1c_s$.

travel measurement are insentive to changes in tire damping; hence confirming the predication about the efficacy of coupling between the motions of the sprung and unsprung masses.

Moreover, in Figure 4.11, the actuator gain is seen to peak at the heave and the wheel-hop frequencies, which indicates that a stable inversion of the vehicle transfer function is taking place by canceling these modes. This feature is reminiscent of the Loop-Transfer-Recovery (LTR) synthesis [16] that applies to square and minimum-phase plants. Therefore, the hybrid algorithm can be viewed as a *loop-shaping* method realized in two-stages. The stages are the minimization of the quadratic criterion in Eq. (4.51) and the interpolation procedure. Although, in principle, it is possible to obtain a desired solution in one step by the LQG methodology, it is not clear how to accomplish this task since the quadratic criterion in Eq. (4.51) involves nine free weights in its most

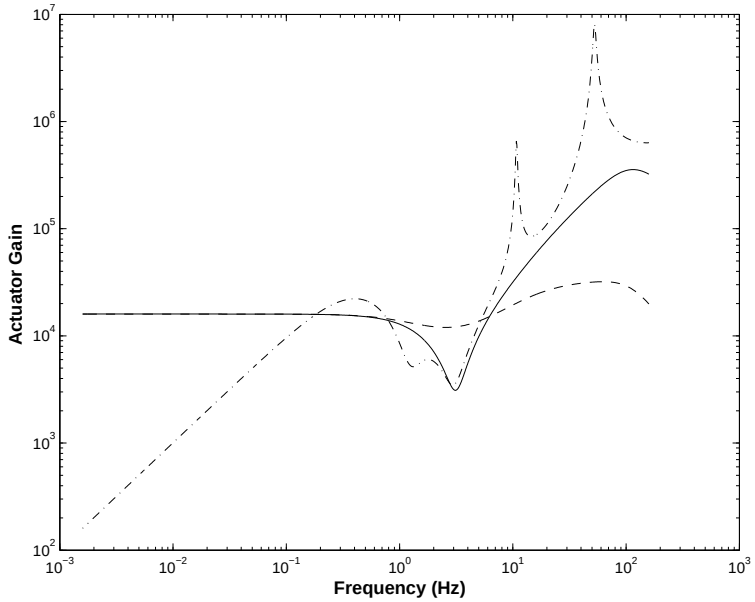

Figure 4.11: The actuator frequency response magnitude using the suspension travel measurement: $-$ the LQG design with tire damping $c_t = 2c_s$; $--$ the LQG design with tire damping $c_t = 0.1c_s$; $-.$ the hybrid algorithm with tire damping $c_t = 0.1c_s$.

general form. Due to the coupling between the modes, it is a non-trivial matter to steer these weights towards a desired solution. The hybrid algorithm, on the other hand, ignores the interactions among the variables z_k, $k = 1, 2, 3$ and u in the first stage. Then, the effect of the interactions is taken care of in the interpolation stage. The reader is cautioned not to draw broad conclusions based on this example solely since hardware limitations and uncertainties may degrade actuator performance.

4.5 Summary

In this chapter, the flexibility of shaping the closed-loop road frequency responses of a quarter-car model by feedback control was investigated. The constraints on the achievable responses of the quarter-car active suspension systems were derived for a wide range of the suspension parameters. The

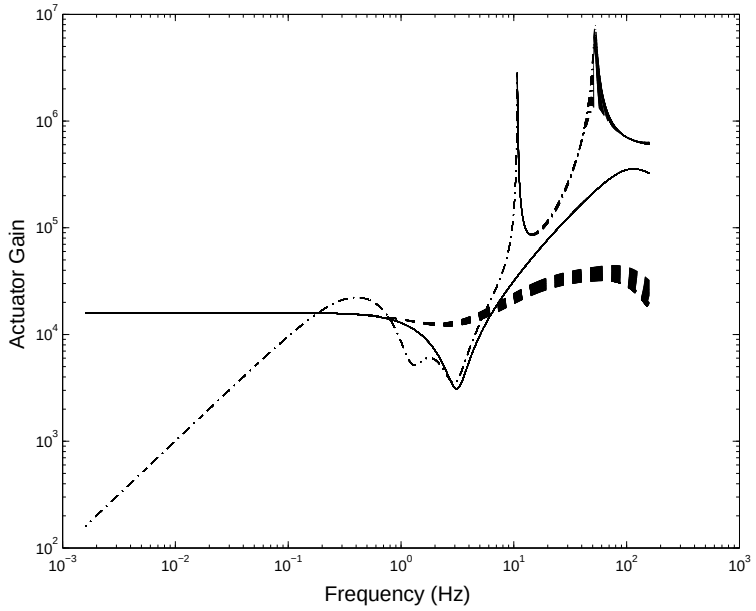

Figure 4.12: The actuator frequency response magnitude using the suspension travel measurement: $-$ the LQG design with tire damping $c_t = 2c_s$; $--$ the LQG design with tire damping c_t at the equally spaced 101 points between and including $0.001c_s$ and $0.1c_s$; $-.$ the hybrid algorithm with tire damping c_t at the same 101 points.

derived constraints complement the existing results in the literature on vehicle dynamics and control. Also, using the factorization approach of the feedback stability, it was shown that tire damping by coupling the motions of the sprung and unsprung masses eliminates a constraint on the wheel-hop mode. The influence of tire damping on the design of an active suspension for a lightly damped quarter-car model by a mixture of the LQG methodology and the interpolation approach was also illustrated. The study of the constraints on the achievable performance has remained largely restricted to pointwise constraints on the frequency responses while ride comfort and safety criteria are mostly expressed in terms of the rms values of the related transfer functions. Hence, a study of the constraints on the achievable rms responses warrants future research.

5 TIRE DAMPING EFFECT ON RIDE QUALITY OF LINEAR QUARTER-CAR ACTIVE SUSPENSIONS

The study of the constraints on the achievable performance has remained largely restricted to pointwise constraints in the frequency domain while ride comfort and safety criteria are mostly expressed in terms of the rms values of the sprung mass vertical acceleration, the suspension travel, and the tire deflection. It is generally agreed that typical road surfaces may be considered as realizations of homogeneous and isotropic two-dimensional Gaussian random processes and these assumptions make it possible to completely describe a road profile by a single power spectral density evaluated from any longitidunal track [52, 53]. Then, the spectral description of the road together with a knowledge of traversal velocity and of the dynamic properties of the vehicle provide an analysis which will describe the response of the vehicle expressed in terms of displacement, acceleration, or stress.

This chapter is organized as follows. In Section 5.1, first, all achievable transfer matrices from the road disturbance to the sprung mass vertical acceleration, the suspension travel, and the tire deflection are parameterized and an optimization problem that aims to minimize a quadratic function of the rms values of the outputs with respect to the class of all stabilizing controllers is formulated. In Subsection 5.1.1, the solution of this optimization problem is numerically obtained for a range of tire damping coefficients. It is observed that tire damping by coupling the motions of the sprung and unsprung masses eliminates a wheel-hop mode constraint; thus reduces the rms vertical acceleration without increasing the rms suspension travel and the rms tire deflection. This result confirms the design procedure outlined in Section 4.4, which is a mixture of the linear-quadratic-regulator and the interpolation methodologies, in an rms setup.

In Section 5.2, first, assuming that tire damping is known, a multi-objective suspension control problem is formulated and solved by using linear matrix inequalities. The control objective is to decrease the rms vertical acceleration while keeping the rms gain of the tire deflection within given bounds. This is the well-known ride comfort–road holding trade-off experienced in the design of active suspension systems. The influence of tire damping on the solution of this constrained optimization problem is studied in Section 5.2.1, and it is demonstrated that for a given upper bound on the tire deflection rms gain, tire damping reduces the rms vertical acceleration obtained with the same suspension system but tire damping omitted. Next, in Section 5.2.2, the assumption that tire damping coefficient is known is dropped and a multi-objective control problem for the suspension models with tire damping coefficient confined to a prescribed interval is formulated. By using LMIs a controller with guaranteed performance over all suspension models in the uncertainty set is obtained. The closed-loop performance of this robust controller is studied. In Section 5.3, the multi-objective control design problem is revisited and it is formulated as a non-convex and non-smooth optimization problem with controller order less than or equal to the quarter-car model order. For a range of controller orders, a similar parametric study is performed to assess the dependence of the closed-loop response on tire damping. The chapter is concluded by Section 5.4.

Multi-objective control of vehicle suspensions by using LMIs is not new. In [2], a constrained $\mathcal{H}_\infty$ control scheme with output and control constraints were studied. In [28], problems with $\mathcal{H}_2$ or $\mathcal{H}_\infty$ cost under positive realness constraint on controller structures were considered. The control objective similar to that of this chapter was studied in [29]. Robust multi-objective controllers were synthesized in [31,32] to cope with parameter uncertainties in system matrices characterized by a given polytope. Application of non-convex and non-smooth optimization algorithms in [33] to suspension control problems is reported in the recent work [34]. In [35], static output feedback $\mathcal{H}_\infty$ controller and non-fragile static output feedback $\mathcal{H}_\infty$ controller design proce-

dures via LMIs and genetic algorithm are presented. The $\mathcal{H}_\infty$ control problem for active vehicle suspension systems with actuator time delay is studied in [36] and a delay-dependent memoryless state feedback $\mathcal{H}_\infty$ controller is designed using LMIs.

This chapter is not about introducing new suspension control methods. In fact, the research on controlled suspension systems is well developed. The sole purpose of this chapter is to provide a detailed study of tire damping effect on ride quality of quarter-car active suspensions based on some popular $\mathcal{H}_2$-optimal control and multi-objective control frameworks. It is the author's belief that together with Chapter 4 this chapter will give a fairly complete picture of tire damping influence on quarter-car active suspensions.

5.1 $\mathcal{H}_2$ Optimal Control of Quarter-Car Active Suspension

Consider the quarter-car model shown in Figure 4.1. Assume that the vehicle travels on a straight profile with a constant velocity v. The road roughness model is as in Section 4.4. This model is simple enough to describe the heave motion of a vehicle traveling on a straight line. The equations of motion were derived in Section 4.1. In this chapter, the rms response of the quarter-car model following a random track described by Eq. (4.50) is studied. The vehicle response variables are as defined in Section 4.1.

For the design of a feedback law, the suspension stroke measurement $y = z_2$ is considered in this section. Note from Eqs. (4.1)–(4.4) that

$$y(s) = G_{21}(s)W(s) + G_{22}(s)U(s) \tag{5.1}$$

where $G_{21}(s)$ and $G_{22}(s)$ denote the bottom elements of $G_{21}(s)$ and $G_{22}(s)$ matrices defined in Eqs. 4.10– 4.11.

Let $K(s)$ denote the transfer function of the controller with input y and the output u. The feedback configuration is shown in Figure 4.2. Recall

that all compensators stabilizing G have the form [17, 132]:

$$K = Q(1 + G_{22}Q))^{-1}, \;\; Q \in \mathcal{RH}_\infty \tag{5.2}$$

With this parameterization, the transfer matrix from w to z denoted by $T_{zw}(s)$ takes a particularly convenient form which is affine in Q:

$$T_{zw} = G_{11} + G_{12}QG_{21}. \tag{5.3}$$

As Q varies over $\mathcal{RH}_\infty$, Eq. (5.3) parameterizes all achievable transfer matrices.

Recall that the feedback law in this section relies only on the suspension travel measurement. This choice is justified by the fact that closed-loop transfer functions obtained with a stabilizing controller that uses the sprung mass vertical acceleration and the suspension travel measurements can be approximated within a specified tolerance for the entire range of frequencies by the closed loop transfer functions of a stabilizing controller that uses only the suspension travel measurement [Proposition 4.3.13].

Now, all achievable rms responses of the quarter-car model to white-noise velocity road inputs are parameterized as follows. The colored-noise case will briefly be discussed in Section 5.1.1. From the first equality in Eq. (4.1), and Eqs. (5.3), (4.6)–(4.6), (4.10)–(4.11),

$$\begin{aligned} T_{zV_i} \;\; = \;\; & -\frac{s}{\Delta}\begin{bmatrix} -(c_t s + k_t)(c_s s + k_s) \\ m_s(c_t s + k_t) \\ m_s m_u s^2 + (m_s + m_u)c_s s + (m_s + m_u)k_s \end{bmatrix} \\ & + \frac{m_s s(c_t s + k_t)}{\Delta^2}\begin{bmatrix} s^2[m_u s^2 + c_t s + k_t] \\ (m_s + m_u)s^2 + c_t s + k_t \\ -m_s s^2 \end{bmatrix} Q. \end{aligned} \tag{5.4}$$

The autocovariance function of z is calculated from Eq. (4.50) as

$$R_z(\tau) = 2\pi n_0^2 \kappa v \int_{-\infty}^{\infty} T_{zV_i}(j\omega) T_{zV_i}^{\sim}(j\omega) e^{j\omega\tau}\, d\omega. \tag{5.5}$$

The square roots of the elements in the diagonal of $R_z(0)$ are equal to the rms vertical acceleration, the rms suspension travel, and the rms tire deflection.

Note from Eq. (5.5) that the weighted sum of the diagonal elements of $R_z(0)$ is given by

$$J(Q;\Lambda) = (2\pi n_0)^2 \kappa v \|\Lambda T_{zV_i}\|_2^2 \tag{5.6}$$

where Λ is a diagonal matrix with nonnegative entries $\lambda_1, \lambda_2, \lambda_3$. The optimized version of Eq. (5.6):

$$J^*(\Lambda) = \inf_{Q \in \mathcal{RH}_\infty} J(Q;\Lambda) \tag{5.7}$$

will be considered in the sequel. Observe that the control input chosen in Eq. (5.7) minimizes $\sum_{k=1}^{3} \lambda_k^2 \, \mathrm{E}[z_k^2]$ with respect to the set of all stabilizing controllers.

5.1.1 $\mathcal{H}_2$ Synthesis and the Influence of Tire Damping

Let

$$F = -\frac{s\Lambda}{\Delta} \begin{bmatrix} -(c_t s + k_t)(c_s s + k_s) \\ m_s(c_t s + k_t) \\ m_s m_u s^2 + (m_s + m_u) c_s s + (m_s + m_u) k_s \end{bmatrix}, \tag{5.8}$$

$$H = \frac{\Lambda}{\Delta} \begin{bmatrix} s^2[m_u s^2 + c_t s + k_t] \\ (m_s + m_u) s^2 + c_t s + k_t \\ -m_s s^2 \end{bmatrix}. \tag{5.9}$$

From Eq. (5.7),

$$J^*(\Lambda) = (2\pi n_0)^2 \kappa v \inf_{Q \in \mathcal{RH}_\infty} \|F - m_s s(c_t s + k_t)\Delta^{-1} H Q\|_2^2. \tag{5.10}$$

Suppose $\lambda_1 > 0$. Then, $H(s)$ has full rank on the imaginary axis including ∞. Furthermore, $m_s s(c_t s + k_t)\Delta^{-1}$ has no zeros in the open right half plane. The right-hand side of Eq. (5.10) does not change when F and H are transposed. Hence, Lemma 6.3.10 in [132] is applicable:

$$J^*(\Lambda) = (2\pi n_0)^2 \kappa v \inf_{Q \in \mathcal{RH}_\infty} \|F - HQ\|_2^2. \tag{5.11}$$

Next, an inner-outer factorization of $H(s)$ is done. In doing so, the first step is to get a spectral factor of $H^{\sim}(s)H(s)$. If the quadruplet (A_H, B_H, C_H, D_H)

denotes a minimal state-space realization of $H(s)$, then a spectral factor denoted by $H_o(s)$ is given by

$$H_o(s) = \left(A_H, B_H, \underline{D}^{-\frac{1}{2}}(D_H^T C_H + B_H^T X), \underline{D}^{\frac{1}{2}}\right)$$

where $\underline{D} = D_H^T D_H$ and X is the stabilizing solution of the Riccati equation:

$$\begin{aligned}(A_H - B_H\underline{D}^{-1}D_H^T C_H)^T X + X(A_H - B_H\underline{D}^{-1}D_H^T C_H) - XB_H\underline{D}^{-1}B_H^T X \\ +C_H^T(I - D_H\underline{D}^{-1}D_H^T)C_H = 0.\end{aligned}$$

The inner factor is then

$$H_i(s) = H(s)H_o^{-1}(s). \tag{5.12}$$

The next step is the calculation of a complementary inner factor $N_\perp$ of H_i, *i.e.,* finding a matrix $N_\perp$ that makes $[H_i\ N_\perp]$ square and inner. If (A_1, B_1, C_1, D_1) is a minimal state-space realization of H_i, then a realization of $N_\perp$ is given by the formula [17][Lemma 13.31]:

$$N_\perp = \left(A_1, -Y^{-1}C_1^T D_\perp, C_1, D_\perp\right) \tag{5.13}$$

where $D_\perp$ is an orthogonal complement of D_1 such that $[D_1\ D_\perp]$ is square and orthogonal and Y is the observability Gramian:

$$A_1^T Y + Y A_1 + C_1^T C_1 = 0. \tag{5.14}$$

Observe that H_i and $N_\perp$ have four common poles. When Λ is nonsingular, $D_\perp$ can be chosen as

$$D_\perp = \begin{bmatrix} 0 & 0 \\ 1 & 0 \\ 0 & 1 \end{bmatrix}. \tag{5.15}$$

Then,

$$\begin{aligned}\inf_{Q\in\mathcal{RH}_\infty} \|F - HQ\|_2^2 &= \|N_\perp^\sim F\|_2^2 + \inf_{Q\in\mathcal{RH}_\infty} \|H_i^\sim F - H_o Q\|_2^2 \\ &= \|N_\perp^\sim F\|_2^2 + \|\Pi^\perp H_i^\sim F\|_2^2\end{aligned} \tag{5.16}$$

with

$$Q = H_o^{-1}\Pi H_i^{\sim} F. \tag{5.17}$$

Hence, from Eqs. (5.11) and (5.16)

$$J^*(\Lambda) = (2\pi n_0)^2 \kappa v \left\{ \|\Pi N_{\perp}^{\sim} F\|_2^2 + \|\Pi^{\perp} N_{\perp}^{\sim} F\|_2^2 + \|\Pi^{\perp} H_i^{\sim} F\|_2^2 \right\}. \tag{5.18}$$

The infimum in Eq. (5.10) is not achieved. However, simple modifications of Q in Eq. (5.17) yield approximations arbitrarily close to $J^*(\Lambda)$. If w is not integrated white-noise, but its derivative is colored-noise, *i.e.,* $V_{\rm i} = \dot{w} = \Psi\eta$ for some minimum phase $\Psi \in \mathcal{RH}_\infty$ and unit-intensity white noise η, it suffices to replace F in Eq. (5.18) with $F\Psi$. From the discussion leading to Eq. (5.11), observe that Ψ is allowed to have zeros on the imaginary axis.

To investigate the influence of tire damping on the optimal cost $J^*(\Lambda)$, it will be more convenient to define a dimensionless quantity:

$$\mu(c_t; \Lambda) = \frac{[J^*(\Lambda)]^{1/2}}{[J(0; \Lambda)]^{1/2}}. \tag{5.19}$$

Thus, $\mu(c_t; \Lambda)$ is a measure of active suspension performance relative to the passive suspension performance in the root–mean–square sense. Since $J(Q; \Delta)$ is proportional to v, $\mu(c_t; \Lambda)$ does not depend on the vehicle speed. Moreover, $\mu(c_t; \Lambda) \leq 1$ for $J^*(\Lambda)$ is obtained by minimizing $J(Q; \Lambda)$ over $\mathcal{RH}_\infty$ and $0 \in \mathcal{RH}_\infty$. In Figure 5.1, $\mu(c_t; \Lambda)$ is plotted versus c_t for the weight $\Lambda = \mathrm{diag}(1, 1, 1)$. This choice of Λ puts equal emphasis on the three output rms values. The impact of tire damping on the active suspension performance is remarkable, in particular for large values of $c_{\rm t}$.

For a vehicle with $c_t = 0$ and traveling at the speed $v = 20$ m/s, the passive suspension has the rms values 0.5424, 0.0046, and 0.0017 for the vertical acceleration, the suspension travel, and the tire deflection, respectively. Thus, the rms vertical acceleration is more than one hundred times the rms suspension travel and the rms suspension travel is more than three times the rms tire deflection. Consequently, the choice $\Lambda = I_3$ results in dramatic reduction of the rms vertical acceleration at the expense of the other responses.

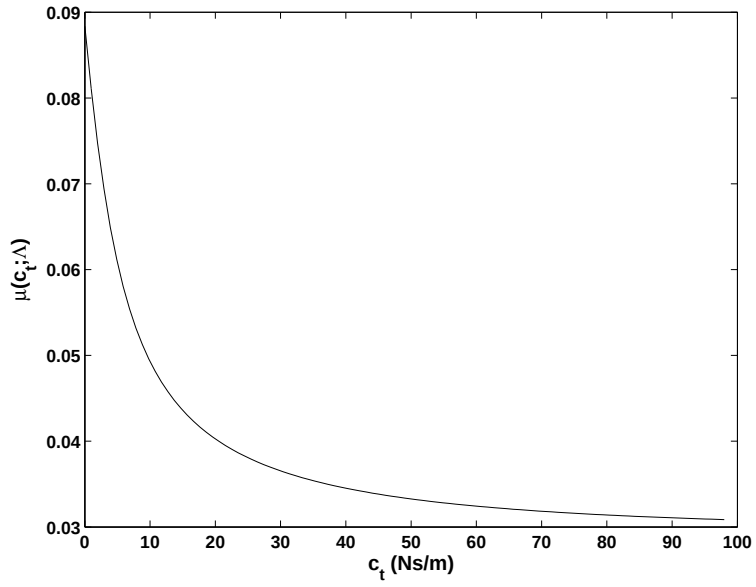

Figure 5.1: The optimized performance index scaled by the open-loop performance index as a function of tire damping coefficient for $\Lambda = \text{diag}(1, 1, 1)$.

Therefore, by setting Λ to I_3, the trade-offs: the sprung mass vertical acceleration versus the suspension travel and the sprung mass vertical acceleration versus the tire deflection are almost entirely neglected. In Figure 5.2, $\mu(c_t; \Lambda)$ is plotted as a function of tire damping coefficient for $\Lambda = \text{diag}(1, 10, 100)$. The latter choice for Λ respects the trade-offs. Although it is not as impressive as in Figure 5.1, the influence of tire damping is strongly felt. In the $\mathcal{H}_2$-optimal control context, this observation reinforces the conclusion in [26, 68] that tire damping can be used to improve ride comfort while maintaining road holding ability and rattle space compactness.

The results in this section show that influence of tire damping on the $\mathcal{H}_2$-optimal design of active suspension systems can be significant. To put it another way, performance of an active suspension system designed by ignoring tire damping may seriously deteriorate. This conclusion has been reached by minimizing a single objective function without paying attention to how its components are being penalized. In fact, $\|F - HQ\|_2$ does not change when F and H are left multiplied by any orthogonal matrix or, more generally, by any square inner matrix. These operations redistributes the trade-offs. In

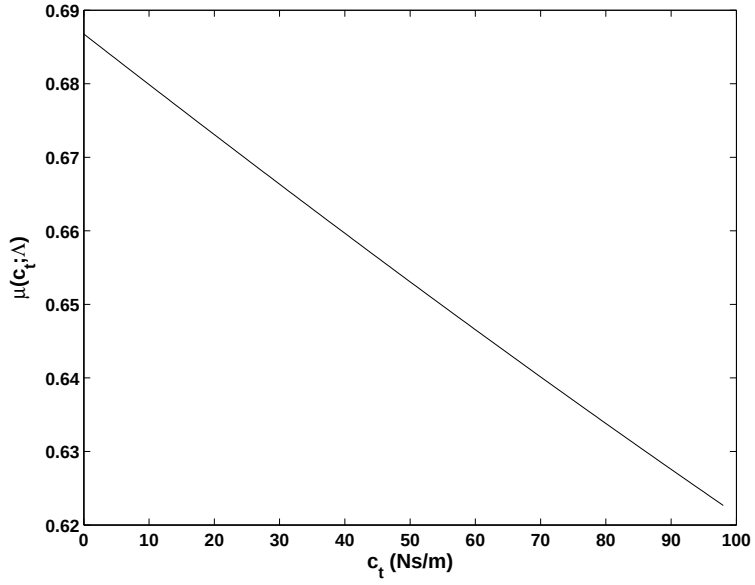

Figure 5.2: The optimized performance index scaled by the open-loop performance index as a function of tire damping coefficient for $\Lambda = \mathrm{diag}(1, 10, 100)$.

addition, controller synthesis must deal with the issues of actuator saturation, parameter and load variations, and robustness to uncertainties in road and tire models. The design problem is then multi-objective synthesis of linear robust output-feedback controllers, for which LMI based solutions have been proposed in the literature [2, 29, 32].

After minor changes in the proofs, the results derived in this section extend without modification to half-car models provided that the road excitation at the front wheel can be modeled as output of a linear-shape filter driven by white-noise. The changes in the proofs are due to the fact that the Q parameter of the stabilizing controller defined in Eq. (5.2) happens to be a 2 by 2 rational matrix in $\mathcal{RH}_\infty$ when the quarter-car model is switched to half-car model. This change in the dimension of the Q parameter requires checking right coprimeness of certain two matrices in $\mathcal{RH}_\infty$. The details can be found in [75]. The parameters of the linear shape-filter can directly be estimated from measured road data [57,65]. In this case, the coefficient defined in Eq. (5.19) depends on v. But, this dependence is weak since in the bandwidth of interest, the power spectrum of the filter output behaves like power spec-

trum of an integrated white-noise process. The temporal correlation between the front and the rear wheels may be predicted by a Pade filter of sufficient order.

5.2 Multi-Objective Control Using LMIs

In designing active suspension systems, one needs to take the following aspects into consideration:

(i) As an indicator of *ride comfort*, $\ddot{x}_1$ should be made as small as possible.

(ii) $x_1 - x_2$ should be kept below the maximum allowable suspension stroke to prevent excessive suspension bottoming, which can result in structural damage and deterioration of ride comfort.

(iii) In order to ensure a firm uninterrupted contact of wheels to road, the dynamic tire load should not exceed the static ones.

(iv) To avoid actuator saturation, u should stay within limits at all times.

Thus, designing control law for suspension systems is a multi-objective control problem where the strategy is to minimize the vertical acceleration while keeping the constraints satisfied. Many other constraints can be added to the above list. However, this list reveals all fundamental design trade-offs. The robustness to variations in tire damping will be studied later. Due to the standing assumption that w is integrated white-noise process, the rms values of z_k, $k = 1, 2, 3$ are scaled by $\sqrt{v}$ for both passive and active suspensions. Hence, vehicle speed does not influence suspension trade-offs and relative performance of active suspension with respect to passive suspension.

Let us consider the state-space realization in Eqs. (4.42)–(4.49). In this section, the following dynamic output feedback structure:

$$\begin{aligned} \dot{\zeta} &= A_K\zeta + B_K y, \\ u &= C_K\zeta + D_K y \end{aligned} \tag{5.20}$$

where the state-space parameters A_K, B_K, C_K, D_K are to be determined will be studied. Recall that $u = D_K y$ with row vector D_K unknown is the static output feedback case. The feedback configuration and the closed-loop transfer function $T_{zV_i}(s)$ are as in Section 5.1. Then, the multi-objective control design problem is:

Problem 5.2.1. *Given $\gamma, \rho_1, \rho_2 > 0$, design an output-feedback controller $u = K(s)y$ that satisfies $\|T_{z_3V_i}\|_\infty < \gamma$ and minimizes $\rho_1\|T_{z_1V_i}\|_2^2 + \rho_2\|T_{z_2V_i}\|_2^2$.*

Before the presentation of the solution, several remarks are in order. First, without the rms gain constraint $\|T_{z_3V_i}\|_\infty < \gamma$ and with $\rho_2 = 0$, the rms vertical acceleration response can be made zero. With tire damping neglected, it is a well-known trade-off that the vertical acceleration can only be decreased at the expense of the tire deflection. The choice between $\|T_{z_3V_i}\|_2$ and $\|T_{z_3V_i}\|_\infty$ is arbitrary since both norms reveal the vertical acceleration–tire deflection trade-off. However, in numerical studies it was observed that $\|T_{z_3V_i}\|_\infty \leq \gamma$ is a tight constraint, *i.e.,* the equality is attained by the minimizing solution. Hence, it directly shapes the optimal solution.

The control design requirements were expressed in the time-domain. The multi-objective control problem formulated above, on the other hand, has the control objective and the constraints in the frequency-domain. A solution based on LMIs will be presented next. This paradigm readily encompasses time-domain constraints at a price of conservatism. By tuning the parameters γ, ρ_1, and ρ_2, the solution of the above design problem can be forced to satisfy time-domain constraints.

In Section 5.1.1, a closed-form expression for the cost function $\sum_{k=1}^{3} \rho_k\|T_{z_kV_i}\|_2^2$ was derived and it was demonstrated that this expression could be made very small provided that ρ_2 and ρ_3 are in the order of ρ_1. As pointed out there, there is not much control over the tire deflection. Nevertheless, this approach does not introduce any conservatism as opposed to LMI based approaches, where a common Lyapunov function is sought for all LMI constraints.

In the following subsection, guidelines how to choose γ, ρ_1, and ρ_2 will be provided. As a final remark, notice that the multi-objective control problem data and consequently the solution of this problem depend on the uncertain parameter c_t. Precise knowledge of tire damping coefficient is an unrealistic assumption. This assumption will be relaxed later and a robust multi-objective suspension control problem will be formulated. But, examination of the influence of tire damping on the solution to the multi-objective control problem is in order.

5.2.1 Influence of Tire Damping

Let $G_{z_kV_i}$ denote the open-loop transfer functions from V_i to the output variable z_k, $k = 1, 2, 3$. The parameters ρ_1, ρ_2, and γ of the multi-objective control problem are chosen as follows. Given c_t, compute $\|G_{z_1V_i}\|_2$, $\|G_{z_2V_i}\|_2$, and $\|G_{z_3V_i}\|_\infty$. For example, when tire damping is absent $\|G_{z_1V_i}\|_2 = 44.57$, $\|G_{z_2V_i}\|_2 = 0.37$, and $\|G_{z_3V_i}\|_\infty = 0.0363$. Now, for some positive parameters λ and μ set $\rho_1 = \|G_{z_1V_i}\|_2^{-1}$, $\rho_2 = \|G_{z_2V_i}\|_2^{-1}\lambda$, and $\gamma = \|G_{z_3V_i}\|_\infty\mu$. By these scalings, it is possible to monitor the progress of the solution with respect to certain benchmark values. The parameters λ and μ control the trade-offs: the vertical acceleration–suspension stroke and the vertical acceleration–tire deflection, respectively. The optimization algorithm is implemented by the `hinfmix` command of MATLAB's LMI Control Toolbox [27]. This command produces a controller of order which is equal to that of the plant.

In Figs. 5.3 and 5.4, the rms values of z_k, $k = 1, 2, 3$ and the tire deflection rms gain of a vehicle traveling with a speed of 20 m/s subjected to white-noise velocity excitation are plotted as functions of tire damping coefficient for both the passive and the active suspension systems designed with two different sets of λ and μ using the vertical acceleration and the suspension travel measurements. As expected, the vertical acceleration–tire deflection and the suspensions travel–tire deflection trade-offs are notable. The declining responses as functions of tire damping indicate that tire damping improves

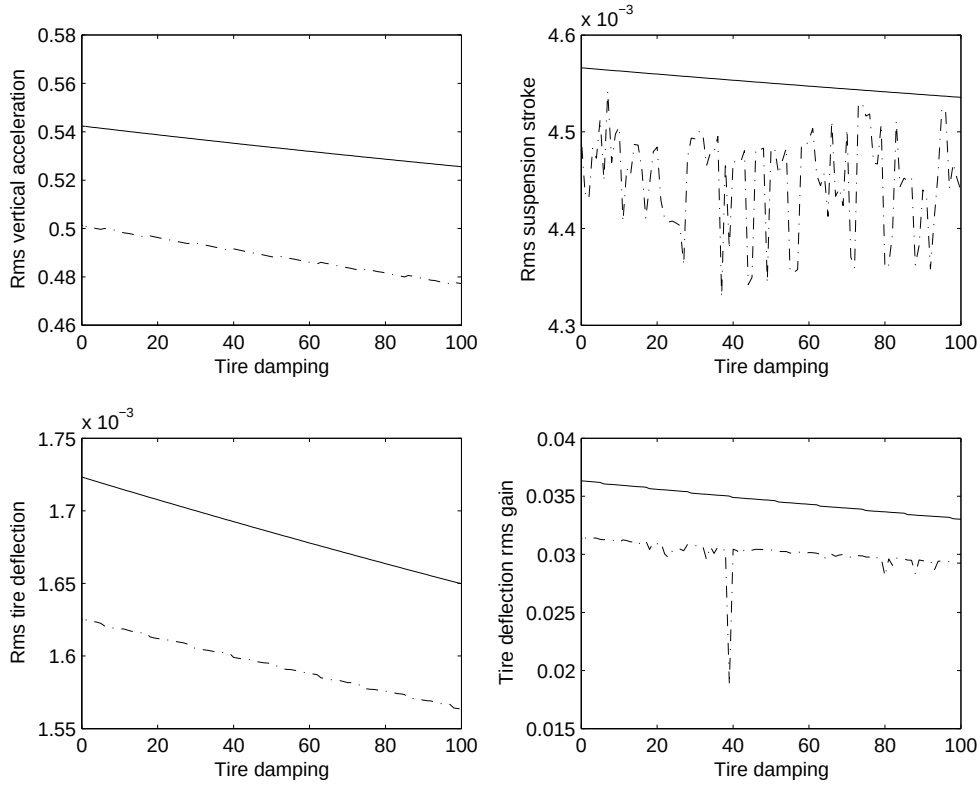

Figure 5.3: The rms values of z_k, $k = 1, 2, 3$ and tire deflection rms gain of the vehicle subjected to white-noise velocity input as a function of c_t: (–) passive suspension; (-.) active suspension with $\lambda = 0.1$ and $\mu = 1$ using vertical acceleration and suspension travel measurements.

passive and active suspension performances. The improvement on the rms vertical acceleration of the active suspension due to tire damping is noteworthy for $\mu = 2$. Moreover, the rms actuator force varies between 59.5 and 62.5 for all $0 \leq c_t \leq 100$. Hence, the actuator saturation is not likely to occur. The rms tire load can not be calculated when $c_t > 0$ since V_i was modeled as a white-noise process.

In Fig. 5.5, the vertical acceleration, the suspension travel, and the tire deflection frequency responses of the active suspension system designed with the parameters $\lambda = 0.1$, $\mu = 2$, and $c_t = 50$ are plotted. The single measurement case, *i.e.*, $y = z_2$ was also investigated. Numerical results that are almost identical to those displayed graphically in Figures 5.1–5.3 were obtained.

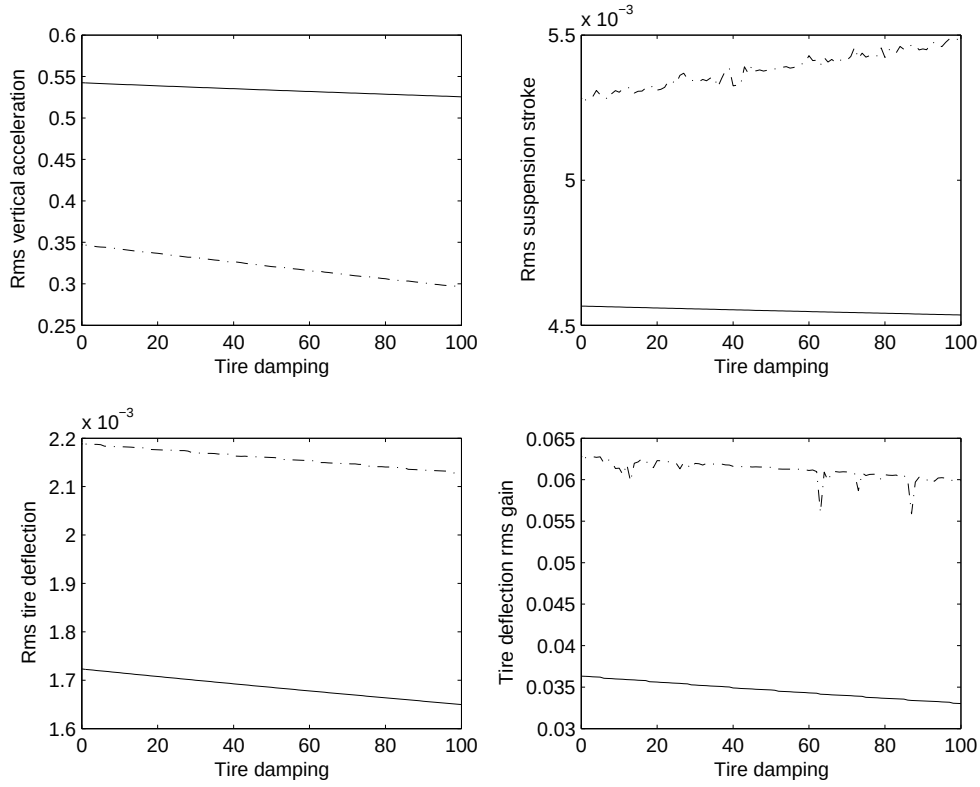

Figure 5.4: The rms values of z_k, $k = 1, 2, 3$ and tire deflection rms gain of the vehicle subjected to white-noise velocity input as a function of c_t: (–) passive suspension; (-.) active suspension with $\lambda = 0.1$ and $\mu = 2$ using vertical acceleration and suspension travel measurements.

To validate the analysis results of the LMI-based multi-objective controller in time-domain, consider the following bump input [36]

$$w(\tau) = \begin{cases} \frac{h}{2}[1 - \cos(2\pi v\tau/l)], & 0 \le \tau \le 1/v \\ 0, & \tau > l/v \end{cases} \tag{5.21}$$

where h and l are the height and the length of the bump. The output of the active suspension whose frequency response magnitudes are plotted in Figure 5.5 to the bump input in Eq. (5.21) are shown in Figure 5.6 for $h =$ 0.10m, $l = 2$m, and $v = 45$ km/h.

As expected from Figure 5.5, the vertical acceleration amplitude is significantly reduced by the feedback while the suspension travel and the tire deflection amplitudes are increased. The influence of tire damping on time-

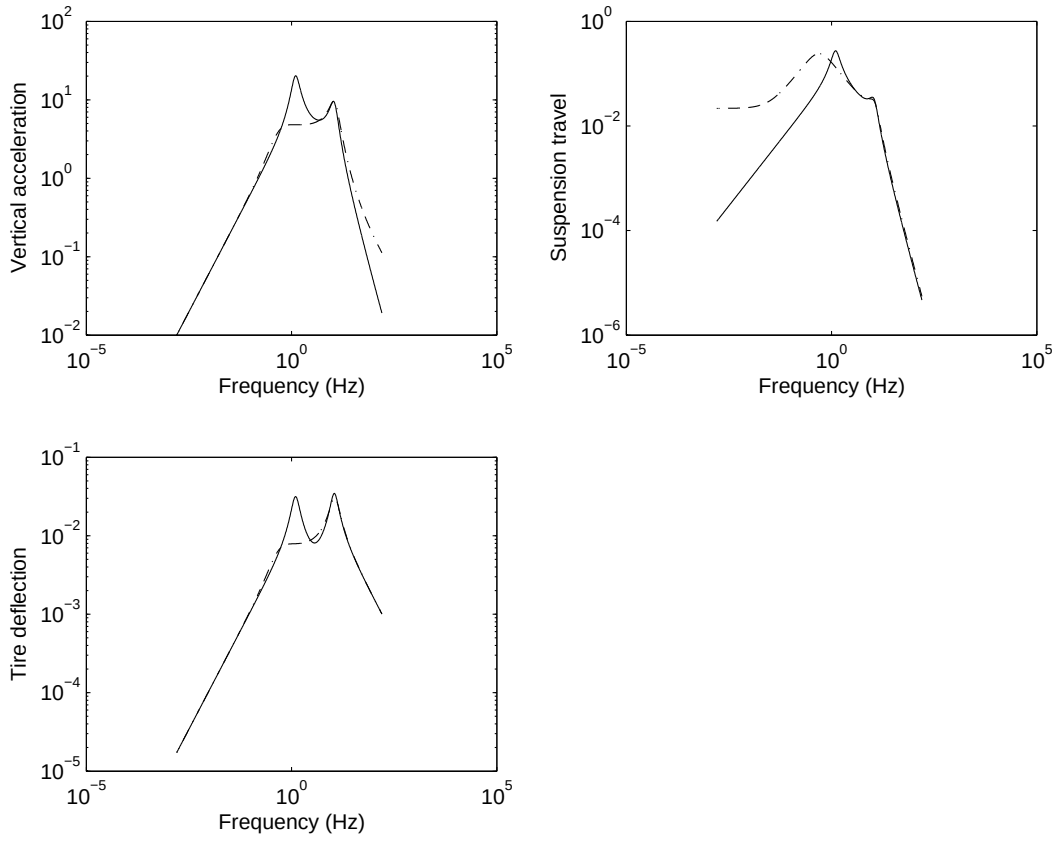

Figure 5.5: Vertical acceleration, suspension travel, and tire deflection frequency responses of the active suspension system designed with the parameters $\lambda = 0.1$, $\mu = 2$, and $c_t = 50$ using vertical acceleration and suspension travel measurements.

domain responses to bump inputs as in Eq. (5.21) can be made transparent by defining the dimensionless quantities:

$$\delta_k(c_t) = 1 - \frac{\sup_{\tau \geq 0} |z_k^{\mathrm{ac}}(\tau)|}{\sup_{\tau \geq 0} |z_k^{\mathrm{p}}(\tau)|}, \qquad k = 1, 2, 3 \tag{5.22}$$

where $z_k^{\mathrm{ac}}(\tau)$ and $z_k^{\mathrm{p}}(\tau)$ denote the regulated output components in Eqs. (4.2)–(4.4) for the active and the passive suspensions, respectively. The quantities δ_k, $k = 1, 2, 3$ plotted in Figure 5.7 as functions of tire damping coefficient change analogously to the rms values of z_k, $k = 1, 2, 3$ displayed in Figure 5.4 when the latter are normalized similarly to Eqs. (4.2)–(4.4); thus, validating the previously drawn conclusions in time-domain.

The numerical studies reported in this section do not hint whether it is

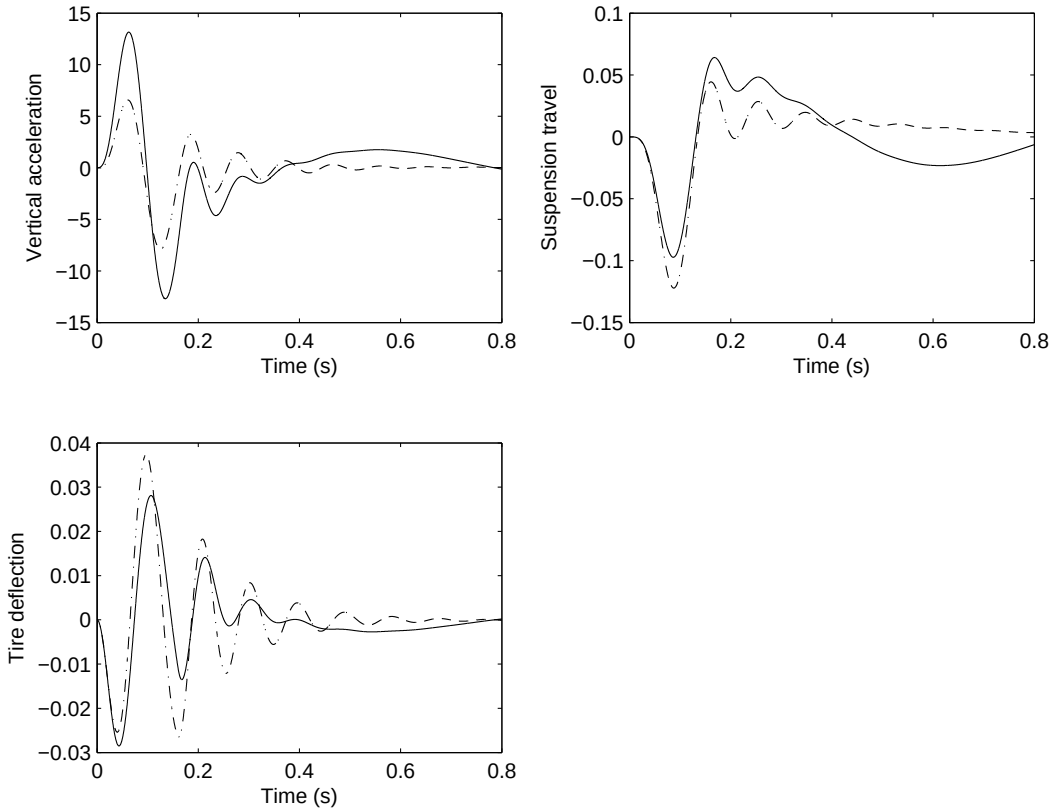

Figure 5.6: The bump responses of the passive and the active suspensions: (–) passive suspension; (-.) active suspension designed with $\lambda = 0.1$, $\mu = 2$, and $c_t = 50$ using the vertical acceleration and the suspension travel measurements.

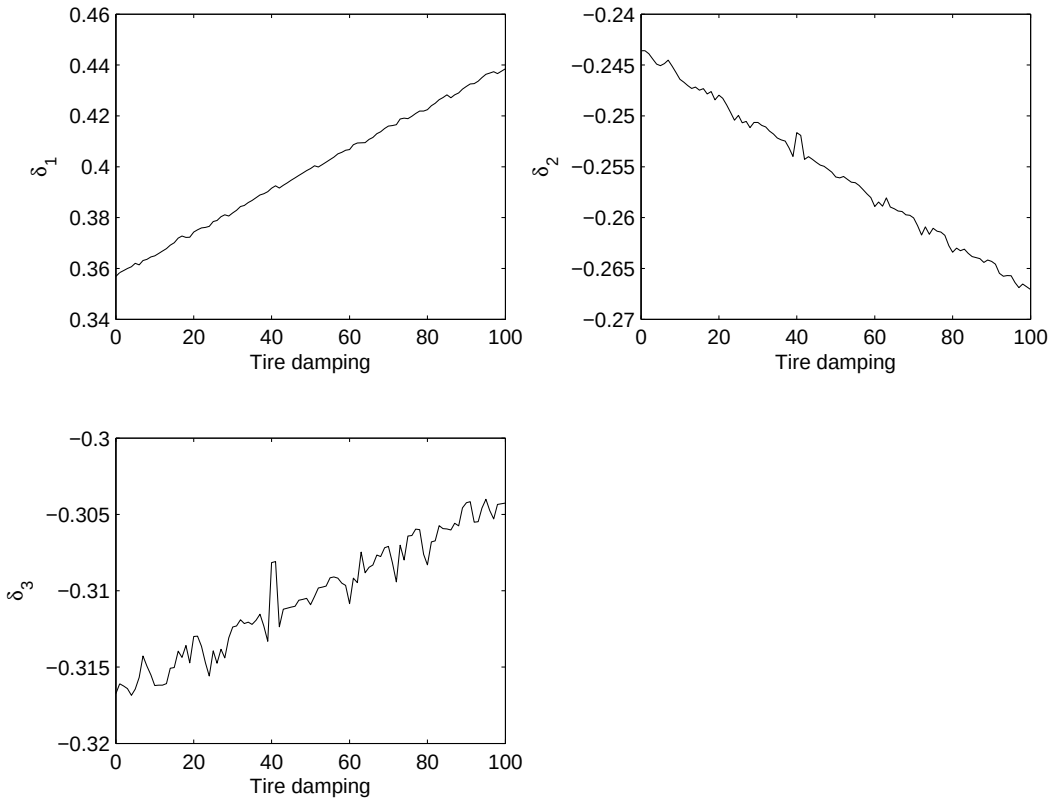

Figure 5.7: The relative performance improvements of the active suspension designed with $\lambda = 0.1$ and $\mu = 2$ using the vertical acceleration and the suspension travel measurements for the bump input.

possible to significantly reduce the rms vertical acceleration without increasing the rms suspension travel and the rms tire deflection. In fact, this is possible as soon as tire damping coefficient is non-zero [26,68]. This result was established in Section 4.4 by using a 17th order controller; but, the order of the resulting closed-loop transfer function is only 8. However, this controller is susceptible to saturation. In general, the order of the controller is dictated by the orders of the plant and the weighting functions. Controllers with lower orders are usually preferable in terms of implementation and computing efforts. Therefore, in Section 5.3 fixed-order robust control algorithms will be used to design $\mathcal{H}_\infty$ controllers with specified orders lower than that of the quarter-car model.

5.2.2 Polytopic Vehicle Suspension Models

The multi-objective control problem solved in Section 5.2.1 assumes exact value of the tire damping coefficient, which is difficult to estimate since it depends on many factors and varies during driving. In this subsection, assuming that c_t takes values in some prescribed interval $[\alpha, \beta]$, a multi-objective controller with guaranteed performance for all possible values of tire damping coefficient will be designed. Note that this uncertainty structure allows fast variations of tire damping.

Let A^0 and B_1^0 denote the matrices A and B_1 in Eqs. (4.46) and (4.47) for $c_t = 0$ and set $A^1 = c_t^{-1}(A - A^0)$ and $B_1^1 = c_t^{-1}(B_1 - B_1^0)$. Define two vertex systems by the quadruplets $P_0 = (A^0, [B_1^0 \;\; B_2], C_1, [0 \;\; D_{12}; 0 \;\; D_{22}])$ and $P_1 = (A^1, [B_1^1 \;\; 0], 0, 0)$ where the MATLAB notation is adopted. Then, the quadruplet P formed conformally with P_0 and P_1 and describing the system studied in Section 5.2.1 can be written as

$$P = P_0 + c_t P_1, \qquad c_t \in [\alpha, \beta] \tag{5.23}$$

which is a line segment in the Euclidean space of state-space parameters. Let $\mathcal{P}$ denote the set of systems defined by Eq. (5.23). Then, the robust multi-objective control design problem is:

Problem 5.2.2. *Given $\gamma, \rho_1, \rho_2 > 0$ and $\mathcal{P}$, design a state-feedback controller $u = Kx$ that satisfies $\|T_{z_3 V_i}\|_\infty < \gamma$ for all $P \in \mathcal{P}$ and minimizes* $\sup_{P \in \mathcal{P}} \rho_1 \|T_{z_1 V_i}\|_2^2 + \rho_2 \|T_{z_2 V_i}\|_2^2$.

Again, this optimization problem can be solved by using LMIs. Its solution is implemented by the `msfsyn` command in MATLAB's LMI Toolbox [27]. For illustration, suppose $\alpha = 25$ and $\beta = 50$. The same formulas for ρ_1, ρ_2, and γ proposed in Section 5.2 can be used provided that the scalings $\|G_{z_k V_i}\|$ are computed with a fixed c_t. For the computations, $c_t = 0$ was picked and the above optimization problem was solved. Let K_p denote the solution which depends on the scalings λ and μ. Using the same msfsyn command with the uncertainty set P_0, which is a singleton, and the same weights, another controller denoted by K_0 was obtained.

Let us see how the robust controller is performing against K_0. Fix c_t and denote the corresponding system in Eq. (5.23) by P_t. Then, compute the closed-loop rms responses of P_t using the controllers K_0 and K_p with $\lambda = 0.1$. The two rms response sets were observed to be slightly different, in particular for small values of μ. For example, when $\mu = 1$ from Table 5.1, the rms vertical acceleration, the rms suspension travel, and the rms tire deflection are read respectively as 0.4856, 0.0045, 0.0016 with K_p and 0.4926, 0.0044, 0.0016 with K_0 for $c_t = 35$. As μ was increased, the rms vertical acceleration of the robust design decreased. This is not unexpected since the slope of the rms vertical acceleration-tire damping curve is steep for large values of μ as seen in Figure 5.4.

As pointed out earlier, the multi-objective control problems studied in this section can be reformulated in several different forms by considering a variety of objective functions and constraints in frequency and time-domains. Then, these objective functions and constraints can be converted into affine functions and LMIs by using the transformations cataloged in [46]. The particular forms chosen in this section have direct implementations in the LMI Toolbox of MATLAB.

Table 5.1: The rms responses of the passive suspension and the robustly designed active suspension for tire damping uncertainties $25 \leq c_t \leq 50$. The active suspension was designed by solving Problem 5.2.2 for $\lambda = 0.1$ and $\mu = 1$.

rms	$c_t = 25$			$c_t = 35$			$c_t = 50$		
	passive	K_0	K_p	passive	K_0	K_p	passive	K_0	K_p
z_1	0.5379	0.4951	0.4881	0.5361	0.4926	0.4856	0.5336	0.4889	0.4818
z_2	0.0046	0.0044	0.0045	0.0046	0.0044	0.0045	0.0046	0.0044	0.0045
z_3	0.0017	0.0016	0.0016	0.0017	0.0016	0.0016	0.0017	0.0016	0.0016

Multi-objective control of a half-car suspension system using LMIs was studied in [73] where the front and the rear road velocity inputs were assumed to be uncorrelated white-noise processes. The parametric tire damping studies did not conform well with the quarter-car results reported here. In particular, the robust controller designed to cope with polytopic tire damping uncertainties did not offer any advantage over the conventional suspension system. The coupling between the heave and the pitch motions appears to be the main source of this discrepancy because the assumed road excitation model ignores this coupling.

5.3 Multi-Objective Control via Fixed-Order Optimization

In this section, the $\mathcal{H}_\infty$ fixed-order optimization (HIFOO) toolbox will be used to design low complexity active suspension systems. More specifically, consider the following multi-objective control design problem:

Problem 5.3.1. *Given $\beta_1 > 0$ and $\beta_2 > 0$ and a specified controller order n_K, find an output-feedback controller $u = K(s)y$ that internally stabilizes the*

closed-loop system and minimizes $\|T_{z_1V_i}\|_\infty$ *while satisfying* $\|T_{z_2V_i}\|_\infty < \beta_1$ *and* $\|T_{z_3V_i}\|_\infty < \beta_2$.

This is a non-convex optimization problem when n_K is less than the order of the passive suspension system. The details on the HIFOO toolbox can be found in [33, 45]. The optimization algorithms in the HIFOO toolbox do not attempt to find global minimum. Hence, their success depend on proper initialization. They have been successfully applied to several benchmark problems [34, 45]. Currently, this toolbox does not accommodate norms other than the supremum norm on either the objective function or the constraints.

As in the LMI design examples of the previous section, choose β_1 and β_2 as follows. Given c_t, set $\beta_1 = \|G_{z_2V_i}\|_\infty$ and $\beta_2 = \|G_{z_3V_i}\|_\infty$. Thus, it is possible to monitor the progress of the solution with respect to the passive suspension. For the same purpose, the objective function may also be scaled with $\|G_{z_1V_i}\|_\infty$. In the implementation of the algorithms in the HIFOO toolbox, the scalings $\|G_{z_1V_i}\|_\infty = 20.2380$, $\|G_{z_2V_i}\|_\infty = 0.2739$, and $\|G_{z_3V_i}\|_\infty = 0.0331$ were used for $c_t = 98$. These scalings result in the choices $\beta_1 = \beta_2 = 1$ and the achieved minimum being less than or equal to one.

Table 5.2: The rms responses of the passively and actively suspended quarter-car model with the HIFOO controllers of order n_K and $c_t = 98$.

rms	Passive	$n_K = 1$	$n_K = 2$	$n_K = 3$	$n_K = 4$
z_1	0.5259	0.4627	0.4746	0.4763	0.4748
z_2	0.0045	0.0040	0.0041	0.0041	0.0040
z_3	0.0017	0.0016	0.0016	0.0016	0.0016

In Table 5.2, the rms values of the vertical acceleration, the suspension travel, and the tire deflection are displayed for the passive and the active suspensions designed by using the HIFOO toolbox with controller orders varying from one to four. The vehicle forward velocity and the road excitation are as in Section 5.2. The performance improvements obtained with the HIFOO

controllers in comparison to the LMI designs in Section 5.2 are impressive. Interestingly, the simplest controller achieves the best performance improvement.

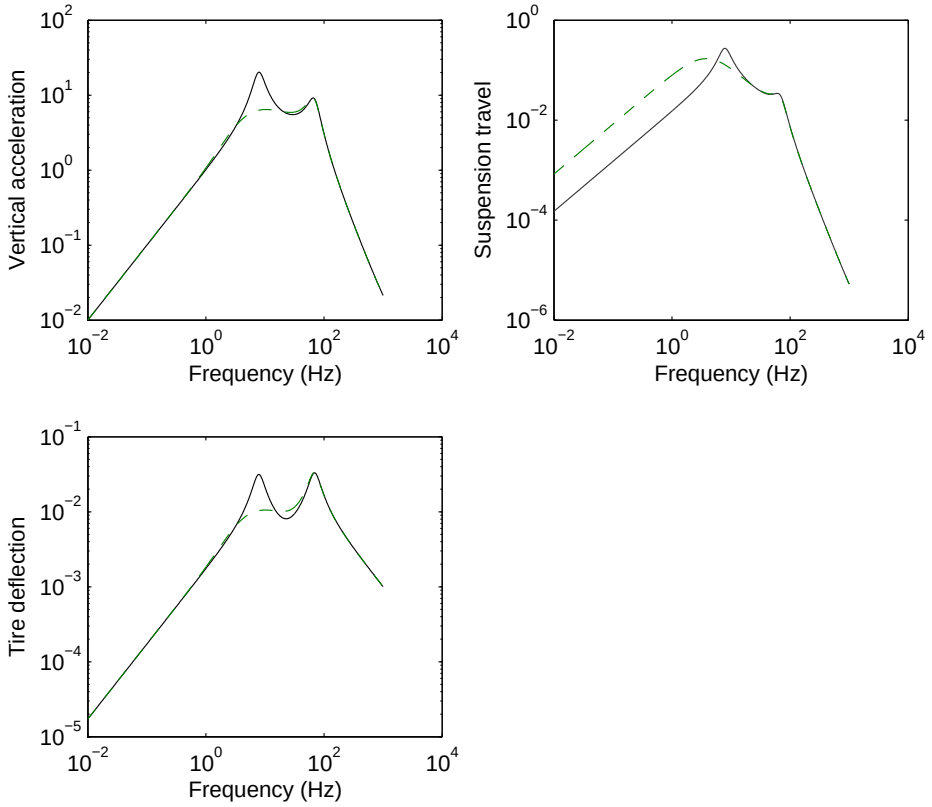

Figure 5.8: Vertical acceleration, suspension travel, and tire deflection frequency response magnitudes of the first-order HIFOO design using suspension travel measurement.

The magnitude responses of the first-order HIFOO controller plotted in Figure 5.8 compare favorably with respect to the responses of the LMI design plotted in Figure 5.5 for $c_t = 50$ and using vertical acceleration and suspension travel measurements. The HIFOO designs were obtained using only suspension travel measurement.

Finally, we investigate influence of tire damping on the closed-loop performance of the HIFOO controllers. In Figures 5.9–5.12, the rms values of $z_k,\ k = 1, 2, 3$ are plotted for $n_K = 1, 2, 3$, and 4 versus c_t. For each n_K

and a range of c_t, the corresponding HIFOO controllers were initialized by the same n_Kth order HIFOO controller whose rms response values are displayed in Table 5.2. For all n_K, the rms vertical acceleration decreases as tire damping increases similar to the patterns observed in Figures 5.3 and 5.4. The rms suspension travel and the rms tire deflection are observed to be non-increasing functions of tire-damping coefficient as in Figures 5.3 and 5.4. Thus, the basic conclusions drawn in Section 5.2, including responses to the bump inputs in Eq. (5.21), carry on, without modification, to the HIFOO designs as well.

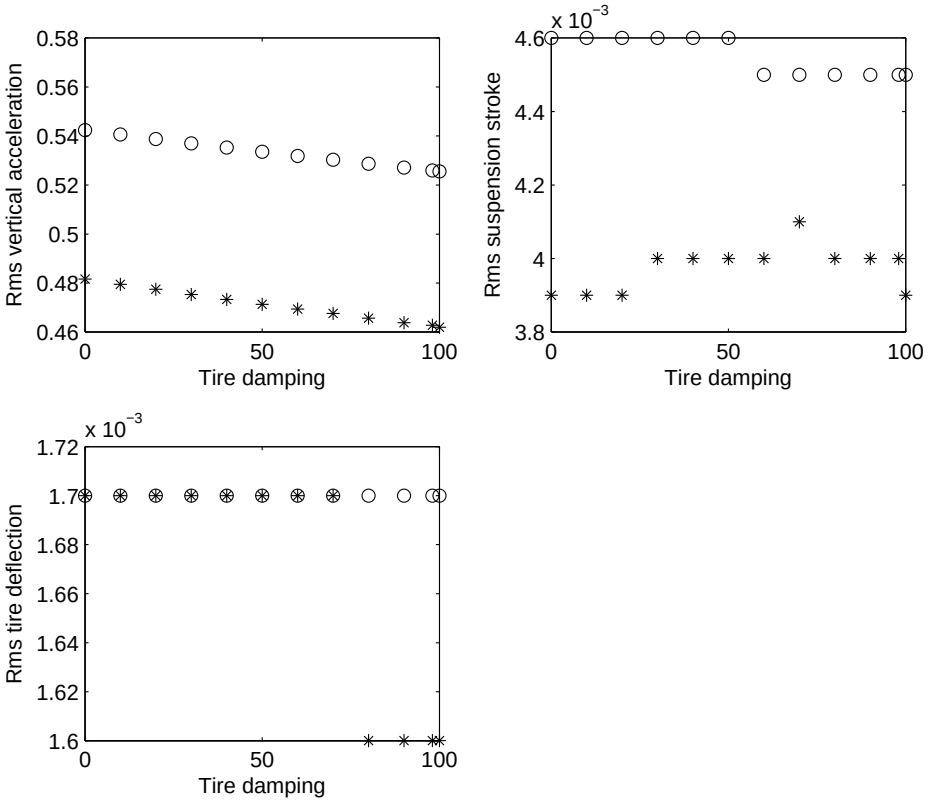

Figure 5.9: The rms responses of the quarter-car model excited by a white-noise velocity input as a function of c_t: (o) passive suspension; ($*$) the HIFOO design with $n_K = 1$ using suspension travel measurement.

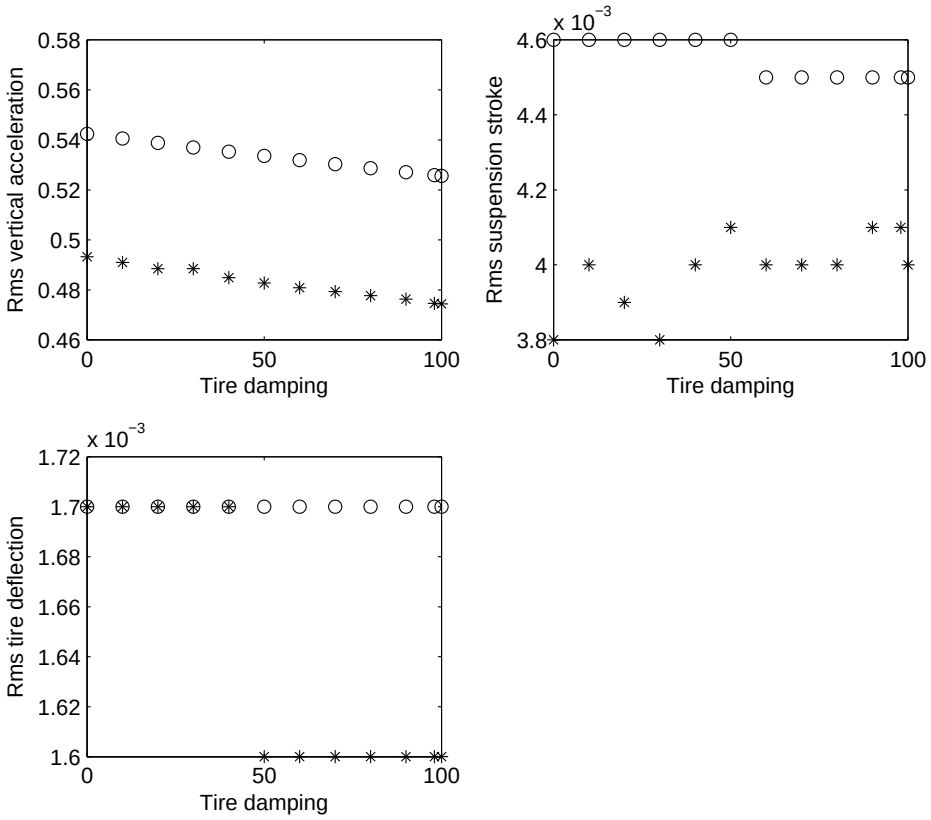

Figure 5.10: The rms responses of the quarter-car model excited by a white-noise velocity input as a function of c_t: (o) passive suspension; ($*$) the HIFOO design with $n_K = 2$ using suspension travel measurement.

5.4 Summary

In this chapter, influence of tire damping on $\mathcal{H}_2$-optimal and multi-objective control of quarter-car suspensions excited by random road disturbances was studied. The multi-objective suspension control problem was first formulated as a convex mixed $\mathcal{H}_2/\mathcal{H}_\infty$ synthesis problem and this problem was solved using LMIs. This formalism gives rise to controllers with orders equal to that of the vehicle model.

Parametric studies showed that the influence of tire damping can not be overlooked in assessing closed-loop performance of actively controlled quarter-car models. This result constitutes a reinforcement, in the root-mean-

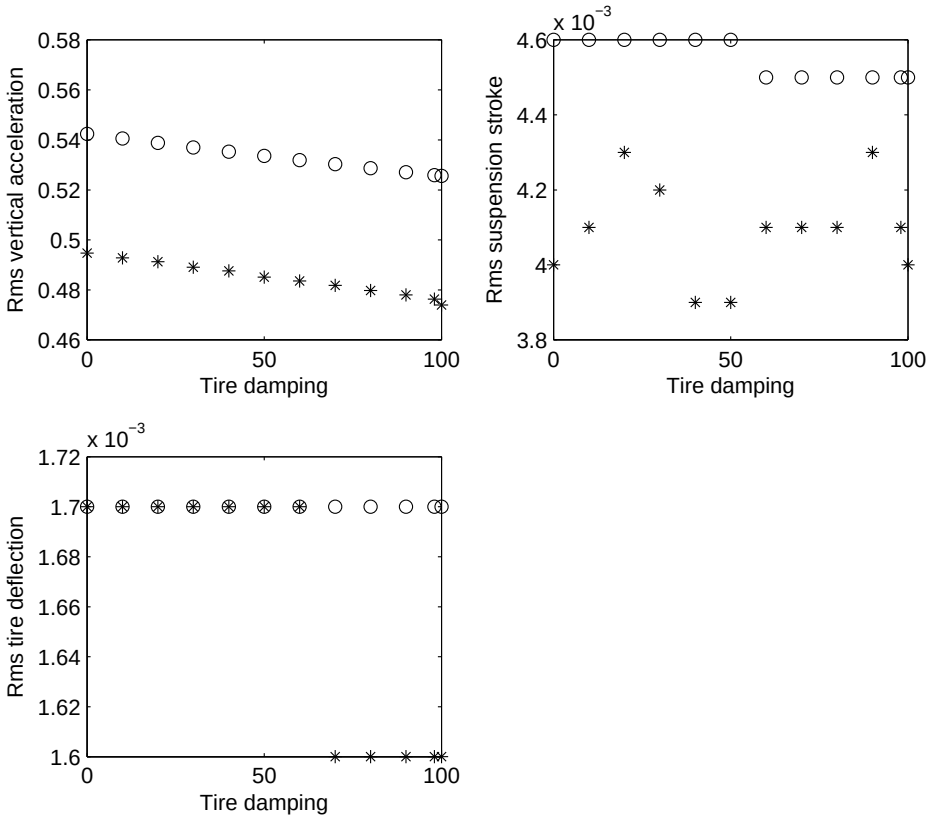

Figure 5.11: The rms responses of the quarter-car model excited by a white-noise velocity input as a function of c_t: (o) passive suspension; ($*$) the HIFOO design with $n_K = 3$ using suspension travel measurement.

square sense, of a conclusion in [26, 68] drawn for pointwise constraints on the achievable frequency responses of the quarter-car model. Then, this result was extended to suspension models with polytopic tire damping uncertainties. Lastly, the multi-objective suspension control problem was re-formulated as a non-convex and non-smooth optimization problem with controller order constrained to be less than or equal to that of the vehicle model. Controllers of various orders were synthesized by using the recently developed optimization algorithms in the HIFOO toolbox. The best performance enhancement was obtained with the lowest order HIFOO controller, showing that there is still room for the application of new techniques to linear suspension control problems. With regard to tire damping, the HIFOO designs were observed to have

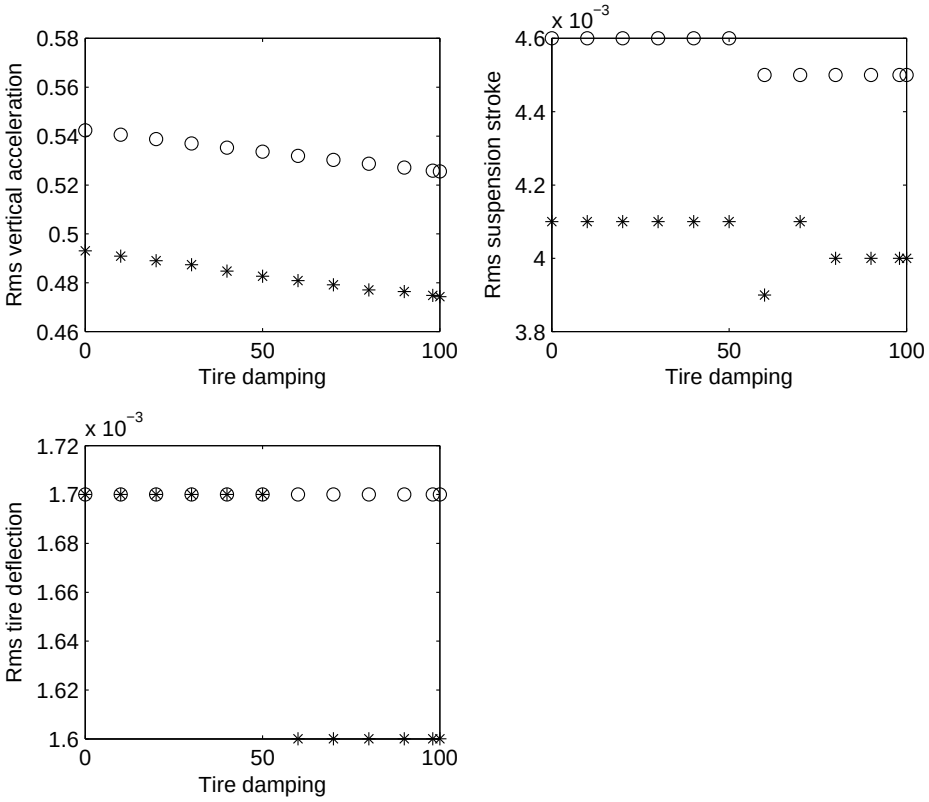

Figure 5.12: The rms responses of the quarter-car model excited by a white-noise velocity input as a function of c_t: (o) passive suspension; ($*$) the HIFOO design with $n_K = 4$ using suspension travel measurement.

closed-loop behavior similar to those of the LMI designs.

Comparing Figures. 5.1–5.12, the following broad conclusions can be drawn. Tire damping reduces both the magnitude and the rms of the sprung mass acceleration for the passive suspension and the active suspensions designed by the $\mathcal{H}_2$-optimal algorithm and the multi-objective control algorithms via LMIs and fixed-order optimization. The coupling between the motions of the sprung and unsprung masses is clearly evident in Figure 5.1 since the optimized performance index rapidly decreases as tire damping coefficient increases. This coupling is, though weakly, observed also in Figure 5.2 by a declining line displaying the optimized performance index versus tire damping and in Figures 5.3 and 5.4, 5.9–5.12 by parallel decreasing lines displaying

the rms vertical acceleration response versus tire damping. The road holding or the tire deflection constraint is a hard constraint as clearly seen in Figures 5.9–5.12. It can be eliminated by exploiting the aforementioned coupling in Chapter 4. However, the design example in Chapter 4 needs to be further tested for robustness, actuator saturation, and controller fragility. In closing, achievable performance and tire damping studies for half and full-car active suspensions in multi-input/multi-output frameworks are left as future research work. In addition, even if tire damping is ignored during a design process, it should be included at validation stage to improve overall simulation accuracy.

6 TIRE DAMPING EFFECT ON HALF-CAR ACTIVE SUSPENSIONS

The contents of this chapter are as follows. In Section 6.1, a four–degrees–of–freedom half-car model is reviewed and achievable rms responses to random road inputs are parameterized. An optimization problem that aims to minimize a weighted sum of the rms values of the outputs with respect to the class of all stabilizing controllers is formulated. The solution of this optimization problem is obtained for a range of tire damping ratios and the vehicle forward velocities. The results derived in this section constitute an extension of the results obtained in Chapter 5 for quarter-car active suspensions to half-car active suspensions.

In Section 6.2, first assuming that tire damping is known, a multi-objective suspension control problem is formulated and solved by using LMIs. The control objective is to decrease the rms vertical and the pitch accelerations while keeping the rms gain of the suspension travels bounded. The influence of tire damping on the solution of this optimization problem is studied; it is observed that tire damping affects only the road holding quality while remaining responses are insensitive to changes of tire damping coefficients in the range considered. Next, the assumption that tire damping coefficients are known is dropped and a multi-objective control problem for suspension models with tire damping coefficients confined to a prescribed box is formulated. By using LMIs, a robust controller with guaranteed performance over all suspension models in the uncertainty set is obtained. The closed-loop performance of the designed suspension system is studied; and it is found that this robust controller does not offer any advantage over an active suspension system designed by neglecting tire damping. Section 6.3 concludes the chapter.

6.1 $\mathcal{H}_2$ Optimal Control of Half-Car Active Suspensions

A four degrees-of-freedom half-car model is shown in Figure 6.1. This model is simple enough to describe the bounce and the pitch motions of a vehicle traveling on a straight line. In this model, the car body is represented by the sprung mass m_s, the pitch moment of inertia by I_p, and the front and the rear wheels are represented respectively by the unsprung masses m_{u1} and m_{u2}. The suspension system consists of two actuators u_1 and u_2 in parallel with the linear passive suspension elements k_{s1}, c_{s1} and k_{s2}, c_{s2}. Each tire is modeled by a simple linear spring in parallel with a linear damping element. The variables x_G and θ stand for the vertical displacement at the center of gravity and the pitch angle of the sprung mass, respectively. The parameter values, except c_{t1} and c_{t2}, are shown in Table 6.1 where G denotes the sprung mass center of gravity.

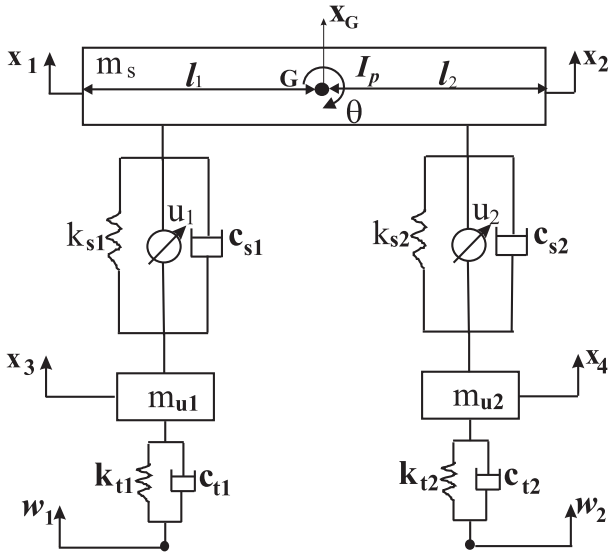

Figure 6.1: The half-car model of the vehicle.

Assuming that the tires behave as point-contact followers that are in contact with the road at all times, the equations of motion take the following

Table 6.1: The vehicle parameters for the half-car model.

Sprung mass	m_s	500 kg
Pitch moment of inertia	I_p	2700 kgm^2
Unsprung masses	m_{u1}, m_{u2}	36 kg
Damping coefficients	c_{s1}, c_{s2}	980 Ns/m
Suspension stiffnesses	k_{s1}, k_{s2}	16,000 N/m
Tire stiffnesses	k_{t1}, k_{t2}	160,000 N/m
Distance of front axle to G	l_1	1.5 m
Distance of rear axle to G	l_2	2.5 m

form:

$$\begin{aligned} m_s\ddot{x}_G &= -k_{s1}(x_1 - x_3) - c_{s1}(\dot{x}_1 - \dot{x}_3) - k_{s2}(x_2 - x_4) \\ &\quad -c_{s2}(\dot{x}_2 - \dot{x}_4) - u_1 - u_2, \end{aligned} \tag{6.1}$$

$$\begin{aligned} I_p\ddot{\theta} &= -l_1k_{s1}(x_1 - x_3) - l_1c_{s1}(\dot{x}_1 - \dot{x}_3) \\ &\quad +l_2k_{s2}(x_2 - x_4) + l_2c_{s2}(\dot{x}_2 - \dot{x}_4) - l_1u_1 + l_2u_2, \end{aligned} \tag{6.2}$$

$$\begin{aligned} m_{u1}\ddot{x}_3 &= k_{s1}(x_1 - x_3) + c_{s1}(\dot{x}_1 - \dot{x}_3) + u_1 \\ &\quad -k_{t1}(x_3 - w_1) - c_{t1}(\dot{x}_3 - \dot{w}_1), \end{aligned} \tag{6.3}$$

$$\begin{aligned} m_{u2}\ddot{x}_4 &= k_s(x_2 - x_4) + c_{s2}(\dot{x}_2 - \dot{x}_4) + u_2 \\ &\quad -k_{t2}(x_4 - w_2) - c_{t2}(\dot{x}_4 - \dot{w}_2) \end{aligned} \tag{6.4}$$

where we assume $c_{t1} = c_{t2} = c_t$ and the front and the rear road disturbances and the control inputs are w_1 and w_2 and u_1 and u_2, respectively. The variables $x_1, x_2,\ x_3,\ x_4,\ w_1,\ w_2$ are measured with respect to an inertial frame. Let $u = (u_1\ \ u_2)^T$ and $w = (w_1\ \ w_2)^T$.

6.1.1 Random Road Excitations

As in the previous chapters, road roughness is typically specified as a random process of a ground displacement power spectral density. It is assumed that w_1 obeys the relation $w_1 = \widetilde{G}\eta$ for some linear shape filter $\widetilde{G}$ where η is a zero mean (spatial) unit-intensity white noise process and the transfer function $\widetilde{G}$ is stable and minimum phase. The latter property means that $\widetilde{G}$ has all finite zeros in the open left-half plane. The relation between $\widetilde{G}$ and the power spectrum of w_1 is given by $S_{w_1}(n) = |\widetilde{G}(j2\pi n)|^2$ where n is the (spatial) frequency measured in cycles/m. The filter $\widetilde{G}$ can be translated to the temporal domain as $\widetilde{G}_{w_1}(s) = \widetilde{G}(sv^{-1})$ where v is the forward velocity of the vehicle assumed to be constant. Hence, $S_\eta(\omega) = v^{-1}$ and $S_{w_1}(\omega) = S_\eta(\omega)|\widetilde{G}_{w_1}(j\omega)|^2$. In this section, we will use a first order linear shape filter:

$$\widetilde{G}(s) = \frac{0.0195}{s + 0.0572}$$

which is the simplest model approximating the spectral data in [52] in the low frequency range.

As the vehicle travels straight on a random road profile with a constant forward velocity a correlation between the front and the rear inputs of the vehicle is induced. The rear wheel is subject to the same road input as the front wheel, but with a time delay T_d: $w_2(t) = w_1(t - T_d)$ where $T_d = (l_1 + l_2)/v$ and $(l_1 + l_2)$ is the wheel base of the vehicle. For control purposes, the pure time delay between the front and the rear inputs may be represented by a finite-dimensional (Pade) approximation. Then, $w_2(t)$ disappears as a variable and the vehicle control problem can be treated in the same way as in the single input case, as far as rms responses are concerned. For this study, a second-order Pade approximation denoted by $L(s)$ is sufficiently accurate.

The objective of this section is to study the rms response of the vehicle. The six response variables are the front and the rear suspension travels, the front and the rear tire deflections, the heave and the pitch accelerations, respectively. These variables form the components of a regulated output vec-

tor z. For the design of a feedback law, we consider the front and the rear suspension travel measurements stacked into a measured output vector y. Passenger comfort requires the rms body accelerations be as small as possible while compactness of the rattle space, good handling characteristics, and improved road-holding quality require the suspension travels and the tire deflections to be kept as small as possible. It is a well-known fact [19] that these objectives can not be met simultaneously with a passive suspension system.

Note that $vS_{w_1}(\omega) \to |\widetilde{G}(0)|^2$ as $v \to \infty$ for every fixed ω. Thus, the effect of the wheel-hop modes on the vehicle random vibration becomes more pronounced and to reduce the wheel-hop induced vehicle vibration, it is necessary that control forces be applied in a large bandwidth of the frequencies. In the absence of tire damping, applying large forces is not sufficient to suppress the wheel-hop modes due to the intrinsic performance limitations as noted earlier [18, 20]. However, as soon as a small damping is allowed in tire model, these limitations disappear and the effect of control becomes more pronounced [26, 68]. Hence, the performance improvement over passive suspensions is expected to be significant in particular at large vehicle speeds due to tire damping.

6.1.2 Achievable Rms Responses

Let $Z(s)$, $Y(s)$, $U(s)$, and $W(s)$ denote respectively the Laplace transforms of z, y, u, and w. Write $Z(s)$ and $Y(s)$ as

$$\begin{aligned} Z &= G_{11}W + G_{12}U, \\ Y &= G_{21}W + G_{22}U. \end{aligned}$$

Now, let $K(s)$ denote the transfer function of the controller with input y and the output u. The stabilization problem is to find a proper feedback transfer function K such that the resulting closed-loop system is *internally stable*. All compensators that stabilize G have the form [17, 132]:

$$K = Q(I + G_{22})^{-1}, \qquad Q \in \mathcal{RH}_\infty$$

With this parametrization, the transfer matrix from w to z denoted by $T_{zw}(s)$ takes a particularly convenient form which is affine in Q:

$$T_{zw} = G_{11} + G_{12}QG_{21}. \tag{6.5}$$

As Q varies over $\mathcal{RH}_\infty$, this equation parametrizes all achievable transfer matrices. Note that the feedback law relies only on the suspension travel measurements.

In this section, we will parameterize all achievable rms responses of the half-car model to random road inputs. From the definition, the auto covariance function of z is given by

$$R_z(\tau) = \frac{1}{2\pi}\int_{-\infty}^{\infty} T_{zw}(j\omega)S_w(j\omega)T_{zw}^{\sim}(j\omega)e^{j\omega\tau}\,d\omega,$$

The square roots of the elements in the diagonal of $R_z(0)$ are the rms values of the suspension travels, the tire deflections at the front and the rear corners of the vehicle, and the body accelerations. Since $w = (w_1 \;\; Lw_1)^T$, $R_z(\tau)$ can be written as

$$R_z(\tau) = \frac{1}{2\pi}\int_{-\infty}^{\infty} T_{zw}\begin{bmatrix}1\\ L\end{bmatrix} S_{w_1}\begin{bmatrix}1\\ L\end{bmatrix}^{\sim} T_{zw}^{\sim}e^{j\omega\tau}\,d\omega.$$

Hence, the sum of the diagonal elements of $R_z(0)$ is given by

$$J(Q) = v^{-1}\left\|T_{zw}\begin{bmatrix}1\\ L\end{bmatrix}\widetilde{G}_{w_1}\right\|_2^2. \tag{6.6}$$

We will consider weighted and optimized version:

$$J^*(\Lambda) = v^{-1}\inf_{Q\in\mathcal{RH}_\infty}\left\|\Lambda T_{zw}\begin{bmatrix}1\\ L\end{bmatrix}\widetilde{G}_{w_1}\right\|_2^2 \tag{6.7}$$

where Λ =diag$\{\lambda_1, ...\lambda_6\}$ with $\lambda_k \geq 0$ for all k. Thus, the optimal control input minimizes $\sum_{k=1}^{6}\lambda_k^2\,\mathrm{E}(z_k^2)$ with respect to all stabilizing controllers. The weighted version of $J(Q)$ in Equation (6.6) is denoted by $J(Q,\Lambda)$.

6.1.3 Root–Mean–Square Performance Analysis

The optimized performance index in Equation (6.7) can be written by using Equation (6.5) as follows:

$$J^*(\Lambda) = v^{-1} \inf_{Q \in \mathcal{RH}_\infty} \|F - HQJ\|_2^2 \tag{6.8}$$

where

$$\begin{aligned} F &= \Lambda G_{11} \begin{bmatrix} 1 \\ L \end{bmatrix} \widetilde{G}_{w_1}, \\ H &= -\Lambda G_{12}, \\ J &= G_{21} \begin{bmatrix} 1 \\ L \end{bmatrix} \widetilde{G}_{w_1} \end{aligned}$$

The following inequality

$$\inf_{Q \in \mathcal{RH}_\infty} \|F - HQJ\|_2 \geq \inf_{Q \in \mathcal{RH}_\infty} \|F - HQ\|_2. \tag{6.9}$$

is obvious. The equality is actually attained as we will see shortly. The argument in showing the equality, however, is different than the argument used in Chapter 5. But, let us first study the right-hand side of Eq. (6.9). The following derivation is parallel to the quarter-car case in Chapter 5.

The matrix H has full column rank on the imaginary axis including infinity. We perform an inner-outer factorization of H. The first step is to get a spectral factor of $H^{\sim}(s)H(s)$. If the quadruplet (A_H, B_H, C_H, D_H) denotes a minimal state-space realization of $H(s)$, then a spectral factor denoted by $H_o(s)$ is given by

$$H_o(s) = (A_H, B_H, \underline{\mathrm{D}}^{-\frac{1}{2}}(D_H{}^T C_H + B_H{}^T X), \underline{D}^{\frac{1}{2}})$$

where $\underline{D} = D_H{}^T D_H$ and X is the stabilizing solution of the Riccati equation:

$$\begin{aligned} &(A_H - B_H \underline{D}^{-1} D_H{}^T C_H)^T X + X(A_H - B_H \underline{D}^{-1} D_H{}^T C_H) \\ &\quad - X B_H \underline{D}^{-1} B_H{}^T X + C_H{}^T (I - D_H \underline{D}^{-1} D_H{}^T) C_H = 0. \end{aligned}$$

The inner factor is then $H_i(s) = H(s)H_o^{-1}(s)$. The next step is the calculation of a complementary inner factor $N_\perp$ of H_i, *i.e.,* finding a matrix $N_\perp$ that makes

$[H_i \;\; N_\perp]$ square and inner. If (A_i, B_i, C_i, D_i) is a minimal state-space realization of H_i, then a realization of $N_\perp$ is given by the formula [17][Lemma 13.31]: $N_\perp = \left(A_i, -Y^{-1}C_i^T D_\perp, C_i, D_\perp\right)$ where $D_\perp$ is an orthogonal complement of D_i such that $[D_i \;\; D_\perp]$ is square and orthogonal and Y is the observability Gramian in $A_i^T Y + Y A_i + C_i^T C_i = 0$. Observe that H_i and $N_\perp$ have the same poles. Thus,

$$\begin{aligned} \inf_{Q\in\mathcal{RH}_\infty} \|F - HQ\|_2^2 &= \|N_\perp^\sim F\|_2^2 + \inf_{Q\in\mathcal{RH}_\infty} \|H_i^\sim F - H_o Q\|_2^2 \\ &= \|N_\perp^\sim F\|_2^2 + \|\Pi^\perp H_i^\sim F\|_2^2 \end{aligned} \tag{6.10}$$

with

$$Q = H_o^{-1}\Pi H_i^\sim F. \tag{6.11}$$

Hence, from Eq. (6.10)

$$vJ^*(\Lambda) = \|\Pi N_\perp^\sim F\|_2^2 + \|\Pi^\perp N_\perp^\sim F\|_2^2 + \|\Pi^\perp H_i^\sim F\|_2^2. \tag{6.12}$$

It remains to establish that Eq.(6.9) holds with equality. For Q in Eq. (6.11), it suffices to find a $\widetilde{Q} \in \mathcal{RH}_\infty$ such that $\widetilde{Q}J = Q$. The left-hand side of Eq. (6.9) does not change when $F - HQJ$ is transposed. Hence, by Lemma 6.3.10 in [132], we can safely assume that J has full column rank on the imaginary axis including infinity. In this case, a necessary and sufficient condition for the solvability of the equation $\widetilde{Q}J = Q$ is that J_1 and J_2 in $J = [J_1 \;\; J_2]^T$ be right coprime over $\mathcal{RH}_\infty$. This is indeed the case since J_1 and J_2 have no open right-half plane zeros in common.

Given Λ, the corresponding optimal cost value is calculated from Eq. (6.12). This formula holds without modification for different measurement set-ups as well. In addition, the rms values of the control inputs can be constrained too by augmenting u to z and expanding Λ to include weights on u. As an application of the above formulas, we will investigate the effect of tire damping on the optimal cost value for a choice of the weighting matrices.

Influence of Tire Damping on the Optimal Cost

Recall the definition of the dimensionless quantity $\mu(c_t;\Lambda)$ introduced in Chapter 5 to quantify the active suspension performance relative to the passive suspension performance in the rms sense. In Figure 6.2, $\mu(c_t;\Lambda)$ is plotted versus c_t for $\Lambda = I_6$. This choice of Λ puts equal emphasis on the six output rms values. The simulation was carried out for the vehicle velocities from 5 to 40 m/s. The impact of tire damping on the active suspension performance is remarkable. The closed-loop performance is further improved by increasing velocities as predicated by the theory.

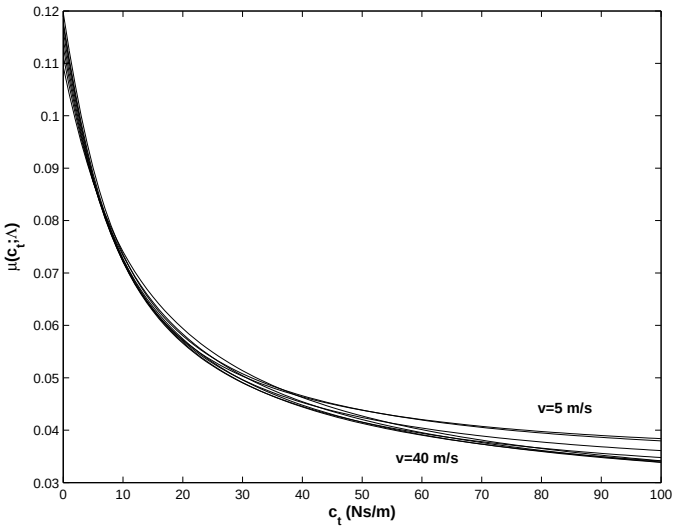

Figure 6.2: The optimized performance index scaled by the open-loop performance index as a function of tire damping coefficient for different vehicle velocities and $\Lambda = I_6$.

It should be noted that the rms vertical acceleration is more than one hundred times the rms suspension travels and the rms suspension travels are about three times the rms tire deflections. Then, the choice $\Lambda = I_6$ results in dramatic reduction of the rms vertical acceleration at the expense of the other responses. Therefore, by setting Λ to I_6, we almost entirely neglect the trade-offs: the sprung mass vertical acceleration and the pitch acceleration versus the suspension travels and the sprung mass vertical acceleration and the pitch acceleration versus the tire deflections. In Figure 6.3, $\mu(c_t;\Lambda)$ is

plotted as a function of tire damping coefficient for $\Lambda = \text{diag}(10I_2, 100I_2, I_2)$ and v ranging from 5 to 40 m/s. The latter choice for Λ respects the trade-offs. Although it is not as impressive as in Figure 6.2, the influence of tire damping is still felt. In the $\mathcal{H}_2$-optimal control context, this observation reinforces the conclusion in [26, 68, 70, 134] that tire damping will help to improve ride comfort while maintaining road holding ability and suspension rattle space compactness. These numerical experiments were repeated with different vehicle parameter values. But, the basic conclusion drawn above did not change.

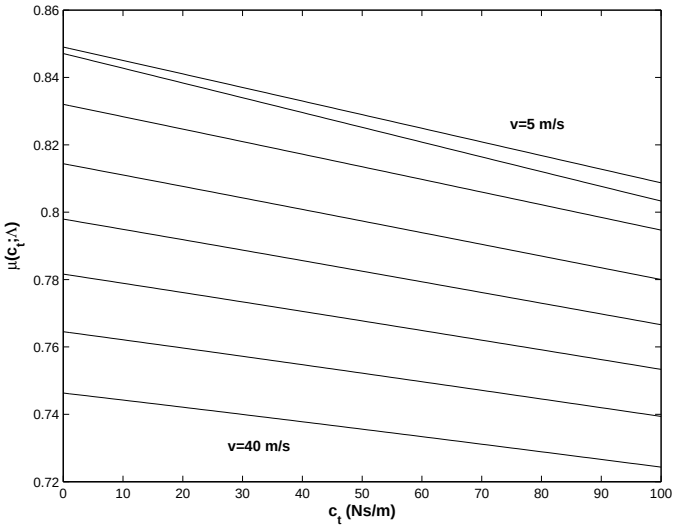

Figure 6.3: The optimized performance index scaled by the open-loop performance index as a function of tire damping coefficient for different vehicle velocities and $\Lambda = \text{diag}(10I_2, 100I_2, I_2)$.

The conclusions similar to the results obtained in Chapter 5 can be drawn as follows. As in Section 5.1.1 the influence of tire damping on the $\mathcal{H}_2$-optimal design of active suspension systems can be significant. In another words, performance of an active suspension system designed by ignoring tire damping may seriously deteriorate due to tire damping. In addition, controller synthesis must address the issues of actuator saturation, parameter and load variations, and robustness to uncertainties in road and tire models. The design problem is then multi-objective synthesis of linear robust output-feedback controllers, for which linear matrix inequality based solutions have been proposed

in the literature [73].

6.2 Mixed $\mathcal{H}_2/\mathcal{H}_\infty$ Synthesis of Half-Car Active Suspensions

Let us put the half-car equations of motions given by Eqs. (6.1)–(6.4) into state-space form. The displacements at the front and the rear wheels of the vehicle are related to x_G and θ by

$$\begin{bmatrix} x_1 \\ x_2 \end{bmatrix} = S \begin{bmatrix} x_G \\ \theta \end{bmatrix}$$

where

$$S = \begin{bmatrix} 1 & l_1 \\ 1 & -l_2 \end{bmatrix}.$$

It will be more convenient to define a new set of state variables in terms of the old state variables and the disturbances as follows:

$$\begin{aligned} \tilde{x}_1 &= x_1 - x_3, \quad \tilde{x}_2 = x_2 - x_4, \quad \tilde{x}_3 = x_3 - w_1, \quad \tilde{x}_4 = x_4 - w_2, \\ \tilde{x}_5 &= \dot{x}_1, \quad \tilde{x}_6 = \dot{x}_2, \quad \tilde{x}_7 = \dot{x}_3, \quad \tilde{x}_8 = \dot{x}_4. \end{aligned} \tag{6.13}$$

Let

$$\begin{aligned} V_i &= [V_{i1} \;\; V_{i2}]^T = \dot{w}, \\ M_s &= \text{diag}(m_s, I_p), \\ K_s &= \text{diag}(k_{s1}, k_{s2}), \\ C_s &= \text{diag}(c_{s1}, c_{s2}), \\ M_u &= \text{diag}(m_{u1}, m_{u2}), \\ K_t &= \text{diag}(k_{t1}, k_{t2}), \\ C_t &= \text{diag}(c_{t1}, c_{t2}). \end{aligned}$$

Then, the equations of motions are given in the state-space form by:

$$\dot{\tilde{x}} = A\tilde{x} + B_1 V_i + B_2 u \tag{6.14}$$

where

$$A = \begin{bmatrix} & I_2 & -I_2 \\ 0_{4\times4} & 0_{2\times2} & I_2 \\ K & C & \end{bmatrix}, \tag{6.15}$$

$$B_1 = \begin{bmatrix} 0_{2\times2} \\ -I_2 \\ N \end{bmatrix}, \tag{6.16}$$

$$B_2 = \begin{bmatrix} 0_{4\times2} \\ W \end{bmatrix},$$

$$K = -\begin{bmatrix} SM_s^{-1}S^TK_s & 0_{2\times2} \\ -M_u^{-1}K_s & M_u^{-1}K_t \end{bmatrix},$$

$$C = -\begin{bmatrix} SM_s^{-1}S^TC_s & 0_{2\times2} \\ -M_u^{-1}C_s & M_u^{-1}(C_s+C_t) \end{bmatrix},$$

$$N = \begin{bmatrix} 0_{2\times2} \\ M_u^{-1}C_t \end{bmatrix},$$

$$W = \begin{bmatrix} -SM_s^{-1}S^T \\ M_u^{-1} \end{bmatrix}.$$

The objective of this section is to study the multi-objective control of a half-car active suspension system excited by random road disturbances. The vehicle response variables that need to be examined are the heave and the pitch accelerations of the sprung mass as indicators of the vibration isolation, the suspension travels as measures of the rattling space, and the tire deflections as indicators of the road-holding characteristic of the vehicle. These variables stacked in the variable z can be written in terms of the state variables and the control inputs as

$$z = (\widetilde{x}_1 \;\; \widetilde{x}_2 \;\; \widetilde{x}_3 \;\; \widetilde{x}_4 \;\; \ddot{x}_G \;\; \ddot{\theta})^T. \tag{6.17}$$

By using state-space parameters, z can be written compactly as follows

$$z = C_1\tilde{x} + D_1u \tag{6.18}$$

where

$$C_1 = \begin{bmatrix} I_4 & 0_{4\times 4} \\ -M_s^{-1}S^T[K_s \;\; 0_{2\times 2} \;\; C_s] & 0_{2\times 2} \end{bmatrix},$$

$$D_1 = \begin{bmatrix} 0_{4\times 2} \\ -M_s^{-1}S^T \end{bmatrix}.$$

For the design of a feedback law, the suspension travel measurements:

$$y = C_2\hat{x} \tag{6.19}$$

will be considered where

$$C_2 = [I_2 \;\; 0_{2\times 6}].$$

The derivative of the road roughness is most commonly specified as a random process $\mu\sqrt{v}\eta(t)$ where v is the vehicle's forward velocity, μ is the road roughness coefficient, and $\eta(t)$ is unit-intensity white-noise process. In this study, v and μ are fixed as $v = 20$ m/s and $\mu = 0.0027$. Thus, the covariance function of V_i denoted by R_{V_i} satisfies

$$R_{V_i}(\tau) = \mu^2 v I_2\, \delta(\tau) \tag{6.20}$$

In contrast to the previous section, in this section we assume that the road excitations at the front and rear wheels are uncorrelated.

6.2.1 Multi-Objective Control of Vehicle Suspension Systems

The primary goal of active suspension design is to improve ride comfort by making the heave and the pitch accelerations of the car body as small as possible while keeping the suspension travels below the maximum allowable suspension stroke to prevent excessive suspension bottoming, which can result in structural damage and deterioration of ride comfort. The dynamic tire loads should not exceed the static ones in order to ensure a firm uninterrupted contact of wheels to road. Meanwhile, active forces should be amplitude bounded to avoid actuator saturations. Thus, the design of active suspension system

is a multi-objective control problem in which the strategy is to reduce the accelerations while keeping the constraints satisfied. Many other constraints can also be taken into consideration. However, the above constraints reveal all fundamental design trade-offs.

In this section, we will consider the following dynamic output feedback structure:

$$\dot{x}_c = A_K x_c + B_K y, \tag{6.21}$$

$$u = C_K x_c + D_K y \tag{6.22}$$

where the state-space parameters A_K, B_K, C_K, D_K of the transfer matrix $K(s) = C_K(sI - A_K)^{-1}B_K + D_K$ are to be determined. The feedback configuration of the generalized plant defined by

$$G(s) = \left[\begin{array}{c|c} G_{11}(s) & G_{12}(s) \\ \hline G_{21}(s) & G_{22}(s) \end{array}\right] \tag{6.23}$$

which maps the pair of inputs $[V_i^T \; u^T]^T$ to the pair of outputs $[z^T \; y^T]^T$ and $K(s)$ is shown in Fig. 6.4.

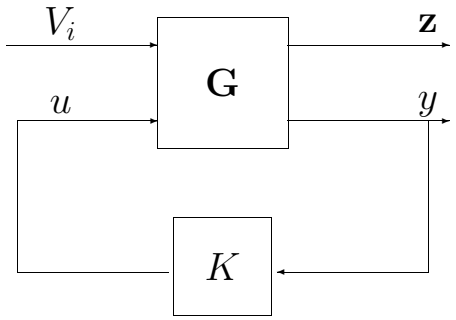

Figure 6.4: Standart block diagram

Let $T_{zV_i}(s)$ denote the closed-loop transfer function from V_i to z. The design specifications mentioned above can be cast into the optimization problem:

$$\mathcal{J}(\Lambda) = \min_{K \in \mathcal{RH}_\infty} \|\Lambda T_{zV_i}\|_2^2 \tag{6.24}$$

The weighting matrix $\Lambda = \mathrm{diag}(\Lambda_1, \cdots, \Lambda_6)$ has non-negative entries. Note from the definition of the $\mathcal{H}_2$-norm and the fact that the power spectrum of V_i denoted by $\mathcal{S}_{V_i}(j\omega)$ satisfies $\mathcal{S}_{V_i}(j\omega) = \mu^2 v I_2$ for all ω, Eq. (6.24) can be written as

$$\begin{aligned}
\mathcal{J}(\Lambda) &= \min_{K \in \mathcal{RH}_\infty} \frac{1}{2\pi} \int_{-\infty}^{\infty} \mathrm{Tr}\{\Lambda T_{zV_i}(j\omega) T_{zV_i}^{\sim}(j\omega) \Lambda\} \, \mathrm{d}\omega \\
&= (\mu^2 v)^{-1} \min_{K \in \mathcal{RH}_\infty} \sum_{k=1}^{6} \frac{\Lambda_k^2}{2\pi} \int_{-\infty}^{\infty} T_{z_k V_i}^{\sim}(j\omega) \mathcal{S}_{V_i}(j\omega) T_{z_k V_i}(j\omega) \, \mathrm{d}\omega \\
&= (\mu^2 v)^{-1} \min_{K \in \mathcal{RH}_\infty} \sum_{k=1}^{6} \Lambda_k^2 \, \mathrm{E}[z_k]^2.
\end{aligned}$$

Hence, the optimal control inputs minimize a weighted combination of the squared rms values of the outputs.

By allowing only a few of the weights in Eq. (6.24) to be non-zero, it is conceivable to make the heave and the pitch accelerations of the body arbitrarily close to zero at the expense of increasing the suspension travels and the tire deflections. To respect the trade-offs, in Eq. (6.24) non-zero weights are assigned to the suspension travels. In addition, an rms gain constraint on the tire deflections:

$$\|\mathcal{W} T_{zV_i}\|_\infty < \gamma, \qquad \gamma > 0 \tag{6.25}$$

where $\mathcal{W} = \mathrm{diag}(0_{2\times 2}, I_2, 0_{2\times 2})$ is imposed and $\Lambda_3 = \Lambda_4 = 0$ is set in Eq. (6.24). This rms gain constraint shapes the optimal solution. The multi-objective control design problem can be summarized as follows:

Problem 6.2.1. *For given numbers $\gamma > 0$, $\Lambda_k = 0$ for $k = 3, 4$ and $\Lambda_k > 0$ otherwise, design an output-feedback controller $u = K(s)y$ that satisfies $\|\mathcal{W} T_{zV_i}\|_\infty < \gamma$ and minimizes $\|\Lambda T_{zV_i}\|_2^2$.*

Some control design requirements were expressed in the time-domain. The multi-objective control problem, on the other hand, has the control objective and the constraint in the frequency-domain. A linear matrix inequality based solution will be presented. This formalism readily encompasses time-domain constraints at a price of conservatism. By tuning the parameters γ

and Λ, the solution of the above design problem can be adjusted to satisfy time-domain constraints. In the next subsection, guidelines will be provided how to choose these tuning parameters.

6.2.2 A Linear-Matrix Inequality Based Solution

Let $G_{z_k V_i}$ denote the open-loop transfer function from V_i to z_k, *i.e.,* the kth row of G_{11} in Eq. (6.23). The weighting matrix Λ and the upper bound γ of the multi-objective control problem are chosen as follows. In Eqs. (6.3) and (6.4), assume c_{t1} is equal to c_{t2} and denote the common value by c_t. Then, given c_t compute $\|G_{z_k V_i}\|_2$ for $k = 1, 2, 5, 6$ and $\|\mathcal{W} G_{11}\|_\infty$. Now, for some positive parameters ρ_1 and ρ_2 set $\Lambda_k = \|G_{z_k V_i}\|_2^{-1} \rho_1$ for $k = 1, 2$, $\Lambda_k = \|G_{z_k V_i}\|_2^{-1}$ for $k = 5, 6$, and $\gamma = \|\mathcal{W} G_{11}\|_\infty \rho_2$. By these scalings, the solution of the optimization problem can be monitored with respect to the passive suspension. The parameter ρ_1 controls the trade-offs between the suspension travels and the sprung mass accelerations while ρ_2 controls the trade-offs between the tire deflections and the sprung mass accelerations. The optimization algorithm is implemented by the `hinfmix` command of MATLAB's LMI Control Toolbox [27]. This command produces a controller of degree which is equal to that of the plant.

In Figs. 6.5 and 6.6, the rms values of z_k, $k = 1, \cdots, 6$ of a vehicle traveling with a speed of 20 m/s subjected to white-noise velocity excitatitions are plotted as functions of tire damping coefficient for both the passive and the active suspension systems designed with $\rho_1 = 0.1$ and $\rho_2 = 1.5$ using the suspension travel measurements. As expected, the trade-offs among the vertical acceleration, the pitch acceleration, the suspension travels, and the tire deflections are notable. In particular, both the vertical and the pitch accelerations are dramatically reduced while the suspension travels are increased by about 60% and the rms tire deflections are slightly increased by about 4 %. The rms values of u_1 and u_2 plotted in Fig. 6.8 for $0 \leq c_t \leq 100$ show that actuator saturations are not likely to occur. In Fig. 6.7, the rms gain of the tire

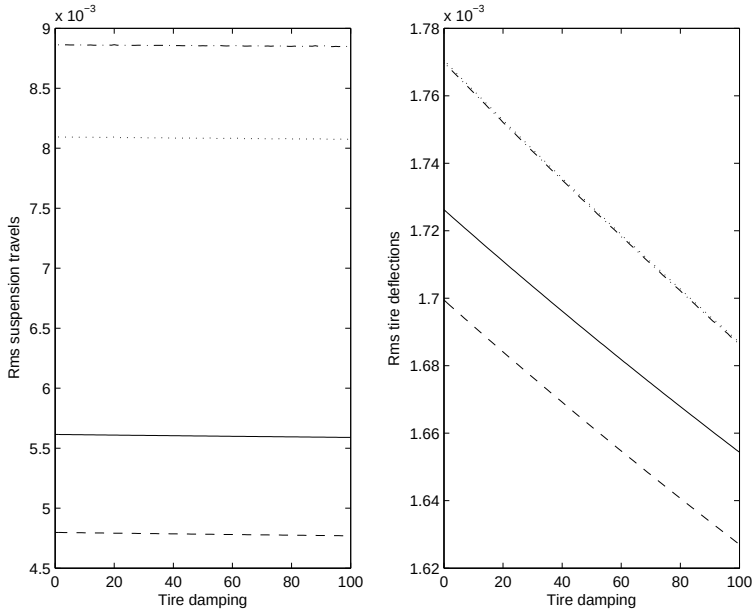

Figure 6.5: The rms values of the suspension travels and the tire deflections of the vehicle subjected to white-noise velocity road inputs as functions of c_t: (-) passive suspension (front); (- -) passive suspension (rear); (-.) active suspension (front); (:) active suspension (rear) with $\rho_1 = 0.1$ and $\rho_2 = 1.5$ using the suspension travel measurements.

deflections is plotted versus tire damping. The rms gain was computed with the formula $\|\mathcal{W}T_{zw}\|_\infty$ instead of $\|\mathcal{W}T_{zV_i}\|_\infty$ since the former more realistically quantifies tire deflection sensitivity to road roughness. The rms values and the rms gain of the tire deflections decrease both for the passive and the active suspensions as tire damping is increased from 0 to 100 while the remaining responses decrease very slowly. In fact, the decreases by percentage are 4.1 and 4.2 for the rms passive suspension tire deflections (front and rear), 4.7 and 4.9 for the rms active suspension tire deflections (front and rear), 8.7 for the rms gain of the passive suspension tire deflections, 9.0 for the rms gain of the active suspension tire deflections, 0.4 and 0.6 for the rms passive suspension travels (front and rear), 0.15 and 0.2 for the rms active suspension travels (front and rear), 0.7 for the passive suspension rms vertical acceleration, 0.2 for the active suspension rms vertical acceleration, 0.6 for the passive suspension rms pitch acceleration, and 0.07 for the active suspension rms pitch acceleration.

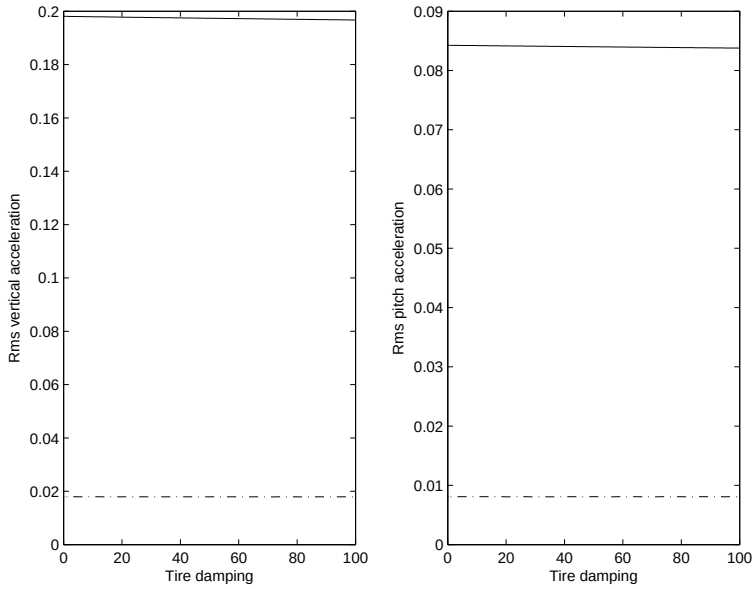

Figure 6.6: The rms values of the vertical and the pitch accelerations of the vehicle subjected to white-noise velocity road inputs as functions of c_t: (-) passive suspension; (-.) active suspension with $\rho_1 = 0.1$ and $\rho_2 = 1.5$ using the suspension travel measurements.

To improve the suspension travel and the tire deflection responses, this design procedure is next repeated with $\rho_1 = 1$ and $\rho_2 = 1$. From Figs. 6.9 and 6.10, it is seen that the rms values of the suspension travels, the tire deflections, the vertical and the pitch accelerations are reduced by about 12%, 3%, 50%, and 45%, respectively, with respect to the passive suspension. From Fig. 6.11, the rms gain of the tire deflections is seen to be reduced by about 4% in comparison to the passive suspension. Note from Fig. 6.12 that the rms values of the control inputs are about 40% of the rms values in the previous case. Thus, the new design is clearly better than the previous one. As noted earlier, only road holding quality is notably influenced by tire damping. As a matter of fact, the decreases by percentage are 4.1 and 4.2 for the rms passive suspension tire deflections (front and rear), 4.0 and 4.0 for the rms active suspension tire deflections (front and rear), 8.7 for the rms gain of the passive suspension tire deflections, 8.0 for the rms gain of the active suspension tire deflections, 0.4 and 0.6 for the rms passive suspension travels (front and rear),

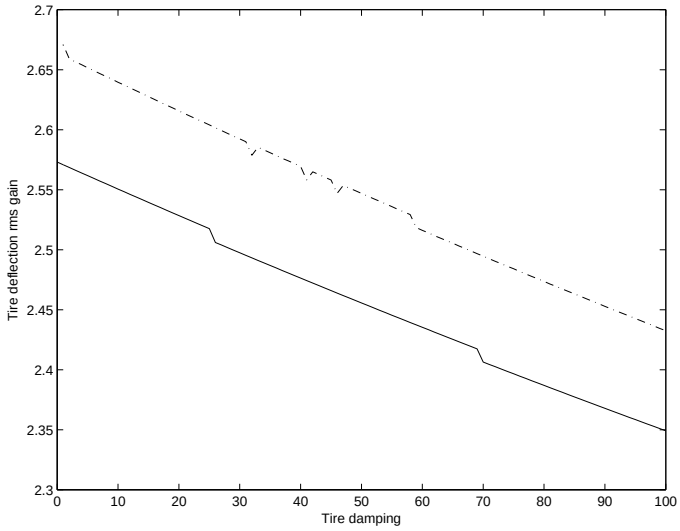

Figure 6.7: $\|\mathcal{W}T_{zw}\|_\infty$ as a function of c_t: (-) passive suspension; (-.) active suspension with $\rho_1 = 0.1$ and $\rho_2 = 1.5$ using the suspension travel measurements.

0.5 and 0.7 for the rms active suspension travels (front and rear), 0.7 for the passive suspension rms vertical acceleration, 0.6 for the active suspension rms vertical acceleration, 0.6 for the passive suspension rms pitch acceleration, and 0.45 for the active suspension rms pitch acceleration.

Based on these observations, it can safely be said that, with the half-car model and the road excitation model in Eq. (6.20) only road holding quality is influenced to some extent by tire damping in both the passive and the active suspension systems. We investigated in Chapter 5 influence of tire damping on the quarter-car suspensions and observed that tire damping significantly reduces all the rms values and the tire deflection rms gains both for the active and the passive suspensions.

The excitation model in Eq.(6.20) presumes that the velocities V_{i1} and V_{i2} are uncorrelated. This assumption is hardly justifiable; however, it guarantees simultaneous excitation of the heave and the pitch motions of the car body. The results in this section show that the body pitch significantly impacts the closed-loop performance of the active suspension system. In other words, decomposition of a half-car model into two independent quarter-car

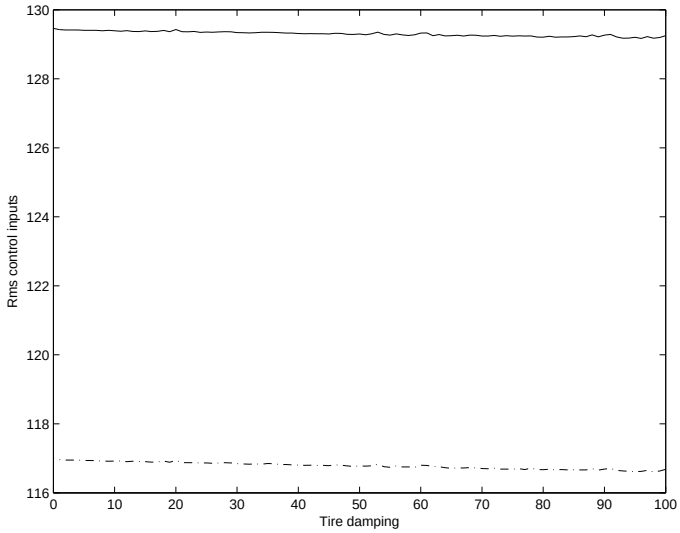

Figure 6.8: The rms values of the actuator forces as functions of c_t: (-) u_1; (-.) u_2 with $\rho_1 = 0.1$ and $\rho_2 = 1.5$ using the suspension travel measurements.

models by a linear transformation is not realistic for a study of the performance limitations and the trade-offs.

The multi-objective control problem and consequently its solution depend on the uncertain parameters c_{t1} and c_{t2}. The purpose of this subsection was to to examine the influence of tire damping on active suspension design using linear matrix inequalities. For a given range of tire damping coefficients, it was observed that only road holding quality was influenced to some extent by tire damping while the rest of the responses were slightly affected. In addition, precise knowledge of tire damping is an unrealistic assumption. In the next subsection, this assumption will be relaxed and a robust multi-objective suspension control problem will be formulated.

6.2.3 Polytopic Vehicle Suspension Models

The multi-objective control problem solved in Section 6.2.2 assumes exact values of the tire damping coefficients, which are difficult to estimate since they depend on many factors and vary during ride. In this subsection, assuming that c_{tk}, $k = 1, 2$ take values in some prescribed intervals $[\alpha_k, \beta_k]$

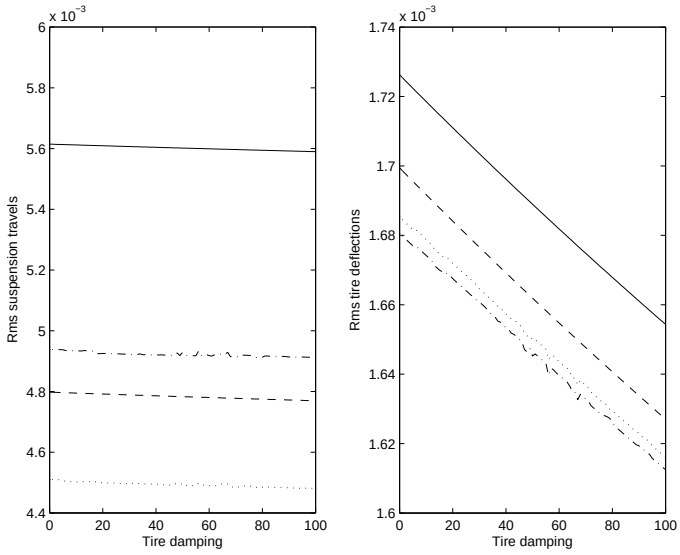

Figure 6.9: The rms values of the suspension travels and the tire deflections of the vehicle subjected to white-noise velocity road inputs as functions of c_t: (-) passive suspension (front); (- -) passive suspension (rear); (-.) active suspension (front); (:) active suspension (rear) with $\rho_1 = 1$ and $\rho_2 = 1$ using the suspension travel measurements.

a multi-objective controller with guaranteed performance for all possible values of tire damping coefficients will be designed. Note that this uncertainty structure allows fast variations of the tire damping coefficients.

Let A^0 and B_1^0 denote the matrices A and B_1 in Eqs. (6.15) and (6.16) evaluated at $c_{t1} = c_{t2} = 0$ and let $A^k = \mathrm{d}A/\mathrm{d}c_{tk}$, $B_1^k = \mathrm{d}B_1/\mathrm{d}c_{tk}$, $k = 1, 2$. Define three vertex systems by the quadruplets $P_0 = (A^0,\ [B_1^0 \quad B_2],\ [C_1; C_2],\ [0 \quad D_1; 0 \quad 0])$ and $P_k = (A^k, [B_1^k \quad 0], 0, 0),\ k = 1, 2$. Then, the quadruplet P formed conformally with P_0, P_1, and P_2 and describing the system studied in Section 6.2.2 can be written as

$$P = P_0 + c_{t1}P_1 + c_{t2}P_2, \qquad c_{tk} \in [\alpha_k, \beta_k],\ \ k = 1, 2, \tag{6.26}$$

which is a box in the Euclidean space of the state-space parameters. Let $\mathcal{P}$ denote the set of systems defined by Eq. (6.26). Then, the robust multi-objective control design problem is:

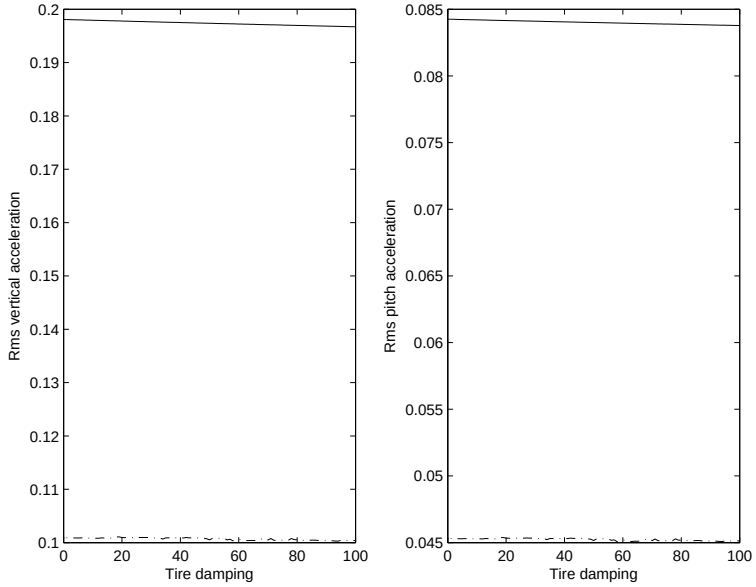

Figure 6.10: The rms values of the vertical and the pitch accelerations of the vehicle subjected to white-noise velocity road inputs as functions of c_t: (-) passive suspension; (-.) active suspension with $\rho_1 = 1$ and $\rho_2 = 1$ using the suspension travel measurements.

Problem 6.2.2. *For given numbers $\gamma > 0$, $\Lambda_k = 0$ for $k = 3, 4$ and $\Lambda_k > 0$ otherwise, and $\mathcal{P}$, design a state-feedback controller $u = K_0\tilde{x}$ that satisfies $\|\mathcal{W}T_{zV_i}\|_\infty < \gamma$ for all $P \in \mathcal{P}$ and minimizes $\sup_{P\in\mathcal{P}} \|\Lambda T_{zV_i}\|_2^2$.*

Again, this optimization problem can be solved by using linear matrix inequalities. Its solution is implemented by the `msfsyn` command in MATLAB's LMI Toolbox [27]. For illustration, suppose $\alpha_k = 0$ and $\beta_k = 100$ for $k = 1, 2$. The same formulas for Λ_k, $k = 1, \cdots, 6$ and γ proposed in Section 6.2.2 can be used provided that the scalings $\|G_{z_k V_i}\|$ are computed with fixed c_{t1} and c_{t2}. For the computations, $c_{t1} = c_{t2} = 0$ were picked and the above optimization problem was solved . Let K_0 denote the solution which depends on the scalings ρ_1 and ρ_2. Using the same msfsyn command with the uncertainty set P_0, which is a singleton, and the same weights, another controller denoted by $\bar{K}_0$ was obtained.

In order to see how the robust controller is performing against $\bar{K}_0$, fix c_{t1} and c_{t2} and denote the corresponding system in Eq. (6.26) by P_t. Then,

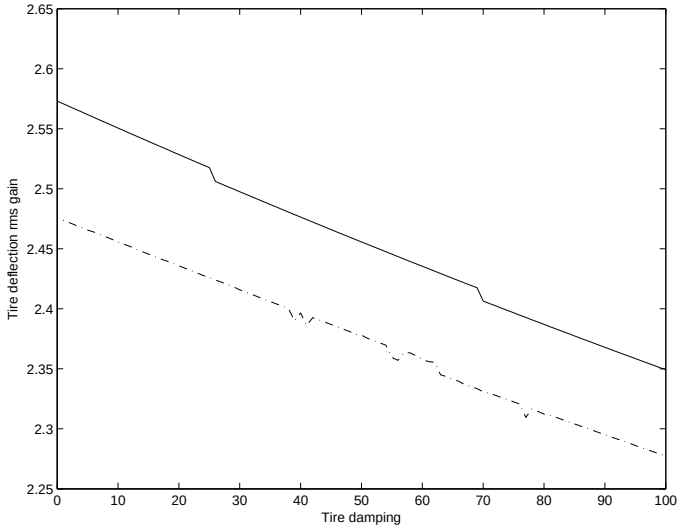

Figure 6.11: $\|\mathcal{W}T_{zw}\|_\infty$ as a function of c_t: (-) passive suspension; (-.) active suspension with $\rho_1 = 1$ and $\rho_2 = 1$ using the suspension travel measurements.

compute the closed-loop responses of P_t using the controllers $\bar{K}_0$ and K_0 with a range of values for ρ_1 and ρ_2. It has been observed that the two response sets are almost identical in all cases. For example, when $\rho_1 = \rho_2 = 1$, the rms vertical accelerations are 0.10145 with K_0 and 0.10160 with $\bar{K}_0$ corresponding to $c_{t1} = c_{t2} = 100$. The last result suggests neglecting tire damping in the design of active suspension systems for half-car models when it is difficult to estimate tire damping coefficients.

6.3 Summary

In this chapter, the rms response of a half-car model excited by random road inputs were studied. First, the road excitation at the front wheel was modeled by a first-order linear shape filter driven by a white-noise input; and the temporal correlation between the front and the rear wheels was predicted by a second order Pade filter. It was demonstrated that the effect of tire damping on the rms performance of actively controlled half-car models can be significant, in particular, at high vehicle velocities. This presents an extension of the result in [70] obtained for quarter-car suspension models to half-car

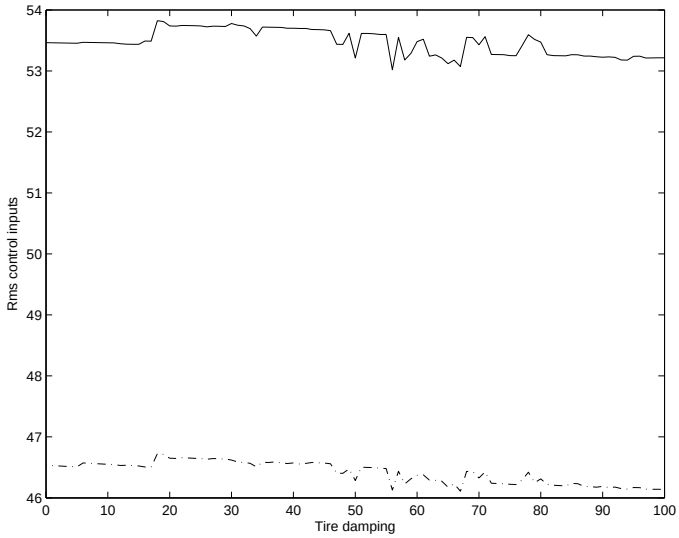

Figure 6.12: The rms values of the actuator forces as functions of c_t: (-) u_1; (-.) u_2 with $\rho_1 = 1$ and $\rho_2 = 1$ using the suspension travel measurements.

suspension models.

Next, the road excitations at the front and the rear wheels were assumed to be uncorrelated and multi-objective control of the half-car suspension system using linear matrix inequalities was studied. It was observed that when the tire damping coefficients are precisely estimated, their values affect to some extent only road holding quality. In the absence of this information, a robust controller was synthesized for a suspension system with polytopic tire damping uncertainties. This robust controller synthesis was seen not to offer any advantage over an active suspension system designed by neglecting tire damping. The last observation is in sharp contrast with a conclusion in [70] drawn for a robustly controlled quarter-car active suspension system. A possible mechanism for this discrepancy is the body pitch which does not allow decomposition of the half-car model in Figure 6.1 into two independent quarter-car models by coupling their vertical motions. This mismatch between the quarter and the half-car active suspension behaviors can not solely be attributed to excessive pitch moment of inertia used in the simulation study. In fact, when the value of the pitch moment of inertia was halved the LMI designs were found to follow the patterns displayed in Figures 6.5–6.12. The robust controller synthesis for

this parameter value was also seen to be ineffective in coping with polytopic tire damping uncertainties as in the previous design. In passing, the study of achievable performance for half-car active suspensions remains future work in a multi-input/multi-output framework.

7 MULTI-OBJECTIVE CONTROL OF FULL-VEHICLE SUSPENSIONS: A CASE STUDY

This chapter is organized as follows. In Section 7.1, a seven-degrees-of-freedom full-car model is reviewed. This model was studied in [41] where a full-state optimal LQG regulator was designed. The LQG regulator designed in [41] improved ride quality as quantified by the rms sprung mass vertical acceleration by approximately 15 % relative to a soft passive suspension while maintaining the rms suspension and tire deflections at reasonable levels. The purpose of this chapter is to obtain further performance improvements via LMIs and the HIFOO controllers.

7.1 The Full-Car Model

A seven degrees-of-freedom full-car model intended to study the heave, the pitch, and the roll motions of a vehicle traveling on a straight line is shown in Figure 7.1. In the figure, the rear anti-roll bar is not shown and the car body is represented by the sprung mass m_s connected to the four unsprung masses m_{u_1}, m_{u_2}, m_{u_3}, and m_{u_4}, denoting respectively the wheel masses at the front-left, the front-right, the rear-left, and the rear-right corners of the vehicle. The sprung mass is assumed to be rigid and has freedoms of motion in the heave, the pitch, and the roll directions while the unsprung masses are free to bounce vertically with respect to the sprung mass. The suspension system between the sprung mass and the unsprung masses consists of the actuators u_i, $i = 1, ..., 4$ in parallel with the linear passive suspension elements of dampers and springs while the tires are modeled as simple linear springs connected in parallel with linear damping elements. The pitch and the roll angles are assumed to be small and in this study tire damping is neglected, *i.e.,* $c_t = 0$. The variables

z_G, θ, and ϕ are the vertical displacement at the center of gravity, the pitch and the roll angles of the sprung mass, respectively. The parameter values are shown in Table 7.1, [41]. Assuming that the tires behave as point-contact followers that are in contact with road at all times, the governing equations of motion of the full-car model are derived as follows.

Table 7.1: The vehicle parameters for the full-car model.

Sprung mass	m_s	1460 kg
Roll moment of inertia	J_x	460 kgm^2
Pitch moment of inertia	J_y	2460 kgm^2
Left and right-front unsprung masses	m_{u1}, m_{u2}	40kg
Left and right-rear unsprung masses	m_{u3}, m_{u4}	35.5 kg
Left and right-front damping coefficients	c_A, c_B	1290 Ns/m
Left and right-rear damping coefficients	c_C, c_D	1620 Ns/m
Left and right-front suspension stiffnesses	k_A, k_B	19,960 N/m
Left and right-rear suspension stiffnesses	k_C, k_D	17,500 N/m
Front auxiliary roll stiffness	K_F	19,200 Nrad/m
Rear auxiliary roll stiffness	K_R	0 Nrad/m
Tire stiffnesses	k_T	175,500 N/m
Longitudinal distance from the front axle c.g. to the sprung mass c.g	l_f	1.011 m
Longitudinal distance from the rear axle c.g. to the sprung mass c.g	l_r	1.803 m
Front track width	t_f	1.522 m
Rear track width	t_r	1.510 m
Longitudinal distance from the sprung mass c.g. to the driver	x_d	0.32 m
Lateral distance from the sprung mass c.g. to the driver	y_d	0.38 m

Let $x_a = [z_{u1}\ z_{u2}\ z_{u3}\ z_{u4}]^T$ denote the vector obtained by stacking the wheel displacements. The body motion vector is defined as $z_q = [z_G\ \ \theta\ \ \phi]^T$. Concatenate the vertical displacements at the corners of the car body as $x_b = [z_1\ \ z_2\ \ z_3\ \ z_4\ ]^T$ and denote the transformation matrix relating z_q to x_b by Ψ,

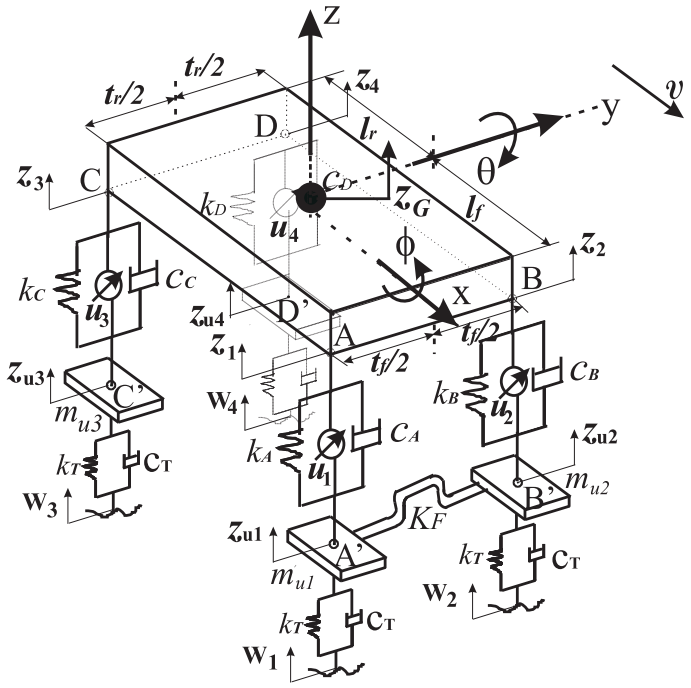

Figure 7.1: The full-car model of the vehicle.

i.e., $x_b = \Psi z_q$. From Figure 7.1, note that Ψ is given by

$$\Psi = \begin{bmatrix} 1 & -l_f & -t_f/2 \\ 1 & -l_f & t_f/2 \\ 1 & l_r & -t_r/2 \\ 1 & l_r & t_r/2 \end{bmatrix}.$$

Stack the road disturbances and the control inputs into two vectors w and u as $w = [w_1 \ w_2 \ w_3 \ w_4]^T$ and $u = [u_1 \ u_2 \ u_3 \ u_4]^T$. The variables x_a, x_b, and w are measured with respect to an inertial frame. Let $\tilde{x} = [z_q \quad x_a]^T$, $K_s = \text{diag}(d_1, d_2)$, $K_t = k_T I_4$, $C_s = \text{diag}(c_A, c_B, c_C, c_D)$ where

$$d_1 = \begin{bmatrix} k_A + K_F/t_f^2 & -K_F/t_f^2 \\ -K_F/t_f^2 & k_B + K_F/t_f^2 \end{bmatrix},$$

$$d_2 = \begin{bmatrix} k_C + K_R/t_r^2 & -K_R/t_r^2 \\ -K_R/t_r^2 & k_D + K_R/t_r^2 \end{bmatrix},$$

Then, the equations of motion can be put into the matrix form:

$$M\ddot{\tilde{x}} = C\dot{\tilde{x}} + K\tilde{x} + Wu + Pw$$

where $M = \text{diag}(m_s, J_y, J_x, m_{u1}, \cdots, , m_{u4})$, $W = [-\Psi \;\; I_4]^T$, $P = [0_{4\times 3} \;\; K_t]^T$,

$$C = \begin{bmatrix} -\Psi^T C_s \Psi & \Psi^T C_s \\ C_s \Psi & -C_s \end{bmatrix},$$

$$K = \begin{bmatrix} -\Psi^T K_s \Psi & \Psi^T K_s \\ K_s \Psi & -K_s - K_t \end{bmatrix},$$

Let $x = [\tilde{x}^T \;\; \dot{\tilde{x}}^T]^T$. Thus, the equations of motion are given in the state-space form by

$$\dot{x} = Ax + B_{11} w + B_2 u \tag{7.1}$$

where $B_{11} = [0_{4\times 7} \;\; P^T M^{-T}]^T$, $B_2 = [0_{4\times 7} \;\; W^T M^{-T}]^T$, and

$$A = \begin{bmatrix} 0_{7\times 7} & I_7 \\ M^{-1}K & M^{-1}C \end{bmatrix}.$$

7.1.1 The Road Excitation Model

A four-wheeled vehicle traveling along a road with a constant forward velocity v is subjected to four imposed displacement excitations, one at each wheel. The road unevenness is commonly modeled as a random excitation process with two kinds of correlations: the cross-correlation between the left and the right tracks and the time delay between the front and the rear wheels. However, in this chapter the displacement excitations will be assumed to be independent by ignoring the correlations among the wheels. This assumption is hardly justifiable; but, guarantees simultaneous excitation of all the three body motions.

The road displacements w_k, $k = 1, \cdots, 4$ are assumed to obey the relation $w_k = \widetilde{G}\eta_k$ for some linear shape filter $\widetilde{G}$ where η_k are independent zero-mean (spatial) unit-intensity white noise processes and the transfer function $\widetilde{G}(s)$ is stable with finite number of zeros in the open left-half plane. The relation between $\widetilde{G}$ and the power spectrum of w_k is given by $S_{w_k}(f) = |\widetilde{G}(j2\pi f)|^2$ where f is the (spatial) frequency measured in cycles per meter. The filter $\widetilde{G}$

is translated to the temporal domain as $\bar{G}(s) = \widetilde{G}(v^{-1}s)$. Hence, $S_{\eta_k}(\omega) = v^{-1}$ and $S_{w_k}(\omega) = S_{\eta_k}(\omega)|\widetilde{G}_{w_k}(j\omega)|^2$.

A first-order linear shape filter $\widetilde{G}(s) = b_w(s+a_w)^{-1}$ has been observed to produce good match to measured road spectra by adjusting the filter parameters b_w and $a_w > 0$ [75]. The parameter values $b_w = 0.0195$ and $a_w = 0.0572$ in [75] are used in the current work. Note that the first-order shape filter results in the road excitation model

$$\dot{w} = -va_w w + \sqrt{v}b_w\xi \tag{7.2}$$

where $\xi(t)$ is a zero-mean vector valued white-noise process with covariance function $R_\xi(\tau) = I_4\delta(\tau)$. If $v = 20$ m/sec, then w_k at this speed can be thought of integrated white-noise, in particular for frequencies larger than 0.2 Hertzs. On the other hand, the natural frequencies of the first three modes corresponding to the vehicle data in Table 7.1 are computed as 0.99, 1.23, and 1.69 Hertzs. Thus, in the bandwidth of interest $\dot{w}$ can be approximated by a vector-valued white-noise process, and it is safe to assume that subsequent controller design procedure is robust to small variations of a_w. Moreover, an active suspension designed in the premises of a road excitation model taking into account all possible couplings among vehicle modes respects the well-known sprung mass accelerations–tire deflections, suspension travels–tire deflections, and sprung mass accelerations–suspension travels trade-offs. In fact, the body modes are highly coupled as evidenced by the closely packed natural frequencies.

7.2 Multi-Objective Control Using LMIs

Let r denote the regulated output obtained by stacking respectively the suspension travels, the tire deflections, the heave, the pitch, and the roll accelerations of the driver located at longitudinal and lateral distances x_d and y_d from the sprung mass center of gravity into a column vector:

$$r = C_1x + D_{11}w + D_{12}u \tag{7.3}$$

where

$$
\begin{aligned}
r &= (x_b^T - x_a^T \;\; x_a^T - w^T \;\; \ddot{z}_d \;\; \ddot{\theta} \;\; \ddot{\phi})^T, \\
C_1 &= \begin{bmatrix} \Psi & -I_4 & 0_{4\times 7} \\ 0_{4\times 3} & I_4 & 0_{4\times 7} \\ \Psi_d[0_{3\times 7} & I_3 & 0_{3\times 4}]A \end{bmatrix}, \\
D_{11} &= \begin{bmatrix} & 0_{4\times 4} & \\ & -I_4 & \\ \Psi_d[0_{3\times 7} & I_3 & 0_{3\times 4}]B_{11} \end{bmatrix}, \\
D_{12} &= \begin{bmatrix} & 0_{8\times 4} & \\ \Psi_d[0_{3\times 7} & I_3 & 0_{3\times 4}]B_2 \end{bmatrix}, \\
\Psi_d &= \begin{bmatrix} 1 & -x_d & y_d \\ 0 & 1 & 0 \\ 0 & 0 & 1 \end{bmatrix}.
\end{aligned}
$$

To improve ride comfort, the heave, the pitch, and the roll accelerations of the driver, should be made as small as possible while keeping the suspension travels below the maximum allowable suspension stroke. This is important for preventing excessive suspension bottoming, which can result in structural damage and deterioration of ride comfort. Also, in order to ensure a firm uninterrupted contact of the wheels to road, dynamic tire loads should not exceed static ones. Thus, designing control law for suspension systems is a multi-objective control problem where the strategy is to reduce the three body accelerations while keeping the constraints satisfied. It is a well-known fact [19] that these conflicting objectives can not be met simultaneously with passive suspensions; but to some extent, they can be resolved by replacing passive suspension with an active or semi-active suspension.

For the design of a feedback law, consider the suspension travel and the velocity measurements:

$$y = (x_b^T - x_a^T \;\; \dot{x}^T)^T.$$

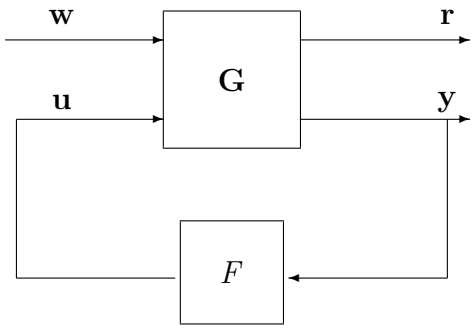

Figure 7.2: Standard block diagram.

Note that the output vector y can be can be written as

$$y = C_2 x \tag{7.4}$$

where

$$C_2 = \begin{bmatrix} \Psi & -I_4 & 0_{4\times 7} \\ 0_{7\times 7} & & I_7 \end{bmatrix}.$$

The dynamic output feedback structure

$$\begin{aligned} \dot{x}_c &= A_K x_c + B_K y \\ u &= C_K x_c + D_K y \end{aligned} \tag{7.5}$$

where the state-space parameters A_K, B_K, C_K, D_K of the transfer function $F(s) : y \mapsto u$ are to be determined will be considered in this chapter. The feedback configuration of $G(s) : [w^T \ u^T]^T \mapsto [r^T \ y^T]^T$ and $F(s)$ is shown in Figure 7.2.

Let $r_{21} = (\ddot{z}_d \ \ddot{\theta} \ \ddot{\phi})^T$, $r_{22} = x_b - x_a$, $r_\infty = x_a - w$, and $r_2 = (r_{21}^T \ r_{22}^T)^T$. Partition r as $r = (r_{22}^T \ r_\infty^T \ r_{21}^T)^T$. Let $T_{r_2 w}(s)$, $T_{r_\infty w}(s)$ and $T_{r_2 \xi}(s)$, $T_{r_\infty \xi}(s)$ denote the closed-loop transfer functions $w \mapsto r_2, r_\infty$ and $\xi \mapsto r_2, r_\infty$. The multi-objective control design problem considered in this section is then as follows.

Problem 7.2.1. *For given two matrices Λ_2 and Λ_∞ and a subset $\mathcal{D}$ of the open left-half plane, design a controller $u = F(s)y$ that minimizes $\|\Lambda_\infty T_{r_\infty \xi}\|_\infty^2 + \|\Lambda_2 T_{r_2 \xi}\|_2^2$ and assigns the closed-loop poles in $\mathcal{D}$.*

The choice of the weights Λ_2 and Λ_∞ is non-trivial due to their large sizes. In this chapter, Λ_2 and Λ_∞ will be picked as block diagonal matrices. In spite of simplicity, this choice leads to controllers capable of effectively suppressing road induced vehicle vibrations without compromising road holding while maintaining suspension travels within limits. As an illustration, let $G_{r_{21}\xi}(s)$, $G_{r_{22}\xi}(s)$, and $G_{r_\infty\xi}(s)$ denote the open-loop transfer matrices from ξ to r_{21}, r_{22}, and r_∞, respectively. Given two numbers $\lambda, \mu \in [0,1]$, set $\Lambda_\infty = \alpha_1 I_4$ and $\Lambda_2 = \mathrm{diag}(\alpha_2 I_3, \alpha_3 I_4)$ where the scalings α_k, $k = 1,2,3$ are defined as $\alpha_1 = \sqrt{\lambda}\,\|G_{r_\infty\xi}\|_\infty^{-1}$, $\alpha_2 = \mu\sqrt{1-\lambda}\,\|G_{r_{21}\xi}\|_2^{-1}$, and $\alpha_3 = (1-\mu)\sqrt{1-\lambda}\,\|G_{r_{22}\xi}\|_2^{-1}$. Thus, the control objective is to minimize $\alpha_1^2\|T_{r_\infty\xi}\|_\infty + \alpha_2^2\mathrm{E}(\ddot{z}_d^2 + \ddot{\theta}^2 + \ddot{\phi}^2) + \alpha_3^2\mathrm{E}\|x_b - x_a\|^2$ over $F(s)$ in (7.5) where $\mathrm{E}(x)$ denotes the expected value of a given random variable x. As the closed-loop pole set, the open rectangle $\mathcal{D} = \{z = a + ib,\ -\gamma < a < 0,\ |b| < \gamma\}$ for a given $\gamma > 0$ is chosen. This simple choice stems from the fact that Problem 7.2.1 can be cast into an LMI problem with pole assignment which requires checking the feasibility of some 171 LMIs for a positive definite unknown matrix of size 18×18. When the pole assignment is not enforced, LMI implementation of any solution of Problem 7.2.1 typically yields high-gain controllers with poles of large moduli.

One may hope to control ride comfort–suspension rattle space compactness, road holding–suspension rattle space compactness, and ride comfort–road holding trade-offs by changing the free parameters μ and λ. Another possibility is to replace $\|\Lambda_\infty T_{r_\infty\xi}\|_\infty^2$ in the cost function with $\|\Lambda_\infty T_{r_\infty w}\|_\infty^2$, which seems to be a more realistic indicator of road holding. Recall the relation $T_{r_\infty\eta}(s) = \widetilde{G}(v^{-1}s)T_{r_\infty w}(s)$. This equality means that $\Lambda_\infty T_{r_\infty\xi}(s)$ converges to $\Lambda_\infty T_{r_\infty w}(s)$ uniformly in finite bands of the frequencies as a_w in (7.2) is increased and b_w is adjusted accordingly.

In Problem 7.2.1, the cost function was expressed in the frequency-domain. A solution based on LMIs will be presented in the sequel. The LMI paradigm encompasses time-domain constraints at a price of conservatism. By tuning the design parameters, the solution of Problem 7.2.1 can also be forced

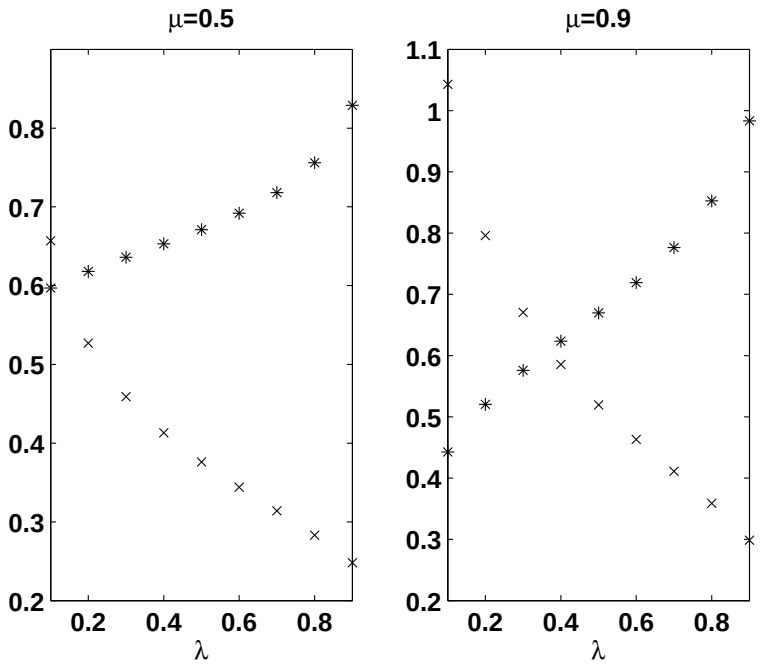

Figure 7.3: The two components of the optimized cost as a function of λ: (x) $\|\Lambda_\infty T_{r_\infty \xi}\|_\infty$; (*) $\|\Lambda_2 T_{r_2 \xi}\|_2$. The multi-objective controllers were synthesized for $\gamma = 200$ and $\mu = 0.5$ and 0.9 using LMIs.

to satisfy possible time-domain constraints.

7.2.1 A Design Example

In this subsection, an example illustrating properties of the multi-objective controller designed by using LMIs is presented. First, μ was fixed as either 0.5 or 0.9 and Problem 7.2.1 was solved for $\gamma = 200$ and $0.1 \leq \lambda \leq 0.9$. In Figure 7.3, $\|\Lambda_\infty T_{r_\infty \xi}\|_\infty$ and $\|\Lambda_2 T_{r_2 \xi}\|_2$ components of the optimized cost function are plotted versus λ for $\mu = 0.5$ and 0.9. Observe that one component increases as λ increases while the other decreases as in quarter-car trade-off studies. Similar trade-off curves are obtained for the boundary cases $\mu = 0$ and $\mu = 1$. The former is the road holding–suspension rattle space compactness trade-off while the latter is the road holding–ride comfort trade-off.

Let us examine a particular solution, for example, the solution obtained for $\lambda = \mu = 0.6$. The rms values of r_{21} and r_{22} are respectively 3.5916

and 0.0722 for the active suspension while the rms gain of $T_{r_\infty \xi}$ is 0.0030. The corresponding values for the passive suspension are respectively 4.7347, 0.0752, and 0.0090. Thus, the rms accelerations are reduced by 24 % without increasing the rms suspension travels and the rms tire deflections. In fact, the rms gain of tire deflections is dramatically reduced by 67 %. These results are in sharp contrast with quarter-car active suspension designs, which can not simultaneously improve the heave acceleration, the suspension travel, and the tire deflection responses and compare favorably with respect to the linear-quadratic-regulator design in [41] which uses the same full-car model of this note. More or less, performance improvements hold component-wise as well, in particular for the three body accelerations. The rms $\ddot{z}_d$, $\ddot{\theta}$, and $\ddot{\phi}$ are respectively 2.17, 1.35, and 3.98 for the passive suspension and 1.69, 1.13, and 2.95 for the active suspension design above.

In Figure 7.4, the magnitudes of the roll-suspension travel, the roll-tire deflection, and the roll-acceleration for the passive suspension and the active suspension to the roll input $w(t) = \delta_r e^{i\omega t}$, $-\infty < t < \infty$ where $\delta_r = [1 \; -1 \; 1 \; -1]^T$ is the roll-direction vector are plotted versus ω. Here, the roll-suspension travel and the roll-tire deflection are defined respectively by $\delta_r^T r_{22}$ and $\delta_r^T r_\infty$. The heave, the pitch, and the warp direction vectors are defined respectively as [1 1 1 1], [1 1 −1 −1], and [1 −1 −1 1] [41]. The magnitude plots of the suspension travels, the tire deflections, and the body accelerations to the heave, the pitch, and the warp inputs resemble Figure 7.4. Thus, once more it is acknowledged that the designed active suspension effectively suppresses body vibrations without increasing the suspension travels and the tire deflections in the bandwidth of interest.

Figure 7.4 reveals that the wheel-hop modes are not essentially affected by the multi-objective controller and it may be possible to replace the 18th order controller with one of the lower-degree controllers. This is indeed the case and the $6th$, the $8th$, or the $10th$ order models obtained by the balanced truncation method are as good as the original high-order controller. More details will be provided on this.

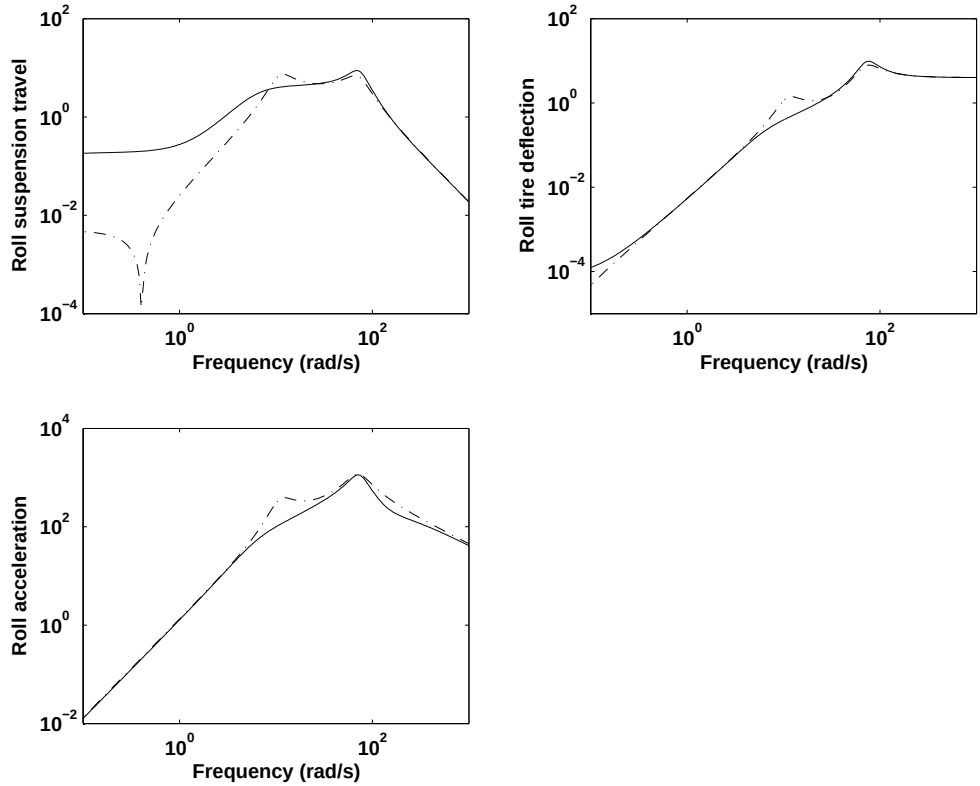

Figure 7.4: The roll-suspension travel, the roll-tire deflection, and the roll-acceleration frequency response magnitudes of the passive suspension and the active suspension system designed by solving Problem 7.2.1 via LMIs to the roll input $w(t) = \delta_r e^{i\omega t}$: (-.) passive suspension; (-) active suspension.

Problem 7.2.1 was re-formulated in many different ways including upper bounds on the $\mathcal{H}_2$ and/or $\mathcal{H}_\infty$ norms of the closed-loop transfer matrices $\Lambda_\infty T_{r_\infty \xi}$ and $\Lambda_2 T_{r_2 \xi}$ with different partitioning of r; but, the basic conclusions drawn above have remained essentially the same.

7.3 Multi-Objective Control via Fixed-Order Optimization

In this section, we consider the following multi-objective control design problem:

Problem 7.3.1. *For given three matrices $\Lambda_1, \Lambda_2, \Lambda_3$, two numbers $\beta_1, \beta_2 > 0$, and a specified controller order n_K, find an output-feedback controller $u =$*

$K(s)$y internally stabilizing the closed-loop system and minimizing $\|\Lambda_1 T_{r_{21}w}\|_\infty$ *while satisfying* $\|\Lambda_2 T_{r_{22}w}\|_\infty < \beta_1$ *and* $\|\Lambda_3 T_{r_\infty w}\|_\infty < \beta_2$.

As we mentioned earlier, this is a non-convex optimization problem solved by using the HIFOO toolbox [45] when n_K is less than the order of the passive suspension system. Recall that the optimization algorithms in the HIFOO toolbox do not attempt to find global minimum. Thus, their success depends on proper initialization. However, they have been successfully applied to several benchmark problems [34]. This toolbox currently does not accommodate norms other than the supremum norms.

The weight matrices and the parameters are chosen as follows. After some feasibility trials, we set $\beta_1 = 1.1$ and $\beta_2 = 1.2$ and let $\Lambda_1^{-1} = \text{diag}(\|G_{\ddot{z}_d w}\|_\infty, \|G_{\ddot{\theta} w}\|_\infty, \|G_{\ddot{\phi} w}\|_\infty)$, $\Lambda_2^{-1} = \|G_{r_{22}w}\|_\infty I_4$, and $\Lambda_3^{-1} = \|G_{r_\infty w}\|_\infty I_4$. Note that the transfer functions in Problem 7.3.1 are from w to the components of r. Also, the diagonal elements of Λ are different.

In Table 7.2, the rms response variables are displayed for the passive and the active suspensions designed by the HIFOO toolbox for different controller orders. In Figure 7.5, the magnitudes of the roll-suspension travel, the roll-tire deflection, and the roll-acceleration for the passive suspension and the HIFOO design for $n_K = 6$ to the roll input in Section 7.2.1 are plotted. Figures 7.4 and 7.5 are nearly the same in spite of the big difference in controller orders.

Performance enhancements by the HIFOO designs (with respect to the passive suspension) are remarkable: the rms accelerations are lowered more than the LQG design in [41] when $n_K > 2$, although numerical results for the latter design are not reported in this chapter. If the LMI design in Section 7.2.1 is followed by balanced truncation, the rms accelerations of the reduced order controllers are slightly less than those of the HIFOO controllers. However, robustness of the HIFOO designs to inaccuracies in road models make them preferable to the LQG and the LMI designs since the latter depend on the parameters of the road model through (7.1) and (7.2).

Table 7.2: The rms responses of the passively and actively suspended full-car model with the HIFOO controllers of order n_K.

rms	$\|T_{r_\infty\xi}\|_2$	$\|T_{r_{22}\xi}\|_2$	$\|T_{\ddot{z}_d\xi}\|_2$	$\|T_{\ddot{\theta}\xi}\|_2$	$\|T_{\ddot{\phi}\xi}\|_2$
Passive	0.0233	0.0752	2.1700	1.3500	3.9800
$n_K = 2$	0.0242	0.0725	2.0381	1.3623	3.6386
$n_K = 4$	0.0238	0.0807	1.9000	1.3189	3.2281
$n_K = 6$	0.0237	0.0765	1.8795	1.3157	3.0871
$n_K = 8$	0.0237	0.0765	1.8815	1.3157	3.0938
$n_K = 10$	0.0263	0.1127	1.7619	1.2023	3.0332

7.4 Summary

In this chapter, multi-objective control of full-car suspension models excited by random road disturbances was studied. The control problem was first formulated as a convex mixed $\mathcal{H}_2/\mathcal{H}_\infty$ synthesis problem and solved using LMIs. This formalism yields a controller with degree equal to the vehicle model order. In a case study, the closed-loop performance of this controller was found superior to the LQG design in [41]. Next, the multi-objective suspension control problem was re-formulated as a non-convex and non-smooth optimization problem with controller order constrained to be less than the vehicle model order. Controllers of various orders were synthesized by using the recently developed optimization algorithms in the HIFOO toolbox. Performance enhancement similar to that of the LMI design was noted especially for low order HIFOO controllers. Thus, multi-objective control of full-car suspensions via LMIs and fixed-order optimization (as implemented by the HIFOO toolbox) presents a promising alternative to existing LQG methods.

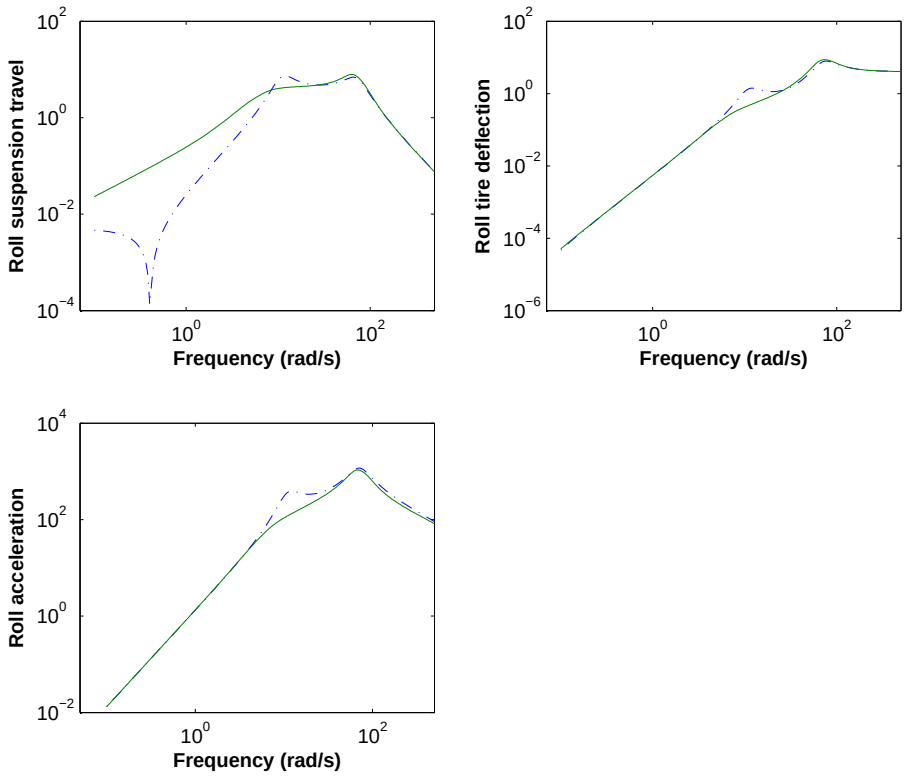

Figure 7.5: The roll-suspension travel, the roll-tire deflection, and the roll-acceleration frequency response magnitudes of the passive suspension and the HI-FOO design for $n_k = 6$ to roll input $w(t) = \delta_r e^{i\omega t}$: (-.) passive suspension; (-) active suspension.

8 ACTIVE SUSPENSION DESIGN FOR IDEALIZED TRUCK CABIN

Heavy road vehicles are typically used for transportation and they have different characteristics than those of a car. For example, heavy road vehicles may have more than two axles and each axle weighs an order of magnitude greater than a typical car axle. In addition, heavy vehicles comprise more than one unit. To accommodate payload volume within practical vehicle dimensions, in a heavy road vehicle the height of the vehicle's center of mass is generally enormous in relation to its track width, compared to cars. The payload mass is often a large proportion of the gross vehicle mass and the payload mass and its distribution along the chassis may also be highly variable. In designing suspension systems, selection of optimum dynamic properties requires performance criteria against which to judge alternatives. For example, infra-structure damage caused by the tires of heavy vehicles traveling over roads and bridges is a major concern while it is not an issue at all with car suspensions. In summary, heavy road vehicles have dynamic behavior which is significantly different than that of cars, and thus require distinct suspension design approaches. In the comprehensive work [135], published literature on suspension design for heavy road vehicles is surveyed and fundamental issues in suspension design for heavy road vehicles that require further attention are identified.

The issue of ride comfort for vehicle operations has generated considerable interest recently, especially in heavy vehicle systems since long-distance drivers are more likely to experience high levels of vibration. Vibration-related health problems and ride comfort assessment criteria and methods are discussed in the survey paper [47]. Cabin and seat suspension (secondary suspension) provides the driver with a comfortable ride without requiring soft primary suspension and consequent problems with vehicle handling, stability, and static deflection. Recent activity [48–51] in the area of cabin and suspension design

has focused on the use of controllable suspension elements which provide ride benefits of active/semi-active primary suspension. In [48], stochastic optimal control was used to design an active cabin suspension for a tractor semitrailer. A pitch-plane modeling including the first bending modes of the frames is used, and the control law is calculated for a range of vehicle speeds. Tong et al. [51] (see, also [50]) proposed a design comprising semi-active cabin and seat suspensions on a tractor-semitrailer. The suspension consists of semi-active dampers with sky-hook controllers. Ride quality was assessed using a dynamic model of the seated driver with only vertical degrees of freedom. Longitudinal and pitch motions of the driver were not considered. The selected vehicle model in [50] is planar and includes a cabin with two-degrees-of-freedom: pitch and vertical displacement.

Very few studies took an integrated look at the primary and secondary suspensions. In [136], elimination of the seat suspension and using softer cabin suspension (with natural frequencies below those of the primary suspension) and stiffer primary suspension was suggested. The author argued that primary suspension dampers are not effective in dissipating the vibration energy due to frame bending. The result is that the driver can experience large levels of vibrations in the longitudinal and vertical directions depending on the cabin mounting and location. It is also a fact that active-suspension control based on rigid body dynamics can cause excitation of unmodelled flexural modes. In [137, 138], flexible frames were incorporated into the authors' ride model and active suspension systems were designed to control the beaming. However, this endeavor resulted with a limited success. In [139], see also [140, 141], the frame of a prototype truck was modeled using the finite-element method. The natural frequencies of the frame were found varying between 5.6 Hz and 31.8 Hz; but, they were neglected in the subsequent semi-active (primary) suspension design. The control objectives were to minimize road-tire forces to prevent road damage and to keep the accelerations of the seated driver and the load at reasonable levels. Due to high center of mass in relation to track width, lateral acceleration of a heavy vehicle leads to significant load transfer

across the axles. This means that there is a strong coupling between yaw and roll motions, which should be taken into account in the design of controlled suspension systems.

Now, we outline the contents of this chapter. In this chapter, we consider a prototype three degrees of freedom cabin model for a mid-sized commercial truck. The purpose of this study is to analyze ride motions of the cabin under random road excitations and to improve its ride performance by designing a suitable compensator. An active suspension system is designed using the LQG design methodology. The simulation results show that the cabin vibrations can effectively be suppressed.

The cabin model considered in this chapter has an additional roll degree of freedom with respect to the models surveyed above. This choice is justified by the fact that during cornering or lane changing, roll and yaw modes of the vehicle are excited by lateral acceleration of the vehicle. Thus, including roll degree of freedom in the cabin model is expected to yield more realistic suspension designs. In addition, excitation forces transmitted to the truck cabin from the vehicle chassis are assumed to be statistically independent. Although this assumption is not realistic since the road disturbances, which are already temporally and spatially correlated, are further filtered by the primary suspension system, it guarantees simultaneous excitation of the heave, the roll, and the pitch modes of the truck cabin. Hence, it suffices to have a crude truck model that relates in the mean-square sense the road disturbances to the chassis displacements at the cabin suspension attachment points to design an active or semi-active suspension system for the cabin. The truck model can be obtained either experimentally by using the spectral estimation algorithm developed in [57] or using a simplified bounce model of the truck. The latter choice is opted in this chapter. Although there are many control design methodologies available, the LQG design method was chosen because it is intuitive and easy to implement.

8.1 The Three–Degrees–of–Freedom Truck Cabin Model

A three degree of freedom truck cabin ride model is shown in Figure 8.1. The displacements at the chassis points $\mathrm{A}', \mathrm{B}', \mathrm{C}', \mathrm{D}'$ with respect to an inertial frame are denoted respectively by w_A, w_B, w_C, w_D. Let z_A, z_B, z_C, z_D denote the displacements at the corners $\mathrm{A}, \mathrm{B}, \mathrm{C}, \mathrm{D}$ of the cabin with respect to an inertial frame. The cabin center of gravity, its mass, and the heave degree of freedom are denoted respectively by G, m_s, and z_G. The pitch and the roll degrees of freedom and their moments of inertia are denoted respectively by θ, ϕ, I_x, and I_y.

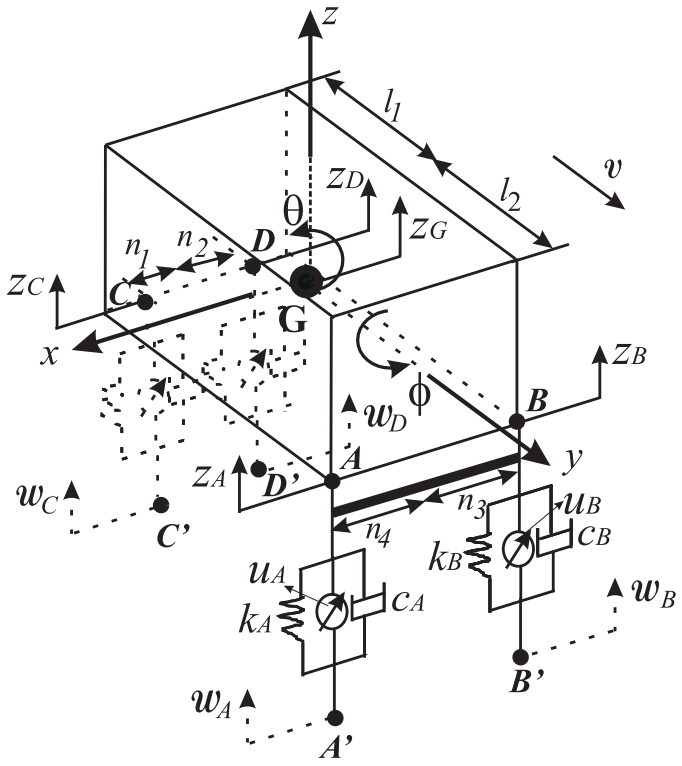

Figure 8.1: Truck cabin model.

The cabin suspension system consists of the actuators u_A, u_B, u_C, u_D in parallel with the linear passive suspension elements: k_A, k_B, k_C, k_D (springs) and c_A, c_B, c_C, c_D (dampers). In front of the cabin, an anti-roll bar denoted by K_F is included. In Table 8.1, the notations for truck cabin parameters and

the parameter values used in this study are shown. These are typical for a mid-sized truck. This cabin model is the most flexible one since it allows all possible cabin motions. In addition to the cabin models surveyed above, in some cabins the front part is practically rigid and the sprung mass can only rotate with respect to the x axis.

Table 8.1: The parameters for the truck cabin model.

Cabin mass	m_c	900 kg
Pitch moment of inertia	I_x	700 kg m^2
Roll moment of inertia	I_y	650 kg m^2
Front-right/left suspension stiffness	k_A, k_B	31,000 N m^{-1}
Rear-right/left suspension stiffness	k_C, k_D	15,500 N m^{-1}
Front-right/left damping coefficient	c_A, c_B	680 Ns m^{-1}
Rear-right/left damping coefficient	c_C, c_D	560 Ns m^{-1}
Front anti-roll bar stiffness	K_F	30,000 N m^{-1}
Distance between front-right/left corner and cabin c. g. along x axis	n_3, n_4	0.84 m
Distance between rear-right/left corner and cabin c. g. along x axis	n_1, n_2	0.68 m
Distance between front-right/left corner and cabin c. g. along y axis	l_2	0.409 m
Distance between rear-right/left corner and cabin c. g. along y axis	l_1	1.091 m

Assuming that the displacements are sufficiently small from the equilibrium, the equations of motion are derived as follows. From Figure 8.1, under the assumption of linearity the following kinematic relations:

$$z_A = z_G + l_2\theta - n_4\phi,$$
$$z_B = z_G + l_2\theta + n_3\phi,$$
$$z_C = z_G - l_1\theta - n_1\phi,$$
$$z_D = z_G - l_1\theta + n_2\phi,$$

or compactly

$$z_S = Sx_s,$$

are easily derived where

$$z_S = \begin{bmatrix} z_A \\ z_B \\ z_C \\ z_D \end{bmatrix}, \quad S = \begin{bmatrix} 1 & l_2 & -n_4 \\ 1 & l_2 & n_3 \\ 1 & -l_1 & -n_1 \\ 1 & l_1 & n_2 \end{bmatrix}, \quad x_S = \begin{bmatrix} z_G \\ \theta \\ \phi \end{bmatrix}.$$

Let $z_A - w_A$ and $z_B - w_B$ denote the suspension strokes at corners A and B. Then, the rotation of the anti-roll bar in the counter-clockwise direction is given by

$$\phi_F = \frac{(z_A - w_A) - (z_B - w_B)}{n_3 + n_4}$$

and accordingly a pair of forces f and $-f$ is formed:

$$f(n_3 + n_4) = K_F \phi_F,$$

or more explicitly,

$$f = K_F \frac{(z_A - z_B) - (w_A - w_B)}{(n_3 + n_4)^2}.$$

Now, let F_A, F_B, F_C, F_D denote respectively the forces at the corners A, B, C, D exerted by the suspension system. Then, the following relations hold for F_A, F_B, F_C, F_D :

$$\begin{aligned} F_A &= -f - k_A(z_A - w_A) - c_A(\dot{z}_A - \dot{w}_A) - u_A, \\ F_B &= f - k_B(z_B - w_B) - c_B(\dot{z}_B - \dot{w}_B) - u_B, \\ F_C &= -k_C(z_C - w_C) - c_C(\dot{z}_C - \dot{w}_C) - u_C, \\ F_D &= -k_D(z_D - w_D) - c_D(\dot{z}_D - \dot{w}_D) - u_D. \end{aligned}$$

Thus,

$$\begin{aligned} m_c \ddot{z}_G &= F_A + F_B + F_C + F_D, \\ I_x \ddot{\theta} &= (F_A + F_B) l_2 - (F_C + F_D) l_1, \\ I_y \ddot{\phi} &= -F_A n_4 + F_B n_3 - F_C n_1 + F_D n_2. \end{aligned}$$

Setting

$$w = \begin{bmatrix} w_A \\ w_B \\ w_C \\ w_D \end{bmatrix}, \quad u = \begin{bmatrix} u_A \\ u_B \\ u_C \\ u_D \end{bmatrix}, \quad \widetilde{z}_S = z_S - w,$$

the following equations of motion:

$$\begin{aligned}
m_c\ddot{z}_G &= -[k_A \;\; k_B \;\; k_C \;\; k_D]\widetilde{z}_S - [c_A \;\; c_B \;\; c_C \;\; c_D]\dot{\widetilde{z}}_S - [1 \;\; 1 \;\; 1 \;\; 1]u, \\
I_x\ddot{\theta} &= -[k_A l_2 \;\; k_B l_2 \;\; -k_C l_1 \;\; -k_D l_1]\widetilde{z}_S - [c_A l_2 \;\; c_B l_2 \;\; -c_C l_1 \;\; -c_D l_1]\dot{\widetilde{z}}_S \\
&\quad -[l_2 \;\; l_2 \;\; -l_1 \;\; -l_1]u, \\
I_y\ddot{\phi} &= \left[(k_A n_4 + \frac{K_F}{n_3+n_4}) \;\; -(k_B n_3 + \frac{K_F}{n_3+n_4}) \;\; k_C n_1 \;\; -k_D n_2\right]\widetilde{z}_S \\
&\quad +[c_A n_4 \;\; -c_B n_3 \;\; c_C n_1 \;\; -c_D n_2]\dot{\widetilde{z}}_S + [n_4 \;\; -n_3 \;\; n_1 \;\; -n_2]u,
\end{aligned}$$

or more compactly

$$M\ddot{x}_S + K\widetilde{z}_S + C\dot{\widetilde{z}}_S + Wu = 0,$$

are obtained where

$$M = \begin{bmatrix} m_c & 0 & 0 \\ 0 & I_x & 0 \\ 0 & 0 & I_y \end{bmatrix},$$

$$K = \begin{bmatrix} k_A & k_B & k_C & k_D \\ k_A l_2 & k_B l_2 & -k_C l_1 & -k_D l_1 \\ -(k_A n_4 + \frac{K_F}{n_3+n_4}) & (k_B n_3 + \frac{K_F}{n_3+n_4}) & -k_C n_1 & k_D n_2 \end{bmatrix},$$

$$C = \begin{bmatrix} c_A & c_B & c_C & c_D \\ c_A l_2 & c_B l_2 & -c_C l_1 & -c_D l_1 \\ -c_A n_4 & c_B n_3 & -c_C n_1 & c_D n_2 \end{bmatrix},$$

$$W = \begin{bmatrix} 1 & 1 & 1 & 1 \\ l_2 & l_2 & -l_1 & -l_1 \\ -n_4 & n_3 & -n_1 & n_2 \end{bmatrix}.$$

Note that from $\widetilde{z}_S = z_S - w = Sx_S - w$,

$$M\ddot{x}_S + KSx_S - Kw + CS\dot{x}_S - C\dot{w} + Wu = 0.$$

For the controlled cabin dynamics, state-space formulas will be derived next. To this end, first let

$$x = \begin{bmatrix} x_S \\ \dot{x}_S \end{bmatrix}$$

denote the state vector and assume that the displacement vector w is the output of the linear shape filter:

$$\begin{aligned} \dot{x}_w &= A_w x_w + B_w \nu, \\ w &= C_w x_w \end{aligned} \tag{8.1}$$

with $\dim(x_w) = n_w$ and $\dim(\nu) = 4$. Further assume that the filter $(A_w, B_w, C_w, 0)$ has a zero at $s = \infty$ with multiplicity at least two. This assumption is not stringent and, for example, is satisfied by the vehicle system under consideration. Then,

$$\dot{w} = C_w A_w x_w + C_w B_w \nu.$$

Now, if $\dot{w}$ is part of the output, the relative degree assumption implies that

$$C_w B_w = 0$$

since, otherwise, the following system

$$\begin{aligned} \dot{x}_w &= A_w x_w + B_w \nu, \\ \dot{w} &= C_w A_w x_w + C_w B_w \nu \end{aligned}$$

would only be proper. Hence,

$$\ddot{x}_S = [-M^{-1}KS \quad -M^{-1}CS \quad M^{-1}(KC_w + CC_wA_w)] \begin{bmatrix} x \\ x_w \end{bmatrix} - M^{-1}Wu.$$

Let

$$\widetilde{x} = \begin{bmatrix} x \\ x_w \end{bmatrix}.$$

Then,

$$\dot{\widetilde{x}} = A\widetilde{x} + B_1\nu + B_2 u \tag{8.2}$$

where

$$A = \left[\begin{array}{cc|c} 0_{3\times 3} & I_3 & 0_{3\times n_w} \\ -M^{-1}KS & -M^{-1}CS & M^{-1}(KC_w + CC_wA_w) \\ \hline 0_{n_w\times 6} & & A_w \end{array}\right],$$

$$B_1 = \left[\begin{array}{c} 0_{3\times n_\nu} \\ 0_{3\times n_\nu} \\ B_w \end{array}\right], \qquad B_2 = \left[\begin{array}{c} 0_{3\times 4} \\ -M^{-1}W \\ 0_{n_w\times 4} \end{array}\right].$$

The filter parameters A_w, B_w, C_w can be obtained from power spectrum measurements at the chassis points A′, B′, C′, D′ using the subspace-based algorithm developed in [57]. Alternatively, a transfer function relating road excitations to w can be derived from first principles. This approach requires a simple physical truck model and it will be discussed in the next section.

For feedback, assume that the accelerometer readings at the corners A, B, C, D and the secondary suspension strokes stacked respectively into the vectors $\ddot{z}_S$ and $\widetilde{z}_S$ which can be expressed as

$$y = \left[\begin{array}{c} \ddot{z}_S \\ \widetilde{z}_S \end{array}\right] = C_2\widetilde{x} + D_{22}u$$

where

$$C_2 = \left[\begin{array}{ccc} -SM^{-1}KS & -SM^{-1}CS & SM^{-1}(KC_w + CC_wA_w) \\ S & 0_{4\times 3} & -C_w \end{array}\right],$$

$$D_{22} = \left[\begin{array}{c} -SM^{-1}W \\ 0_{4\times 4} \end{array}\right]$$

are available.

Table 8.2: The parameters for the truck bounce model.

Cabin mass	m_c	900 kg
Sprung mass	m_s	5,100 kg
Unsprung mass	m_u	1,000 kg
Primary suspension stiffness	k_s	3,600,000 N/m
Secondary suspension stiffness	k_c	90,000 N/m
Primary damping coefficient	c_s	5,000 Ns/m
Secondary damping coefficient	c_c	2,500 Ns/m
Tire stiffness	k_T	8,000,000 N/m

8.2 Bounce Model of the Truck

A simplified bounce model of the truck is sketched in Figure 8.2. The model parameters shown in Table 8.2 have been obtained by considering 'heave only' motion of a twelve degrees of freedom full truck model.

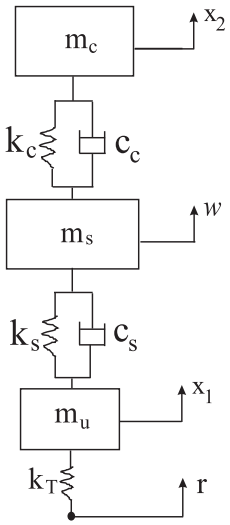

Figure 8.2: Bounce model of the truck.

Assuming that the tires are in contact with the road at all times, the equations of motion are given by

$$
\begin{aligned}
m_c\ddot{x}_2 &= -k_c(x_2 - w) - c_c(\dot{x}_2 - \dot{w}),\\
m_s\ddot{w} &= k_c(x_2 - w) + c_c(\dot{x}_2 - \dot{w}) - k_s(w - x_1) - c_s(\dot{w} - \dot{x}_1),\\
m_u\ddot{x}_1 &= k_s(w - x_1) + c_s(\dot{w} - \dot{x}_1) - k_T(x_1 - r)
\end{aligned}
$$

where x_2, w, and x_1 are respectively the vertical displacements of the cabin, the sprung and the unsprung masses. The sprung and the unsprung masses represent respectively the truck body and the assembly of the wheels and the axles. The variable r denotes the road unevenness. Even though we use common symbols, these variables are not the same as the state variables and the chassis displacements introduced in the previous section.

Next, change the state variables as:

$$
\bar{x}_1 = x_2 - w,\ \ \bar{x}_2 = w - x_1,\ \ \bar{x}_3 = x_1 - r,\ \ \bar{x}_4 = \dot{x}_2,\ \ \bar{x}_5 = \dot{w},\ \ \bar{x}_6 = \dot{x}_1,
$$

and set $\zeta = \dot{r}$. Then, the transfer function $G_{\dot{w}\zeta}(s)$ mapping ζ to $\dot{w}$ is given by the following state-space representation:

$$
\begin{aligned}
\dot{\bar{x}} &= \tilde{A}\bar{x} + \tilde{B}\zeta,\\
\dot{w} &= \tilde{C}\bar{x}
\end{aligned}
\tag{8.3}
$$

where

$$
\tilde{A} = \begin{bmatrix}
0 & 0 & 0 & 1 & -1 & 0\\
0 & 0 & 0 & 0 & 1 & -1\\
0 & 0 & 0 & 0 & 0 & 1\\
-\dfrac{k_c}{m_c} & 0 & 0 & -\dfrac{c_c}{m_c} & \dfrac{c_c}{m_c} & 0\\
\dfrac{k_c}{m_s} & -\dfrac{k_s}{m_s} & 0 & \dfrac{c_c}{m_s} & -\dfrac{c_c + c_s}{m_s} & \dfrac{c_s}{m_s}\\
0 & \dfrac{k_s}{m_u} & -\dfrac{k_T}{m_u} & 0 & \dfrac{c_s}{m_u} & -\dfrac{c_s}{m_u}
\end{bmatrix},\ \tilde{B} = -\begin{bmatrix} 0\\0\\1\\0\\0\\0 \end{bmatrix},
$$

$$
\tilde{C} = \begin{bmatrix} 0 & 0 & 0 & 0 & 1 & 0 \end{bmatrix}.
$$

As in Section 6.2 (see Eq. (6.20)) we will assume that the derivative of the road roughness *i.e.*, ζ is a random variable $\mu\sqrt{v}\eta(t)$ where v is the vehicle's forward velocity, μ is the road roughness coefficient, and $\eta(t)$ is unit intensity white-noise process. In this study, v and μ were fixed as $v = 20$ ms^{-1} and $\mu = 0.0027$. Thus, the covariance function of ζ denoted by R_ζ satisfies

$$R_\zeta(\tau) = \mu^2 v\delta(\tau). \tag{8.4}$$

The power spectral density of w is computed from Eqs. (8.3) and (8.4) as

$$S_w(\omega) = \mu^2 v\,|\omega^{-1}\tilde{C}(j\omega I_6 - \tilde{A})^{-1}\tilde{B}|^2. \tag{8.5}$$

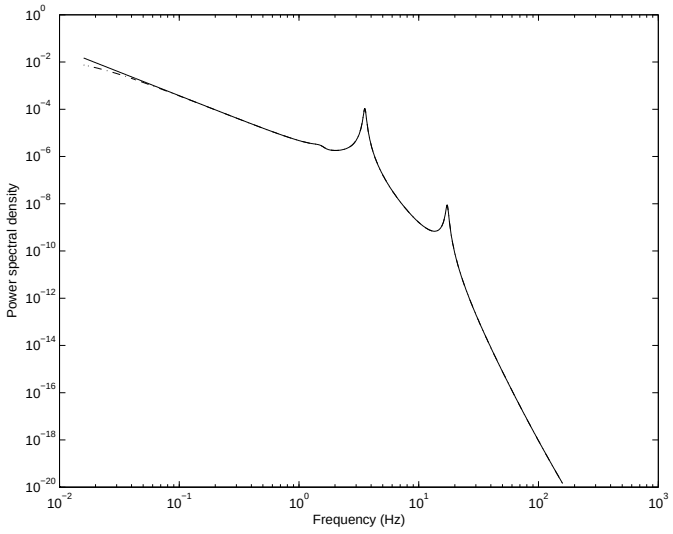

Figure 8.3: Power spectral densities of the sprung mass displacement for a white-noise velocity road input $\zeta(t) = \mu\sqrt{v}\eta(t)$ and its approximation by $\mu^2 v|H_\lambda(j\omega)|^2$ defined in(8.6) for $\lambda = 0.1$.

Let λ be a positive number and consider the system given by the transfer function

$$H_\lambda(s) = \frac{1}{s+\lambda}\,\tilde{C}(sI_6 - \tilde{A})^{-1}\tilde{B}. \tag{8.6}$$

As $\lambda \to 0$, the output power spectral density of this system driven by $\zeta(t)$ approaches to the spectral density in Eq. (8.5). In fact, from Figure 8.3 this approximation is seen to be very accurate for all $|\omega| \geq 0.02$ Hz and $\lambda \leq 0.1$. Henceforth, we fix λ as $\lambda = 0.1$.

Now, let the quadruplet $(\hat{A}_w, \hat{B}_w, \hat{C}_w, 0)$ denote a state-space realization of $H_{0.1}(s)$. Observe that $(\hat{A}_w, \hat{B}_w, \hat{C}_w, 0)$ has a zero at $s = \infty$ with multiplicity at least two as required. Finally, the shape-filter parameters in Eq. (8.1) are obtained by setting

$$A_w = I_4 \otimes \hat{A}_w, \quad B_w = I_4 \otimes \hat{B}_w, \quad C_w = I_4 \otimes \hat{C}_w.$$

This choice presumes that the displacements at the chassis points $\mathrm{A}', \mathrm{B}', \mathrm{C}', \mathrm{D}'$ are uncorrelated and have identical second-order statistics. This assumption is hardly justifiable; however, guarantees simultaneous excitation of the heave, the pitch, and the roll motions of the truck cabin as demonstrated in the controller design example of the next section. It is worth mentioning that the parameter values in Tables 8.1 and 8.2 have been obtained by approximating true values and linearizing the spring and the damper nonlinearities.

8.3 Active Suspension Design for the Truck Cabin

Recall the model derived in Section 8.1:

$$\begin{aligned} \dot{\widetilde{x}} &= A\widetilde{x} + B_1\nu + B_2u \\ y &= C_2\widetilde{x} + D_{22}u + \xi \end{aligned} \tag{8.7}$$

where ξ is an artificially introduced sensor noise with a covariance εI_8. Here, ε is a small positive number to be used as a design variable, say 10^{-5}. The separation principle of the linear-quadratic-design methodology will be used. More precisely, assume the following covariance structure:

$$\mathrm{E}\left(\nu\nu^T\right) = I_4, \qquad \mathrm{E}\left(\nu\xi^T\right) = 0_{4\times 8}, \qquad \mathrm{E}\left(\xi\xi^T\right) = \varepsilon I_8$$

on the stochastic processes $\nu(t)$ and $\xi(t)$. The filter gain K_f is computed by the `lqew` command in MATLAB. Thus, the state estimator has the form:

$$\dot{\hat{x}} = A\hat{x} + B_2u + K_f(y - C_2\hat{x} - D_{22}u). \tag{8.8}$$

The feedback gain K_r is computed by solving the linear-quadratic regulator problem:

$$\min J \qquad \text{subject to} \qquad J = \int (\ddot{x}_S^T Q \ddot{x}_S + u^T R u)\, \mathrm{d}t$$

where Q is a diagonal matrix and $R = \rho I_4$ with $\rho > 0$. In the simulation, $\rho = 10^{-3}$ was picked and the entries of Q were chosen as the inverses of the covariances $\mathrm{E}(\ddot{z_G})^2$, $\mathrm{E}(\ddot{\theta})^2$, and $\mathrm{E}(\ddot{\phi})^2$. Finally, u is given by

$$u = -K_r \hat{x}. \tag{8.9}$$

8.3.1 The Closed-Loop Performance

The closed-loop state-space equations can be calculated from Eqs. (8.7), (8.8), and (8.9) by letting $\xi = 0$ in (8.7) as follows

$$\begin{bmatrix} \dot{\widetilde{x}} \\ \dot{\hat{x}} \end{bmatrix} = \begin{bmatrix} A & -B_2 K_r \\ K_f C_2 & A - B_2 K_r - K_f C_2 \end{bmatrix} \begin{bmatrix} \widetilde{x} \\ \hat{x} \end{bmatrix} + \begin{bmatrix} B_1 \\ 0_{34\times 4} \end{bmatrix} \nu$$

$$\begin{bmatrix} \ddot{x}_S \\ u \end{bmatrix} = - \begin{bmatrix} M^{-1}[KS & CS & -(KC_w + CC_w A_w) & WK_r] \\ 0_{4\times 34} & K_r & & \end{bmatrix} \begin{bmatrix} \widetilde{x} \\ \hat{x} \end{bmatrix}.$$

For ν satisfying Eq. (8.4), the rms heave, pitch, and roll accelerations were computed respectively as 0.710, 0.595, and 1.339 for the passively suspended cabin and 0.519, 0.455, and 0.842 for the actively suspended cabin. The performance improvements are then by 27%, 23.5%, 37%, respectively for the rms heave, pitch, and roll accelerations. The rms values of u_A, u_B, u_C, u_D computed as 113.2, 113.2, 82.5, and 82.5, respectively, show that actuator saturations are not likely to occur.

The frequency response magnitudes of the truck cabin to the warp input $\nu = e^{j\omega t}[1\ 0\ 0\ -1]^T$ shown in Figures 8.4–8.6 clearly indicate that cabin vibrations due to the road unevenness are effectively suppressed by the controlled secondary suspension. Observe that the frequency response magnitudes do not change at the heave and the wheel-hop natural frequencies of the truck bounce model. This is not unexpected since these modes can not

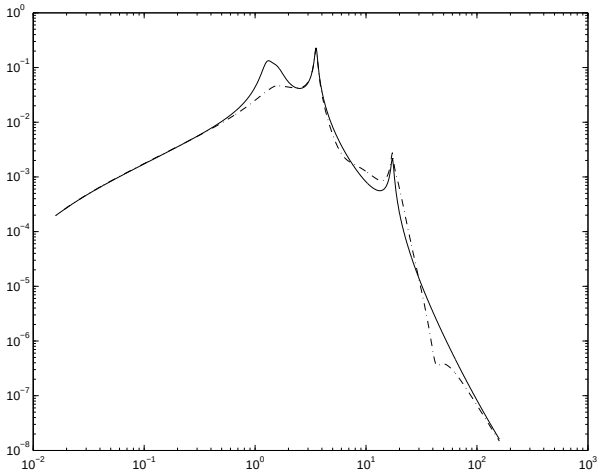

Figure 8.4: The heave acceleration frequency response magnitude of the cabin for the warp input $\nu = e^{j\omega t}\,[1\ 0\ 0\ -1]^T$: (–) passive suspension,(-.) active suspension.

be controlled by the actuators in the secondary suspension system. Moreover, the secondary suspension has little influence on the primary suspension as indicated by a hardly visible peak at 1.6 Hz in Figure 8.3, which is roughly the heave natural frequency of the cabin. In passing, it should be mentioned that this active suspension system has been designed for a truck without payload which is the most critical situation for ride comfort.

8.4 Summary

In this chapter, a three-degrees-of- freedom cabin ride model of a commercial truck was developed for an active/semi-active suspension application. The control design methodology based on this model is particularly simple in that it relies on the accelerometer readings and the suspension travel measurements of the cabin. An analytical model relating random excitations at the wheels to the accelerometer readings of the chassis at the cabin suspension attachment points can be obtained by using either well-established spectral estimation methods or a simplified bounce model of the truck derived from

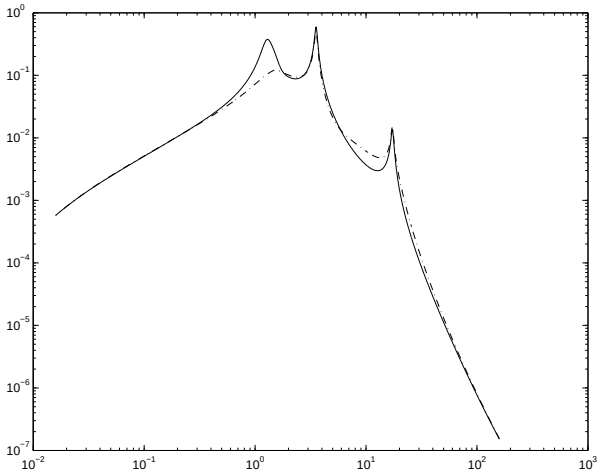

Figure 8.5: The pitch acceleration frequency response magnitude of the cabin for the warp input $\nu = e^{j\omega t}\,[1\ 0\ 0\ -1]^T$: (–) passive suspension, (-.) active suspension.

first principles with certain assumptions on the road profile. The latter route was pursued in this chapter though the former was easy to implement since it yields results which are irrespective of the complicacies of the primary suspension system and the road profile. For a commonly used road model in vehicle dynamics literature, an active cabin suspension system was designed using the LQG design methodology. The results demonstrate that the cabin vibrations can effectively be suppressed. Experimental verification of the derived results on full truck models and real trucks remains future work.

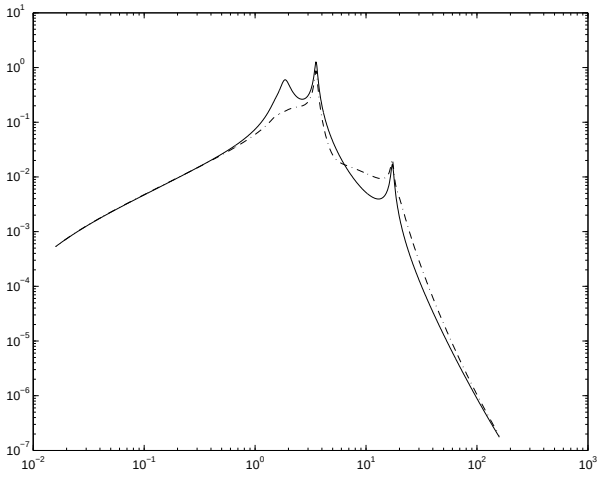

Figure 8.6: The roll acceleration frequency response magnitude of the cabin for the warp input $\nu = e^{j\omega t}\,[1\ 0\ 0\ -1]^T$: (–) passive suspension, (-.) active suspension.

9 CONCLUDING REMARKS

9.1 Contributions

The contributions of this thesis are as follows:

- A strongly consistent subspace algorithm to identify discrete-time, linear time invariant systems from nonuniformly spaced power spectrum measurements was presented. This algorithm was illustrated with one practical example that solves a stochastic road modeling problem. A byproduct subspace algorithm to construct analytic functions from evaluations of their real or imaginary parts on finite subsets of the unit circle was developed.

- A connection between the proposed subspace identification algorithm and the Lagrange–Sylvester rational interpolation method was established.

- Constraints and trade-offs at certain frequencies of closed-loop frequency responses of quarter-car suspension models were derived. These constraints and trade-offs complement the existing results in the literature. The influence of tire damping on the achievable quarter-car active suspension performance was analyzed in detail. A numerical example utilizing rational interpolation in the active suspension design was provided.

- The rms and the rms gain constraints for the quarter, half, and full-car suspension models were studied in the $\mathcal{H}_2$-optimal and multi–objective control frameworks. For the quarter and half-car models, the dependance of closed-loop rms responses on the tire damping was investigated. The multi-objective control problem was first formulated as a convex mixed $\mathcal{H}_2/\mathcal{H}_\infty$ synthesis problem for the quarter, half, and full-car models and solved by using LMIs. The LMI paradigm necessarily yields controllers

with complexity equal to plant complexity. Next, multi-objective suspension control problem was re-formulated as a non-convex and non-smooth optimization problem for the quarter and full-car models. This problem was solved by using the HIFOO toolbox. In the latter problem formulation, the designer is free to choose controller complexity. Best performance enhancements were obtained with simplest HIFOO controllers, showing that there is still room for the application of new techniques to linear suspension control problems. Lastly, for the quarter and half-car models the assumption that tire damping coefficient is exactly known was relaxed and robust controllers to cope with polytopic tire damping uncertainties were designed.

- In a case study for half-car models, we have observed that active suspension performance depends also on the correlation structure between the wheels. An explanation is that the body pitch by coupling vertical motions doesn't allow decomposition of half-car model into two independent quarter-car models. This observation holds also for the full-car models which in the literature have been suggested to be decomposed into the heave, the pitch, and the roll components for the vehicle body and additional warp for the wheels in contact with the road. We demonstrated that multi-objective control methods can be applied to such large-scale problems without relying on motion decoupling schemes.

- A three–degree–of–freedom cabin ride model for a commercial truck was derived and an active cabin suspension system was designed by using the LQG method and a simplified truck bounce model. The preliminary results showed that cabin vibrations can effectively be suppressed by the actively controlled suspension. The multi-objective control methods studied in this thesis can equivalently be applied to this design problem.

9.2 Recommendations for Further Research

The following topics need further attention:

- Our study of constraints on the achievable performance of controlled vehicle suspensions is complete as far as the quarter-car model is concerned. An essential tool in this study was the use of Youla factorization. For more complicated vehicle models, *i.e*, half and full-car models the development of effective tools remains an open problem.

- The conclusions drawn on the design trade-offs were based on numerical studies only for all car models. Unlike pointwise constraints derived for the quarter-car model, closed-form expressions for the rms and/or the rms gain performance limits were not derived for any of the vehicle models. This subject warrants future work.

- We have not addressed the issues of sensitivity, robustness, suspension nonlinearities (except for tire uncertainty), parameter variations, and unmodelled dynamics in our studies. In realistic designs they have to be taken into account.

- Although tire damping might be diffucult to estimate and too small to consider its effect in a design process, it should be included at the validation stage to improve overall simulation accuracy.

- The preliminary design results obtained with the optimization algorithms in the HIFOO toolbox are encouraging. Further numerical experiments are necessary to confirm the good performance of non-convex and non-smooth optimization techniques.

- Our results on the control of a cabin model for a commercial truck are preliminary. Multi-objective control methods, *i.e*, mixed $\mathcal{H}_2/\mathcal{H}_\infty$ synthesis and the optimization algorithms in the HIFOO toolbox could be used to design realistic active suspension systems for truck cabins.

- The systems considered in this thesis are assumed to be "fully-active". The practical realization details for the controlled actuations and the associated energy requirements should be considered.

APPENDIX A

A.1 Proof of Lemma 2.2.1

Equation (2.22) implies that

$$\begin{aligned} X_{\mathrm{C}}^{\mathrm{c}}(\theta) &= (e^{j\theta} I_n - A)^{-1} F \\ X_{\mathrm{C}}^{\mathrm{ac},p}(\theta) &= e^{j(p-1)\theta}(e^{-j\theta} I_n - A^T)^{-1} C^T. \end{aligned}$$

The matrix $\begin{bmatrix} \mathcal{W}_{\mathrm{C}} \\ \mathcal{X}_{\mathrm{C}} \end{bmatrix}$ is rank deficient if and only if there exists a row vector

$$[\alpha_1 \ \cdots \ \alpha_p \ \ \beta \ \ \gamma] \neq 0 \tag{A.1}$$

with $\alpha_k^T \in \mathbf{R}^m$, $k = 1, \cdots, p$ and $\beta^T, \gamma^T \in \mathbf{R}^n$ such that

$$[\alpha_1 \ \cdots \ \alpha_p \ \ \beta \ \ \gamma] \begin{bmatrix} \mathcal{W}_{\mathrm{C}} \\ \mathcal{X}_{\mathrm{C}} \end{bmatrix} = 0$$

$$\Longleftrightarrow$$

$$\mathcal{J}(z_k) = 0, \quad k = 1, \cdots, N \tag{A.2}$$

where

$$\begin{aligned} \mathcal{J}(z) &= \sum_{k=1}^{p} \alpha_k z^{k-1} + \gamma z^p (I_n - zA^T)^{-1} C^T \\ &\quad + \beta (zI_n - A)^{-1} F. \end{aligned} \tag{A.3}$$

Since $\mathcal{J}(z)$ is a real-rational matrix, z_k is a zero of it if and only if z_k^* is a zero of it. Thus, each element of $\mathcal{J}(z)$ has at least $2N - 2$ zeros whenever (A.2) holds. (If $z_k \notin \mathbf{R}$ for all k, then the number of zeros is precisely $2N$).

Let $\rho(A)$ be the spectral radius of A, *i.e.,* the largest of the magnitudes of the eigenvalues of A. The Laurent series of $\mathcal{J}(z)$ converges in the annulus:

$$\mathbf{D}_A=\{z \in \mathbf{C} : \rho(A) < |z| < [\rho(A)]^{-1}\}. \tag{A.4}$$

Each element in the rational vector $\mathcal{J}(z)$ is either identically zero or has at least $2N-2$ zeros at $e^{\pm j\theta_k}$; but each element of $\mathcal{J}(z)$ can have at most $p+2n-1$ zeros. Since $2N \geq p+2n+2$, we then have $\mathcal{J}(z) \equiv 0$. This implies that all the coefficients in the Laurent expansion of $\mathcal{J}(z)$ are zero. Since the Laurent series of $\gamma z^p(I_n - zA^T)^{-1}C^T$ starts with $\gamma C^T z^p$ and converges in the disk

$$\mathbf{D}_\rho=\{z \in \mathbf{C} : \ |z| < [\rho(A)]^{-1}\}, \tag{A.5}$$

the three terms on the right hand side of (A.3) are independent; and therefore they are identically zero. Hence,

$$\alpha_k = 0, \quad k = 1, \cdots, p;$$

$$\gamma(z^{-1}I_n - A^T)^{-1}C^T \equiv 0;$$

$$\beta(zI_n - A)^{-1}F \equiv 0.$$

The minimality of (A, B, C, D) implies the minimality of $(A, F, C, \frac{1}{2}E)$. Thus, from the controllability of the pairs (A, F) and (A^T, C^T) we have $\beta = \gamma = 0$. Hence, (A.1) is violated. Finally, note that $\begin{bmatrix} \mathcal{W}_{\mathrm{C}} \\ \mathcal{X}_{\mathrm{C}} \end{bmatrix}$ is rank deficient if and only $\begin{bmatrix} \mathcal{W} \\ \mathcal{X} \end{bmatrix}$ is rank deficient. The last assertion is due to the fact that for any complex matrix Z,

$$x^T Z = 0 \Longleftrightarrow x\,[\mathrm{Re}\, Z \ \ \mathrm{Im}\, Z] = 0.$$

A.2 Proof of Lemma 2.2.3

The first two claims are obvious. From (2.67),

$$A''T^{-1} = T^{-1}A', \qquad A''\Pi = \Pi A'. \tag{A.6}$$

Now, partition T^{-1} and Π as

$$T^{-1} = [t_1 \ \cdots \ t_{2n}], \qquad \Pi = [\pi_1 \ \cdots \ \pi_{2n}].$$

If $n_i = 1$, put $l = n_1 + \cdots + n_i$. Then, from (2.67)

$$A''t_l = \mu_i t_l, \qquad A''\pi_l = \mu_i \pi_l$$

which shows that t_l is an eigenvector of Σ_c associated with the eigenvalue μ_i. Thus, for some $\Lambda_{n_i} \in \mathbf{R}$

$$\pi_l = \Lambda_{n_i} t_l.$$

This equality is due to the fact that eigenvectors corresponding to a simple real eigenvalue span a one dimensional subspace of $\mathbf{R}^n$. If $n_i = 2$, again putting $l = n_1 + \cdots + n_i$, from (2.67) we get

$$\begin{aligned} A''[t_l \ t_{l+1}] &= [t_l \ t_{l+1}]\Sigma_i, \\ A''[\pi_l \ \pi_{l+1}] &= [\pi_l \ \pi_{l+1}]\Sigma_i \end{aligned}$$

which shows that t_l and t_{l+1} are eigenvectors of Σ_c associated with the eigenvalues $\mu_i \pm j\nu_i$. It is known that eigenvectors corresponding to a pair of simple complex eigenvalues form a two dimensional subspace of $\mathbf{R}^n$. Hence, for some $\beta \in \mathbf{R}^{2\times 2}$

$$\begin{aligned} \pi_l &= \beta_{11} t_l + \beta_{12} t_{l+1} \\ \pi_{l+1} &= \beta_{21} t_l + \beta_{22} t_{l+1}. \end{aligned} \tag{A.7}$$

Multiplying both sides of the first equation in (A.7) with A'' and using the equations in (A.7), we get

$$(\beta_{12} + \beta_{21})\nu_i t_l + (\beta_{22} - \beta_{11})\nu_i t_{l+1} = 0.$$

Since $\nu_i \neq 0$ and t_l and t_{l+1} are linearly independent vectors, we then must have

$$\beta_{11} = \beta_{22}, \qquad \beta_{21} = -\beta_{12}.$$

It follows that

$$[\pi_l \ \pi_{l+1}] = \Lambda_i [t_l \ t_{l+1}]$$

where

$$\Lambda_i = \begin{bmatrix} \beta_{11} & \beta_{12} \\ -\beta_{12} & \beta_{11} \end{bmatrix}.$$

Let

$$\Lambda_{\mathrm{c}} = \begin{bmatrix} \Lambda_1 & 0 & \cdots & 0 \\ 0 & \Lambda_2 & \cdots & 0 \\ \vdots & \vdots & \ddots & \vdots \\ 0 & 0 & \cdots & \Lambda_k \end{bmatrix}.$$

Then, Λ_{c} is compatible with Σ_{c} and

$$[\pi_1 \ \cdots \ \pi_n] = \Lambda_{\mathrm{c}} [t_1 \ \cdots \ t_n]. \tag{A.8}$$

Likewise, for some Λ_{ac} compatible with Σ_{ac} we get

$$[\pi_{n+1} \ \cdots \ \pi_{2n}] = \Lambda_{\mathrm{ac}} [t_{n+1} \ \cdots \ t_{2n}]. \tag{A.9}$$

Since Σ_{ac} is compatible with Σ_{c}, Λ_{ac} is compatible with Σ_{c}. Thus, combining (A.8) and (A.9), we get (2.70). The last claims are easy to verify.

A.3 Proof of Theorem 2.2.3

Let

$$\widetilde{\mathcal{S}}_N(z) = \widehat{\chi}(z)\, \check{F} + \check{F}^T\, \widehat{\chi}^T(z^{-1}) + \check{E}.$$

The least-squares problem (2.92) can be written as

$$\widehat{E}, \widehat{F} = \arg\min_{\check{E},\check{F}} (\widehat{Q}_N - \widehat{T}_N + D_N) \tag{A.10}$$

where

$$\begin{aligned} \widehat{Q}_N &= \frac{1}{N} \sum_{k=1}^{N} \|\mathcal{R}_k^{-\frac{1}{2}} \widetilde{\mathcal{S}}_N(z_k)\|_F^2, \\ \widehat{T}_N &= \frac{1}{N} \sum_{k=1}^{N} \mathrm{Tr}\{S_k^H \mathcal{R}_k^{-1} \widetilde{\mathcal{S}}_N(z_k) + \widetilde{\mathcal{S}}_N^H(z_k) \mathcal{R}_k^{-1} S_k\}, \\ D_N &= \frac{1}{N} \sum_{k=1}^{N} \|\mathcal{R}_k^{-1/2} S_k\|_F^2. \end{aligned}$$

In the derivation of (A.10), we have used the facts that $\mathrm{Tr}(AB) = \mathrm{Tr}(BA)$ and $\mathrm{Tr}(A) = \mathrm{Tr}(A^T)$ for any matrices A and B of compatible sizes. The boundedness of fourth order moments means the boundedness of second order moments. More precisely, $\mathrm{E}\|\eta_k\|_F^2 \leq [\mathrm{E}\|\eta_k\|_F^4]^{\frac{1}{2}}$. Hence from (2.11) and the chain of (in)equalities

$$\begin{aligned}[\sigma_{\max}^{\frac{1}{2}}(\mathcal{R}_k)]^2 &= \sigma_{\max}^2(\mathcal{R}_k^{\frac{1}{2}}) \\ &\leq \|\mathcal{R}_k^{\frac{1}{2}}\|_F^2 = \mathrm{Tr}(\mathcal{R}_k) = \mathrm{E}\|\eta_k\|_F^2,\end{aligned}$$

we get $\sigma_{\max}(\mathcal{R}_k) \leq M_\eta^{\frac{1}{2}}$. Let $\sigma_{\min}$ denote the smallest singular value. The inequality $\|XY\|_F \geq \sigma_{\min}(X)\,\|Y\|_F$ valid for any matrices of X and Y of compatible sizes then yields

$$\widehat{Q}_N \geq \frac{1}{M_\eta^{\frac{1}{2}} N} \sum_{k=1}^{N} \|\widetilde{\mathcal{S}}_N(z_k)\|_F^2. \tag{A.11}$$

From (2.91), we have for each $\check{E}$ and $\check{F}$

$$\lim_{N\to\infty} \|\widetilde{\mathcal{S}}_N - \check{S}\|_\infty = 0, \qquad \text{w.p.1} \tag{A.12}$$

where

$$\check{S}(z) = \chi(z)\,\check{F} + \check{F}^T\,\chi^T(z^{-1}) + \check{E}. \tag{A.13}$$

Hence,

$$\lim_{N\to\infty} \inf \widehat{Q}_N \geq M_\eta^{-\frac{1}{2}} \lim_{N\to\infty} \inf \frac{1}{N} \sum_{k=1}^{N} \|\check{\mathcal{S}}(z_k)\|_F^2, \ \text{ w.p.1.}$$

We claim that if $\check{E}$ and $\check{F}$ is a nontrivial pair, then $\check{S}(z)$ can vanish only at a finite number of points z_k. To establish this claim, suppose that

$$\check{S}(z_k) = 0, \qquad k = 1, \cdots, M.$$

Then, from $\check{S}(z_k^{-1}) = \check{S}^T(z_k)$ we see that these inequalities are also satisfied with z_k^{-1}, $k = 1, \cdots, M$. Thus, using the same argument in the proof of Lemma 2.2.1, if $2M-2 > 2n$ and the frequencies are distinct, we conclude that $\check{S}(z)$ is identically zero (since its each entry can have at most $2n$ zeros). Let $\mathbf{D}_A$ and $\mathbf{D}_\rho$ be as in (A.4) and (A.5), respectively. Then, all the coefficients in the Laurent expansion of $\check{\mathcal{S}}(z)$, which converges in $\mathbf{D}_A$, are zero. The Laurent

series of $\check{F}^T\,\chi^T(z^{-1})$ starts with $z\check{F}^T[J_{\rm f}\mathcal{K}U_{2n}\Pi_{\rm c}]^T$ and converges in the disk $\mathbf{D}_\rho$. Therefore, the three terms on the right hand side of (A.13) are independent; and thus they are identically zero. Hence,

$$\check{E}=0, \qquad \check{F}^T\,(z^{-1}I_n-\Sigma_{\rm c}^T)^{-1}\Lambda_{\rm c}^TC^T\equiv 0. \tag{A.14}$$

Let $x\in\mathbf{R}^m$ be such that $\check{F}x{=}\beta\neq 0$. This is possible since $\check{E}=0$ implies $\check{F}\neq 0$. Then, from the second equation in (A.14) we have

$$\beta^T\,(z^{-1}I_n-\Sigma_{\rm c}^T)^{-1}\Lambda_{\rm c}^TC^T\equiv 0$$

which means that $(\Sigma_{\rm c}^T,\Lambda_{\rm c}^TC^T)$ is not a controllable pair. Since $\Lambda_{\rm c}$ is nonsingular, this means (A^T,C^T) is not controllable, *i.e.,* (A,C) is not observable. Thus, we reach a contradiction and $\check{S}(z)$ is nonzero in the complement of at most $2n$ points. Since $\|\check{S}(z)\|_F^2$ is uniformly continuous on the unit circle, a standard compactness argument then yields

$$\|\check{S}(e^{j\theta})\|_F^2\geq\gamma, \qquad \theta\in\cup_{i=1}^r[a_i,b_i]$$

for some $\gamma>0$ and disjoint intervals $[a_i,b_i]\subseteq[0,2\pi]$ satisfying $\sum_{i=1}^r(b_i-a_i)>\pi$. Thus, from (2.12) we obtain for all sufficiently large N

$$\frac{1}{N}\sum_{k=1}^N\|\check{\mathcal{S}}(z_k)\|_F^2\geq\delta\gamma\pi.$$

We have shown that

$$(\check{E},\check{F})\neq 0\Longleftrightarrow\lim_{N\to\infty}\inf\widehat{Q}_N>0,\ \text{ w.p.1.} \tag{A.15}$$

Let

$$\check{\Gamma}{=}\left[\begin{array}{c}\mathrm{vec}(\check{E})\\ \mathrm{vec}(\check{F})\end{array}\right].$$

For eack k, we can write $\mathrm{vec}(\widetilde{\mathcal{S}}_N(z_k))$ and $\mathrm{vec}(\check{\mathcal{S}}_N(z_k))$ as linear functions in $\check{\Gamma}$:

$$\widetilde{\mathcal{A}}_{N,k}\,\check{\Gamma}=\mathrm{vec}(\widetilde{\mathcal{S}}_N(z_k)),\quad \check{\mathcal{A}}_{N,k}\,\check{\Gamma}=\mathrm{vec}(\check{\mathcal{S}}_N(z_k)). \tag{A.16}$$

for some matrices $\widetilde{\mathcal{A}}_{N,k}$ and $\check{\mathcal{A}}_{N,k}$. To be specific on this, let $\widehat{\chi}_i(z_k)$ and $\chi_i(z_k)$ denote the ith rows of $\widehat{\chi}$ and $\chi(z_k)$, respectively. Let for each k,

$$\widetilde{\mathcal{B}}_{N,k} = \begin{bmatrix} e_1^T \otimes \widehat{\chi}(z_k) + I_m \otimes \widehat{\chi}_1^*(z_k) \\ \vdots \\ e_m^T \otimes \widehat{\chi}(z_k) + I_m \otimes \widehat{\chi}_m^*(z_k) \end{bmatrix},$$

$$\check{\mathcal{B}}_{N,k} = \begin{bmatrix} e_1^T \otimes \chi(z_k) + I_m \otimes \chi_1^*(z_k) \\ \vdots \\ e_m^T \otimes \chi(z_k) + I_m \otimes \chi_m^*(z_k) \end{bmatrix}.$$

Then,

$$\widetilde{\mathcal{A}}_{N,k}=\begin{bmatrix} I_{m^2} & 0 \\ 0 & \widetilde{\mathcal{B}}_{N,k} \end{bmatrix}, \qquad \check{\mathcal{A}}_{N,k}=\begin{bmatrix} I_{m^2} & 0 \\ 0 & \check{\mathcal{B}}_{N,k} \end{bmatrix}.$$

Hence,

$$\widehat{Q}_N = \frac{1}{N}\sum_{k=1}^{N} \|(I_m \otimes \mathcal{R}_k^{-\frac{1}{2}})\mathrm{vec}(\widetilde{\mathcal{S}}_N(z_k))\|_F^2 = \check{\Gamma}^T \widehat{\Xi}_N \check{\Gamma}$$

where

$$\widehat{\Xi}_N=\frac{1}{N}\sum_{k=1}^{N} \widetilde{\mathcal{A}}_{N,k}^H (I_m \otimes \mathcal{R}_k^{-1})\widetilde{\mathcal{A}}_{N,k}.$$

From (A.15), note that $\widehat{\Xi}_N$ is positive definite for all large N w.p.1. Likewise, we can write $\widehat{T}_N$ as

$$\widehat{T}_N = \Upsilon_N \check{\Gamma}$$

where

$$\begin{aligned} \Upsilon_N &= \frac{1}{N}\sum_{k=1}^{N} [\mathrm{vec}(S_k^*)]^T (I_m \otimes \mathcal{R}_k^{-1})\widetilde{\mathcal{A}}_{N,k} \\ &\quad + \frac{1}{N}\sum_{k=1}^{N} [\mathrm{vec}(S_k)]^T (I_m \otimes \mathcal{R}_k^{-1})\widetilde{\mathcal{A}}_{N,k}^*. \end{aligned}$$

Let $\widehat{\Gamma}_N$ denote the least-squares solution of (2.92) in stacked form:

$$\widehat{\Gamma}_N=\begin{bmatrix} \mathrm{vec}(\widehat{E}_N) \\ \mathrm{vec}(\widehat{F}_N) \end{bmatrix}.$$

Then,

$$\widehat{\Gamma}_N = \mathrm{Re}\{\widehat{\Xi}_N^{-1}\}\frac{1}{N}\sum_{k=1}^{N}\mathrm{Re}\{\widetilde{\mathcal{A}}_{N,k}^H(I_m\otimes\mathcal{R}_k^{-1})\mathrm{vec}(S_k)\}.$$

Split $\widehat{\Gamma}_N$ as

$$\widehat{\Gamma}_N = \bar{\Gamma}_N + \widetilde{\Gamma}_N$$

where

$$\begin{aligned}\bar{\Gamma}_N &= \mathrm{Re}\{\widehat{\Xi}_N^{-1}\}\frac{1}{N}\sum_{k=1}^{N}\mathrm{Re}\{\widetilde{\mathcal{A}}_{N,k}^H(I_m\otimes\mathcal{R}_k^{-1})\mathrm{vec}(S(z_k))\};\\ \widetilde{\Gamma}_N &= \mathrm{Re}\{\widehat{\Xi}_N^{-1}\}\frac{1}{N}\sum_{k=1}^{N}\mathrm{Re}\{\widetilde{\mathcal{A}}_{N,k}^H(I_m\otimes\mathcal{R}_k^{-1})\mathrm{vec}(\eta_k)\}.\end{aligned}$$

Let Γ denote the unknowns in stacked form:

$$\Gamma = \begin{bmatrix}\mathrm{vec}(E)\\ \mathrm{vec}(F)\end{bmatrix}.$$

Observe that if $N \geq (p/2)+n+1$ and $\eta_k = 0$ for all k, then $\widehat{\chi}(z) = \chi(z)$ for all z and from (A.16)we have

$$\mathrm{vec}(S(z_k)) = \check{\mathcal{A}}_{N,k}\,\Gamma = \widetilde{\mathcal{A}}_{N,k}\,\Gamma, \qquad \text{for all } k.$$

Hence,

$$\begin{aligned}\widehat{\Gamma}_N &= \mathrm{Re}\{\widehat{\Xi}_N^{-1}\}\frac{1}{N}\sum_{k=1}^{N}\mathrm{Re}\,\{\widetilde{\mathcal{A}}_{N,k}^H(I_m\otimes\mathcal{R}_k^{-1})\widetilde{\mathcal{A}}_{N,k}\,\Gamma\}\\ &= \mathrm{Re}\{\widehat{\Xi}_N^{-1}\}\mathrm{Re}\,\{\widehat{\Xi}_N\}\,\Gamma = \Gamma.\end{aligned}$$

This proves Lemma 2.2.4.

Now, from (2.91) we have uniformly in k

$$\lim_{N\to\infty}\|\widetilde{\mathcal{A}}_{N,k} - \check{\mathcal{A}}_{N,k}\|_F, \qquad \text{w.p.1.} \tag{A.17}$$

Recall that $\widehat{\Xi}_N^{-1}$ is bounded away from zero w.p.1 for all large N; and $\widetilde{\mathcal{A}}_{N,k}$ is also uniformly bounded in k w.p.1 for all large N. Thus, the following series

$$\begin{aligned}\bar{\Gamma}_N &= \Gamma + \mathrm{Re}\{\widehat{\Xi}_N^{-1}\}\frac{1}{N}\sum_{k=1}^{N}\mathrm{Re}\,\{\widetilde{\mathcal{A}}_{N,k}^H(I_m\otimes\mathcal{R}_k^{-1})\\ &\qquad\cdot(\widetilde{\mathcal{A}}_{N,k} - \check{\mathcal{A}}_{N,k})\}\Gamma\end{aligned}$$

converges w.p.1 to Γ as N tends to infinity.

Finally, we study the noise term $\widetilde{\Gamma}_N$. Let

$$\begin{aligned} c_{N,k} &= \mathrm{Re}\{\widehat{\Xi}_N^{-1}\}\mathrm{Re}\,\{\widetilde{\mathcal{A}}_{N,k}^H(I_m \otimes \mathcal{R}_k^{-1})\}, \\ d_{N,k} &= \mathrm{Re}\{\widehat{\Xi}_N^{-1}\}\mathrm{Im}\,\{\widetilde{\mathcal{A}}_{N,k}^H(I_m \otimes \mathcal{R}_k^{-1})\}, \\ \xi_k &= \mathrm{vec}(\mathrm{Re}(\eta_k)), \\ \zeta_k &= \mathrm{vec}(\mathrm{Im}(\eta_k)). \end{aligned}$$

Then, we can write $\widetilde{\Gamma}_N$ as

$$\widetilde{\Gamma}_N = \frac{1}{N}\sum_{k=1}^{N} c_{N,k}\xi_k + \frac{1}{N}\sum_{k=1}^{N} d_{N,k}\zeta_k.$$

Let us assume for a moment that $c_{N,k}$ and $d_{N,k}$ are bounded sequences of deterministic matrices denoted by $\bar{c}_{N,k}$ and $\bar{d}_{N,k}$. Then, $\bar{c}_{N,k}\xi_k$ and $\bar{d}_{N,k}\zeta_k$ are sequences of independent zero mean random variables with uniformly bounded fourth order moments. Thus, from the strong law of large numbers [142] each series above tends to zero w.p.1 as N tends to infinity. Now, let

$$\check{\Xi}_N = \frac{1}{N}\sum_{k=1}^{N} \check{\mathcal{A}}_{N,k}^H(I_m \otimes \mathcal{R}_k^{-1})\check{\mathcal{A}}_{N,k}$$

and

$$\begin{aligned} \bar{c}_{N,k} &= \mathrm{Re}\{\widehat{\Xi}_N^{-1}\}\mathrm{Re}\,\{\check{\mathcal{A}}_{N,k}^T(I_m \otimes \mathcal{R}_k^{-1})\}; \\ \bar{d}_{N,k} &= \mathrm{Re}\{\widehat{\Xi}_N^{-1}\}\mathrm{Im}\,\{\check{\mathcal{A}}_{N,k}^T(I_m \otimes \mathcal{R}_k^{-1})\}. \end{aligned}$$

From (A.17),

$$\lim_{N\to\infty} \|\widehat{\Xi}_N - \check{\Xi}_N\|_F, \qquad \text{w.p.1;}$$

and thus

$$\begin{aligned} \lim_{N\to\infty} \|c_N - \bar{c}_N\|_\infty &= 0, \qquad \text{w.p.1;} \\ \lim_{N\to\infty} \|d_N - \bar{d}_N\|_\infty &= 0, \qquad \text{w.p.1} \end{aligned} \tag{A.18}$$

where $\|c_N\|_\infty = \sup_{1\le k\le N} \sigma_{\max}(c_{N,k})$. The series

$$\widetilde{\vartheta}_N = \frac{1}{N}\sum_{k=1}^{N}(c_{N,k} - \bar{c}_{N,k})\xi_k - \frac{1}{N}\sum_{k=1}^{N}(d_{N,k} - \bar{d}_{N,k})\zeta_k$$

is dominated (absolutely) by the series

$$\|c_N - \bar{c}_N\|_\infty \frac{1}{N}\sum_{k=1}^{N}\|\xi_k\|_2 + \|d_N - \bar{d}_N\|_\infty \frac{1}{N}\sum_{k=1}^{N}\|\zeta_k\|_2$$

where $\|x\|_2$ is the Euclidean norm of $x \in \mathbf{R}^n$ defined by $\|x\|_2 = (\sum_{j=1}^{n}|x_j|^2)^{\frac{1}{2}}$. From the strong law of large numbers, we have

$$\lim_{N\to\infty}\left[\frac{1}{N}\sum_{k=1}^{N}\|\xi_k\|_2 - \frac{1}{N}\sum_{k=1}^{N}\mathrm{E}\,\|\xi_k\|_2\right] = 0, \qquad \text{w.p.1;}$$

$$\lim_{N\to\infty}\left[\frac{1}{N}\sum_{k=1}^{N}\|\zeta_k\|_2 - \frac{1}{N}\sum_{k=1}^{N}\mathrm{E}\,\|\zeta_k\|_2\right] = 0, \qquad \text{w.p.1.}$$

From (2.10), we have

$$\begin{aligned}\frac{1}{N}\sum_{k=1}^{N}\mathrm{E}\,\|\xi_k\|_2 &= \frac{1}{N}\sum_{k=1}^{N}\mathrm{E}\,\|\mathrm{Re}\,\eta_k\|_F = \frac{1}{2N}\sum_{k=1}^{N}\mathrm{Tr}(\mathcal{R}_k)\\ &\le \frac{m}{2N}\sum_{k=1}^{N}\sigma_{\max}(\mathcal{R}_k) \le \frac{m}{2}M_\eta^{\frac{1}{2}}.\end{aligned}$$

Thus,

$$\lim_{N\to\infty}\sup\frac{1}{N}\sum_{k=1}^{N}\|\xi_k\|_2 \le \frac{m}{2}M_\eta^{\frac{1}{2}}, \qquad \text{w.p.1.}$$

Likewise,

$$\lim_{N\to\infty}\sup\frac{1}{N}\sum_{k=1}^{N}\|\zeta_k\|_2 \le \frac{m}{2}M_\eta^{\frac{1}{2}}, \qquad \text{w.p.1.}$$

Hence, from (A.18) $\widetilde{\vartheta}_N$ converges to zero w.p.1 as N tends to infinity; and therefore $\widetilde{\Gamma}_N$ converges to zero w.p.1 as N tends to infinity. It follows that $\widehat{\Gamma}_N$ converges to Γ w.p.1 as N tends to infinity.

APPENDIX B

B.1 Proof of Lemma 3.1.1

The matrix $\begin{bmatrix} \mathcal{W} \otimes I_m \\ \mathcal{X} \end{bmatrix}$ is rank deficient if and only if there exists a row vector

$$[\alpha_0 \ \cdots \ \alpha_{q-1} \ \beta] \neq 0 \tag{B.19}$$

with $\alpha_k^T \in \mathrm{R}^m,\ k = 0, \ldots, q-1$, and $\beta^T \in \mathrm{R}^n$ such that

$$[\alpha_0 \ \cdots \ \alpha_{q-1} \ \beta] \begin{bmatrix} \mathcal{W} \otimes I_m \\ \mathcal{X} \end{bmatrix} = 0. \tag{B.20}$$

From (3.36), (3.27), and (3.35), (3.33), equation (B.20) holds if and only if

$$[\alpha_0 \ \cdots \ \alpha_{q-1} \ \beta] \frac{d^j}{dz^j} \begin{bmatrix} \mathcal{Z}_q(z) \otimes I_m \\ \mathcal{X}_{\mathrm{C}}(z) \end{bmatrix}_{z=z_k} = 0, \quad 0 \leq j \leq N_k,\ k = 1, \ldots, L,$$

$$\Updownarrow$$

$$\frac{d^j}{dz^j} E(z)\Big|_{z=z_k} = 0, \quad 0 \leq j \leq N_k,\ k = 1, \ldots, L, \tag{B.21}$$

where

$$E(z) = \sum_{k=0}^{q-1} \alpha_k z^k + \beta(zI_n - A)^{-1}B.$$

Equation (B.21) implies that for each k the elements of the rational vector $E(z)$ have common zeros at z_k with multiplicity $N_k + 1$. Since $E(z)$ is real-rational, z_k is a zero of $E(z)$ if and only if z_k^* is also a zero of $E(z)$. Therefore, $E(z)$ happens to have a total number of N zeros counting multiplicities. However, the elements of $E(z)$ have numerator degrees not exceeding $n + q - 1$. Hence, any element of $E(z)$ cannot have N zeros. Thus, $E(z) \equiv 0$. This implies that

$\alpha_k = 0$ for all k and $\beta(zI_n - A)^{-1}B \equiv 0$. The latter result follows from the fact that $\beta(zI_n - A)^{-1}B$ is analytic and has a zero at $z = \infty$; hence it is orthogonal to $\sum_{k=0}^{q-1} \alpha_k z^k$. Recall that (A, B) is an uncontrollable pair if and only if it is possible to find a vector $\beta \neq 0$ such that $\beta(zI_n - A)^{-1}B \equiv 0$. Finally, note that $\begin{bmatrix} \mathcal{F} \\ \hat{\mathcal{X}} \end{bmatrix}$ is rank deficient if and only if $\begin{bmatrix} \mathcal{W} \otimes I_m \\ \mathcal{X} \end{bmatrix}$ is rank deficient. The last assertion is due to the fact that, for any complex matrix Z and real vector x,

$$x^T Z = 0 \Longleftrightarrow x\,[\mathrm{Re}Z\ \mathrm{Im}Z] = 0.$$

B.2 Proof of Lemma 3.1.2

The matrix $\mathcal{Y}$ is rank deficient if and only if there exists $\begin{bmatrix} B \\ D \end{bmatrix} \neq 0$ such that

$$\mathcal{Y} \begin{bmatrix} B \\ D \end{bmatrix} = 0 \quad \Longleftrightarrow \quad \frac{d^j}{dz^j} G(z)\Big|_{z=z_k} = 0, \quad 0 \leq j \leq N_k,\ k = 1, \ldots, L.$$

As in the proof of Lemma 3.1.1, this equation implies that every element of $G(z)$ has a total number of N zeros counting multiplicities, a contradiction if $G(z)$ is not identically zero unless $N \leq n$.

BIBLIOGRAPHY

[1] A. Alleyne and J. K. Hedrick. Nonlinear adaptive control of active suspensions. *IEEE Transactions on Control Systems Technology*, 3:94–101, 1995.

[2] H. Chen and K. H. Guo. Constrained H_∞ control of active suspensions: An LMI approach. *IEEE Transactions on Control Systems Technology*, 13:412–421, 2005.

[3] I. Fialho and G. J. Balas. Road adaptive suspension design using linear parameter-varying gain scheduling. *IEEE Transactions on Control Systems Technology*, 10:43–54, 2002.

[4] D. Hrovat. Application of optimal control to advanced automative suspension design. *Transaction of the ASME, Journal of Dynamic Systems, Measurement, and Control*, 115:328–342, 1993.

[5] D. Hrovat. Survey of advanced suspension developments and related optimal control applications. *Automatica*, 33:1781–1817, 1997.

[6] D. Hrovat, D. L. Margolis, and M. Hubbard. An approach toward the optimal semi-active suspension. *Transactions of the ASME, Journal of Dynamic Systems, Measurement, and Control*, 110:288–296, 1988.

[7] D. Karnopp. Active and semi-active vibration isolation. *Transactions of the ASME, Journal of Mechanical Design*, 117 B:177–185, 1995.

[8] D. Karnopp, M. J. Crodby, , and R. A. Harwood. Vibration control using semi-active force generators. *Transactions of the ASME, series B,*

Journal of Engineering for Industry, 96:619–626, 1974.

[9] A. G. Thompson. Design of active suspensions. In *Proceedings of the Institution of Mechanical Engineers*, volume 185, pages 553–563, 1970-1971.

[10] A. G. Thompson. An active suspension with optimal linear state feedback. *Vehicle System Dynamics*, 5:187–192, 1976.

[11] H. D. Tuan, E. Ono, , and P. Apkarian. Nonlinear H_∞ control for an integrated suspension system via parameterized linear matrix inequality characterizations. *IEEE Transactions on Control Systems Technology*, 9:175–185, 2001.

[12] M. Yamashita, K. Fujimori, K. Hayakawa, and H. Kimura. Application of H_∞ control to active suspension systems. *Automatica*, 30:1717–1729, 1994.

[13] P. Gaspar, I. Szaszi, and J. Bokor. Design of robust controllers for active vehicle suspension using the mixed mu synthesis. *Vehicle System Dynamics*, 40:193–228, 2003.

[14] K. Hayakawa, K. Matsumoto, M. Yamashita, Y. Suzuki, K. Fujimori, and H. Kimura. Robust H_∞ feedback control of decoupled automobile active suspension systems. *IEEE Transactions on Automatic Control*, 44:392–396, 1999.

[15] D. Hrovat. A class of active LQG optimal actuators. *Automatica*, 18(1):117–119, 1982.

[16] G. Stein and M. Athans. The LQG/LTR procedure for multivariable feedback-control design. *IEEE Transactions on Automatic Control*, 32:105–114, 1987.

[17] K. Zhou, J. C. Doyle, and K. Glover. *Robust and Optimal Control*. Prentice-Hall, Upper Saddle River, 1996.

[18] J. K. Hedrick and T. Butsuen. Invariant properties of automative suspensions. In *Proceedings of the Institution of Mechanical Engineers. Pt.D. Journal of Automobile Engineering*, volume 204, pages 21–27, 1990.

[19] D. Karnopp. Theoretical limitations in active suspensions. *Vehicle System Dynamics*, 15:41–54, 1986.

[20] M. C. Smith. Achievable dynamic responsefor automotive active suspensions. *Vehicle System Dynamics*, 24:1–34, 1995.

[21] M. C. Smith and G. W. Walker. Performance limitations and constraints for active and passive suspensions: A mechanical multi-port approach. *Vehicle System Dynamics*, 33:137–168, 2000.

[22] C. Yue, T. Butsuen, and J. K. Hedrick. Alternative control laws for automotive active suspensions. *Transactions of the ASME, Journal of Dynamic Systems, Measurement, and Control*, 111:286–291, 1989.

[23] G. Jianmin, R. Gall, and W. Zuomin. Dynamic damping and stiffness characteristics of the rolling tire. *Tire Science and Technology*, 29:258–268, 2001.

[24] B. S. Kim, C. H. Chi, and T. K. Lee. A study on radial directional natural frequency and damping ratio in a vehicle tire. *Applied Acoustics*, 68:538–556, 2007.

[25] H. B. Pacejka. *Tyre and Vehicle Dynamics*. Butterworth-Heinemann, Burlington,Massachusetts, 2nd edition, 2006.

[26] J. A. Levitt and N. G. Zorka. Influence of tire damping in quarter car active suspension models. *Transactions of the ASME, Journal of Dynamic Systems, Measurement, and Control*, 113:134–137, 1991.

[27] P. Gahinet, A. Nemirowski, A. J. Laub, and M. Chilali. *LMI Control Toolbox*. Natick, MA: The Mathworks, 1st edition, 1995.

[28] C. Papageorgiou and M. C. Smith. Positive real synthesis using matrix inequalities for mechanical networks: Application to vehicle suspension. *IEEE Transactions on Control Systems Technology*, 14:423–435, 2006.

[29] J. Wang and D. A. Wilson. Mixed $GL_2/H_2/GH_2$ control with pole placement and its application to vehicle suspension systems. *International Journal of Control*, 74:1353–1369, 2001.

[30] T. Shimomura, Y. Yamasaki, and T.Fujii. LMI-based iterative synthesis of strictly positive real H_2 controllers. In *Proceedings of the American Control Conference*, Chicago, IL, 2001.

[31] H. Chen, P. Y. Sun, and K. H. Guo. A multi-objective control design for active suspensions with hard constraints. In *Proceedings of the American Control Conference*, volume 1, pages 4371–4376, 2003.

[32] H. Gao, J. Lam, and C. Wang. Multi-objective control of vehicle active suspension systems via load-dependent controllers. *Journal of Sound and Vibration*, 290:654–675, 2006.

[33] M. L. Overton. HIFOO: H-infinity fixed order optimization: A matlab package for fixed-order controller design. Available: <http://www.cs.nyu.edu/overton/software/hifoo>.

[34] S. Gümüşsoy and M. L. Overton. Fixed-order H^∞ controller design with HIFOO, a specialized nonsmooth optimization package. In *Proceedings of American Control Conference*, pages 2750–2754, Seattle, WA, 2008.

[35] H. Du, J. Lam, and K. Y. Sze. Non-fragile output feedback H_∞ vehicle suspension control using genetic algorithm. *Engineering Applications of Artificial Intelligence*, 16:667–680, 2003.

[36] H. Du and N. Zhang. H_∞ control of active vehicle suspensions with actuator time delay. *Journal of Sound and Vibration*, 301:236–252, 2007.

[37] M. C. Smith and F. C. Wang. Controller parameterization for disturbance response decoupling: Application to vehicle active suspension control. *IEEE Transactions on Control Systems Technology*, 10:393–407, 2002.

[38] F. C. Wang and M. C. Smith. Disturbance response decoupling and achievable performance with application to vehicle active suspension. *International Journal of Control*, 75:946–953, 2002.

[39] G. W. Walker. *Constraints upon the Achievable Performance of Vehicle Suspension Systems*. PhD thesis, University of Cambridge, 1997.

[40] K. M. Malek and J. K. Hedrick. Decoupled active suspension design for improved ride quality/handling performance. *Vehicle System Dynamics*, 15:383–398, 1986. supplement.

[41] R. M. Chalasani. Ride performance potential of active suspension systems - part ii: Comprehensive analysis based on a full car model. *ASME-AMD*, 80:187–204, 1986.

[42] S. B Choi, H. S. Lee, and Y. P. Park. H_∞ control performance of a full-vehicle suspension featuring magnetorheological dampers. *Vehicle System Dynamics*, 38:341–360, 2002.

[43] N. Yağiz and İ. Yüksek. Sliding mode control of active suspensions for a full vehicle model. *International Journal of Vehicle Design*, 26:264–276, 2001.

[44] İ. Eski and S. Yıldırım. Vibration control of vehicle active suspension systems using a new robust neural network. *Simulation Modelling Practice and Theory*, 17:778–793, 2009.

[45] S. Gümüşsoy, D. Henrion, M. Millstone, and M. L. Overton. Multiobjective robust control with HIFOO 2.0. In *IFAC Symposium on Robust Control Design*, Haifa, Israel, 2009.

[46] C. Scherer, P. Gahinet, and M. Chilali. Multiobjective output-feedback control via LMI optimization. *IEEE Transactions on Automatic Control*, 42:896–911, 1997.

[47] Z. Y. Jiang, D. A. Streit, and M. El-Gindy. Heavy vehicle ride comfort: Literature survey. *Heavy Vehicle Systems–International Journal of Vehicle Design*, 8:258–284, 2001.

[48] M. M. ElMadany. Stochastic optimal control of highway tractors with active suspensions. *Vehicle System Dynamics*, 17:193–210, 1988.

[49] M. Kawana and T. Shimogo. Active suspension of truck seat. *Shock and Vibration*, 5:pp. 35–41, 1998.

[50] R. T. Tong and F. Amirouche. Truck cab suspension design: optimisation and vibration control. *Heavy Vehicle Systems–International Journal of Vehicle Design*, 5:236–260, 1998.

[51] R. T. Tong, F. Amirouche, and L. Palkovics. Ride control-a two state suspension design for cabs and seats. *Vehicle System Dynamics Supplement*, 33:578–589, 1999.

[52] C. J. Dodds and J. D. Robson. The description of road surface roughness. *Journal of Sound and Vibration*, 31(2):175–183, 1973.

[53] K. M. A. Kamash and J. D. Robson. Implications of isotrophy in random surface. *Journal Sound and Vibration*, 54(1):1–13, 1977.

[54] P. Van Overschee, B. De Moor, W. Dehandschutter, and J. Swevers. A subspace algorithm for the identification of discrete time frequency domain power spectra. *Automatica*, 33:2147–2157, 1997.

[55] H. Kimura. Directional interpolation approach to H^{∞}-optimization and robust stabilization. *IEEE Transactions on Automatic Control*, AC-32:1085–1093, 1987.

[56] D. J. N. Limebeer and B. D. O. Anderson. An interpolation theory approach to H^∞-controller degree bounds. *Linear Algebra Applications*, 98:347–386, 1988.

[57] H. Akçay and S. Türkay. Frequency domain subspace-based identification of discrete-time power spectra from nonuniformly spaced measurements. *Automatica*, 40:1333–1347, 2004.

[58] H. Akçay and S. Türkay. Frequency domain subspace-based identification of discrete-time power spectra from nonuniformly spaced measurements. In *43rd IEEE Conference on Decision and Control*, pages 851–856, Paradise Island, Bahamas, 2004.

[59] H. Akçay and S. Türkay. Frequency domain subspace-based identification of discrete-time power spectra from nonuniformly spaced measurements. In *Proceedings of International Workshop, SCTW 2005*, pages 1–11, Gebze, Turkey, 2005.

[60] H. Akçay and S. Türkay. Rational interpolation of analytic functions from real or imaginary parts of frequency-response data: A subspace-based approach. In *48th IEEE Conference on Decision and Control and 28th Chinese Control Conference*, pages 3359–3363, Shangai, P.R. China, 2009.

[61] H. Akçay and S. Türkay. Rational interpolation of analytic functions from real or imaginary parts of frequency-response data: A subspace-based approach. *IEEE Signal Processing Letters*, 16:350–353, 2009.

[62] T. McKelvey, H. Akçay, and L. Ljung. Subspace-based multivariable system identification from frequency response data. *IEEE Transactions on Automatic Control*, 41:960–979, 1996.

[63] H. Akçay and S. Türkay. A subspace-based approach to Lagrange-Sylvester interpolation of rational matrix functions. In *44th IEEE Conference on Decision and Control and European Control Conference*, pages

7102–7107, Seville, Spain, 2005.

[64] H. Akçay and S. Türkay. On the subspace-based interpolation of rational matrix functions. In *3rd IFAC Symposium on System, Structure and Control*, Foz do Iguaçu, Brazil, 2007.

[65] H. Akçay and S. Türkay. A subspace-based method for solving Lagrange-Sylvester interpolation problems. *SIAM Journal on Matrix Analysis and Applications*, 29:377–395, 2007.

[66] S. Türkay and H. Akçay. Effect of tire damping on the ride performance potential of active suspension systems. In *SICE Annual Conference 2007*, Kagawa University, Takamatsu City, Kagawa, Japan, 2007.

[67] S. Türkay and H. Akçay. On the performance limitations of quarter-car active suspension models. In *Proceedings of 5th IFAC Symposium on Advances in Automotive Control*, Monterey Coast, California, 2007.

[68] S. Türkay and H. Akçay. Aspects of achievable performance for quarter-car active suspensions. *Journal of Sound and Vibration*, 311:440–460, 2008.

[69] S. Türkay and H. Akçay. Influence of tire damping on the ride performance limitations and optimal H_2 design for quarter-car active suspensions. In *Proceedings of the 47th IEEE Conference on Decision and Control*, pages 4390–4395, Cancun, Mexico, 2009.

[70] H. Akçay and S. Türkay. Rms performance limitations and constraints for quarter-car active suspensions. In *Proceedings of the 16th Mediterranean Conference on Control and Automation*, pages 425–430, Ajaccio, France, 2008.

[71] H. Akçay and S. Türkay. Influence of tire damping on multi-objective control of quarter-car suspensions. In *Proceedings of the International Conference on Industrial Technology*, pages 62–66, Viña del Mar - Valparaiso, Chile, 2010.

[72] H. Akçay and S. Türkay. Influence of tire damping on actively controlled quarter-car suspensions. *Transactions of ASME, Journal of Vibration and Acoustics*, 2009. Submitted.

[73] H. Akçay and S. Türkay. Influence of tire damping on mixed H_2/H_∞ synthesis of half-car active suspensions. *Journal of Sound and Vibration*, 322:15–28, 2009.

[74] S. Türkay and H. Akçay. Influence of tire damping on the H_2 optimally designed half-car active suspension. In *Proceedings of the 2008 IEEE Multi-conference on Systems and Control*, pages 444–449, San Antonio, Texas, 2008.

[75] S. Türkay and H. Akçay. Tire damping effect on H_2 optimal control of half-car active suspensions. *Transactions of the ASME, Journal of Vibration and Acoustics.*, 132:024502, 2010.

[76] S. Türkay and H. Akçay. Multi-objective control of full-vehicle suspensions: A case study. *Transactions of the ASME, Journal of Dynamic Systems Measurement and Control.*, 2010. Submitted.

[77] H. Akçay and S. Türkay. Active suspension design for an idealized truck cabin. In *Proceedings of the ECC'09 European Control Conference*, pages 4392–4397, Budapest, Hungary, 2009.

[78] S. Kay. *Modern Spectral Estimation, Theory and Application.* Englewood Cliffs, NJ: Prentice-Hall, 1988.

[79] M. B. Priestley. *Spectral Analysis and Time Series.* Academic Press, London, England, 1989.

[80] P. Stoica and R. Moses. *Introduction to Spectral Analysis.* Prentice-Hall, Upper Saddle River, 1997.

[81] K. Glover and J. Willems. Parametrization of linear dynamical systems: cananical forms and identifiability. *IEEE Transactions on Automatic Control*, AC-19:640–645, 1974.

[82] R. Guidorzi. Canonical structures in the identification of multivariable systems. *Automatica*, 11:361–374, 1974.

[83] R. Guidorzi. Invariants and canonical forms for systems structural and parametrice identification. *Automatica*, 17:117–133, 1981.

[84] A. J. M. Van Overbeek and L. Ljung. On-line structure selection for multivariable state space models. *Automatica*, 18:529–543, 1982.

[85] L. Ljung. *System Identification: Theory for the User*. Prentice-Hall, Englewood Cliffs, 2nd edition, 2000.

[86] W. E. Larimore. Canonical variate analysis in identification, filtering and adaptive control. In *Proceedings of the 29th Conference on Decision and Control*, pages 596–604, Hawai, USA, 1990.

[87] P. Van Overschee and B. De Moor. *Subspace Identification for Linear Systems: Theory–Implementation–Applications*. Kluwer Academic Publishers, Dordrecht, 1996.

[88] M. Verhaegen. Identification of the deterministic part of MIMO state space models given in innovations form from input-output data. *Automatica*, 30:61–74, 1994. Special Issue on Statistical Signal Processing and Control.

[89] M. Viberg. Subspace methods in system identification. *Automatica*, 31:1835–1852, 1995. Special Issue on Trends in System Identification.

[90] K. Liu, R. N. Jacques, and D. W. Miller. Frequency domain structural system identification by observability range space extraction. In *Proceedings of the American Control Conference*, volume 1, pages 107–111, Baltimore, MD, 1994.

[91] T. McKelvey, H. Akçay, and L. Ljung. Subspace-based identification of infinite-dimensional multivariable systems from frequency response data. *Automatica*, 32:885–902, 1996.

[92] P. Van Overschee and B. De Moor. Continuous-time frequency domain subspace identification. *Signal Processing*, 52:179–194, 1996. Special Issue on Subspace Methods for Detection and Estimation.

[93] J. Schoukens and R. Pintelon. *Identification of Linear Systems: A Practical Guideline to Accurate Modeling*. Pergamon, London, 1991.

[94] M. Verhaegen. A subspace model identification solution to the identification of mixed causal, anti-causal LTI systems. *SIAM Journal on Matrix Analysis and Applications*, 17:1835–1852, 1996.

[95] R. Fraanje, M. Verhaegen, V. Verdult, and R. Pintelon. A frequency domain subspace algorithm for mixed causal, anti-causal LTI systems. In *Proceedings of the 13th IFAC Symposium on System Identification*, Rotterdam, The Netherlands, August 2003.

[96] P. Caines. *Linear Stochastic Systems*. Wiley Series in Probability and Mathematical Statistics, Wiley, New York, 1988.

[97] B. D. Moor. The singular value decomposition and long and short spaces of noisy matrices. *IEEE Transactions on Signal Processing*, 41:2826–2838, 1993.

[98] S. Türkay and H. Akçay. A study of random vibration charecteristics of the quarter-car model. *Journal of Sound and Vibration*, 282:111–124, 2005.

[99] P. J. Parker and B. D. Anderson. Hilbert transforms from interpolation data. *Mathematics of Control, Signals, and Systems*, 3:97–124, 1990.

[100] A. V. Oppenheim and R. W. Schafer. *Discrete-Time Signal Processing*. International edition, Prentice-Hall, New Jersey, 1989.

[101] J. B. Garnett. *Bounded Analytic Functions*. Academic Press, New York, 1981.

[102] K. Hinnen, M. Verhaegen, and N. Doelman. Robust spectral factor approximation of discrete-time frequency domain power spectra. *Automatica*, 41:1791–1798, 2005.

[103] B. D. O. Anderson and A. C Antoulas. Rational interpolation and state-variable realizations. *Linear Algebra and Its Applications*, 137/138:479–509, 1990.

[104] A. C Antoulas and B. D. O. Anderson. On the scalar rational interpolation problem. *IMA Journal of Mathematical Control and Information*, 3:61–88, 1986.

[105] A. C. Antoulas and B. D. O. Anderson. On the problem of stable rational interpolation. *Journal of Linear Algebra and Applications*, 122/123/124:301–329, 1989.

[106] A. C Antoulas, J. A. Ball, J. Kang, , and J. C. Willems. On the solution of the minimal rational interpolation problem. *Linear Algebra and Its Applications*, 137/138:511–573, 1990.

[107] J. A. Ball, I. Gohberg, and L. Rodman. *Interpolation of Rational Matrix Functions*. Birkhäuser, Basel, Switzerland, 1990.

[108] J. A. Ball, I. Gohberg, and L. Rodman. Two-sided Lagrange-Sylvester interpolation problem for rational matrix functions. In *Proceedings of Symposia in Pure Mathematics*, pages 17–83, 51, AMS, Providence, RI, 1990.

[109] J. A. Ball and J. Kang. Matrix polynomial solution of tangential Lagrange-Sylvester interpolation conditions of low mcmillan degree. *Linear Algebra and Its Applications*, 137/138:699–746, 1990.

[110] A. Blomqvist, A. Lindquist, and R. Nagamune. Matrix-valued nevanlinna-pick interpolation with complexity constraints: An optimization approach. *IEEE Transactions on Automatic Control*, 48:2172–2190, 2003.

[111] T. Boros, A. H. Sayed, and T. Kailath. A recursive method for solving unconstrained tangential interpolation problems. *IEEE Transactions on Automatic Control*, 44:454–470, 1999.

[112] I. P. Fedcina. A description of the solution of the Nevanlinna-Pick tangent problem. *Akad. Nauk Armyan. SSR. Dokl.*, 60:37–42, 1975. (in Russian).

[113] I. P. Fedcina. The Nevanlinna-Pick tangent problem with multiple points. *Akad. Nauk Armyan. SSR. Dokl.*, 61:214–218, 1975. (in Russian).

[114] A. H. Sayed, T. Constantinescu, and T. Kailath. Time-variant displacement structure and interpolation problems. *IEEE Transactions on Automatic Control*, 39:960–976, 1994.

[115] A. H. Sayed, T. Kailath, H. Lev-Ari, and T. Constantinescu. Recursive solutions of rational interpolation problems via fast matrix factorization. *Integral Equations Operator Theory*, 20:84–118, 1994.

[116] J. Kamali, T. Boros, T. Kailath, and G. Franklin. Q-parametrization for unstable plants: A displacement structure approach. pages 4401–4402, 1995.

[117] R. S. Smith and J. C. Doyle. Model validation: A connection between robust control and identification. *IEEE Transactions on Automatic Control*, 37:942–952, 1992.

[118] D. C. Youla and M. Saito. Interpolation with positive-real functions. *Journal of Franklin Institute*, 284:77–108, 1967.

[119] C. I. Byrnes, T. T. Georgiou, and A. Lindquist. A new approach to spectral estimation: A tunable high-resolution spectral estimator. *IEEE Transactions on Signal Processing*, 48:3189–3205, 2000.

[120] C. Mosquera and F. Pérez. Algebraic solution to the robust spr problem for two polynomials. *Automatica*, 37:757–762, 2001.

[121] H. Langer and A. Lasarow. Solution of a multiple Nevanlinna-Pick problem via orthogonal rational functions. *Journal of Mathematical Analysis and Applications*, 293:605–632, 2004.

[122] R. E. Kalman. On partial realization, transfer-functions and canonical forms. *Acta. Polytech. Scand. Math.*, 31:9–32, 1979.

[123] Nikolai K. Nikolski. Operators, functions, and systems: An easy reading. In *Hardy, Hankel, and Toeplitz*, volume Vol. 1, 2002. AMS, Providence, RI.

[124] J. Chen and G. Gu. *Control Oriented System Identification: An H_∞ Approach*. Wiley-Interscience, New York, 2000.

[125] K. Y. Osipenko. *Optimal Recovery of Analytic Functions*. Nova Science Publishers, New York, 2000.

[126] J. A. Ball, I. Gohberg, and L. Rodman. Simultaneous residue interpolation for rational matrix functions. *Integral Equations Operator Theory*, 13:611–637, 1990.

[127] T. Kailath. *Linear Systems*. Prentice–Hall, Englewood Cliffs, NJ, 1980.

[128] J. A. Ball, M. A. Kaashoek, G. Groenewald, and J. Kim. Column reduced rational matrix functions with given null-pole data in the complex plane. *Linear Algebra and Its Applications*, 203/204:111–138, 1994.

[129] L. Ljung. *Linear system identification as curve fitting*, pages 203–215. Directions in Mathematical Systems Theory and Optimization, A. Rantzer and C. I. Byrnes, eds., LNCIS 286. Springer-Verlag, Berlin, Heidelberg, 2003.

[130] A. G. Thompson. Effect of tyre damping on the performance of vibration absorbers in active suspension. *Journal of Sound and Vibration*, 133:457–465, 1989.

[131] A. Zaremba, R. Hampo, and D. Hrovat. Optimal active suspension design using constrained optimization. *Journal of Sound and Vibration*, 207:351–364, 1997.

[132] M. Vidyasagar. *Control System Synthesis: A Factorization Approach*. MIT Press, Cambridge, Massachusetts, 1985.

[133] G. C. Goodwin and M. M. Seron. Fundamental design trade-offs in filtering, prediction, and smoothing. *IEEE Transactions on Automatic Control*, 42:1240–1251, 1997.

[134] J. Lieh. Tire damping effect on ride quality of vehicles with active control suspensions. *Transactions of the ASME, Journal of Vibration and Acoustics*, 131, 2009. Paper no 031011.

[135] D. J. Cole. Fundamental issues in suspension design for heavy road vehicles. *Vehicle System Dynamics*, 35:319–360, 2001.

[136] F. Uffelman. Truck development trends in ride behavior. *SAE Transactions*, pages 910–920, 1993. Paper 933010.

[137] A. Hac, I. Youn, and H. H. Chen. Control of suspensions for vehicles with flexible bodies-part i: active suspensions. *Transactions of the ASME, Journal of Dynamic Systems, Measurement, and Control*, 118:508–517, 1998.

[138] A. Hac, I. Youn, and H. H. Chen. Control of suspensions for vehicles with flexible bodies-part ii: semi-active suspensions. *Transactions of the ASME, Journal of Dynamic Systems, Measurement, and Control*, 118:518–525, 1998.

[139] M. Valášek, V. Stejskal, Z. Šika, O. Vaculín, and J. Kovanda. Dynamic model of truck for suspension control. *Vehicle System Dynamics Supplement*, 28:496–505, 1998.

[140] M. Valášek, M. Novák, Z. Šika, and O. Vaculín. Extended ground-hook–new concept of semi-active control of truck's suspension. *Vehicle System Dynamics*, 27:289–303, 1997.

[141] M. Valášek, V. Stejskal, Z. Šika, and O. Vaculín. Control concepts of semi-active damping of truck suspension for road friendliness. *Vehicle System Dynamics Supplement*, 28:766–771, 1998.

[142] K. L. Chung. *A Course in Probability Theory.* Academic Press, New York NY, 2nd edition, 1997.